The University Of Sheffield.

S.M. Gilgannon

Origin of overdeepened bedrock basins and valleys in ice sheet settings

A thesis submitted in partial fulfilment of the requirements for the degree of Doctor of Philosophy

2021

Origin of overdeepened bedrock basins and valleys in ice sheet settings

Sean Michael Gilgannon

A thesis submitted in partial fulfilment of the requirements for
the degree of Doctor of Philosophy

The University of Sheffield
Faculty of Social Sciences
Department of Geography

December 2021

For Mom & James.

ABSTRACT

Understanding the controls on focused glacial erosion is important given its impact on ice sheet development and dynamics. Previous work has assumed that large glacial erosional landforms such as troughs and overdeepenings are morphologically distinct from glaciofluvial landforms such as tunnel valleys. However, there are many examples of large-scale glacial bedrock incisions (channelised glacioerosional bedrock landform (CGBL)) that are difficult to categorise as either glacial or subglacial-fluvial, and process-based morphological criteria for distinguishing between the two are lacking.

This thesis presents the findings of a semi-automated GIS-based morphological analysis of both the long- and cross-profiles of CGBL features identified in foreland or foreland-like settings. The thesis identifies over 13,900 individual bedrock CGBLs and analyses changes in average cross-sectional morphologies of CGBL features in four main study regions (northern Switzerland; Finger Lakes; Humboldt glacier; and British Columbia) against erosional end-member examples (glacial, subaerial fluvial, and subglacial fluvial). Changes in cross sectional morphology are further analysed along features in relation to changes in bed slope and the regional context (e.g. bedrock erodibility, faulting, topographic confinement) in Northern Switzerland and the Finger Lakes.

The results show that CGBL features are found across most currently and previously glaciated foreland-settings, and that these have average cross-sectional morphologies that range from subaerial fluvial eroded V-shaped to glacially eroded U-shaped. The results also show that CGBL development is highly influenced by the bed slope morphology and regional contextual factors.

The major conclusion is that CGBL features such as "overdeepenings" and "tunnel valleys" are part of a continuum of features which form from both glacial and subglacial fluvial erosive processes, and that the relative level of influence of these processes are highly influenced by a wide range of contextual factors including geology and topography.

Give a man a fire and he's warm for a day, but set fire to him and he's warm for the rest of his life.

— Terry Pratchett

ACKNOWLEDGEMENTS

Many thanks go to my supervisor team, Darrel Swift, Stephen Livingston, Urs Fischer, and John Menzies for their infinite wisdom, patience, and guidance throughout the PhD. Also to my family and friends; especially my brother who was always happy to sit and listen to an ever flowing stream of consciousness with accompanying badly drawn diagrams; Sarah who was always happy to improve my enthusiastic attempts at spelling and grammar; Joe who help me overcome my befuddlement of Matlab and laugh throughout the ups and downs of the PhD; and my Mom, without their never ending support and encouragement I would not have been able to have the courage to strive so far into the wonderful world of academia.

This work was funded by through the ACCE (Adapting to the Challenges of a Changing Environment) NERC DTP and the project CASE (Collaborative Awards in Science and Engineering) partner Nagra (the Swiss National Cooperative for the Disposal of Radioactive Waste).

A final thanks must go to the whole Geography department of the University of Sheffield which has truly been a joy and a privilege to have been welcomed into for this wonderful adventure.

DECLARATION

I, the author, confirm that the Thesis is my own work. I am aware of the University's Guidance on the Use of Unfair Means (www.sheffield.ac.uk/ssid/unfair-means). This work has not been previously been presented for an award at this, or any other, university.

CONTENTS

I INTRODUCTION AND BACKGROUND

1 INTRODUCTION 3

1.1 Rationale . . . 3

1.2 Terminology used in this thesis . . . 5

1.2.1 Overdeepenings . . . 6

1.2.2 Tunnel Valleys . . . 8

1.2.3 Channelised Glacioerosional Bedrock Landforms . . . 9

1.3 Thesis Aims and Objectives . . . 12

1.3.1 Research Questions . . . 12

1.3.2 Objectives . . . 12

1.4 Structure and outline of thesis . . . 13

2 BACKGROUND 15

2.1 Introduction . . . 15

2.2 Key landforms and process-form linkages . . . 15

2.2.1 Incision by ice . . . 15

2.2.2 Incision by glacial melt water . . . 23

2.2.3 Tunnel valleys . . . 27

2.3 Outstanding questions and Summary . . . 32

II DATA AND PROCESSING

3 DATA SYNTHESIS AND SITE SELECTION 37

3.1 Introduction . . . 37

3.2 Northern Switzerland . . . 37

3.3 Analogue Sites . . . 40

3.3.1 The United States of America . . . 41

3.3.2 Canada, British Columbia . . . 63

3.3.3 New Zealand . . . 74

3.3.4 Greenland . . . 82

3.3.5 Antarctica . . . 92

3.4 Additional potential analogue regions . . . 96

3.4.1 European Tunnel Valleys . . . 96

3.4.2 South America (Peru) . . . 96

3.5 Study site selection . . . 96

3.6 End member selection . . . 97

4 DATA PREPROCESSING 99

4.1 Introduction . . . 99

4.2 DEM availability and resolution . . . 99

4.3 Feature Mapping . . . 104

4.4 Feature long- and cross-profile extraction . . . 106

4.4.1 Centreline creation . . . 106

4.4.2 Cross-profile creation . . . 107

4.4.3 Long-profile creation . . . 108

4.4.4 Identification of foreland and alpine boundary 114

III MORPHOLOGICAL ANALYSIS

5 CROSS-SECTIONAL FORM OF BEDROCK CGBLS 119
5.1 Introduction 119
5.2 Study Sites 121
5.2.1 Channel-like glacial-erosional bedrock landform (CGBL) 121
5.2.2 End members of erosion 121
5.3 Methods 122
5.3.1 Cross-sectional analysis 122
5.3.2 Feature morphology averaging 125
5.4 Results 125
5.4.1 CGBL width and depth 125
5.4.2 CGBL Morphology 126
5.5 Discussion 133
5.6 Summary 140

6 VARIATION IN MORPHOLOGY ALONG PROFILE FORM OF BEDROCK CGBLS 141
6.1 Introduction 141
6.2 Method 142
6.2.1 Morphometric methods 142
6.2.2 Qualitative analysis of long-profile change in form 143
6.2.3 Quantitative analysis of variation in long-profile form 143
6.2.4 Statistical analysis of relationships between form metrics 143
6.2.5 Hypothesis testing: controls on long-profile and cross-profile form 143
6.2.6 Statistical analyses 147
6.3 Results 147
6.3.1 Initial description of long-profile variation in form 147
6.3.2 General morphometrics of CGBLs per region 148
6.3.3 Statistical morphological trend within features 151
6.3.4 Normal and adverse slopes 152
6.3.5 Changes in Topographic Confinement 153
6.3.6 Tributary valleys 158
6.3.7 Lithology 160
6.3.8 Inferred faults vs sub-basins 165
6.4 Discussion 166
6.4.1 General CGBL morphology 166
6.4.2 Variability due to specific influences 166
6.5 Summary 172

IV DISCUSSION AND CONCLUSION

7 DISCUSSION 177
7.1 Introduction 177
7.2 Overview of Results 177
7.2.1 Global synthesis 177
7.2.2 Average cross-sectional morphology 178
7.2.3 Variation of morphology along profile 178
7.3 Discussion of CGBL Formation Hypothesis 179

7.3.1 Existing formation hypotheses 179
7.3.2 Proposed broad model of formation 184
7.4 Wider Implications 188
7.5 Limitations 189
7.5.1 Data quality for long-profile analysis 189
7.5.2 Is b vs V-index a better way of seeing process trends? 189
7.5.3 The benefit of using the KDE to see a dominant process 190
8 CONCLUSIONS AND FUTURE WORK 191
8.1 Conclusion 191
8.1.1 What is the current understanding of CGBL formation and development? 191
8.1.2 Are overdeepenings and tunnel valleys parts of a continuum of features that can be described as 'CGBLs' or are they distinct phenomena formed by different processes (i.e. glacial versus fluvial)? 191
8.1.3 What can morphological analysis indicate regarding the role of ice (i.e. quarrying and abrasion) and fluvial erosion in relation to CGBLs formation? 192
8.1.4 What role does changes in feature slope (e.g. adverse and normal slope) and regional context (e.g. geology and topography) play in terms of variability in CGBL morphology, both within individual features and between different CGBL features? 192
8.2 Future works 193

BIBLIOGRAPHY 195

V APPENDIX
A APPENDIX A 221
B APPENDIX B 229

LIST OF FIGURES

Figure 1.1	Location of proposed repository sites	5
Figure 1.2	Lake-filled overdeepenings	6
Figure 1.3	Schematic diagram of overdeepenings	7
Figure 1.4	The Vejle tunnel valley in Denmark	9
Figure 1.5	The Finger Lakes region of New York	10
Figure 2.1	Development of a characteristic glacial U-shaped valley cross-profile	17
Figure 2.2	Fluvial valley long-profiles	18
Figure 2.3	Sognefjord fjord long-profile	20
Figure 2.4	Schematic diagram of theoretical overdeepenings	21
Figure 2.5	Schematic diagram of overdeepenings formed by quarrying	23
Figure 2.6	Schematic diagram showing inner gorge morphology	25
Figure 2.7	Inner gorge near Bern	26
Figure 2.8	Tunnel valley in Wisconsin	28
Figure 2.9	Development of tunnel valleys in soft sediment beds through piping	29
Figure 2.10	Tunnel valley development propoesed by Wingfield 1990	30
Figure 3.1	CGBLs located in the NSF near Zurich	38
Figure 3.2	Geological map of area covered by Figure 3.1.	39
Figure 3.3	Schematic cross section of geological setting of potential repositories and the potential effect of future glaciations.	39
Figure 3.4	Map showing geographical locations of potential areas of interest for the analogue study of the NSF-style CGBLs	40
Figure 3.5	Map of maximum spatial extent of the Laurentide Ice Sheet inrealtion to Finger Lakes	42
Figure 3.6	Location map of the 11 Finger Lakes.	43
Figure 3.7	Bedrock geological map of the region of the Finger Lakes.	44
Figure 3.8	Schematic cross section of averaged geological units	44
Figure 3.9	Piston cores and sedimentary stratigraphic interpretation of seismic reflectors of Cayuga Lake	45
Figure 3.10	Selected transverse and longitudinal interpreted bedrock profiles and sediment fills of 8 of the Finger Lakes.	48
Figure 3.11	Map of maximum spatial extent of the LIS (dark blue line) and names of each lobe and their flow direction in the region of the great lakes. Red box marks the location of the CGBLs Studied by Sjogren. Figure from Margold et al. (2015).	51
Figure 3.12	Hill shaded topographic map of Michigan.	52
Figure 3.13	Map of location of Michigan CGBLs shown by dashed box labelled by Sjorgen as Fig. 3. From Sjogren et al. (2002).	52
Figure 3.14	Figure showing the different tunnel valley morphologies produced from either parallel or transverse flows. Figure from Sjogren et al. (2002).	54

Figure 3.15 Figure from Sjogren et al. (2002) showing surface elevation (not bedrock) maps, and the interpreted idealised sedimentary and bedrock cross sections. 54
Figure 3.16 Map of location and names of major lakes, glaciers, and streams created from the 1968 U.S.G.S. topographic sheet N4813 (Scale 1:00 000). Figure from Mullins et al. (1991). 57
Figure 3.17 Geological map of the area around Lake McDonald 58
Figure 3.18 Contour map of erosion below lake level (depth to bedrock) for Lake McDonald. 59
Figure 3.19 Photograph and interpretation of seismic reflection profile from Lake McDonald. 60
Figure 3.20 Annotated photographs of the axial portions of seismic profiles 60
Figure 3.21 Location of sedimentary basin data in the northern Okanagan valley, south-central British Columbia. Figure from Vanderburgh and Roberts (1996). 64
Figure 3.22 Bedrock surface contour map produced from seismic profiles. Figure from Eyles et al. (1991). 65
Figure 3.23 Bedrock topography map produced from seismic profiles of Kalamalka. 68
Figure 3.24 Bedrock surface topography map. Figure from Eyles and Mullins (1997). 71
Figure 3.25 Map showing geographic location of the largest lakes in New Zealand (left), and map of mapped Quaternary ice limits for New Zealand (right). Figures from Barrell (2011). 75
Figure 3.26 Map of New Zealand's southern island's simplified geology, from Fitzsimons and Veit (2001). 76
Figure 3.27 Map of locations of published morphologies. 76
Figure 3.28 Sketched bathymetric map of Lake Tekapo from Irwin (1978) using measurements published by Irwin (1973). 77
Figure 3.29 Schematic longitudinal profile of bathymetry and lake sediments in Lake Tekapo, 1971. 78
Figure 3.30 Bathymetric map of Lake Ohau, with irregular contour intervals selected to best show the measured bathymetry. Figure from Carter and Lane (1996) originally measured by Irwin in (1970). 79
Figure 3.31 Bathymetric map of Lake Coleridge, with irregular contour intervals selected to best show the measured bathymetry. Figure from Carter and Lane (1996) originally measured by Flain in (1970). 79
Figure 3.32 Bathymetric map of Lake Te Anau, with irregular contour intervals selected to best show the measured bathymetry. Figure from Carter and Lane (1996) originally measured by Irwin in (1971). 80
Figure 3.33 Map of Greenland bed topography produced by Morlighem et al. (2017). 83
Figure 3.34 Geological map of Greenland with interpretation of sub-ice bedrock geology from White et al. (2016), modified from Dawes (2009). 85

Figure 3.35 Map of locations of overdeepening used in the metric dataset (Table 3.10). Black polygons are overdeepenings that have been classified as topographically confined (i.e. those depressions where the mean relief within a small (20 km) buffer of the depression perimeter exceeds 500 m) Figure from Patton et al. (2016b). 86
Figure 3.36 Humboldt Glacier CGBL location maps. 90
Figure 3.37 Humboldt Glacier Ice penetrating radargram profiles 90
Figure 3.38 Bed topography map of Antarctica from Bedmap2 (Fretwell et al., 2013) 92
Figure 4.1 Workflow chart showing steps taken in the creation of the Finger Lakes DEM using data from Mullins et al. (1996) and the USGS bedrock topography map. 102
Figure 4.2 Example images from selected stages of the DEM creation. . . . 103
Figure 4.3 Workflow chart showing steps taken in the mapping of CGBL feature in the northern Swiss, Finger Lakes, and British Columbia study regions. 105
Figure 4.4 Figure showing differences between feature polygon centrelines and long-profiles and how cross-sections from each may be affected. 106
Figure 4.5 Workflow chart showing steps taken in the mapping of the centrelines of CGBL features in the northern Swiss, Finger Lakes, and British Columbia study regions. 107
Figure 4.6 Example figure for northern Switzerland feature 1 centreline creation and trimming of tributary lines. 109
Figure 4.7 Workflow chart showing steps taken in the mapping of cross-profiles at 100 m intervals for CGBL features in the northern Swiss, Finger Lakes, and British Columbia study regions, as well as end member study sites. 110
Figure 4.8 Schematic diagram showing locations where cross sections would require manual clipping to edges of feature polygons. . 111
Figure 4.9 Workflow chart showing steps taken in the mapping line of deepest erosion along the long-profile of CGBL features in the northern Swiss, Finger Lakes, and British Columbia study regions.112
Figure 4.10 Schematic diagram showing how the location of the deepest point in a cross-profile can vary from the geographic centre of the cross-profile, highlighting how the Zonal statistics method calculates the location of the deepest points at each cross-profile.113
Figure 4.11 Location of alpine foreland boundary in relation to 1000 m elevation line in the region of northern Switzerland 114
Figure 4.12 Example elevation profile line manually placed across the study site of northern Switzerland 114
Figure 4.13 Location of alpine-foreland boundary in relation to CGBL features115
Figure 5.1 Site Location map 120
Figure 5.2 Schematic diagram of glacial and subaerial valley erosion and the resultant valley cross-profiles. 121

Figure 5.3 Schematic valley cross-section showing the dimensions each metric records. Grey area shows bedrock location. 123
Figure 5.4 Example cross-profiles and associated measured mean b values and V-index values. 124
Figure 5.5 Example 2D KDE surfaces for the end-member cross-sections. . 125
Figure 5.6 Loglog scatter plots of feature maximum depth against maximum width. 126
Figure 5.7 Box plots of the *b*-exponent (A), form ratio (Fr) (B) and V-index (C) for each CGBL. 127
Figure 5.8 Scatter plots of b/Fr relationships from the peak mean KDE (for calculated sites) and reported b/Fr for previously published sites.131
Figure 5.9 Scatter plots of peak KDE mean *b*-exponent against peak KDE V-index values for CGBL study sites and example end-members of erosion. 132
Figure 5.10 Scatter plots of peak KDE mean *b*-exponents against peak KDE width and peak KDE depth. 136
Figure 5.11 Scatter plots of peak KDE V-index against peak KDE width and peak KDE depth. 137
Figure 5.12 Example cross-profiles of study sites, additional comparison sites, and erosional end members. 139
Figure 6.1 Workflow chart showing steps taken in the identifying normal and adverse slopes in line of deepest erosion in CGBL features in northern Switzerland. 144
Figure 6.2 Example of how normal and adverse slopes were categorised. . 145
Figure 6.3 Schematic diagram showing how topographic confinement is calculated 145
Figure 6.4 Map showing location of published mapped geological faults in northern Switzerland and CGBL features. 146
Figure 6.5 Long-profiles of the features of northern Switzerland showing the line of deepest erosion 149
Figure 6.6 Long-profiles of the features of the Finger Lakes showing the line of deepest erosion 150
Figure 6.7 Scatter plot hexbins for morphometric relationships present in the CGBL features of northern Switzerland. 154
Figure 6.8 Scatter plot hexbins for morphometric relationships present in the Finger Lake CGBL features. 155
Figure 6.9 Slope angle frequency distribution graphs for all normal and adverse slopes of the features in northern Switzerland. 156
Figure 6.10 Changes in confinement for CGBLs of northern Switzerland and the Finger Lakes. 157
Figure 6.11 Scatter plot hexbins of topographic confinement for the northern Switzerland. 158
Figure 6.12 Scatter plot hexbins of topographic confinement for Finger Lakes.159
Figure 6.13 Geology maps for CGBLs of northern Switzerland and the Finger Lakes. 161

Figure 6.14 Contoured KDE scatter plots for the Finger Lakes for scale (depth and width) and cross-sectional morphology by underlying lithology. 163
Figure 6.15 Contoured KDE scatter plot for northern Switzerland for scale (depth and width) and cross-sectional morphology divided by erodibility of underlying lithology. 164
Figure 6.16 Scatter plot for northern Switzerland for number of mapped faults within 10 km Buffer of features against number of nested basins present in features. 165
Figure 6.17 Schematic diagram normal and adverse slopes of a theoretical CGBL feature formed in an alpine setting. 169
Figure 6.18 Schematic diagram of a theoretical CGBL feature formed across an alpine and foreland setting. 174
Figure 7.1 Schematic long-profile diagram showing how quarrying may be active on the steeper slopes of the CGBL normal slopes. . . . 182
Figure 7.2 Schematic cross-sectional diagram of potential processes active during variations in meltwater flow for bedrock with lower RMS values. 184
Figure 7.3 Schematic diagram of a theoretical CGBL feature formed across an alpine and foreland setting. 187
Figure A.1 Bedrock geologic map of Finger Lakes, New York, (1:250,000). . 227
Figure A.2 Geologic map of Glacier National Park, Montana (1:100,000). . . 228
Figure B.1 Long-profiles of the features of northern Switzerland showing changes in feature width 230
Figure B.2 Long-profiles of the features of the Finger Lakes showing changes in feature width 231
Figure B.3 Long-profiles of the features of northern Switzerland showing changes in form ratio (Fr) along feature 232
Figure B.4 Long-profiles of the features of the Finger Lakes showing changes in form ratio (Fr) along feature 233
Figure B.5 Scatter plot hexbin of topographic confinement for foreland features of northern Switzerland. 234

LIST OF TABLES

Table 1.1 Morphometries of Weischselian tunnel valleys (as reviewed by Kehew et al., 2012). 11
Table 3.1 NSF metrics for main features. See Figure 3.1 for locations. . . . 38
Table 3.2 Finger Lakes published statistics. Table from Mullins et al. (1996). 47
Table 3.3 Finger Lakes data availability. 50
Table 3.4 Michigan data availability table. 56
Table 3.5 Glacier National Park data availability table 62
Table 3.6 Okanagan Lake data availability table. 66

Table 3.7 Kalamalka Lake data availability table. 69
Table 3.8 Shuswap Lake data availability table. 73
Table 3.9 New Zealand data availability table. 81
Table 3.10 Greenland overdeepening morphometries measured by Patton et al. (2016b). 87
Table 3.11 Greenland data availability table. 88
Table 3.12 Humboldt Glacier, Greenland data availability table. 91
Table 3.13 Antarctic overdeepening morphometries measured by Patton et al. (2016b). 94
Table 3.14 Antarctica data availability table. 95
Table 4.1 Table of CGBL features and data sources 101
Table 5.1 Cross-section morphometrics 129
Table 6.1 r^2 values of morphological relationships for each of the CGBL features of northern Switzerland 151
Table 6.2 r^2 values of morphological relationships for each of the CGBL features of the Finger Lakes. 152
Table 6.3 Mapped geological units, formations and groups crosscut by CGBLs in the Finger Lakes region. 162
Table 6.4 Table showing mapped geological erodibility groups crosscut by CGBLs in northern Switzerland. 164
Table 7.1 Table outlining morphological evidence for and against the existing formation hypotheses. 180
Table A.1 Table of all potential analogue sites found and the potential available published data. 222
Table B.1 Table showing the location of faults and its effect on location of nested features 229
Table B.2 Table showing northern Switzerland 229
Table B.3 Table showing Finger Lakes 229

Part I

INTRODUCTION AND BACKGROUND

1 INTRODUCTION

1.1 RATIONALE

Landforms arising from focused, deep incision of bedrock are common in glacial landscapes (Cook and Swift, 2012; Kehew et al., 2012; Livingstone and Clark, 2016; Patton et al., 2016b; Kirkham et al., 2020). Ice is typically assumed to be the dominant agent of erosion in such landscapes, and deep incision by ice is generally thought to occur where ice flow has been focused and steered by pre-existing topography (such as preglacial valleys). However, glaciation is also associated with the production of large volumes of surface melt that reaches the ice-bed via englacial pathways, where, in conjunction with subglacial-origin meltwater, it can form organised subglacial drainage networks that are guided in large part by the ice surface slope and in part by the subglacial topography. Water, too, may therefore be an effective erosional agent of focused subglacial bedrock incision (Fountain and Walder, 1998; Greenwood et al., 2007; Kehew et al., 2012; Livingstone and Clark, 2016).

Understanding large-scale glacial erosional landforms and their associated erosional processes has long been of interest in the scientific community due to these features having significant influence on subglacial drainage system distribution, morphology, and transmissivity, the location of basal ice, the transport and deposition of subglacial sediments, and the processes and dynamics of ice flow (Cook and Swift, 2012). However, the nature of glacial erosion and its potential to drastically change the landscape in which it occurs has once again become of interest to the much wider global community. This renewed interest has been due to the potential impact large scale glacioerosional landforms may have on a wide range of scientific communities. Understanding development of such features has been shown to affect our understanding of ice sheet dynamics and therefore how accurately current and future numerical models will be able to predict changes in both ice sheets (such as the Greenland ice sheet and the Antarctic ice sheet) (Cook and Swift, 2012; Patton et al., 2015; Patton et al., 2016b) and mountain glaciers (Colonia et al., 2017). These changes have been shown to result in potential significant hazard, including the exposure of new lakes in the deepened basins during glacier retreat that may catastrophically drain, and the potential increase in retreat rates of ice masses on adverse slopes which may affect the rate of ice mass loss (Cook and Swift, 2012). Better understanding of the processes that form large scale glaciaoerosional landforms also affects countries that rely on current glaciation as a fresh water resource (Colonia et al., 2017). Several studies have attempted to map the locations and morphologies of current glacial overdeepened features, and to model the location of future feature emergence (Haeberli et al., 2016; Colonia et al., 2017; Magnin et al., 2020). This work has been done to allow policy makers to plan future freshwater resource management in the event of the loss of the current glaciers due to climate change. Large scale overdeepenings in lowland areas have also been shown to be of import to large scale infrastructure works, including the placement of deep geological repositories for the storage of nuclear waste

(Stumm, 2010; Haeberli and Whiteman, 2015; Fischer et al., 2017). Notably, the location, morphometrics and infill of these features have been shown to be important when considering the potential impact of future glaciation on geological repositories for nuclear waste (Fischer et al., 2017).

The present study was undertaken in partnership with Nagra (the Swiss National Cooperative for the Disposal of Radioactive Waste; i.e., the technical competence centre for deep geological disposal of radioactive waste in Switzerland), who provided partial funding for this project under a CASE studentship ('Collaborative Awards in Science and Engineering') arrangement. At the time of writing, Nagra has selected five potential sites in Switzerland for the placement of a deep geological repository for the storage of high-level nuclear waste. All of the proposed sites are located approximately 500m below ground level (b.g.l.) in the Opalinus clay geological formation in the north of Switzerland in the foreland region at the foot of the southern Jura mountains (Fig.1.1). Nagra's interest in large-scale glacial erosional landforms is a result of their siting criteria requiring environmental stability for the next 1 million years. The presence of several large sediment- and water-filled glacially eroded basins (overdeepenings) across the Swiss foreland suggest that significant bedrock erosion has occurred in the siting locations during previous glacial cycles (Jordan, 2010; Dürst Stucki and Schlunegger, 2013; Magrani et al., 2020) and thus may occur here in future (Fischer et al., 2017). The exact nature of the erosional processes which may have occurred during the formation of these features, and how they will develop in future glaciations is still uncertain, and this uncertainty poses a significant issue for the safety assessment of the proposed repositories. Nagra has therefore commissioned several different projects and reports to determine the potential for future glacial erosion at the proposed repository sites. The first three chapters of this thesis have been adapted from two reports produced for Nagra on the formation and morphology of bedrock landforms produced by focused glacial and glaciofluvial incision, including potential of features elsewhere being analogue sites for features on the Northern Swiss Foreland (NSF) (Gilgannon et al., 2019; Gilgannon et al., 2020).

In both this thesis and the previous Nagra reports, the identification of sites that are potential analogues for features on the NSF was undertaken to permit site comparisons that would elucidate the fundamental formational processes of the features, while minimising the influence of external factors that may have only modified these processes. The degree of analogue potential was therefore based on similarity of feature morphology (e.g. planform size and shape, depth) and topographic setting to the Swiss foreland features. Key morphological and contextual characteristics of the NSF features (Fig.1.1) were assumed to be their channel-like planform morphology, their large geometry (up to approximately 64 km long and approximately 4.6 km wide), their incision into (sedimentary) bedrock, their 'overdeepened longitudinal and transverse profile morphology (see below), and their formation in an area of relatively low-relief (in this instance, in a foreland area at the foot of a high-mountain chain; i.e. the Alps). Inclusion of potential analogue sites was prioritised by data availability, with the availability of bedrock elevation data suited to detailed morphological analysis of the features being the key criterion.

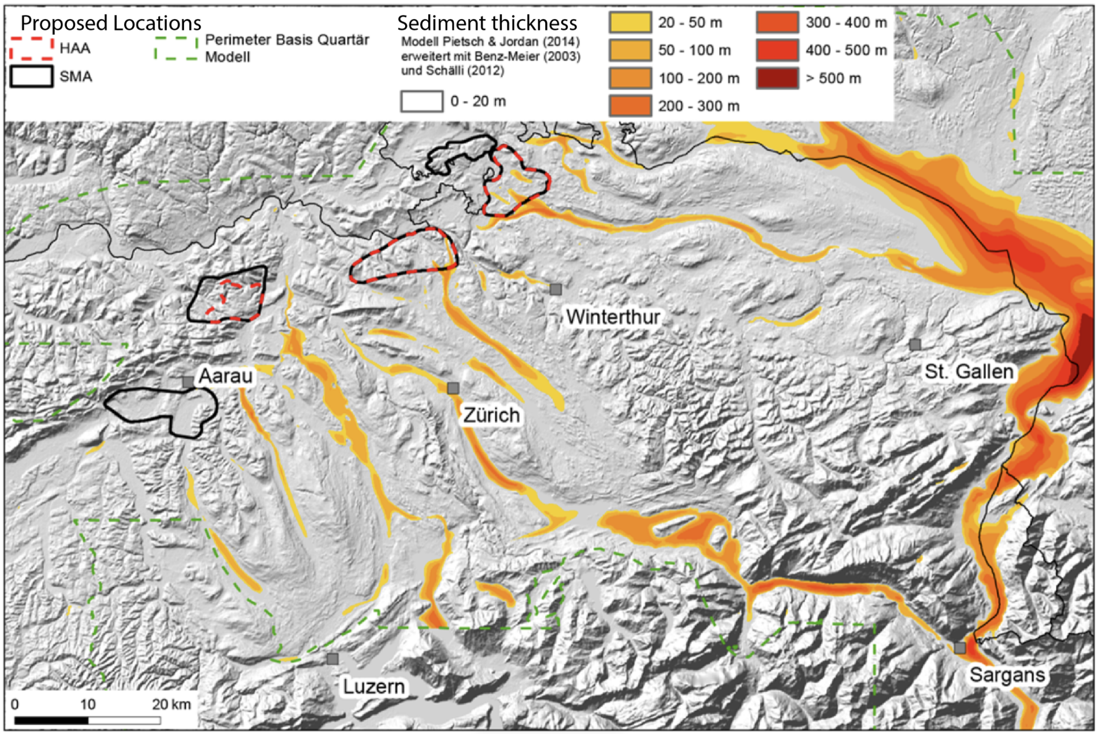

Figure 1.1: Location of proposed sites for deep geological repositories for nuclear waste in the NSF near Zurich. Figure from Fischer et al. (2017)

The thesis therefore primarily focuses on an examination of the morphological variation between the features of the Northern Swiss Foreland and those of selected analogue regions, as well as selected example "end-members" of glacial, subaerial fluvial, and subglacial fluvial erosion, with the overarching aim of improve our understanding of large-scale glacioerosional bedrock landforms.

1.2 TERMINOLOGY USED IN THIS THESIS

Landforms associated with focused, deep bedrock incision under glacial conditions are identified in the literature using a variety of names (e.g. *overdeepening, trough, tunnel valley, linear incision feature*) and research into these landform types has sometimes been undertaken in largely separate scientific communities. As a result, many names and descriptive terms exist for superficially similar features or phenomena, with only a few names being well-used or understood across the whole scientific community. In addition, some names imply a particular formation process, whereas others do not. Feature names that are assumed to be well-used and understood across different communities include the terms *glacial valley* (also *U-shaped valley* or *glacial trough*), *cirque, fjord, fluvial valley* (also *V-shaped valley*), *inner gorge* (i.e. *fluvial gorge*), and *meltwater channel*. Below we list names and associated descriptive terms for features about which there may be some confusion and we provide clear descriptions and definitions of each.

1.2.1 *Overdeepenings*

Overdeepenings (e.g. Linton, 1963; Sugden and John, 1976; Cook and Swift, 2012)(Fig.1.2 and 1.3) are closed topographic basins found in the floors of cirques and glacially deepened valleys in mountainous regions, including the floors of glacial fjords. Overdeepenings are also observed beneath piedmont glacier lobes (Tweed et al., 2005; Magnusson et al., 2012), in continental shelf locations where ice has advanced 'offshore' (e.g. Patton et al., 2016b), and where ice lobes have advanced over thick sediments (e.g. Spedding and Evans, 2002). They may be incised into bedrock (e.g. Hooke, 1991) or sediment (e.g. Motyka et al., 2006). The direction of ice flow in and out of palaeo-overdeepenings is typically easy to define from their position within formerly glaciated landscapes (or, for features associated with contemporary ice masses, by observation of current ice flow patterns). Overdeepenings have therefore been described (e.g. Patton et al., 2015) as having a 'normal' slope, down which ice at the base of the glacier flows as it enters the basin, and an 'adverse' slope, which ice within the basin must ascend as it exits the basin. In some literature, adverse slopes have been described as 'reverse' slopes.

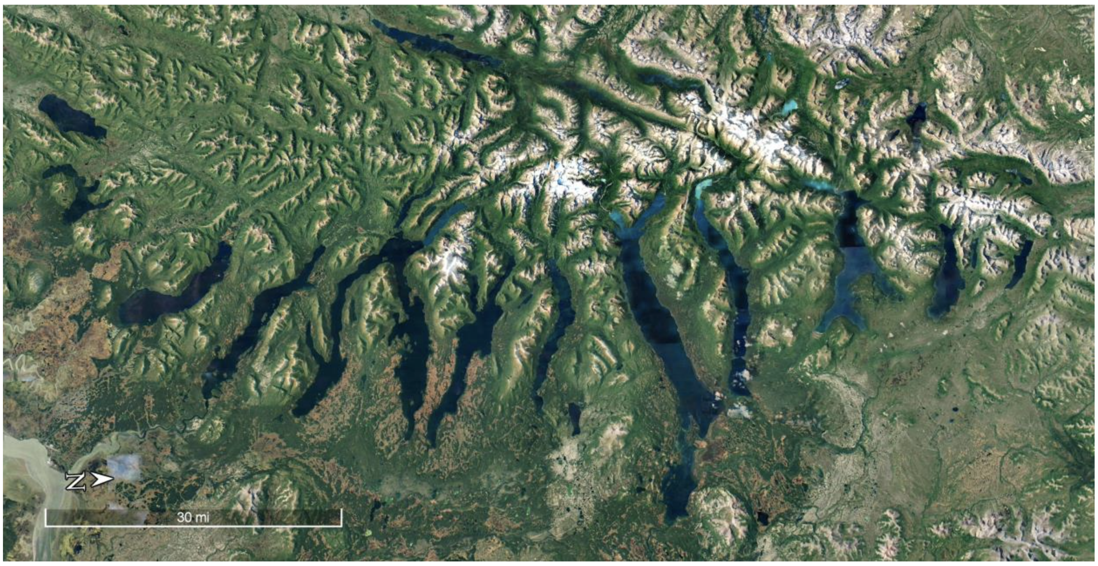

Figure 1.2: Satellite image (Google Earth) of lake-filled overdeepenings occupied by ice during the Last Glacial Maximum in the Wood-Tikchik State Park and upper Togiak River basin and surrounding area, Alaska, USA.

Overdeepening planform morphology is variable. Smaller examples are typically ovoid and larger examples are ribbon-like (Fig.1.2), with the longest axis oriented in the direction of ice flow. Overdeepenings are assumed to be produced by glacial erosion largely because of their large planform area (above), their incision below fluvial base level, and because the transverse profiles of overdeepened valley sections appear to retain the classic glacial 'U'-shape. Thus, overdeepenings appear to be basins created simply by the undulating nature of U-shaped glacial valley longitudinal profiles, where undulations reflect along-flow variation in the depth of erosion (Fig.1.3). For example, overdeepenings have been observed at valley constrictions (i.e. narrowings), where deeper erosion of the valley profile has occurred due to a localised speed-up of ice flow (Gudmundsson, 1997; Hindmarsh et al., 2006; Kessler et al., 2008). In addition, overdeepenings have been observed at valley confluences, where an increase in ice flux is also likely to cause a speed-up of ice flow (Lloyd, 2015). However, areas of deep glacial erosion can also be associated with availability of meltwater. Notably, faster basal sliding occurs where surface melt reaches the bed of glaciers, and glacial sliding is likely to be more effective at eroding bedrock where water is available to transport erosion products (Alley et al., 1997; Herman et al., 2011; Cook and Swift, 2012).

The term 'overdeepening' has, historically, been applied to sometimes different aspects of glacial landscape evolution (Cook and Swift, 2012). However, today it is mainly used to describe a closed (typically bedrock) basin in a glacier or ice sheet bed where, for bedrock examples, the principal physical erosion processes are assumed to have been due to sliding ice (i.e. quarrying and abrasion), and where water may have had a role in facilitating ice-erosion (rather than contributing to bedrock erosion directly) (Swift et al., 2018). In this context, sections of glacial valleys or areas of valley floor where a closed-basin is created by ice-erosion can are described as 'overdeepened'. However, it must be noted that overdeepenings incised into sediment beds may be achieved almost entirely by entrainment and evacuation by subglacial water flow (e.g. Motyka et al., 2006).

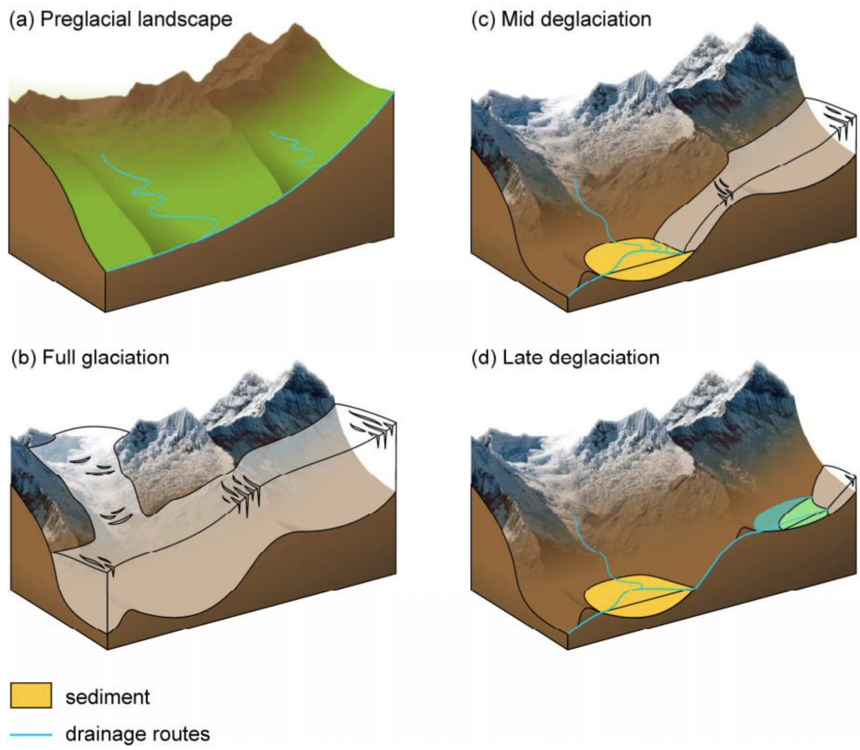

Figure 1.3: Schematic diagram showing the typical glacial and post-glacial context of overdeepened basins in mountainous topography, although note, overdeepenings also form beneath ice sheets and piedmont glacier tongues. Figure: Cook and Swift (2012)

Use of the terms 'overdeepening' and 'overdeepened' appears to have varied subtly since these terms were first coined in the late 19th Century (e.g. Gannett, 1898; Penck, 1900). Both terms were originally used to describe the apparent deepening by glacial erosion of valley floors *beyond the depth that would be expected to have occurred under processes of fluvial erosion alone* (cf. Gilbert, 1877) (i.e. beyond the level of the expected graded fluvial profile, though not necessarily forming a closed basin). The terms are now generally used in either a genetic or non-genetic way in relation to the erosional processes involved in feature formation and development. The genetic nomenclature defines that only features formed by dominant ice erosion should be referred to as overdeepenings (Cook and Swift, 2012), while the non-genetic uses of the terms combine glacially eroded "overdeepened" features with their subglacial fluvial "tunnel valley" counterparts (Magrani et al., 2020). Cook and Swift (2012) have recommended use of the term 'glacially deepened', rather than overdeepened, to indicate valleys deepened by glacial erosion but not necessarily deepened to an extent that closed basins are present.

1.2.2 *Tunnel Valleys*

Tunnel valleys are 'open' or sediment-filled overdeepened valleys (Fig.1.4) incised into bedrock or sediment and these features are typically found in lowland areas within the footprint of former large ice sheets (e.g. Ussing, 1903; Wright, 1973; Attig et al., 1989; Wingfield, 1990; Piotrowski, 1994; Patterson, 1997; Huuse and Lykke-Andersen, 2000; Jørgensen and Sandersen, 2006; Stumm, 2010; Kehew et al., 2012; Livingstone and Clark, 2016; Wenau and Alves, 2020; Kirkham et al., 2020). These features typically extend for tens of kilometres, and are up to several kilometres wide and tens to hundreds of metres deep (Table.1.1). Similar to overdeepenings, they are orientated broadly parallel to ice flow (mainly because it is the ice surface slope that directs the flow of subglacial meltwater), and, like many overdeepenings, have (a) undulating long-profiles and (b) typically terminate at or near former ice margins (e.g. Sandersen et al., 2009; Livingstone and Clark, 2016; Dove et al., 2017; Kirkham et al., 2020). However, many tunnel valleys form anastomosing or cross-cutting networks, the latter being unusual for glacial overdeepenings and troughs. Thus, tunnel valley formation has been typically ascribed to subglacial meltwater erosion (cf. Ó Cofaigh, 1996). This attribution is supported by other tunnel valley attributes, including their greater sinuousity and elongation values, fluvial-like network characteristics, flat-floored cross profiles, and association with other glaciofluvial features, such as outwash fans and eskers (Ó Cofaigh, 1996; Kehew et al., 2012).

The term *tunnel valley* was first coined by Ussing in 1903, although *tunnel channel, palaeovalley, subglacial meltwater channel* (or *incision*), and *linear incision*, are all terms that have been used (Ehlers and Wingfield, 1991). Clayton et al. (1999) used the term *tunnel channel* to indicate smaller (within-) valley features incised by flows under bankfull conditions (e.g. Russell et al., 2007), and *tunnel valley* to indicate larger valley features incised by meandering subglacial rivers. However, the erosion of both valley- and channel-like tunnel features is contentious, with both gradual (i.e. steady-state) and outburst mechanisms invoked (cf. Ó Cofaigh, 1996; Kehew et al., 2012; van der Vegt et al., 2012). In this thesis, the term *tunnel valley* is used in its broadest morphological sense, meaning it is used to refer to any incised glacial valley or channel feature known to have been formed exclusively by subglacial meltwater.

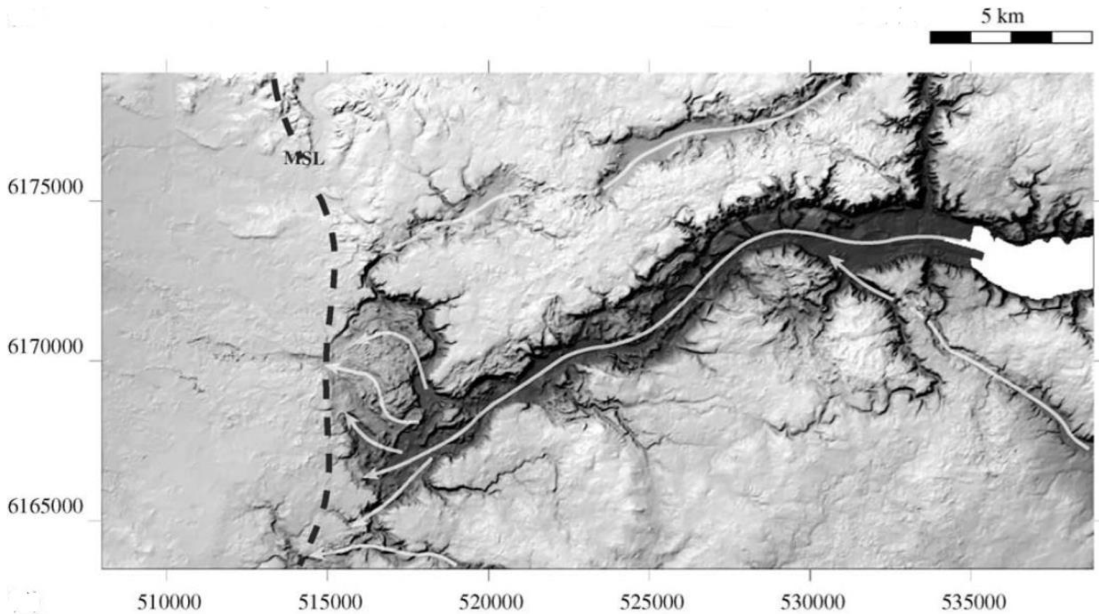

Figure 1.4: The Vejle tunnel valley in Denmark. The dashed 'MSL' line indicates the maximum ice extent during the Last Glacial Maximum. Grey arrows indicate inferred routes of meltwater. Figure: Jørgensen and Sandersen (2006)

Tunnel valleys are frequently 'overdeepened' because subglacial hydraulic gradients permit water to flow uphill, meaning tunnel valleys can be eroded below the subaerial fluviatile base level. Within the literature, features described as *tunnel valleys* have typically been located in flat, lowland regions (e.g. Kehew et al., 2012; Livingstone and Clark, 2016)(Table.1.1), whereas closed-basins found in mountainous environments have been described as overdeepenings (Cook and Swift, 2012). This distinction has been made mainly because lower topographic relief in foreland regions means ice flow is presumed to be less focused, meaning potential for focused, deep incision by ice is reduced (personal communication Prof. Haeberli (University of Zurich) and Prof. Schlunegger (Universität Bern); Cook and Swift (2012)), meaning erosion by meltwater flow has been sometimes considered a more plausible explanation. *Tunnel valleys* have also been distinguished from *overdeepenings* based on their association with other meltwater features such as outwash fans and eskers (Cutler et al., 2002), their erosion into sediment rather than bedrock (e.g. Livingstone and Clark, 2016), evidence of cross-cutting relationships that reveal a palimpsest signature of incision (e.g. Kristensen et al., 2007), and their valley infill characteristics (e.g. van der Vegt et al., 2012). Further, numerous *tunnel valleys* may occur beneath a single ice lobe, arranged in a 'bird's foot' pattern conforming to the likely orientation of subglacial drainage pathways (e.g. van der Vegt et al., 2012).

1.2.3 *Channelised Glacioerosional Bedrock Landforms*

Certain deep bedrock-incision phenomena are not easily categorised on morphological grounds alone as either overdeepenings or tunnel valleys. For example, features observed in the bedrock topography of northern Switzerland (Fig.1.1) exhibit a context (e.g. bedrock incision, U-shaped cross-profiles in several locations) that appears more consistent with overdeepening (i.e. ice erosion), but morphological characteristics that are potentially consistent with subglacial fluvial erosion (specifically, their elongation and network characteristics). Similarly, the Finger Lakes in North America (Fig.1.4) are typically described as tunnel valleys (e.g. Mullins and Hinchey, 1989; Stumm, 2010) but are incised into bedrock and share many morphological similarities with the features in Switzerland. The bedrock context of the Finger Lakes features stands in particular contrast to the sediment-erosion context of the great majority of all other tunnel valleys formed along the southern margin of the former Laurentide Ice Sheet (e.g. Kehew et al., 2012; Livingstone and Clark, 2016).

In this thesis we have therefore introduced a new 'non-genetic' term *channelised glacioerosional bedrock landform* (CGBL) to refer to landforms that reflect deep incision of bedrock in glacial environments by organised flows of ice or subglacial water (or both) *where the specific formational mechanism cannot (as yet) be known or assumed*. The term does not therefore presume a specific formation process, and is more appropriate for use when referring to landforms of an as-yet undetermined origin than the terms *overdeepening* or *tunnel valley*.

Figure 1.5: The Finger Lakes region of New York, USA (Google Earth). The lake-filled ribbon-like overdeepened valleys have both overdeepening-like and tunnel valley-like characteristics.

Table 1.1: Morphometries of Weischselian tunnel valleys (as reviewed by Kehew et al., 2012). Number of features measured taken from Kehew et al. (2012) and referenced papers. Not all papers report the total number of observations of individual features used to calculate size and depth values. star (*) Authors have not stated explicitly how many features were used in calculating measurements.

Location	Substrate	Length	Width	Depth	Number of features measured	Reference
Northern Europe:						
Ireland	Bedrock		<3 km	200 m	5	Knight, 2002
East Anglia	Bedrock	≤30 km	≤500 m	>100 m	Not stated	Galon, 1983
Northern Germany and the Netherlands	Bedrock and Sediment	≤150 km	3-5km	≥500 m - <80 m	>8* >15* >10* Not stated	Ehlers et al., 1984 Stackebrandt, 2009 Bosch et al., 2009 Piotrowski, 1999
The North Sea	Sediment	≤100 km	≤6 km	≤500 m	2 Full and ~6 partial. >20* Not stated >18* >20* 15 >25* >8* 3 generations of features 1 Not stated Not stated >15* Not stated	Kristensen et al., 2007 Stewart and Lonergan, 2011 Stoker et al., 1983 Kluiving et al., 2003 Praeg, 2003 Kristensen et al., 2008 Huuse and Lykke-Andersen, 2000 Lonergan et al., 2006 Lutz et al., 2009 Piotrowski, 1994 Cameron et al., 1987 Ehlers and Wingfield, 1991 Bradwell et al., 2008 Wingfield, 1989
Denmark North Sea	Sediment	≤100 km	100 m – 2-3 km		>18* >3* Not stated >10*	Jørgensen and Sandersen, 2006 Jørgensen et al., 2003a,b Jørgensen and Sandersen, 2009a Jørgensen et al., 2009
Denmark	Bedrock	≤30 km	~1 km	≤350 m	Not stated	Jørgensen and Sandersen, 2009b
Northern Jutland	Bedrock	5-10 km	1 km	>180 m	>11*	Sandersen et al., 2009
North America:						
Southern Sector of Laurentide Ice Sheet	Bedrock and Sediment	200 m – ~90 km	30 m – 9 km	Not stated	1931	Livingstone and Clark, 2016
Minnesota	Not stated	~150 km			Not stated Not stated >10* Not stated Not stated	Wright et al., 1964 Patterson, 1994 Patterson, 1997 Patterson, 1998 Jennings, 2006
Alberta	Sediment (with inferred Bedrock)		≤5 km	≤100 m	6 Not stated 10* Not stated >20*	Beaney, 2002 Rains, et al., 1993 Evans et al., 2006 Evans et al., 2008 Sjogren et al., 2002
Southern Alberta	Bedrock	10 km	>1k m	≤100 m	3	Rains et al., 2002
Southern Ontario	Bedrock and Sediment			≤30 m	>30* 5	Brennand and Shaw, 1994 Brennand et al., 2006

1.3 THESIS AIMS AND OBJECTIVES

The aim of this thesis is to determine the formational origins of large scale CGBLs. The thesis will achieve this through exploration of the following research questions and related objectives:

1.3.1 *Research Questions*

Four main research questions were proposed, and are listed here in chronological order in relation to the thesis structure:

RQ1: What is the current understanding of CGBL formation and development?

RQ2: Are overdeepenings and tunnel valleys parts of a continuum of features that can be described as 'CGBLs' or are they each a distinct phenomenon with a different formation process (i.e. glacial versus fluvial)?

RQ3: What can morphological analysis indicate regarding the role of ice (i.e. quarrying and abrasion) and fluvial erosion in relation to CGBLs formation?

RQ4: What role do changes in feature slope (e.g. adverse and normal slope) and regional context (e.g. geology and topography) play in terms of variability in CGBL morphology, both within individual features and between different CGBL features?

1.3.2 *Objectives*

Objective 1 (O1): ***Determine the current understanding of CGBLs' formation, morphology, and distribution. (RQ1)***

Approach: Review extant literature and available published and unpublished data on the distribution and morphology of CGBLs.

Objective 2 (O2): ***Develop tools to semi-automate identification, measurement, and analysis of CGBL feature cross and long profiles. (RQ2, RQ3, RQ4)***

Approach: Use existing published morphometric methodologies in Python, MATLAB, and ArcGIS to develop semi-automated methods for extracting and analysing multiple long and cross profiles of CGBL features.

Objective 3 (O3): ***Determine the average morphology of "known" glacial and fluvial end members of erosion and compare them against CGBLs from different regions around the world to elucidate their formation. (RQ2)***

Approach: Use published and unpublished data to extract morphological measurements for statistical comparison. The comparison will focus on metrics related to the nature of the CGBL long and cross profiles and will be compared against those for erosional end member landforms. The extraction of measurements will be undertaken through the development and application of new and existing geomorphological analytical techniques (O2).

Objective 4 (O4): ***Determine the influence of regional context on the morphology of CGBLs. (RQ3, RQ4)***

Approach: Use the methods applied in objective 2 to investigate the influence of internal (normal and adverse slope) and external factors of topography (topographic confinement and tributary valleys) and geology (lithology and faulting).

1.4 STRUCTURE AND OUTLINE OF THESIS

The focus of the thesis on the features of the Northern Swiss Foreland (NSF) has been influenced by the requirements of the collaboration with the project partner (Nagra), and the resulting required project deliverables. This influence has been seen in the project structure, with the focus on understanding the features of northern Switzerland, and the aforementioned production of two reports outlining the current knowledge of the location and morphology of potential analogue features in foreland or foreland-like regions, as well as the current data availability of each of the potential analogue sites. These reports were written in collaboration with my Sheffield University supervisors Dr Darrel Swift and Dr Stephen Livingstone, and were reviewed by Dr Urs Fischer and Dr Angela Landgraf of Nagra, before being internally published by Nagra (Gilgannon et al., 2019; Gilgannon et al., 2020) (Gilgannon et al., 2019 awaiting internal publication at time of writing). Both reports have been used as part of this chapter and the following chapters 2 and 3.

The thesis has been divided into three main sections. Section 1 reviews previous work (O1) and synthesizes existing morphological and topographic data (Chapters 2 and 3). Section 2 focuses on analysing the morphologies of identified CGBLs. This is done in two ways. First, a global study of average morphological properties (Chapter 4) and second a focused study of morphological changes within CGBL features (Chapter 5). The global study compares the chosen CGBLs to known end members of glacial erosion to determine if typical CGBL features are a product of distinct erosional processes (glacial or fluvial) or if they are formed from a combination of erosion types (O2, O3). The second method of investigation analyses internal changes in cross-sectional and longitudinal profiles, and relates these changes in morphology to each other, and external regional factors such as geology and topography (O2, O4). The final third section focuses on using the findings of sections 1 and 2 to evaluate existing formation hypotheses and propose how they relate to the morphologies of the features studied herein.

2 BACKGROUND

2.1 Introduction

The following chapter reviews the morphologies, scales, and formation hypotheses for the most common large-scale channelised glacial erosional landforms that are present in current and formerly glaciated landscapes and that are associated with incision by ice or glacial meltwater. The key findings of this literature review are summarised at the end of the chapter, with an emphasis on identification of current gaps in understanding of the erosional processes involved in CGBL formation.

2.2 Key landforms and process-form linkages

Glacial erosional landforms and landscapes are typically considered highly distinctive and easy to distinguish from non-glacial, fluvial-origin landforms on simple morphological grounds (Menzies, 2009). In addition, tunnel valleys, which are typically incised into sediment and are more ribbon-like than other glacial erosional landforms (e.g. Stumm, 2010; Kehew et al., 2012), are assumed to be highly distinctive from their bedrock-incised glacial and subaerial fluvial counterparts. Nonetheless, there are examples of subglacial fluvial incision into bedrock (e.g. Kehew et al., 2012), and flows of water and ice both form organised flows that are steered in part by topography. Further, it is physically possible for landforms incised by both types of flow to exhibit adverse slopes. It follows that the assumption (implicit in many studies) that glacial and subglacial fluvial forms are morphologically distinct may not always hold true. In addition, although there are no published studies (at present) that conclusively demonstrate landforms created by contributions from both glacial and glaciofluvial erosion, the abundance of meltwater in glacier ablation zones means at least some contribution of glaciofluvial erosion to the development of certain glacial forms (and vice-versa) is certainly likely.

The purpose of this section is to review the key morphological characteristics of glacial and subglacial fluvial landforms (the latter focus being mainly on tunnel valleys) with the aim of identifying their distinguishing morphological characteristics. In the first section, the focus is on incision by ice, but it is instructive to consider how landforms incised into bedrock by ice differ from those incised by fluvial processes in non-glacial environments.

2.2.1 *Incision by ice*

In glaciated landscapes, the pattern of glacial bedrock incision is dictated largely by the pattern of ice flow and, as a result, the spatial and temporal pattern of sliding at the glacier bed. Steering of ice by topography (e.g. Kessler et al., 2008) means the fastest sliding rates and zones of maximum potential incision occur at the base of pre-existing valleys. Polythermal regimes of ice sheets and ice caps also restrict sliding to the base of pre-existing valleys (Staiger et al., 2005; Cook and Swift, 2012). The finer details of the incision pattern, including the location of maximum incision, are dictated by local variations in sliding controlled by variability in ice flux and subglacial hydrology (Cook and Swift, 2012), local basal thermal conditions (Lai and Anders, 2021), and by variations in lithology (bedrock geology and structure) (Swift et al., 2008).

2.2.1.1 *Glacial valleys, troughs and fjords*

Sliding beneath glaciers increases predictably from the glacier margin to the centreline, causing ice to incise broad-bottomed valleys with characteristic U-shaped cross-profiles (Fig.2.1a) (Harbor, 1992; Amerson et al., 2008; Augustinus, 1995). This is most evident where flow is constrained by topography, such as in alpine regions or regions of high elevation beneath or bordering large ice sheets (Young et al., 2011; Kessler et al., 2008). This U-shape transverse morphology is characteristic of cirques, glacial valleys, and fjords, including overdeepened sections of the aforementioned features, and can be described mathematically (Fig.2.1b, c). In contrast, gradual non-glacial fluvial incision into bedrock causes valleys to exhibit V-shaped transverse profiles with narrow valley bottoms (Horton, 1945). Sedimentation in 'alluvial' reaches of fluvial systems (i.e. the growth of 'floodplains') can produce flat-floored transverse valley profiles, but these can be distinguished from glacial profiles by the abrupt change in gradient that occurs where alluvium meets the valley sides.

Longitudinal profiles of glacially incised landforms are also distinctive from those arising from gradual fluvial incision. Fluvial incision produces a concave parabolic ('graded') longitudinal profile because stream power dissipates exponentially in the downstream direction (Gilbert, 1877; Mackin, 1948). Glacial incision, in contrast, is characterised by a flatter longitudinal profile (e.g. Brocklehurst and Whipple, 2006) (Fig.2.2a) because glacier power initially increases in the downstream direction (as ice thickens and flow velocities increase) but then decreases in the downstream direction within the ablation area as ice is lost (MacGregor et al., 2000). Further, in fluvial systems, changes in base level stimulate adjustment in the fluvial longitudinal profile, giving rise to knickpoints – local changes in profile gradient – that track headward (i.e. upstream) from the place of base level change (Lewis, 1945). Glacial longitudinal profiles are not affected by base level change, responding instead to changes in climate that control the equilibrium line elevation (Oerlemans, 1984; MacGregor et al., 2000), thereby changing the glacial mass balance and leading to changes in ice thickness, flux, and down-valley extent.

Glacial longitudinal profiles do, nonetheless, exhibit 'knickpoint-like' steps (Fig.2.2b, c). These steps may reflect structural or lithological changes (Duhnforth et al., 2010), or may be preglacial features of similar origin. However, steps also reflect changes in ice flux, which occur most abruptly where topography steers ice into confluences or through narrow troughs (e.g. Cooper et al., 2016). Thus, modelling studies that relate erosion rate to ice flux via basal sliding have produced steps by simulating increases in flux, for example at confluences with tributaries and trough heads caused by narrowing of glacial valleys below their accumulation basins (MacGregor et al., 2000; Anderson et al., 2006), and at decreases in flux at the ice margin (MacGregor et al.,

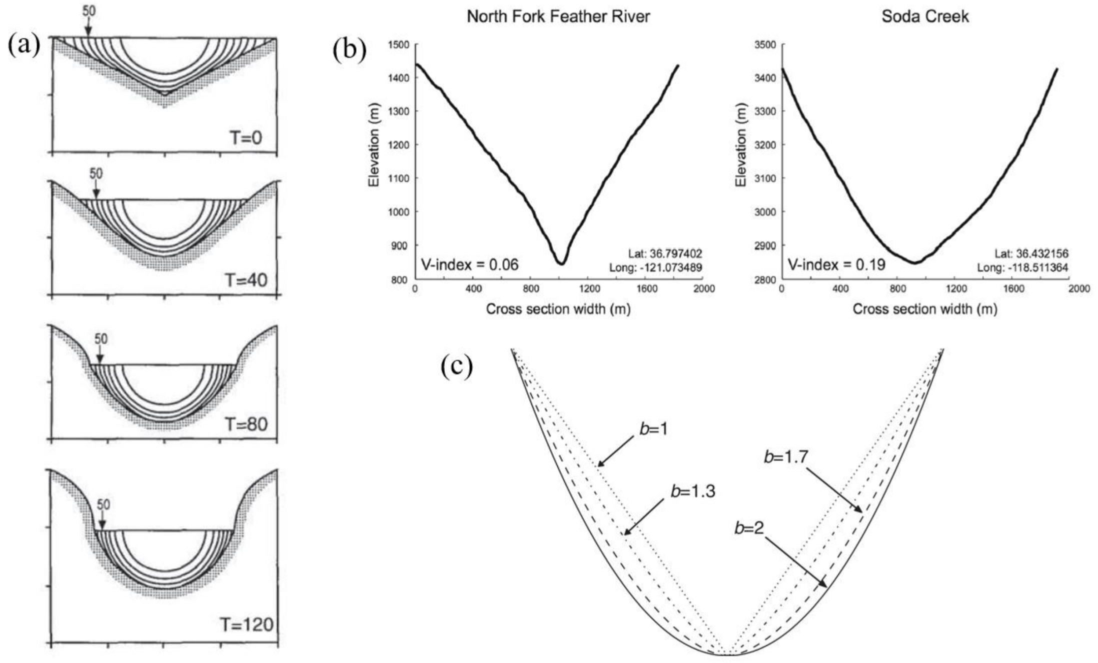

Figure 2.1: (a) Development of a characteristic glacial U-shaped valley cross-profile from a fluvial profile in a simple glacial erosion model; time (T) in ka (Harbor, 1992). (b) Cross-profiles of non-glaciated (North Fork Feather River) and glaciated (Soda Creek) valleys and associated V-index values (Zimmer and Gabet, 2018). (c) Idealised V-shaped (fluvial – dotted line) and U-shaped (glacial – solid line) valleys and associated b-values obtained by fitting the shape with a power-law equation (Prasicek et al., 2015).

2009), leaving a bedrock 'threshold' marking the former ice-front position (Fig.2.2c) Such steering of flux by topography is presumably also a significant influence on the development of trough heads in fjord systems (cf. Kessler et al., 2008).

Less attention has been given to the influence of lithology on incision patterns and valley morphology, even though modelling (e.g. Harbor, 1992) and field studies (e.g. Augustinus, 1991) have emphasized a significant control of lithology on the cross-profile form of glacial valleys (cf. Zimmer and Gabet, 2018). Augustinus (1991) demonstrated significantly deeper and narrower glacial valley incision by ice in 'harder' lithologies, as did Swift et al. (2008), who further found that fjord sections in harder lithologies may be substantially more 'overdeepened'. The influence of lithology on incision patterns, such as trough size and spacing, is likely to some extent controlled by positions of major faults (e.g. Glasser and Ghiglione, 2009; Duhnforth et al., 2010). Notably, Swift et al. (2008) observed striking changes in fjord network characteristics, including size, sinuosity and spacing, apparently influenced by lithology in East Greenland. Additionally, several studies (Camerlenghi et al., 2001; Studinger et al., 2003; Tabacco et al., 2002) have shown that some of the largest troughs and basins in Antarctica have a strong tectonic component, being associated with grabens or other tectonic basins (Cook and Swift, 2012).

Advances in numerical modelling have permitted exploration of the influence of different glacial erosion laws (e.g. Egholm et al., 2012; Ugelvig et al., 2016), different models of ice physics (Braedstrup et al., 2016), variability in the availability of melt (e.g. Herman et al., 2011) (Fig.2.2d), and erosive tools (Ugelvig et al., 2018) on the details of glacial valley incision. However, such studies have not applied detailed examination of the results in terms of transverse valley or long-profile morphology.

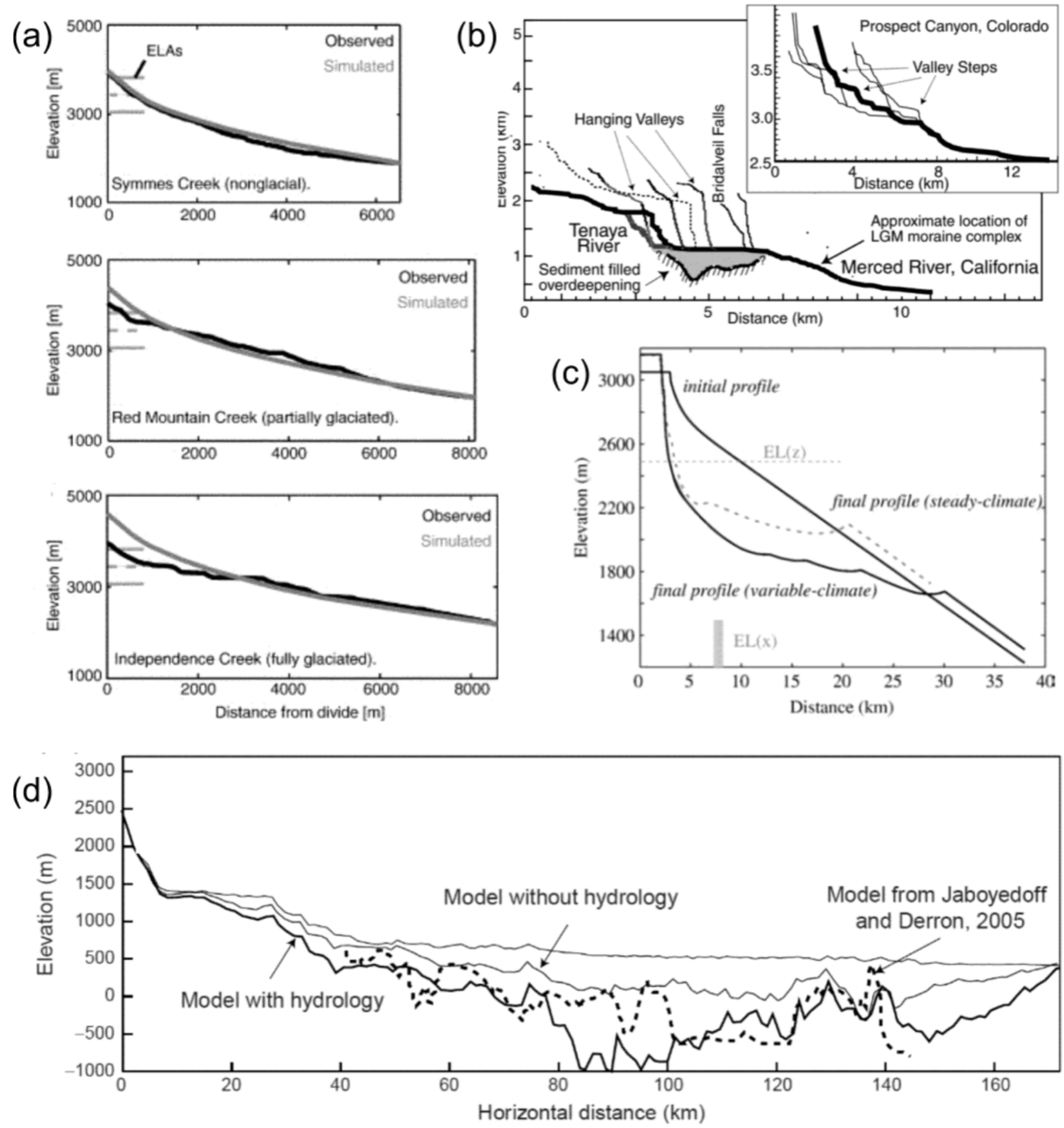

Figure 2.2: (a) Simulated fluvial and observed valley long-profiles in nonglacial and fully glaciated catchments (Brocklehurst and Whipple, 2006). (b) Long-profile of Yosemite Valley and Prospect Canyon and their tributaries, showing stepped and overdeepened profiles (MacGregor et al., 2000). (c) Long-profiles modelled using a simple glacier erosion model (MacGregor et al., 2009). (d) Observed and modelled bedrock long-profiles of the Rhone Valley (Herman et al., 2011).

2.2.1.2 *Overdeepenings*

A key feature of glacial incision in mountain glacier and ice sheet settings is the presence of closed basins (overdeepenings) in the longitudinal profile (Patton et al., 2016b; Cook and Swift, 2012; Dürst Stucki and Schlunegger, 2013; Haeberli et al., 2016). Overdeepenings are ubiquitous beneath both marine and terrestrial ice masses, and common beneath even small glaciers and ice caps.

Overdeepening morphology varies greatly. Mountain glacier, outlet glacier and ice stream tributary beds typically exhibit multiple overdeepenings, separated by bedrock highs, that range in length from 10^2 to 10^4 m, and may be regularly or irregularly sized and spaced, and typically reaching several tens to hundreds of metres in depth (Hooke, 1991; Cook and Swift, 2012). Larger ice stream and outlet glacier systems may exhibit even longer overdeepened profiles, sometimes exceeding 1 km in depth relative to the basin 'lip' (i.e. the exit point for ice, sediment and water), and sometimes containing smaller sub-overdeepenings, that terminate at a prominent high or 'threshold' (Fig.2.3). In marine settings, such thresholds may serve as important 'grounding line' positions (Cook and Swift, 2012; Patton et al., 2016b). Intermediate thresholds in mountain glacier and fjord beds may form prominent bedrock bars (i.e. riegels) that affect (and possibly slow) ice flow (Hanson et al., 1998). Marine thresholds and the overdeepenings behind them presumably form in a similar manner to steps located at the termini of terrestrial glaciers (e.g. MacGregor et al., 2009).

In fluvial systems, scour creates small basins, but the energy of the flow and its ability to scour the bed diminishes rapidly as basin depth increases and flow begins to 'pond'. In contrast, the high viscosity of ice means glacier flow continues to exert shear forces on the bed as it deepens. Flow overcomes the topographic obstacles created by the adverse slopes of such basins through a combination of (1) longitudinal coupling, where ice motion is maintained by the pushing force of ice upglacier of the adverse slope and the pulling force of ice downglacier of it, and (2) by thickening until the ice-surface gradient is steep enough to generate shear stresses that maintain flow through the basin. In addition, changes in hydrology within basins that promote higher basal water pressures and sediment deposition should cause sliding rates in overdeepenings to increase. However, high water pressure and sediment deposition both act to reduce contact between ice and the bed (i.e. bedrock), implying a slowing of erosion with increasing basin depth (Cook and Swift, 2012; Patton et al., 2016b). Further, the enlargement of the basin locally enlarges the valley cross-sectional area and, assuming conservation of ice flux, is likely therefore to lead to a slowing of ice flow within the basin.

Overdeepening morphology is determined primarily by patterns of ice flux, and topographic steering of flow likely has a very important control, particularly in areas of high topography (e.g. Kessler et al., 2008). Precise details of overdeepening location and morphology, however, likely relate to the specific erosion process responsible, the availability of water for sliding and flushing, the availability of erosive tools, and the operation of both positive and negative (i.e. stabilising) feedbacks associated with

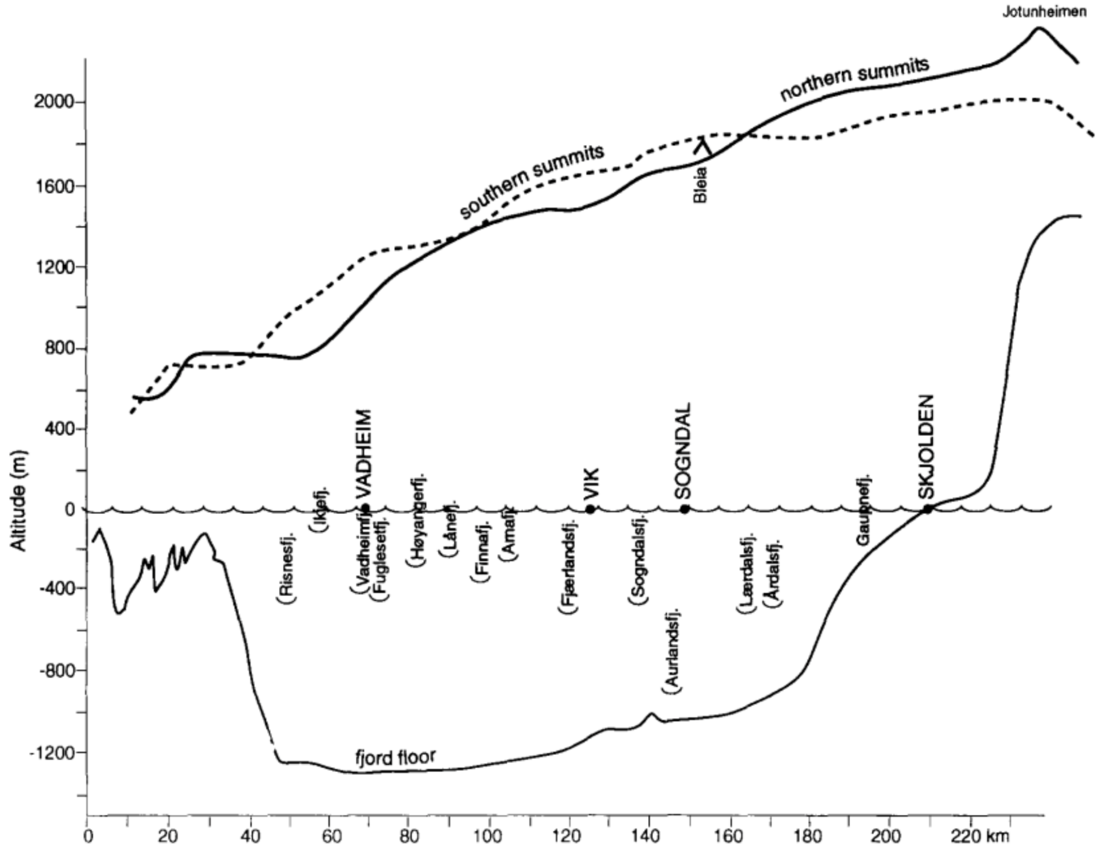

Figure 2.3: Long valley profile of the Sognefjord fjord Nesje and Whillans (1994) demonstrating a relatively flat, overdeepened fjord-floor with a steep adverse slope rising to a prominent bedrock threshold at the overdeepening 'lip'.

these (Fig.2.4). Overdeepening formation in low-relief foreland and continental shelf areas, where flux is presumed to decline because of ice ablation and divergent ice flow vectors, provides evidence for the existence of these additional processes and feedbacks (Cook and Swift, 2012).

The importance of quarrying for overdeepening formation has been emphasized by Hooke (1991), who proposed a positive ice-water-erosion feedback related to it. Quarrying is the physical process of fracturing bedrock and entraining the resulting blocks in basal transport, with fracturing favoured by spatially and temporally varying ice and water pressure fluctuations at the bed (Iverson, 2012). Hooke (1991) argued that quarrying would exploit pre-existing irregularities in ice-bed topography (perhaps due to lithology), and that ice flow over these irregularities would cause crevasse formation at the ice surface that would direct surface melt to the bed, where it would thus enhance the quarrying rate (Fig.2.4d). This implies that overdeepenings erode headwards by quarrying (Hooke, 1991) (see also Fig.2.5), which is consistent with analyses that demonstrate a typically asymmetric overdeepening long-profile morphology (Patton et al., 2016b). However, overdeepening formation has also been simulated by numerical studies that do not explicitly include quarrying or related feedbacks, and which instead use erosion rules based only on glacier sliding (e.g. Oerlemans, 1984; MacGregor et al., 2000; Herman et al., 2011).

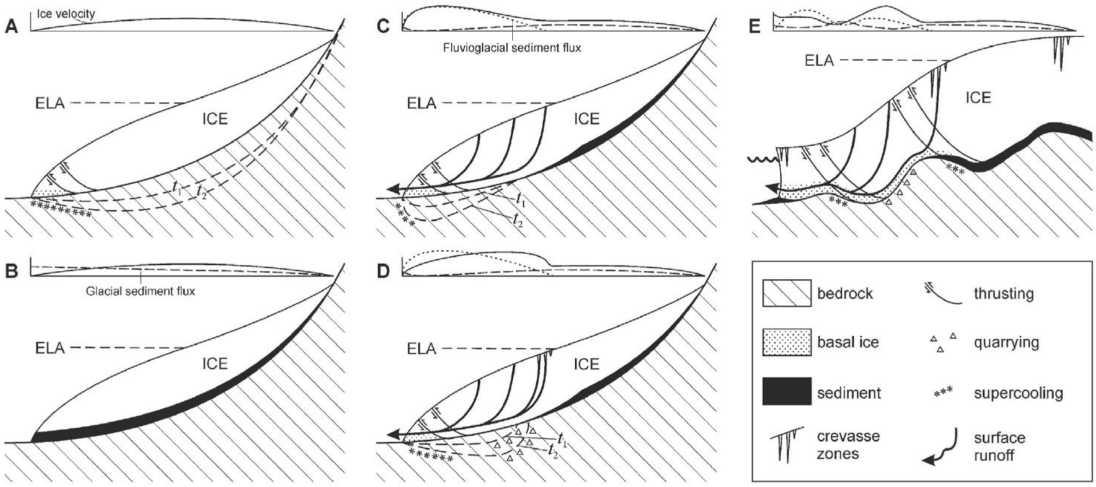

Figure 2.4: Schematic diagram showing the different erosion processes and development of different morphologies of theoretical overdeepenings. Dashed lines indicate time horizons during the erosion of major subglacial basins. (A) Shows the theoretical symmetrical erosion pattern that would occur if there were no hydrological forcing of basal sliding and sediments produced by erosion are flushed from the glacier bed. (B) Shows how no overdeepening will form when sediments are not flushed away and accumulate to form a thick basal sediment layer that protects the bed. (C) Shows the development of a strong overdeepening underneath the ablation area, as a result of surface runoff enhancing both basal sliding and basal sediment evacuation. (D) Shows a headward evolution of an overdeepening resulting from focussed delivery of surface runoff and local steepening of the bed enhancing quarrying and abrasion at the overdeepening head. (E) Shows the development of multiple overdeepenings and complex spatial patterns of erosion resulting from variation in climate and hence ELA position and glacier extent. Figure: Patton et al. (2016b), modified from Cook and Swift (2012).

Numerical studies that have explicitly used formulations of the quarrying process (e.g. Ugelvig et al., 2016) do indeed produce overdeepenings, but the details do not appear to differ substantially from models that employ sliding-based erosion formulations, where patterns of sliding are only forced by seasonal melt (e.g. Herman et al., 2011). Because melt is produced mainly in the ablation area and motivates fastest sliding near the upper part of this area, where channelized drainage is less efficient, the model used by Herman et al. (2011) produced headward erosion of an overdeepening with an asymmetric long-profile as bed erosion caused the ablation area to ‘erode’ headwards. Further, forcing the model using a non-steady climate was able to produce multiple overdeepenings, as shown by the earlier model of MacGregor et al. (2009). Whether the morphological details produced by these models really are different, however, requires further analysis.

An alternative formation mechanism is that overdeepenings should preferentially form near to glacier termini where ice surface gradients are steepest (i.e. able to drive water along steep adverse gradients) and there is abundant meltwater to flush the sediment created by erosion (Cook and Swift, 2012) (Fig.2.4c). This mechanism, which does not invoke quarrying caused by an initial bedrock irregularity, may account for the large number of overdeepenings located beneath glacier termini.

Regardless of formation mechanism, non-steady climate will lead to complex patterns of overdeepening formation (cf. Herman et al., 2011) (Fig.2.4e), and changes in mass balance and terminus position will lead to changes in ice surface slopes overlying overdeepenings, leading to repeated episodes of sediment evacuation and erosion within individual basins.

Hooke (1991) also proposed a potentially important stabilising control on overdeepening morphology that was later elaborated on by Alley et al. (2003), the process of glaciohydraulic supercooling (GSC). GSC causes water in subglacial sheets and channels to freeze and arises when the gradient of the overdeepening adverse slope exceeds that of the ice surface slope (which is in the opposite direction) by a factor of two. At this threshold, flow in subglacial channels distributes across the bed (Cook and Swift, 2012; Werder, 2016), and sediment carried by the water is deposited on the adverse slope, and some of the sediment is entrained into glacial transport by basal ice formation. The protection afforded to bedrock by thick sediments should therefore cause overdeepening adverse slope gradients to stabilise at this threshold, and thereafter growth must be limited to headward extension. Borehole studies showing persistent near-overburden water pressures within overdeepenings provide support for the breakdown of efficient subglacial drainage within overdeepened areas (e.g. Hooke, 1991), which itself should act to slow erosion within basins by decoupling basal ice from the bed. However, Werder (2016) has shown that the threshold is variable and dependent on the pressure of water in the subglacial drainage system downglacier of the overdeepening lip. Further, Creyts et al. (2013), Cook and Swift (2012) and Patton et al. (2016b) have advocated explanations for variation in the adverse slope threshold that are related to the sediment carrying capacity of subglacial water flow.

The flattish floors of overdeepened marine outlet glacier troughs (i.e. fjords) (Fig.2.3) also suggest stabilising feedbacks on overdeepening depth. A fundamental feedback is flotation, which will cause ice to decouple from the glacier bed. Further, Patton et al. (2016b) have suggested that these flattish profiles occur because stabilising feedbacks on adverse slopes slow erosion at the base of overdeepenings and focus erosion on the intervening thresholds (Fig.2.5). This would eventually lead to a uniformly overdeepened profile where the bed profile is graded by the energy available for subglacial fluvial transport of sediment, which is dictated by the subglacial hydraulic gradient, much the same as fluvial long-profiles are graded to available stream power (Cook and Swift, 2012). This situation may be unlikely to arise in alpine regions where tectonic uplift maintains steep glacier (and valley) profiles, but is at least plausible in passive settings in high topography at the margins of relatively stable continental ice sheets.

Overdeepening depth varies greatly, with some marine outlet glacier examples exceeding 1000 m in depth relative to the basin lip (i.e. the bedrock threshold at the fjord-end; e.g. Fig.2.3). Erosion to such depths requires large ice thicknesses and surface gradients that can maintain ice-bed coupling and the evacuation of basal water and sediment. Flow resistance provided by lateral and basal shear, together with backstress (i.e. form drag) provided by the development of an adverse slope and bedrock threshold at the fjord lip (Fig.2.3), is therefore likely to be an important factor.

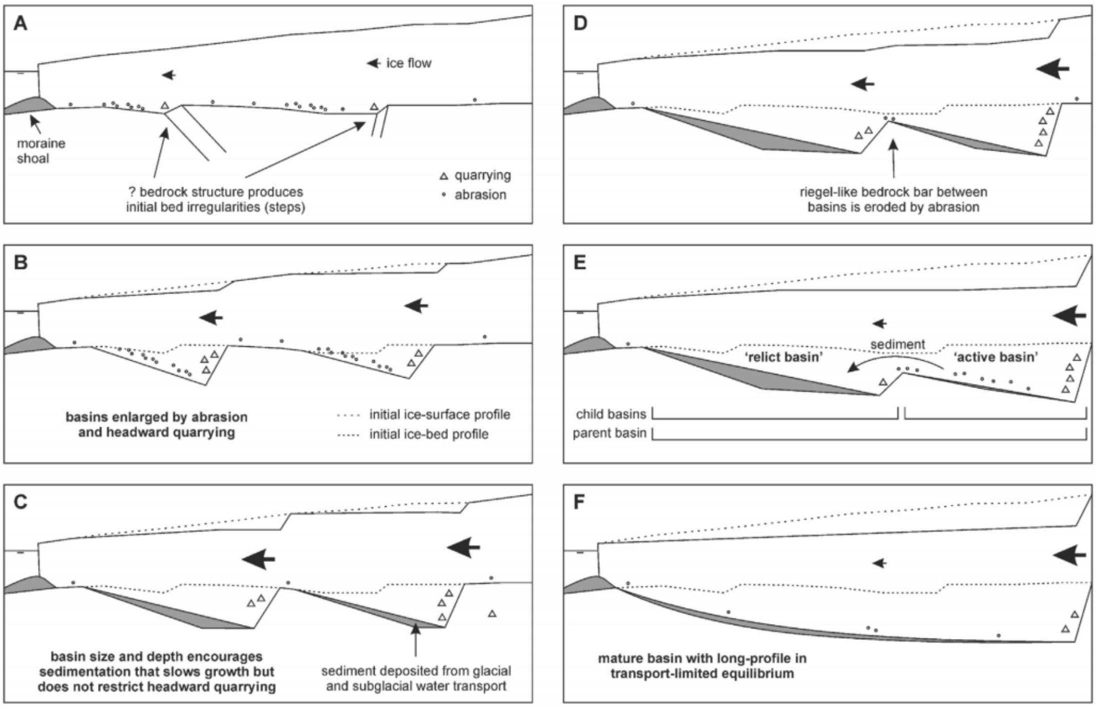

Figure 2.5: Schematic diagram showing hypothesized development of long-flat floored overdeepenings characteristic of large outlet glacier or ice stream systems. Multiple initial overdeepenings coalesce through headward erosion by quarrying but also because abrasion is focused upon intervening thresholds. Figure: Patton et al. (2016b).

High lateral shear provided by the narrow valley sides may, for example, account for the deep basin beneath Byrd Glacier, Antarctica (Patton et al., 2016b), and perhaps observations of deeper overdeepenings in narrow valleys formed in more resistant lithologies (e.g. Swift et al., 2008). Where there is an absence of marginal topography that creates lateral shear, backstress provided by the bedrock threshold is presumably extremely important. This may account for the deep basin occupied by Thwaites Glacier, Antarctica (Joughin et al., 2009). It should be noted that many of the deepest overdeepenings are fault controlled; these antecedent conditions will provide deep pre-existing valleys and weaken the underlying bedrock thus having a strong influence on the depth to which the ice is able to erode (Camerlenghi et al., 2001; Studinger et al., 2003).

2.2.2 *Incision by glacial melt water*

Fluvial incision can occur during glacial conditions if suitable volumes of water are generated by glacial melt and routed via the bed, either directly or indirectly (i.e. indirectly meaning via storage and release in a catastrophic event or series of events). Such incision may occur subglacially or proglacially, and will not necessarily create landforms that are morphologically distinctive or physically separate from features associated with fluvial erosion during interglacial periods. Landforms of subglacial fluvial incision, such as tunnel valleys and smaller bedrock meltwater channels, typically show system characteristics that are discordant with present subaerial drainage, such as abrupt start- and end-points and undulating long- profiles (see section 2.2.1). However, inner gorges (or slot gorges) may arise from proglacial incision during periods of deglaciation (Jansen et al., 2014). Though these sometimes exhibit 'valley-in-valley' transverse profiles (Fig.2.6) characteristic of a history of variable incision rates under changing discharge regimes, these typically form part of (and grade into) the post-glacial fluvial system.

Erosion by subglacial meltwater occurs via the same three mechanical and chemical processes as in subaerial fluvial systems: corrasion (a mechanical processes similar to that of glacial abrasion), cavitation, and corrosion (chemical weathering) (Knighton, 2014). Water under glaciers is drawn both from the surrounding ice through pressure melting at the ice bed interface, geothermal flux and frictional melting, and from surface melt water. Surface melt water can reach the bed through moulins and crevasses, which act as point sources to the ice bed interface, as well as from sudden releases of water stored subglacially, supraglacially or at the ice-margin. These different melt sources with variable temporal rates and magnitudes (Chandler et al., 2013), combined with the pressurisation of flow by overlying ice, results in a drainage network morphology, distribution and routing that may be notably different from subaerial systems, and which may evolve through time from distributed to well-ordered channels and back again (Fountain and Walder, 1998), sometimes rapidly. The largest differences are the abrupt beginning and ending of channels, and the ability of subglacial meltwater to flow up-slope (Shreve, 1972) and therefore create undulating channel longitudinal profiles (Ó Cofaigh, 1996; Greenwood et al., 2007; Grau Galofre et al., 2018). Numerical modelling of erosion by such systems has been very limited (e.g. Herman et al., 2011; Beaud et al., 2014; Beaud et al., 2016; Beaud et al., 2018b).

2.2.2.1 *N-channels and inner gorges*

N-channels (after Nye (1973)) are subglacially eroded bedrock channels exposed by glacial retreat and are typically of small scale (10s-100s of meters). N-channels have been described as having a trapezoidal cross profile morphology by Grau Galofre et al. (2018). However, previous work by Clapperton (1968) and Glasser and Sambrook Smith (1999) suggests that the cross-profile morphologies can vary depending on the ice conditions under which they formed, as well as the pre-existing subglacial topography. Glasser and Sambrook Smith (1999) show that, depending on the type of substrate over which the channels have formed, the channels can develop a narrow profile (bedrock) and a wider profile (sediments). The reported lengths of meltwater channels are on the kilometre scale (1-2 km) (Grau Galofre et al., 2018), while widths range from 40-60 m at the channel head up to 150-300 m at the mouth. Grau Galofre et al. (2018) and Greenwood et al. (2007) report depths of <5 m at the channel head and over 10 m deep at the mouth. Glasser and Sambrook Smith (1999) report 4 different types of meltwater channel in their study of the northwest of England with channel lengths that range from 75 m up to 3.5 km. The channels range from single isolated long channels to short steep chutes incised into bedrock ridges. Glasser and Sambrook Smith (1999) also report that the channels with lengths ranging from 75 m to 2.75 km showed both isolated channels and integrated networks of channels with several tributaries connecting to larger main channels.

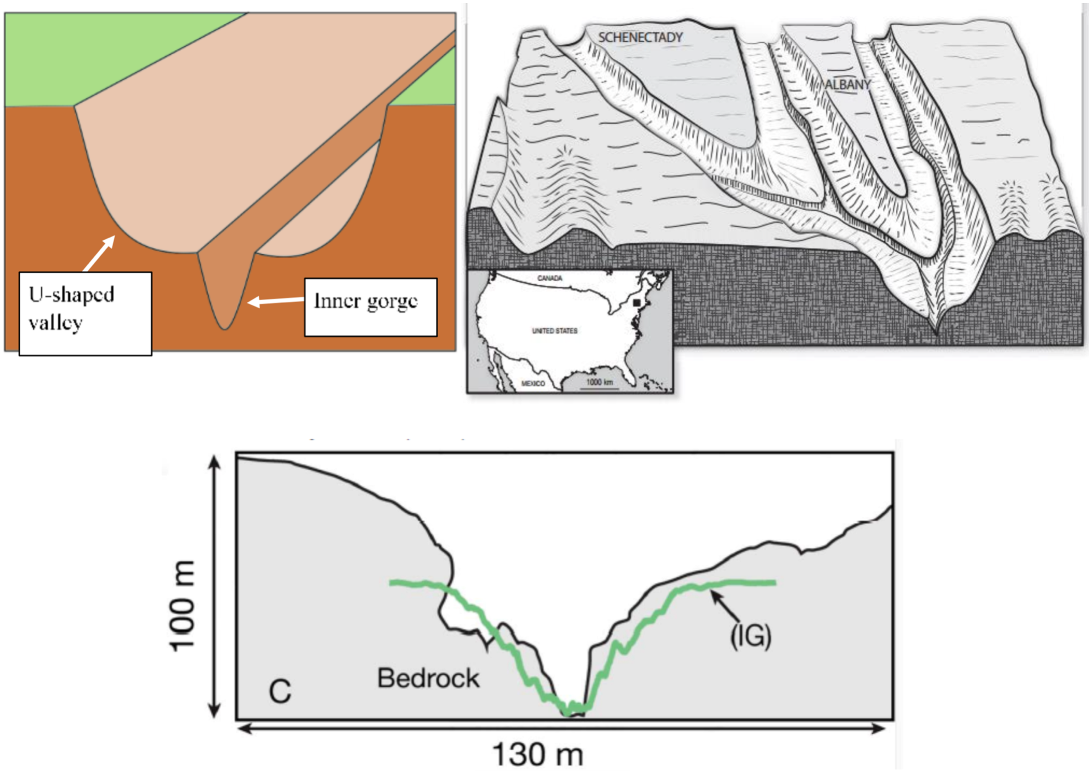

Figure 2.6: Upper Left: schematic diagram showing inner gorge morphology. Upper Right: morphology of an inner gorge located in the northeast of the United states (Lajeunesse, 2014). Below: Cross-profile of a bedrock channel (IG) modelled using a subglacial fluvial erosion model, with the cross-profile of an inner gorge feature for comparison (Beaud et al., 2018b).

Inner gorges, sometimes called slot gorges or slot canyons (Korup and Schlunegger, 2007), are found at the base of some glacial valleys and are presumed to have some connection to glacial melt (Fig.2.7). Inner gorges are often distinctive because they demonstrate a valley-within-valley morphology (Fig.2.6). Formation in both subglacial and subaerial contexts has been proposed (Jansen et al., 2014), with leading formation theories being (1) subglacial meltwater erosion during periods of high surface melting (Jansen et al., 2014; Beaud et al., 2018b); (2) pre-glacial river incision due to base-level fall or shift in sediment supply (Lajeunesse, 2014); (3) interglacial fluvial incision, possibly over multiple interglacials, with gorges filled with sediment that preserves them during glacial advances but is flushed out by subaerial fluvial erosion after glacial retreat (Montgomery and Korup, 2011); and (4) a combination of both glacial and interglacial incision (Dürst Stucki et al., 2012). Modelled erosion by water in subglacial channels produces bedrock incision features that are similar in shape and scale to inner gorges (Beaud et al., 2018b).

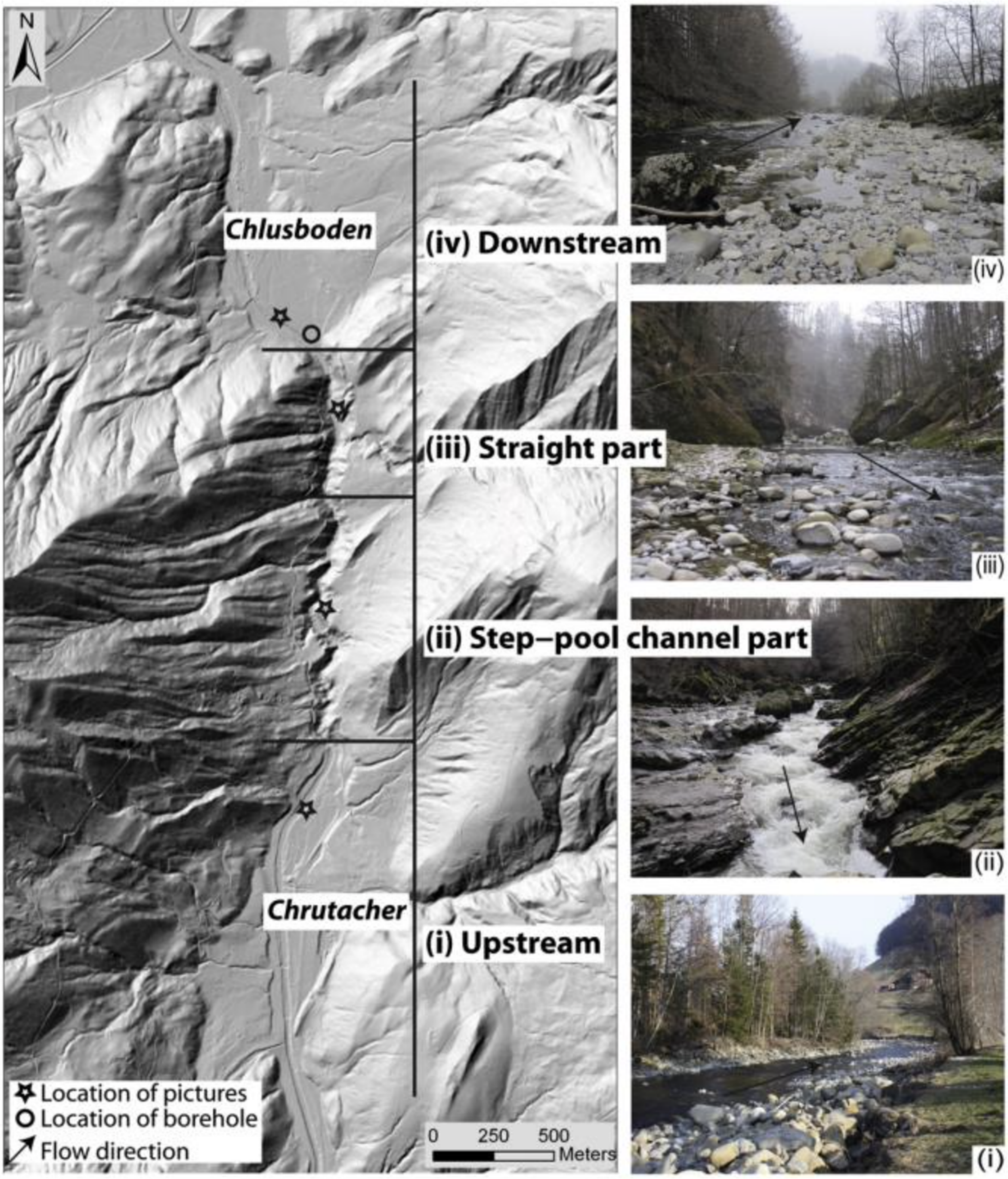

Figure 2.7: Photographs (right) illustrating morphology of an inner gorge (left, shown using a hillshaded-DEM) near Bern, Switzerland. Gorge incision here is inferred to have been subglacial. Figure: Dürst Stucki et al. (2012).

2.2.3 *Tunnel valleys*

Tunnel valleys range from <20 to 150 km in length, are up to 5 km wide and 500 m deep (Praeg, 2003; Stackebrandt, 2009; Stumm, 2010; Livingstone and Clark, 2016) (Table.1.1, Fig.2.8). They are found across a wide range of previously glaciated landscapes, including Europe (e.g. Smed, 1998; Piotrowski et al., 1999; Huuse and Lykke-Andersen, 2000; Jørgensen and Sandersen, 2006; Kristensen et al., 2007; Stewart et al., 2013), North America (e.g. Mullins and Hinchey, 1989; Atkinson et al., 2013; Livingstone and Clark, 2016), Antarctica (e.g. Wellner et al., 2006; Rose et al., 2014) and Greenland (Livingstone et al., 2017). Most of the tunnel valleys described in literature are incised into sediment and not bedrock, though many bedrock examples have been reported (Mullins and Hinchey, 1989; Brennand and Shaw, 1994; Regis et al., 2003; Denton and Sugden, 2005)(see both Stumm (2010) and Kehew et al. (2012) for comprehensive reviews). Numerous tunnel valleys may occur beneath a single ice lobe, arranged in a 'bird's foot' pattern that conforms to the likely former subglacial drainage pattern (e.g. van der Vegt et al., 2012).

The formation of tunnel valleys has been extensively discussed, but formation mechanisms are controversial and many questions about the timing (i.e. glacial period, stage of (de)glaciation) and rate of formation (e.g. Stumm, 2010) also remain. The three main hypotheses of tunnel valley formation are (1) sapping of deformable (or fluidised) subglacial sediment or weak bedrock (Boulton and Hindmarsh, 1987; Mullins and Hinchey, 1989; Clayton et al., 1999; Boulton et al., 2009), (2) time-transgressive formation close to the ice margin, extending headwards during ice retreat (Huuse and Lykke-Andersen, 2000; Kristensen et al., 2008), and (3) catastrophic flood events arising from the release of stored water (Shaw et al., 1989; Huuse and Lykke-Andersen, 2000; Jørgensen and Sandersen, 2006).

2.2.3.1 *Sapping of deformable subglacial sediment or weak bedrock*

This mechanism envisages tunnel valleys to be the product of a steady-state 'sapping' process (process of subglacial channel and bank failures) within the underlying sedimentary/fractured bedrock materials, and to form gradually in response to prolonged, low-magnitude groundwater flows within arterial, subglacial drainage pathways (e.g. Boulton et al., 2009). These pathways develop due to "piping" at the ice sheet margins (Fig.2.9) in response to high hydraulic gradients and increased subglacial water discharge in these locations. Piping involves the establishment of numerous small and inefficient (and hence high-pressure) channels within sediment or weak bedrock at the ice-bed interface. Piping then permits the subglacial hydrological network to develop into a network of larger, more efficient (and hence low pressure) R- or N-channels, which promotes further flow of groundwater through the substrate (and possibly wholescale flow of fluidised substrate/sediment) towards the trunk channel system.

The formation of tunnel valleys by sapping of deformable sediments or bedrock was first proposed by Boulton and Hindmarsh (1987) (Fig.2.9). The flow of fluidised sediments towards channels as a means of forming large valleys in sediment has also been advocated by Clayton et al. (1999), and the sapping of weakly lithified bedrock

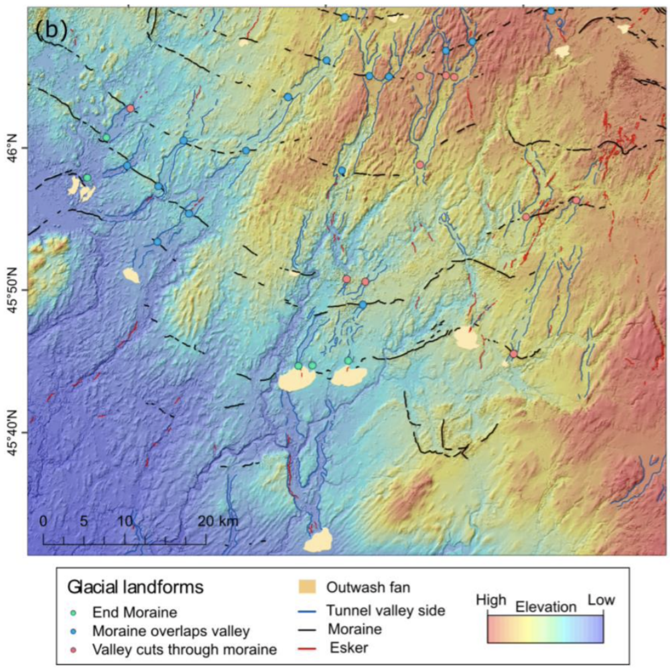

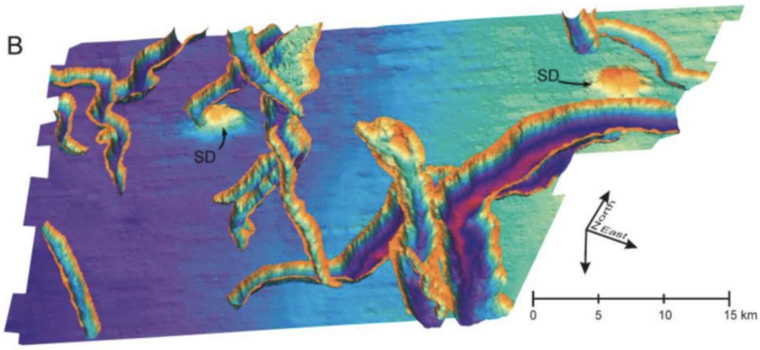

Figure 2.8: Above: Plan view of tunnel valleys incised into ice-moulded Quaternary deposits of Wisconsin near the southern limit of the former Laurentide Ice Sheet. Image: Livingstone and Clark (2016). Below: 3D perspective view of sediment-incised tunnel valleys in the North Sea (SD = salt diapir). Figure: Kristensen et al. (2007).

to form tunnel valleys dating from the Ordivician has been invoked by Ravier et al. (2014). Some authors doubt the ability of sediment to deform towards channels at a rate sufficient to permit the formation of large valleys in the substrate (e.g. Ó Cofaigh, 1996), but observations at alpine glaciers (e.g. Hubbard et al., 1995; Swift et al., 2005) indicate that diurnally varying water pressures within channels, which lead to a diurnally reversing hydraulic gradient between channels and the adjacent distributed system, may encourage sediment deformation towards channels as discharges and pressures within channels decline following the diurnal peak. Alternatively, the same mechanism, by means of sweeping sediment from large areas of bed adjacent to major subglacial drainage axes (or 'meltwater corridors') (Sjogren et al., 2002; Peterson and Johnson, 2018), could facilitate direct glacial erosion of bedrock in those areas and therefore result in linear glacial bedrock incisions guided by subglacial hydrology.

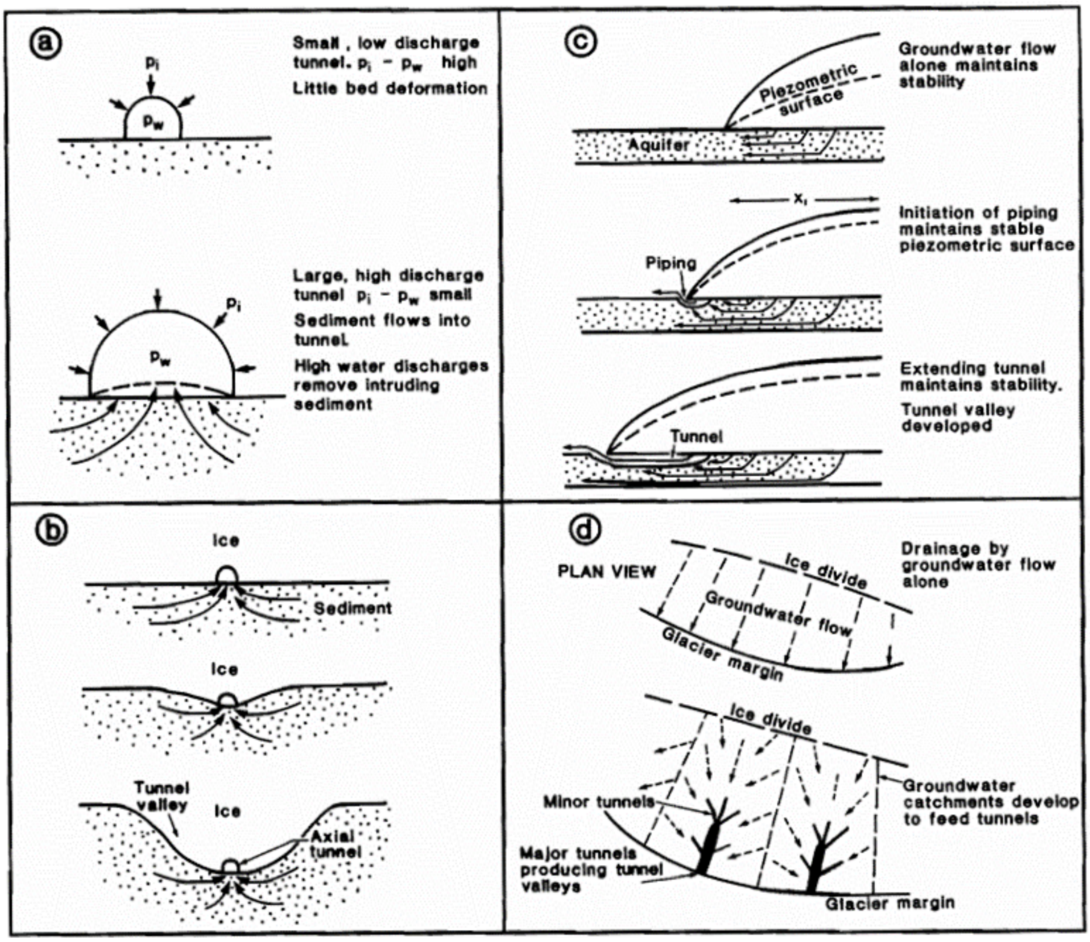

Figure 2.9: Development of tunnel valleys in soft sediment beds through piping (Boulton and Hindmarsh, 1987).

Kehew et al. (2013) observed that tunnel valley morphology beneath the former Saginaw Lobe of the Laurentide Ice Sheet was composite, with uppervalley sections (i.e. those 'proximal' to tunnel valley heads) exhibiting regular spacing and smaller depths characteristic of lower energy flows, and therefore potentially consistent with a mechanism reflecting steady-state subglacial drainage. It is notable that tunnel valleys appear to be unusual on impermeable, crystalline bedrock (Stumm, 2010), where sapping would be less effective than in weaker, porous sedimentary rocks. In these locations, eskers are typically found, and these are sometimes considered the 'counterpart' of tunnel valleys in areas where ice covered hard bedrock (Clark and Walder, 1994; Boulton et al., 2009).

2.2.3.2 *Time-transgressive formation close to the ice margin during ice retreat*

Time transgressive tunnel valley formation through meltwater erosion close to the margin during glacial retreat was first put forward by Moores (1989). Several subsequent studies have also invoked formation by repeated incision events of varying magnitude over time (Cutler et al., 2002; Jørgensen and Sandersen, 2006; Kehew et al., 2013). Moores (1989) and Kehew et al. (2013) have both proposed that tunnel valleys are formed by abundant supraglacial melt water produced during deglaciation, which is transported to the ice bed interface through moulins. The meltwater passages created by these flows extended headward beneath the ice through the linking of new moulins and crevasses (cf. Nienow et al., 1998) as the ice retreats and climate warms, eventually resulting in the formation of large-scale tunnel valley features.

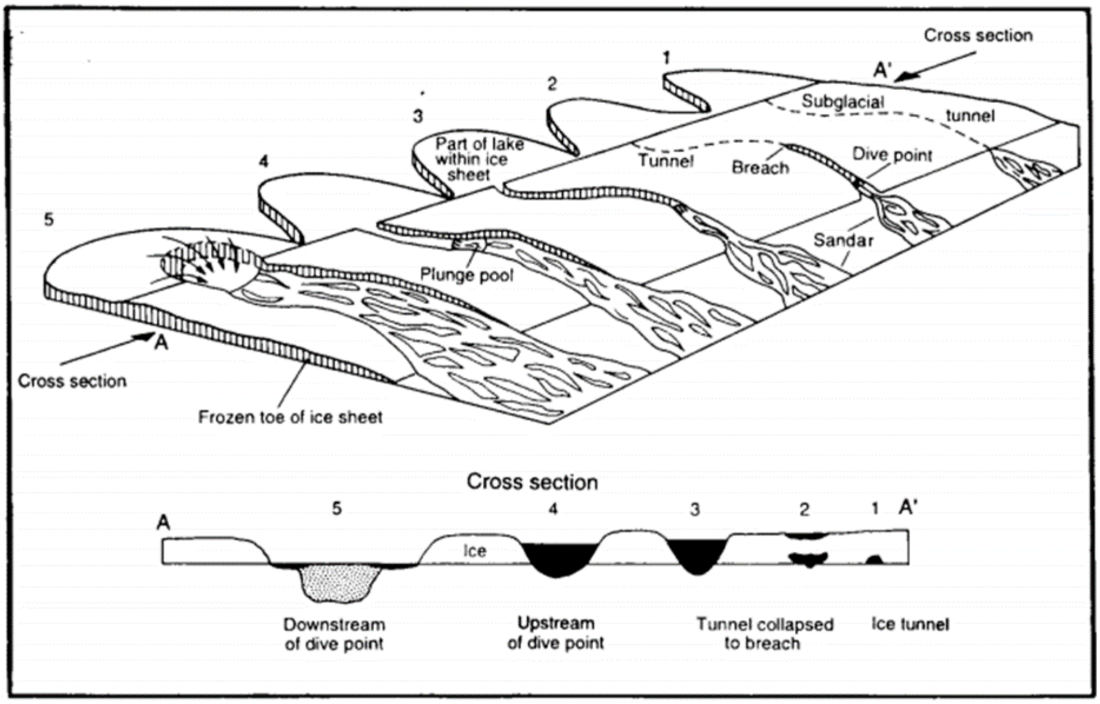

Figure 2.10: Cartoon showing stages in the development of tunnel valleys as envisaged by Wingfield (1990). Figure: Wingfield (1990) in Ó Cofaigh (1996). The tunnel valley initiates from an ice tunnel (R-channel) formed at the ice margin (1), which then collapses (2), causing progressive headward incision into the ice and substrate (3 to 5).

Kehew et al. (2013) invoked this explanation for the distal (from tunnel valley heads) valley morphology of the composite system beneath the Saginaw Lobe, which exhibits irregular spacing, deep incision, and infill comprising coarse gravels. Further, bedrock incised tunnel valleys in Denmark mapped by Jørgensen and Sandersen (2009) exhibit dendritic networks and examples of valley bifurcation (notably, near the ice margin) that may indicate formation over a prolonged period, from multiple water sources, during which there were changes in hydraulic gradient resulting from changes in ice-surface or ice-margin geometry. Time transgressive erosion is a theory particularly associated with the formation of sediment-incised tunnel valleys in the North Sea (Kristensen et al., 2008), where clinoforms at the downstream end appear to suggest incremental sediment redeposition on the adverse slope beneath the ice margin, possibly as a result of glaciohydraulic supercooling (Alley et al., 1998; Werder, 2016). Sediment deposition at the ice margin due to changes in flow velocity, either subglacially due to glaciohydraulic supercooling, or proglacially due to water exiting from an ice-roofed channel, may explain bifurcations in tunnel valleys leading up to the ice margin, because sedimentation will locally steepen the adverse gradient and, where ice-bed topography allows, encouraging water to divert laterally to follow lower adverse gradients.

A particular type of time transgressive formation that is related to catastrophic drainage was proposed by Wingfield (1990). In this theory (Fig.2.10), tunnel valleys are formed by jökulhlaups from subglacial lakes that first form ice tunnels (i.e. R-channels) that then collapse, resulting in water being required to incise into the sediment substrate below. The initiation of flow causes hydrostatic lift and erosion of an R-channel by means of frictional melting; the 'over-enlarged' tunnel then collapses, causing water to incise into sediment, and forming a waterfall at a 'breach head' at the upper end of the collapsed section. This style of evolution proceeds along the route of the tunnel until the collapse reaches the source of the jökulhlaup (Fig.2.10). Ó Cofaigh (1996) is highly critical of this theory due to the lack of field evidence for large-scale marginal outwash fans, hyper concentrated flow deposits indicative of jökulhlaups events, highly braided network patterns within the channels, and down-flow proximal to distal fining of sediments in the channels.

2.2.3.3 *Catastrophic flooding events*

Catastrophic flood hypotheses have generally developed to explain tunnel valleys incised into bedrock, where the rates of erosion required to form them are considered unlikely under steady state R-channel flow (e.g. Boyd et al., 1988; Kehew et al., 2012; Kehew et al., 2013; Stumm, 2010) (although see recent modelling work by Beaud et al. (2018b) and papers indicating formation of bedrock tunnel valleys over multiple glaciations, e.g. Lowe and Anderson (2003)). For example, the Labyrinth tunnel-channel system in the Dry Valleys is presumed to reflect a series of repeated outburst events, in part because it is bedrock-incised and in part due to its highly anastomosing network characteristics (Sugden et al., 1991). Further, Kehew et al. (2013) proposed that the formation of 'proximal' sections of valleys beneath the Saginaw Lobe may have been aided by moderate and repeated or even large releases of stored water on account of their incision into soft but low-permeability bedrock that was considered unlikely to permit 'sapping'.

The general premise of the catastrophic flood hypothesis is that subglacial lakes, potentially trapped behind a frozen permafrost wedge or in a basin with a steep adverse slope, catastrophically drain resulting in the formation of individual tunnel valleys or entire tunnel valleys networks during one or several large erosional events (Wright, 1973; Nye and Frank, 1973; Ehlers and Linke, 1989; Brennand and Shaw, 1994; Beaney, 2002). The breaches in the subglacial lakes are then closed through ice creep and till deformation, or the water pressure dropping and stopping flow up the adverse slope. Hooke and Jennings (2006) linked catastrophic drainage to tapping of stored water by piping (see 2.2.2.1) development through regions of the ice margin of the southern Laurentide Ice Sheet that were underlain by permafrost. The theory implies that the rate of incision and development of the resulting tunnel valleys would increase as the features (initially narrow R-channels) developed until the point of catastrophic outburst. After the outburst and formation of the tunnel valley, Hooke and Jennings (2006) propose that the valleys would then be filled with ice and sediment, until the next outburst flood. A similar formation mechanism that culminates in an outburst flood was put forward by Cutler et al. (2002) for three tunnel valleys in Wisconsin. Cutler et al. (2002) concluded that one of two scenarios must have occurred to allow for the deposition of 2 m-diameter boulders seen in the sedimentary fans associated with the channels. The first scenario, described as the "early" scenario, is one in which the tunnel valley was initiated by an outburst flood through a permafrost wedge, with the tunnel valley later being occupied by ablation-derived melt flows. The second and preferred scenario, described as the "late" scenario, is one where channels were initiated by normal meltwater erosion of ice and sediment that enlarges a pathway through a permafrost "seal" at the ice margin, culminating in an outburst flood that rapidly drains a subglacially impounded water source.

The association of tunnel valleys with catastrophic floods has also been implied by proponents of the controversial mega-flood hypothesis of drumlin formation (e.g. Kor et al., 1991; Brennand and Shaw, 1994). This theory of tunnel valley formation is considered by Ó Cofaigh (1996) and Clarke et al. (2005) as being controversial, due to two main problems: first, that the theory does not account for the volume of meltwater needed to be produced to form all the drumlin fields that are used as evidence for the large scale flooding; and second, that the theory ignores evidence for tunnel valley incision under less catastrophic conditions (see above).

2.3 OUTSTANDING QUESTIONS AND SUMMARY

The work presented in this thesis aims to address the question related to the variations in morphology of CGBL feature present in foreland-like settings. The preceding review indicates several areas of uncertainty regarding understanding of the formation and morphology of CGBLs that present areas of opportunity for future work:

- There is limited bedrock topography data available for detailed analysis of CGBL morphologies, and available data has limited quality and resolution. The morphological analyses undertaken on the available data by previous studies has also been of varying quality and consistency, leaving significant room for more sophisticated analyses (e.g. of transverse and long-profile form). Data availability for bedrock tunnel valley morphology is particularly sparse, and there are few analyses of tunnel valley morphology, especially those incised into bedrock.

- Bedrock-incised tunnel valleys are not uncommon, and are typically assumed in published literature to be associated with catastrophic rather than steady formation mechanisms, but insufficient morphological analysis has been undertaken to confirm such assumptions.

- It is uncertain whether the presumed morphological distinctions between subglacial fluvial and glacial forms really hold true, and what this might mean for identification of glaciofluvial- origin CGBLs. For example, are glacial valleys, including overdeepened sections, consistently U-shaped, and are glaciofluvial CGBLs consistently V-shaped or trapezoidal? Further, do different formation mechanisms for glaciofluvial CGBLs (catastrophic, fluctuating, and steady) indicate differences in morphology that may be helpful for constraining their origin?

- Bifurcation of tunnel valleys near the ice margin has been observed in bedrock-incised valleys, but the reasons for this behaviour have not been scientifically explored. The phenomenon may be related to sediment deposition beneath or in front of the ice margin due to changes in water flow velocity associated with glaciohydraulic supercooling or subglacial-to-subaerial flow transition.

- Evidence for direct glacial erosion of tunnel valleys is unconvincing (e.g. Stumm, 2010), yet some degree of interaction of glacial and subglacial fluvial erosion processes is extremely likely. For example, potential flushing of sediment from wide areas of glacier beds by diurnally reversing hydraulic gradients (e.g. Hubbard et al., 1995) is likely to result in enhanced bedrock erosion by glacial processes along subglacial drainage axes (or 'meltwater corridors'). This could lead to zones of glacial erosion migrating if water is diverted, for example, by sedimentation near to or in front of the ice margin.

- It is still uncertain as to how CGBL morphology is influenced by geology. Notably, evidence of significant changes in glacial U-shape valley characteristics driven by geology could indicate that geology will be a significant obstacle to discriminating glacial from glaciofluvial CGBLs.

- Controls on CGBL depth remain uncertain, with supercooling- and flotation-related thresholds being likely key for glacial CGBLs, and some evidence for supercooling-thresholds being important for sediment-incised tunnel valleys (e.g. Kristensen et al., 2008). However, the importance of the supercooling threshold and its theoretical basis remains uncertain (e.g. Stumm, 2010; Cook and Swift, 2012). Further, such thresholds are dictated largely by ice surface slope, which for paleo-features can be difficult to reconstruct, meaning relationships between incision depth and other crucial factors, such as ice thickness, remain enigmatic. Nonetheless, statistical evidence of deepest overdeepenings occurring in narrower valleys in high topography (Patton et al., 2016b), indicates that lateral drag may be important for developing thick ice able to incise very deeply (see also Haeberli et al. (2016)), with form drag possibly also playing a crucial role as an adverse slope develops behind a bedrock threshold. This further implicates lithology, because harder lithologies appear to result in incision of narrower glacial valleys (Augustinus, 1992; Swift et al., 2008).

- It is clear that numerical models have the potential to provide quantitative insight into complex morphological questions. Although presently in a state of rapid development and with complex erosional, depositional and transport processes not yet fully incorporated, current models are nevertheless still able to provide important insight into subglacial erosional processes (e.g. Beaud et al., 2014; Beaud et al., 2018b; Beaud et al., 2018a). By challenging even simple models to reproduce the morphological characteristics of known landforms we can begin to investigate underlying controls (e.g. geology, hydrology and climate). As new numerical models and tools are developed this capability will only increase.

- Model simulations are also capable of exploring the timescale required for processes to produce particular forms, and therefore offer great potential to assist morphological studies that aim to discriminate the many of mechanisms of CGBL formation. However, certain processes are not well represented in models, due to computational or observational constraints (i.e. lack of data). For example, in the glaciofluvial erosion model of Beaud et al. (2014) and Beaud et al. (2018b), water and sediment transport is simulated in only one dimension (along a longitudinal ice-flow profile), whereas drainage morphology and sediment and water sources within such systems vary in four dimensions (three physical dimensions, plus time).

Part II

DATA AND PROCESSING

3. GLOBAL CGBL DATA SYNTHESIS AND SITE SELECTION

3.1 INTRODUCTION

To achieve the thesis aims of understanding the morphology, distribution and erosional processes involved in CGBLs, we must first understand the current knowledge on the distribution and data coverage of CGBL features. To this end, the first step in this project is to produce a global synthesis of existing data and morphological properties of CGBLs in foreland or foreland-like settings. The synthesis has been undertaken on a global scale to increase the likelihood of capturing the most suitable analogue of the CGBL features present in northern Switzerland, while still capturing the maximum number of potential features.

The following chapter has two main foci. The first is a very brief introduction to the features present in the Northern Swiss Foreland (NSF) and their regional context. Northern Switzerland has high data availability, with access to data facilitated by Nagra. The second is a review of sites globally that were considered to have potential as analogues for the Swiss features. The latter section reviews how each of the features have been interpreted within published literature; their topographical, geological and climatic similarities to northern Switzerland; and the level of data availability and its quality. The review only covers potential analogue sites that had at least some open source published data available. The results of this chapter, and those of chapters 1 and 2 have been compiled as two reports internally published within Nagra (Gilgannon et al., 2019; Gilgannon et al., 2020).

3.2 NORTHERN SWITZERLAND

Northern Switzerland contains a large number of sediment-filled and part-filled CGBLs that all have an orientation roughly perpendicular to the approximate ENE-WSW orientation of the Alpine mountain front and many reach as far as the Jura Mountains (Fig.3.1). The geology of the region can be subdivided into three main units: Molasse conglomerate; limestone Malmkalk; and the Opalinus clay (Fig.3.2 and 3.3). The three main geological units are inclined and dip in a south-easterly direction towards the Alpine mountains (their source; Fig.3.2 and 3.3). The CGBLs of the NSF vary greatly in length, depth (to bedrock), and width, with the largest features reaching lengths up to approximately 166 km, and widths of up to 12.1 km, and depths to bedrock of up to 847 m, respectively (Table.3.1). Figure 3.1 also shows the five possible siting regions for the geological repository under consideration by Nagra as of 2017. The siting areas are not of direct relevance to this thesis – which focuses on establishing formation processes for CGBLs in general – and are given only for reference.

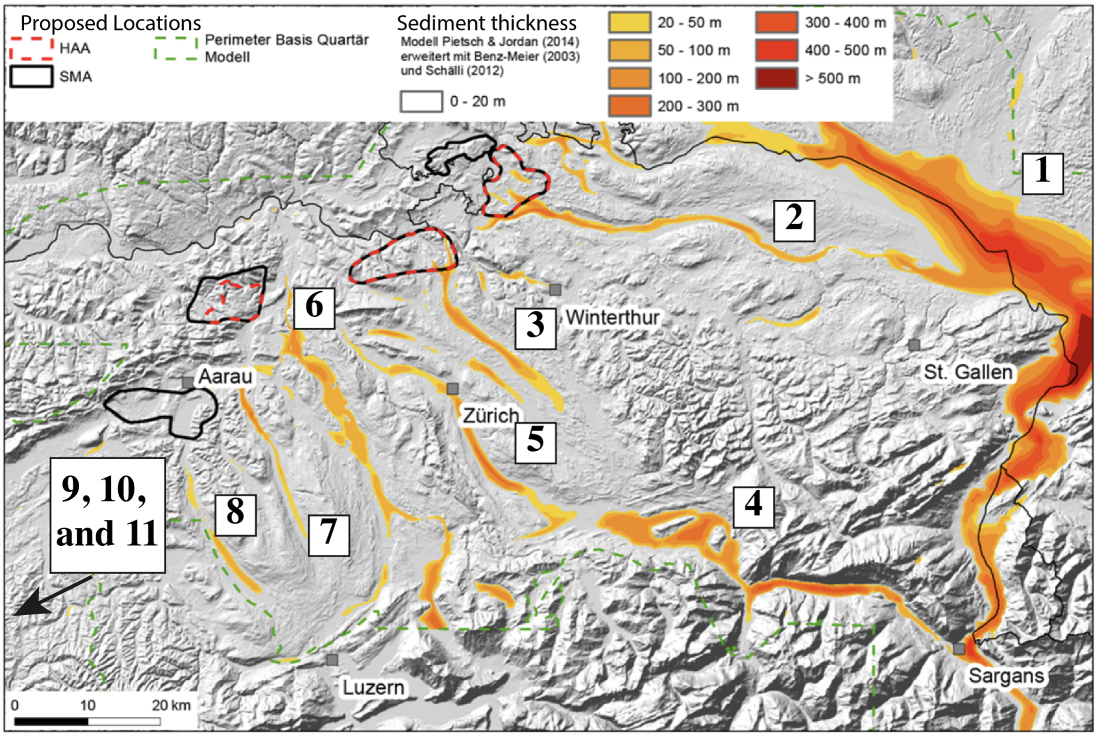

Figure 3.1: CGBLs located in the NSF near Zurich and the 5 potential nuclear storage facility sites. Figure from Fischer et al. (2017).

Table 3.1: NSF metrics for main features. See Figure 3.1 for locations.

Feature	Depth[1] (m)	Width[2] (km)	Length (km)	Elongation ratio[3]	Area (km^2)
1	671	1523	166	109	1043
2	319	-	71	-	-
3	260	1356	33	24	49
4	378	955	58	60	124
5	328	1039	45	43	67
6	270	983	39	39	65
7	330	1719	27	16	41
8	159	2828	23	8	22
9	844	3207	71	22	158
10	463	1782	119	67	486
11	847	6621	100	15	625

[1] = To bedrock at deepest point
[2] = Average
[3] = Length/Width

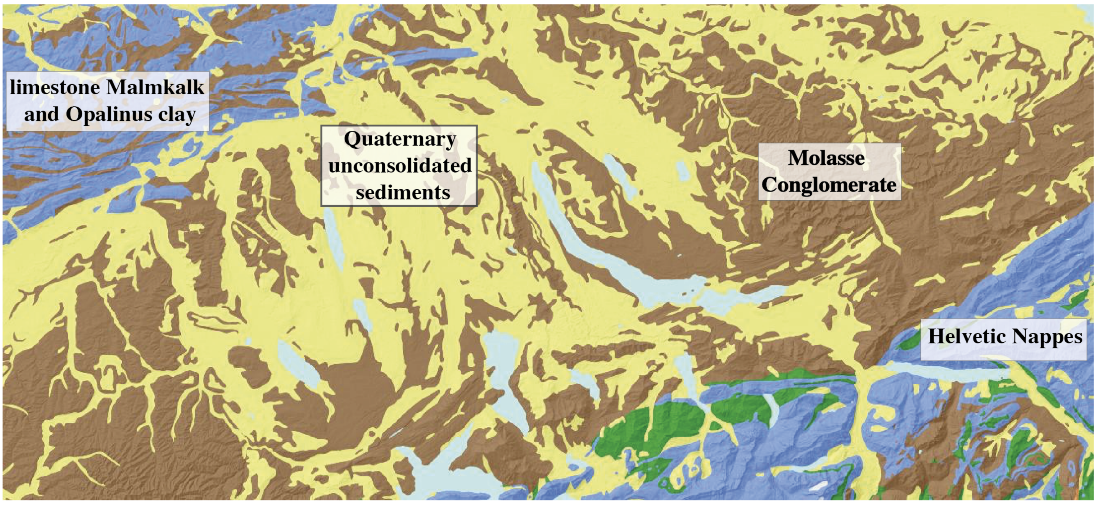

Figure 3.2: Geological map of area covered by Figure 3.1. Map from the Swiss Geological Survey. Section of geological map from https://map.geo.admin.ch on 01/06/18. Yellow unit: Quaternary unconsolidated sediments; brown unit: Molasse conglomerate (Clastic sedimentary rocks); northern blue unit: limestone Malmkalk and Opalinus clay (Biogenic sedimentary and evaporites and clastic sedimentary rocks). Southern blue units containing the Helvetic Nappes (Biogenic sedimentary and evaporites and clastic sedimentary rocks).

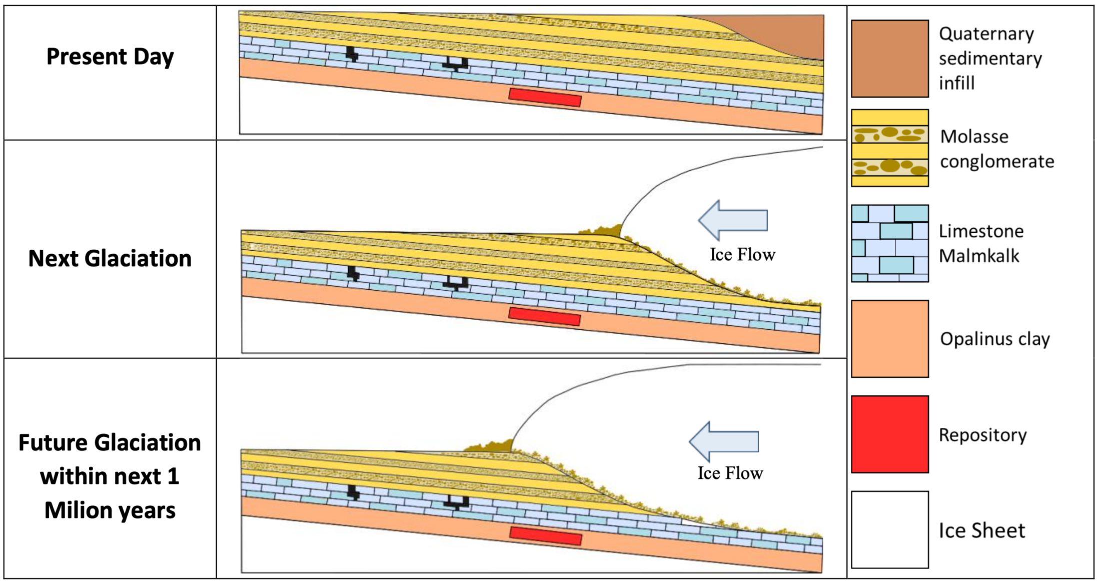

Figure 3.3: Schematic cross section of geological setting of potential repositories and the potential effect of future glaciations. Figure adapted from Fischer et al. (2017).

3.3 ANALOGUE SITES

This section presents an overview of sites that may constitute analogues for the northern Switzerland region in terms of past environment and process. Sites were initially selected on the basis of presence of CGBLs with some morphological similarity to the northern Switzerland features, and a full list of considered sites is presented in Table.A.1 in the Appendix. Sites were then prioritised according to the level of data availability required for full morphological analysis, including availability of data on depth to bedrock. Only the latter sites are covered here (below); sites with little analogue potential or little available data have been excluded.

The areas that passed the minimum threshold of data availability were: several regions of the United States, including the Finger Lakes region of New York State, and Glacier National Park; British Columbia (Canada); The Southern Alps (New Zealand); Greenland, focusing on features beneath the Humboldt Glacier; Peru and Antarctica (Fig.3.4). For each area, the general characteristics of the CGBLs and their context are described, focusing on CGBLs of specific interest in terms of data availability or published morphology. Where possible an assessment of the analogue potential of the area or region is presented, with the site potential ranked by means of comparison with key characteristics with those of CGBLs in northern Switzerland. The key characteristics in question are general morphological characteristics, geological and topographic setting, and past climatic settings during past glaciation.

Figure 3.4: Map showing geographical locations of potential areas of interest for the analogue study of the NSF-style CGBLs

3.3.1 *The United States of America*

3.3.1.1 *Finger Lakes*

Introduction

The large glacial erosional features present in the Finger Lakes region, New York State, USA, have several strong similarities with the NSF CGBLs. The main similarities of the region with that of the NSF are the first-order morphologies and spatial distribution of the 11 large glacially eroded basins now occupied by lakes in the region (Fig.3.6 and 3.7), which have been extensively studied by Mullins and Hinchey (1989) and Mullins et al. (1996). In addition, similarities include the lithologies and geological structures present (Rickard and Fisher, 1970a), and the dry climatic conditions that prevailed during past glaciations (Anderson et al., 1997).

The region is located beneath the former southern margin of the Laurentide Ice Sheet (LIS) from 27-30 ^{14}C ka before Present (BP) until approximately 14 ^{14}C ka BP (Fig.3.5)(Margold et al., 2015). The ice flow from the LIS and the Oneida Lobe which covered the region had a southerly flow direction, reaching its maximum extent at the Valley Heads moraine, approximately 12.95-14.1 ^{14}C ka BP. Mullins et al. (1996) proposed a link between the sedimentary infilling of the Finger Lakes and the timing of Heinrich event H-1 (Mullins et al., 1996; Broecker et al., 1992), which was a consequence of surging of the eastern margin of the Laurentide Ice Sheet during its retreat from its last glacial maximum (LGM) (Mullins et al., 1996; Broecker et al., 1992).

The climate of the region of the Finger Lakes and the rest of the northeast of North America has been reconstructed using pollen analogues by Prentice et al. (1991) for the time period between 18 ka BP and time of publication. Their findings suggest that the region would have experienced a very cold and dry climate at approximately 18 ka BP, which would have warmed quite rapidly during deglaciation. By approximately 9 ka BP, the climate had changed, experiencing a greater annual temperature range than experienced today.

Margold et al. (2015) and Mickelson and Colgan (2003) both proposed large discharges of subglacial water in this region under the LIS: Margold et al. (2015) on the basis of field evidence of large ice streams that fed adjacent ice lobes (Huron-Erie Lobes) and which required large volumes of subglacial meltwater to occur in areas of otherwise unfavourable geology and topography; and Mickelson and Colgan (2003) based on the presence of drumlins and inter-drumlin channels to the north of the Finger Lakes. Brennand and Shaw (1994) propose that these channels were formed during the waning flows of a thick flood-related water layer, as the bed of the ice sheet settled back on the underlying sediment/bedrock bed.

The regional bedrock and sedimentary geology (Fig.3.7) show similarities to that of the NSF, specifically relating to the orientation of the different units to the direction of past ice flow, and the orientation of the CGBLs (Yager et al., 2001; Rickard and Fisher,

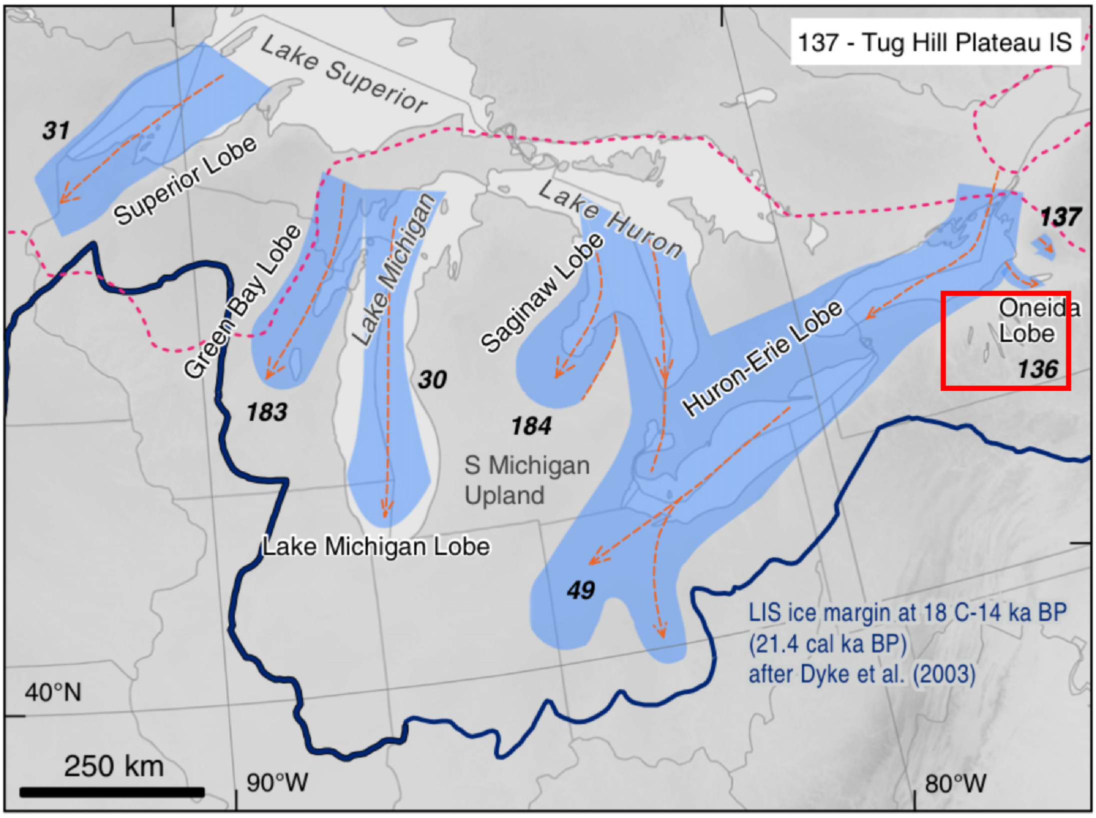

Figure 3.5: Map of maximum spatial extent of the Laurentide Ice Sheet and names of each lobe and their flow direction in the region of the great lakes. Red box marks the location of the CGBLs studied by Mullins et al. (1996). Figure from Margold et al. (2015).

1970a; Cadwell and Muller, 1986). However, the main difference between the NSF and the Finger Lakes region is the direction of ice flow with respect to topography and bedding (NSF: south to north, Finger Lakes north to south, while both bedrock units dip broadly south). Figures 3.7 and 3.8 show how the geological units are perpendicular to the longitudinal CGBL axis and the past ice flow direction. The schematic cross sections show how, in the NSF, the geological units dip in the opposite direction to ice flow (Fig.3.8) when compared to the dip of the geological units of the Finger Lakes region, which dip in the direction of ice flow (Fig.3.8).

Topographic setting

The local topography is generally low lying up-ice to the north of the Finger Lakes (~216-110 m a.s.l.) (USGS, 2018), with drumlin fields found between the lakes and the shore of Lake Ontario ~41 km to the north. However, the Finger Lakes themselves are situated in valleys confined by higher topography. Each of these valleys and adjacent ridge lines of higher topography run in a general north- south orientation, with the ridges reaching maximum heights of just under 500 m a.s.l. in the south of the region. In other words, the northern region where the lakes 'begin' has typically lower maximum elevations, and the region to the south (where the lakes are located) quickly grades into high ground associated with the Appalachian Mountains.

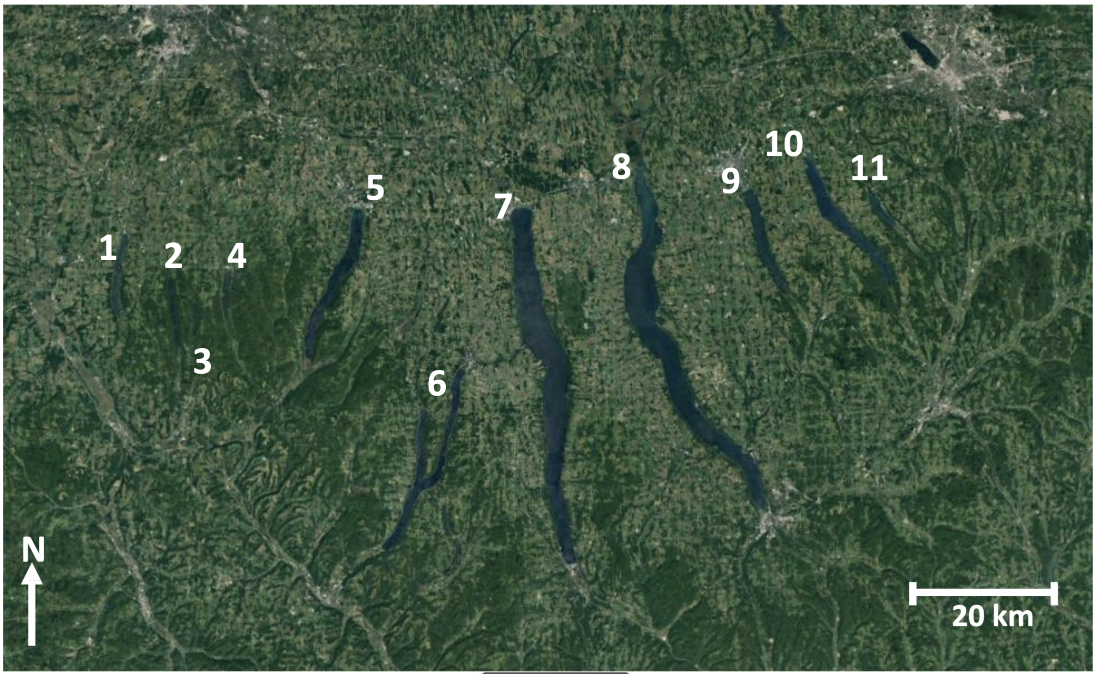

Figure 3.6: Location map of the 11 Finger Lakes. 1) Lake Conesus; 2) Lake Hemlock; 3) Lake Canadice; 4) Lake Honeoye; 5) Lake Canandaigua; 6) Lake Keuka; 7) Lake Seneca; 8) Lake Cayuga; 9) Lake Owasco; 10) Lake Skaneateles; 11) Lake Otisco. This figure was recreated from Mullins et al. (1996). Satellite imagery: Google Earth.

The topography of the surrounding areas of the Finger Lakes is dominated by the large basin of Lake Ontario to the north, which runs east to west (maximum depth to bedrock >220 m to the south east). The areas to the northeast, east, and south of the Finger Lakes are dominated by the mountains of the Adirondacks, which covers an area of over 25,500 km^2 and reaches a maximum height of just over 1,630 m a.s.l., and the Appalachian Mountains which reach maximum heights of over 800 m a.s.l. in the regions south of the Finger Lakes.

The topography of the Finger Lakes is therefore notably different from that of the NSF, as the flow of ice was from the low-ground into the more topographically confined regions, while the NSF flowed into the less confined foreland. In contrast to northern Switzerland, where the ice cap grew from the topographic highs into the low-relief foreland, the LIS margin thinned against the Appalachian Mountains. These topographic differences are also evident in that the Finger Lakes region was covered by an ice lobe fed from an ice sheet, in contrast to the NSF which was covered by several piedmont style lobes of an ice cap.

Bedrock Geology

The bedrock of the Finger Lakes is made up of shales, siltstones, limestones, dolostones, and sandstones (Fig.3.7)(Rickard and Fisher, 1970a). All the units show bedding dipping in a southerly direction, with a strike in an east-west direction, and therefore perpendicular to the direction of LGM ice flow (Yager et al., 2001). As noted above, the direction of dip in relation to ice flow is the opposite to that seen in the

NSF. Figure 3.8 shows a schematic averaged geological cross-section highlighting the location of the CGBLs in relation to the underlying lithologies. It is important to note that the CGBLs of the Finger Lakes region have not been reported to, or appear to start and end uniformly in any specific geological unit (See Appendix Fig.A.1).

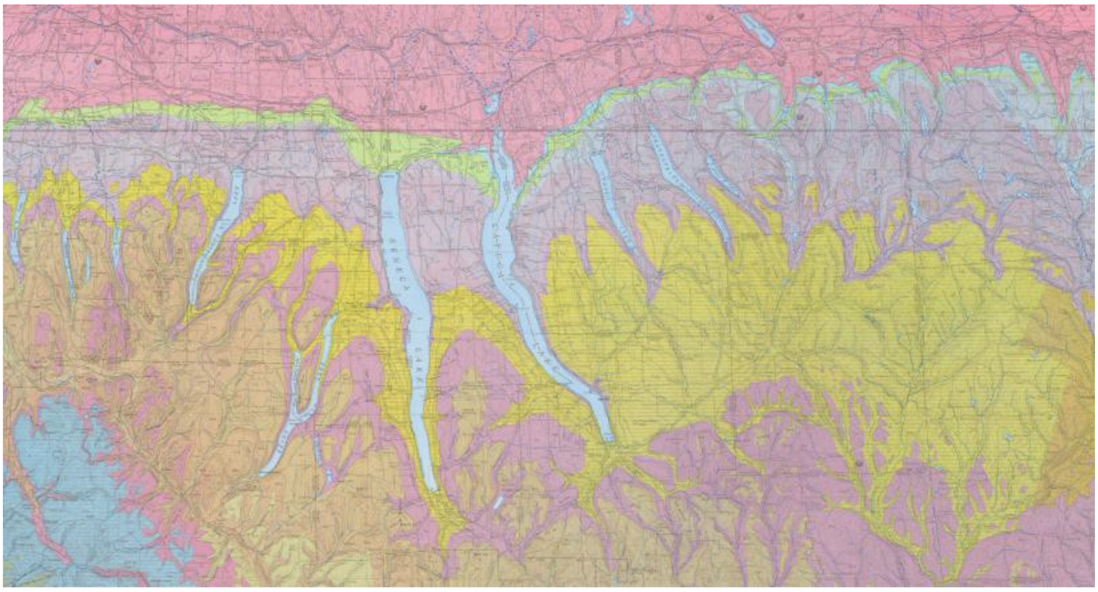

Figure 3.7: Bedrock geological map of the region of the Finger Lakes. Map sections sourced from Rickard and Fisher (1970a). See full map in Appendix A for descriptions of each geological unit and location of geological cross-section.

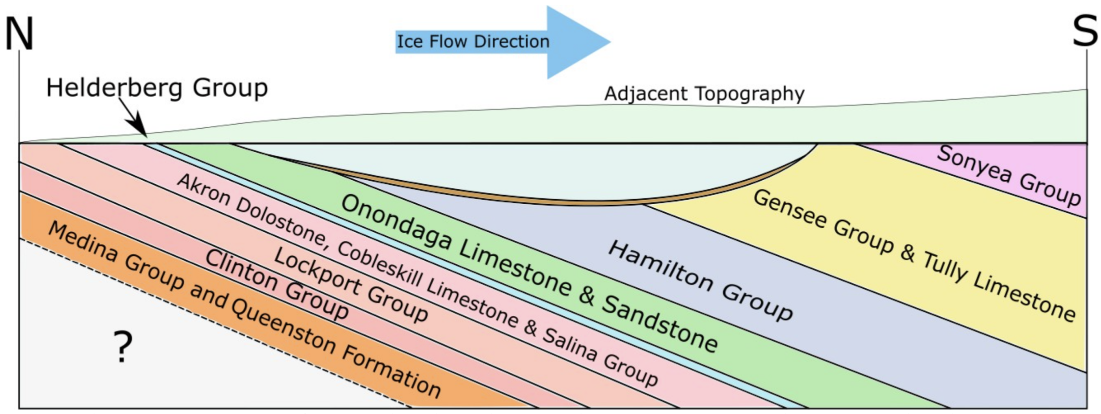

Figure 3.8: Schematic cross-section of averaged geological units and structures present under Seneca Lake. The units shown in the cross-section are, Medina Group and Queenston Formation; Clinton Group; Lockport Group; Akron Dolostone, Cobleskill Limestone and Salina Group; Onondaga Limestone and Sandstone; Hamilton Group [Shale, Limestone, Sandstone, and Siltstone]; Gensee Group and Tully Limestone, [Shale, Limestone, and Siltstone]; Sonyea Group [Shale and Siltstone]; West Fall Group. The figure was created using geological data extracted from Rickard and Fisher (1970a).

Published morphology

The 3D bedrock and sedimentary infill morphologies of the Finger Lakes has been mapped extensively by Mullins and Hinchey (1989) and Mullins et al. (1996), who obtained seismic profiles of sufficient quality for 8 of the 11 Finger Lakes to have seismic bedrock profiles produced and interpreted, as well as sedimentary core data from three of the lakes (Fig.3.9a, and 3.10).

Typically, cross profiles appear to be qualitatively more V-shaped than U-shaped, as shown in Figures 3.9b, and 3.10, although this was not quantified in the aforementioned studies. The maximum recorded bedrock depths of the Finger Lakes range from 94 m to 442 m below lake level, with the area of maximum erosion occurring on average in the centre of the lakes or slightly south of the centre (i.e. in the down ice flow direction). The asymmetry of the longitudinal erosion towards the south of the features is also highlighted by Mullins and Hinchey (1989), who describe the Finger Lakes as forming broad and shallow profiles in the north, becoming deeper and more narrow (i.e. gorge like) to the south. The lakes range in length from 5–61 km and reach a maximum width of 0.6–5.6 km. The areas of maximum width occur a small distance to the north of the middle of the lakes, which is somewhat offset with regards to the location of greatest depth. Each of the lakes have reasonably linear and non-sinuous central lines along features.

Mullins and Hinchey (1989) also report, in the north of the lakes, collapse or melt-out structures in the sedimentary infill of the lake, indicative of grounded ice, and in the northern sections of both Owasco Lake and Seneca Lake (compare Fig.3.9) they identified esker like ridges, which are indicative of subglacial meltwater channels occupying the base of the features. Both of these depositional features are associated with late-stage glaciation after the erosion of the lake basins.

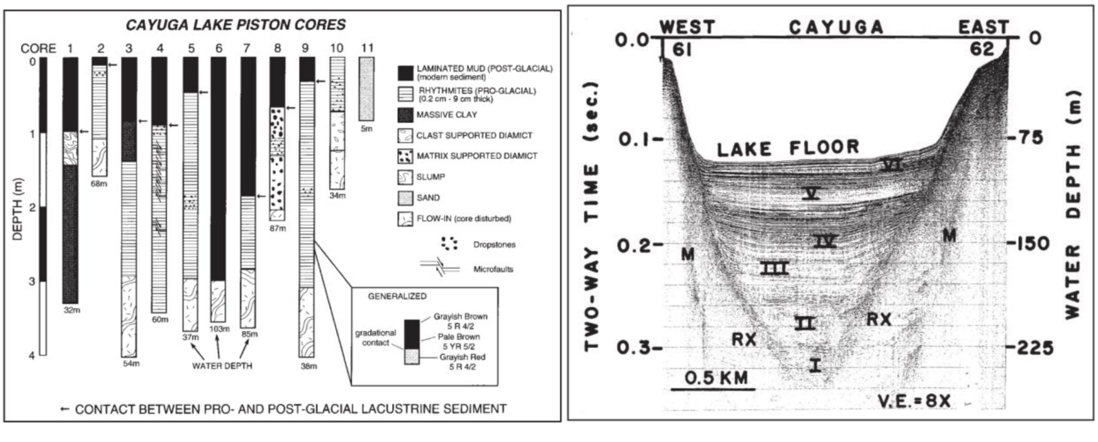

Figure 3.9: Mullins et al. (1996) Piston cores and sedimentary stratigraphic interpretation of seismic reflectors of Cayuga Lake. Sedimentary stratigraphy descriptions and interpretations are outlined in the sedimentary geology and infill section below.

The sediments overlying the bedrock and filling the valleys have been studied by several different authors (Mullins et al., 1996; Yager et al., 2001; Fischer et al., 2017) at different resolution. The most comprehensive of these was undertaken by Mullins et al. (1996) who divided the sedimentary infill of the lakes by the sediments' seismic reluctance into six distinct units, outlined below.

Calculated ages of deposition

Several absolute uncalibrated ^{14}C dates have been reported for the sediments of the Finger Lakes and the surrounding area. One radiocarbon date is reported from a wood fragment recovered from sedimentary sequence VI by Mullins et al. (1996) providing an age of 8,320 ±70 yrs BP, which was used to extrapolate an estimated age for sequence VI of 13.4 ka. This age correlates well with another radiocarbon date reported by King et al. (1983) of 13,925 ±700 yrs BP obtained from the boundary of the VI-V sequence in Seneca Lake. Two other AMS (Accelerator Mass Spectrometry) bulk organic ages are reported, 13,865 ± 100 yrs BP from above VI-V sequence sedimentary boundary in Seneca Lake (Mullins et al., 1996) and another radiocarbon age of 13.6 ± 0.2 ka BP from above VI-V sequences sedimentary contact in the Canandaigua Valley (Mullins et al., 1996). The last radiocarbon age reported for the Finger Lakes by Mullins et al. (1996) was for an *in situ* peat layer just below Canandaigua Lake's sedimentary sequence VI. The reported age is 13,650 ± 210 yrs BP, and has been used to infer that there was rapid sedimentation around 14.4 ka BP. This date was obtained from the Valley Head moraine to the south of the lakes, dated by Wellner and Petruccione (1996), Muller and Calkin (1993) and Krall (1977), to 13.6 ± 0.2 ka BP coincident with the formation of the peats.

These calculated and inferred ages suggest that the whole sedimentary sequence was deposited approximately between 14.4 ka BP and 13.5 ka BP.

The valley infill descriptions and interpretations by Mullins et al. (1996) have been presented below. The authors divide the sediments into six distinct seismic units. The sedimentary thickness has been recorded by the authors to reach a maximum of 275 m in the southern section of Seneca Lake (Table 3.2).

Table 3.2: Finger Lakes published statistics. Table from Mullins et al. (1996).

Lake	Map number (Figure 1)	Seismic Profiles (km)	Piston Cores (Number)	Drill Data (Yes/No)	Length (km)*	Maximum Width (km)*	Elevation (m)*	Water Volume ($10^6 m^2$)*	Surface Area (km^2)*
Conesus	1	n.a.	0	No	13	1.3	249	157	14
Hemlock	2	30	0	No	11	0.8	276	106	7
Canadice	3	14	0	No	5	0.6	334	43	3
Honeoye	4	n.a.	0	No	7	1.4	245	35	7
Canandaigua	5	120	0	Yes	25	2.4	210	1,640	42
Keuka	6	180	0	No	32	3.3	218	1,434	47
Seneca	7	400	15	No	57	5.2	136	15,540	175
Cayuga	8	150	11	Yes	61	5.6	116	9,379	172
Cwasco	9	75	0	No	18	2.1	217	781	27
Skaneateles	10	80	0	No	24	3.3	263	1,563	36
Otisco	11	n.a.	0	No	9	1.2	240	78	8

Lake	Drainage Area (km^2)*	DA/SA	Maximum Water Depth (m)	Maximum Sedimentary Thickness (m)	Maximum Erosion Below Lake Level (m)	Maximum Erosion Relative to Sea Level (m)
Conesus	168	12	18*	n.a.	n.a.	n.a.
Hemlock	96	14	29	149	173	+103
Canadice	32	11	27	68	94	+240
Honeoye	95	14	9*	n.a.	n.a.	n.a.
Canandaigua	407	10	84	202	261	−51
Keuka	405	9	57	146	193	+25
Seneca	1,181	7	186	270	442	−306
Cayuga	1,870	11	132	226	358	−242
Cwasco	470	17	52	95	140	+77
Skaneateles	154	4	84	140+	255	+8
Otisco	94	12	20*	n.a.	n.a.	n.a.

* Based on Bloomfield, 1978.
n.a = not applicable
DA/SA = Drainage area to surface area ratio

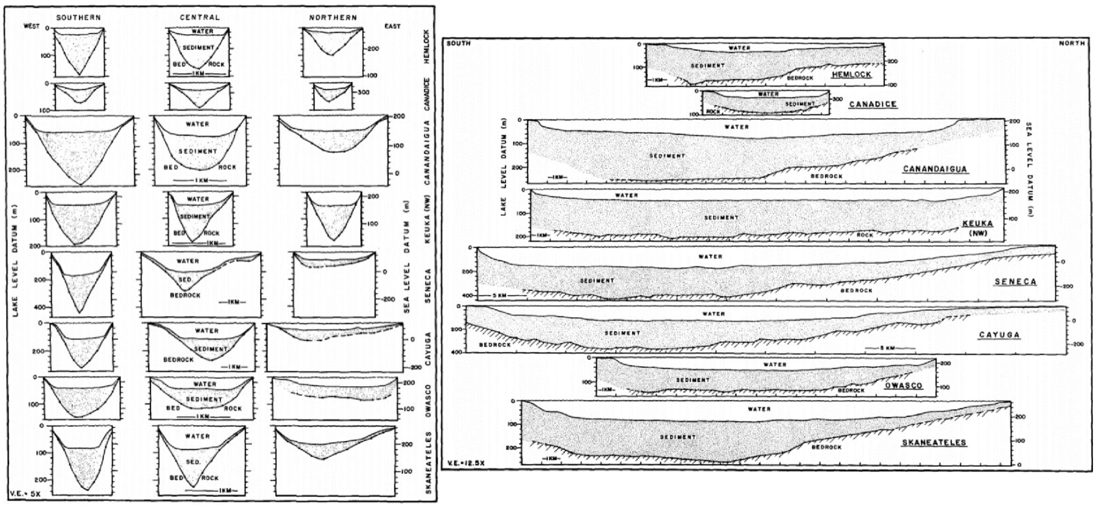

Figure 3.10: Selected transverse and longitudinal interpreted bedrock profiles and sediment fills of 8 of the Finger Lakes. Each profile is shown relative to each individual lake level and not metres above sea level. All the scales of the longitudinal profiles are consistent except those of Seneca and Cayuga lake. The vertical exaggeration is constant for all profiles (V.E. = 5× and 12.5×, respectively). Figures from Mullins et al. (1996).

Sediment geology and infill

The following subsection describes the subdivisions of the sedimentary units found in the Finger Lakes as described by Mullins and Hinchey (1989) and Mullins et al. (1996).

Unit I (oldest sequence)

Unit I is dominated by chaotic seismic reflectors, with a hummocky upper surface, which lies underneath and is onlapped by the other younger units. The spatial distribution of the unit is reported by Mullins et al. (1996) as only occurring in the south of the lakes. Mullins et al. (1996) report Unit I comprising of the coarse-grained Valley Heads Moraine, with a depositional age of ~14.4 ka. No error value has been reported for these radiocarbon ages.

Unit II

Unit II is dominated by strong lateral changes in the seismic reflectors, transitioning from hummocky high-amplitude reflectors in the north portion of the unit into smoother low-amplitude reflectors in the southern portion (Mullins et al., 1996). Mullins and Hinchey (1989) report the unit being present in the southern two thirds of the lakes.

Unit III

Unit III is dominated by a reflection-free seismic profile, which has been interpreted by the authors to represent rapid deposition of fine-grained sediment (Mullins et al., 1996), and occurs throughout each of the lake basins.

Unit IV

Unit IV is dominated by continuous, high-frequency, high-amplitude reflectors, and in conjunction with the piston cores has been found to be spatially widespread across the lakes. This has been interpreted as being fine-grained varve-like rhythmites with dropstones and thin sandy turbidites (Mullins et al., 1996). The depositional unit has been recorded to occur in all of the lake basins in the Finger Lakes.

Unit V and Unit VI (youngest sequence)

Both Unit V and Unit VI are dominated by low-amplitude, continuous reflector profiles that onlap the older sequences in the north. These have been interpreted by Mullins and Hinchey (1989) as indicating a southerly sediment source. The change in direction of the sediment influx represents the change in dominant basin flow and the end of the glacial influence, with all the sedimentary deposits being dated to have occurred between 14.4 ka and 13.5 ka BP.

Data availability

There is relatively good seismic and sedimentological data on the sediment/bedrock depth and morphology of 8 of the 11 lakes from a variety of published seismic lines and cross- and long-profiles undertaken by Mullins and Hinchey (1989) and Mullins et al. (1996). However, this data exists only in published diagrams, the original paper seismic lines being lost with time (Prof Scholz, Syracuse University, pers. Comm.). For this thesis, the published diagrams have therefore been digitised at the University of Sheffield (see Chapter 4). High-resolution chirp data on the sedimentary infill of Skaneateles Lake, and Multichannel seismic of Seneca and Cayuga Lakes, has been collected by the Finger Lakes Research Program at Syracuse University, NY, USA under Professor Scholz, and it is anticipated that this data will be published in the near future. The table below (Table 3.3) outlines the main data sources found for the lakes and the Finger Lakes region.

Table 3.3: Finger Lakes data availability.

Data type	Data source	Reference publication
Bedrock Geological map	Geological Map of New York, Finger Lakes Sheet (scale 1:250,000)	Rickard and Fisher (1970a)
Sedimentary Geological map	Surficial Geological Map of New York, Finger Lakes Sheet (scale 1:250,000)	Cadwell and Muller (1986)
Seismic stratigraphy	Seismic reflection data collected using an EGG Uniboom, with a resolution of <1m.	Mullins and Hinchey (1989), Mullins et al. (1996)
Sedimentary core logs	15 5m max piston cores (pc) from Seneca Lake and 11 pcs from Cayuga Lake. 72 ~3m pcs from the southern half of Cayuga Lake. 13 drill records from dry lake valley south of Cayuga Lake.	Mullins et al. (1996), Ludlam (1967), Tarr (1904)
Ice extent maps	-	Margold et al. (2015), Mickelson and Colgan (2003)
Regional Surface DEM	United States Interagency Elevation Inventory USGS Lidar Point Cloud	USGS (2018)
Regional Bedrock topography DEM	USGS Map of Bedrock Topography	Soller and Garrity (2018)

Analogue potential

The Finger Lakes appear to be a very good analogue site for the NSF features, due to the similar morphology and scale of the features, the underlying sedimentary bedrock geology, with the features being incised deeply into bedrock, the topographic setting, and the similar proposed climatic conditions during formation (however, under an ice sheet not a piedmont lobe). The Finger Lakes also have good data availability, specifically bedrock topography and sedimentary infill data.

3.3.1.2 *Michigan*

Introduction

The recorded CGBL features in the state of Michigan are generally located in the northeast of the state and do not appear to have been well studied (Fig.3.11-3.13). The location of the features suggest that they are connected with the Saginaw Lobe of the LIS, and therefore LGM in age (Fig.3.11 and 3.12). Sjogren et al. (2002) comments on the spatial relation and distribution of the features, describing them as tunnel channels and associating them with large volumes of subglacial melt water, which also formed the hummocky terrain seen in the area.

The published literature states that deposits associated with the Saginaw Lobe have been dated to ~15 ka BP (Monaghan et al., 1986). Margold et al. (2015) extensive work on the timing and extent of the LIS shows that this region of the ice sheet reached its maximum extent at ~18 ka BP. Ice limits and flow directions at this time are shown in Figures 3.11 and 3.12.

The regional setting of the features in low lying topography at the edge of the LIS, as opposed to occupying the foreland of a mountain range, is similar to that of the Finger Lakes features. The region does not have any reported large-scale faulting or other geological structure in either the published literature or the published bedrock geological maps, which could affect the morphology and formation of the mapped features.

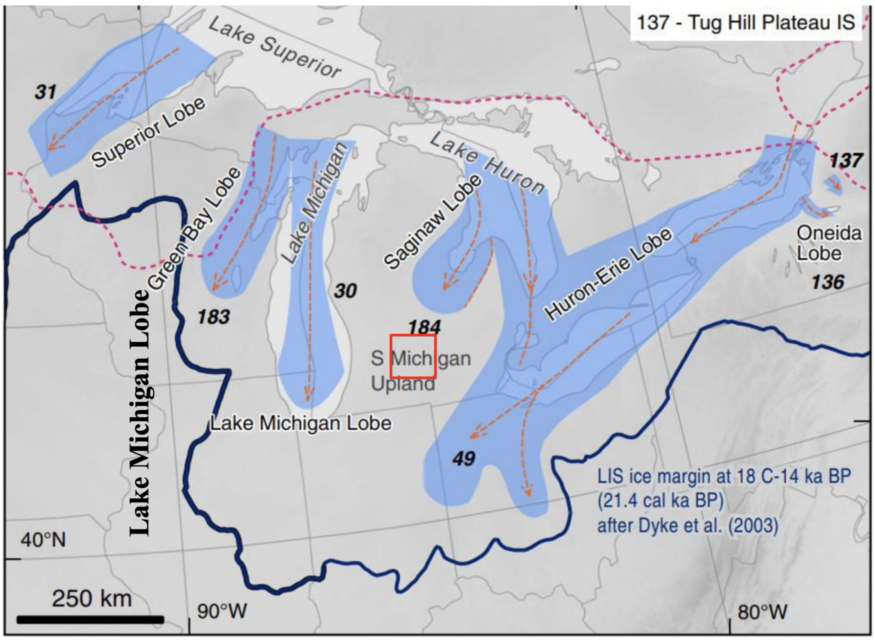

Figure 3.11: Map of maximum spatial extent of the LIS (dark blue line) and names of each lobe and their flow direction in the region of the great lakes. Red box marks the location of the CGBLs Studied by Sjogren. Figure from Margold et al. (2015).

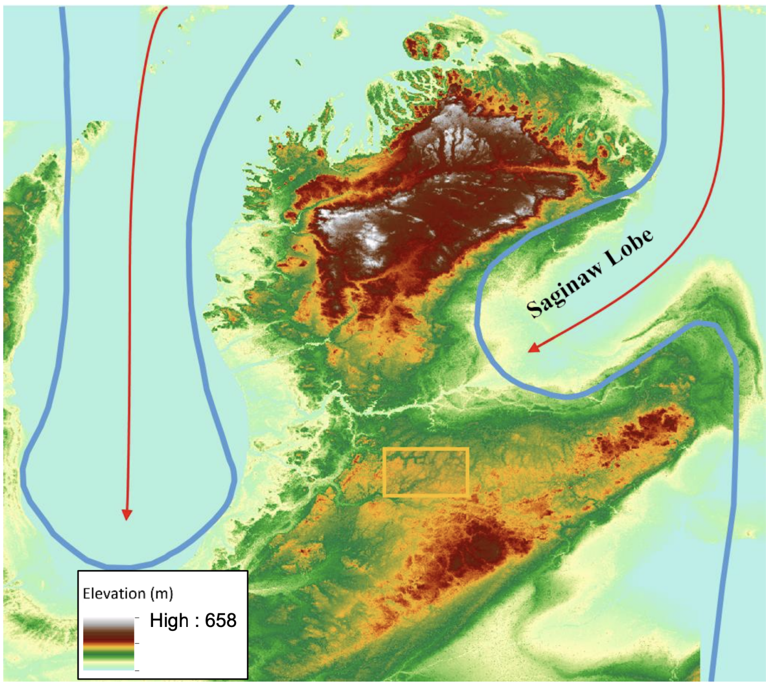

Figure 3.12: Hill shaded topographic map of Michigan. Blue lines indicate mapped locations of ice stream lobes and red arrows show ice flow direction (Margold et al., 2015), however the whole area was ice covered at the LGM (compare figure 3.11). Orange box shows location of Sjogren et al. (2002) study site. Map from 30m resolution STRM DEM.

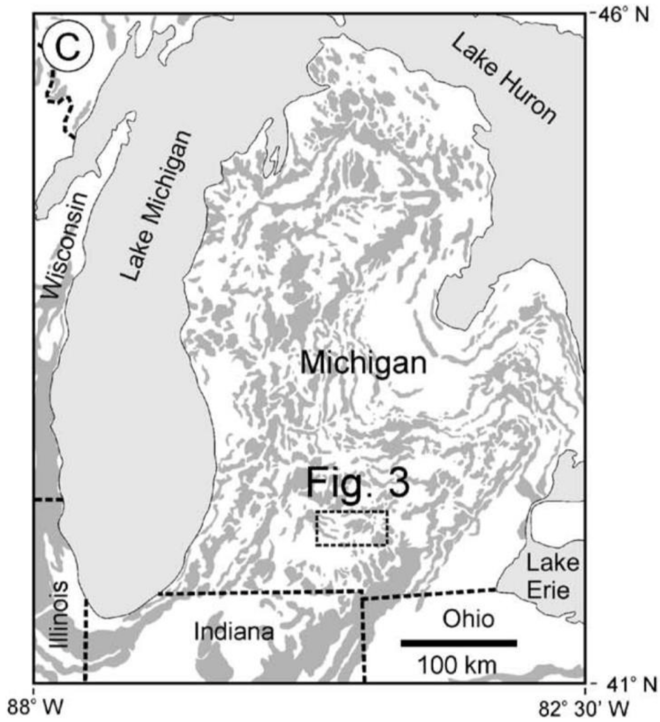

Figure 3.13: Map of location of Michigan CGBLs shown by dashed box labelled by Sjorgen as Fig. 3. From Sjogren et al. (2002).

Topographic setting

The Michigan CGBLs are located along the previous southern margin of the LIS, with four of the great lakes (Lake Michigan, Lake Superior, Lake Huron, and Lake Erie) located to the west, north, and east of the location of the studied tunnel valleys (Fig.3.11 and 3.12) (Sjogren et al., 2002; Fisher and Taylor, 2002; Kehew and Kozlowski, 2007). The area of interest is located in the south of the state at the southern end of the Saginaw Lobe. The Saginaw Lobe followed a topographic low between a large area of high ground to the northwest (Roscommon State Forest) and a much more low-lying area to the southeast.

Bedrock geology

The work by Sjogren et al. (2002) on the Michigan CGBLs does not specifically discuss the bedrock in the area of the features, but does show the features cutting into the bedrock, described as sandstone, in several diagrams (see Fig. 3.14 below). The geology of the area has been mapped independently and documents the geology as being part of the Saginaw formation, which is predominately made up of Pennsylvanian sandstones and shales, with a small amount of limestone and coal ("Bedrock Geology of Michigan", 1987, 1:500,000 scale)

The bedrock geology of Michigan state comprises a basin of Jurassic, Pennsylvanian, Mississippian, Devonian, Silurian, Ordovician, Cambrian, and Precambrian formations (see geological map in Appendix A).

The lithologies of the main geological formations are outlined below in stratigraphic order from youngest to oldest. The first is that of the Red Beds made up of Jurassic mudstone and shales, then the Grand River Formation of Pennsylvanian Sandstones and Shales; the Saginaw formation of Pennsylvanian sandstones, shales, limestones and coal; the Bayport limestone of Mississippian limestones, dolostones, sandstones, shales, chert and evaporite; the Michigan formation of shales, black-shales, dolostone, gypsum, limestone, sandstone and evaporite; the Marshall formation of sandstone and siltstone; and finally the Coldwater formation of shale, dolostone, sandstone, limestone and siltstone ("Bedrock Geology of Michigan", 1987, 1:500,000 scale).

Published morphologies

Sjogren et al. (2002) did not include long- or cross-profiles of the CGBLs and none appear to exist. However, Sjogren et al. (2002) do provide a map of the spatial distribution and cross-cutting relationship of the tunnel valleys, as well as schematic diagrams of the interpreted bedrock and sediment profiles (Fig.3.14 and 3.15, as well as in Appendix A).

The mapped network of CGBLs is ~70 km by 30 km and was studied in conjunction with a larger area in Alberta, Canada. Sjogren et al. (2002) identified three different types of channel morphology (Fig.3.14) and related the changes in morphology to the underlying bedrock and sedimentary cover. The first two types are formed in thicker deposits of till, forming narrower channels with more pronounced hummocks in the channel base. The third type is formed in areas of thin till, forming wider, flat-bottomed channels that appear to cut deeper into the underlying bedrock (Fig.3.14). All three types of channel morphology are reported by Sjogren et al. (2002) to be present in the Michigan study area, with the type 3 bedrock incised CGBLs being reported to be found in the lowland areas of the state.

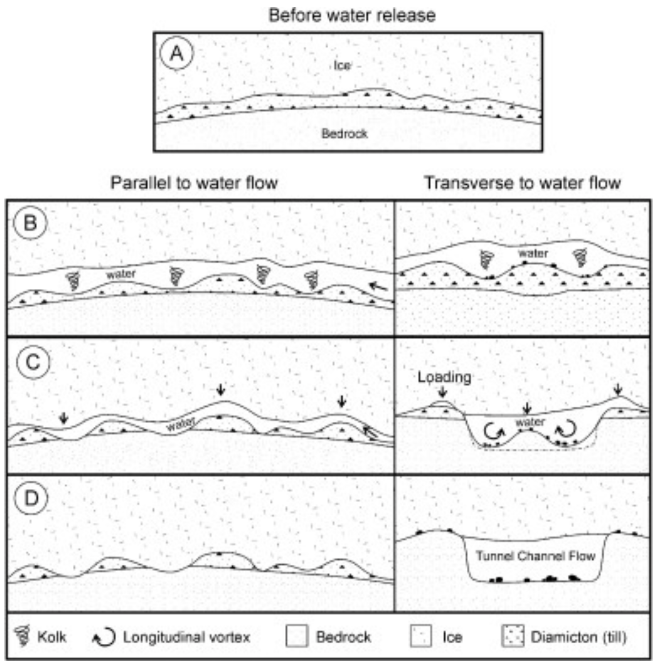

Figure 3.14: Figure showing the different tunnel valley morphologies produced from either parallel or transverse flows. Figure from Sjogren et al. (2002).

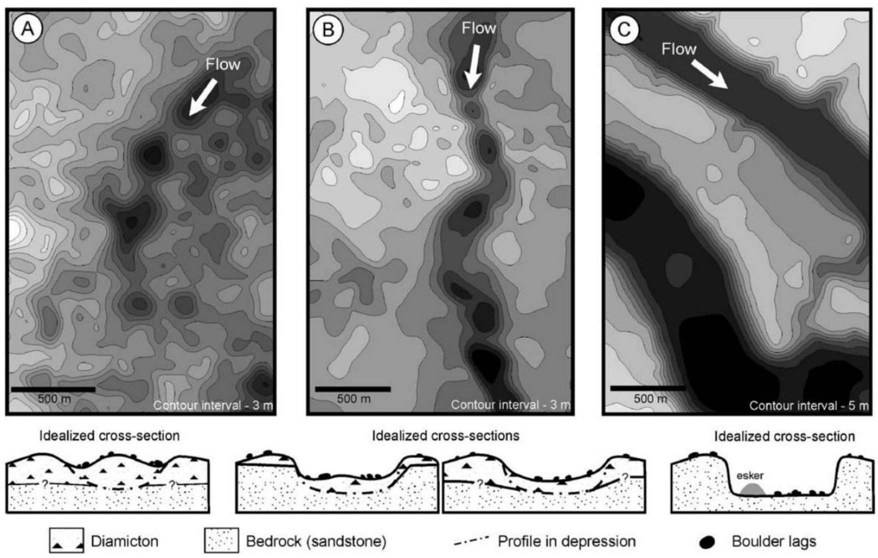

Figure 3.15: Figure from Sjogren et al. (2002) showing surface elevation (not bedrock) maps, and the interpreted idealised sedimentary and bedrock cross sections.

Sediment geology and infill

The sedimentary infill of the features reported by Sjogren et al. (2002) (schematically shown in Figure 3.15) is reported to be thin sandy diamictons over glaciofluvial sands and gravels. No dates have been reported for the deposition of these sediments.

The sedimentary Quaternary geology of the state of Michigan was mapped extensively by Farrand and Bell (1982) to 1:500,000 scale. The sedimentary cover is dominated by coarse grained glacial outwash, coarse to fine grained glacial till, and lacustrine deposits. The northwest of the state also contains extensive deposits of peat, thin to discontinuous till over bedrock, and dune sands. The sediments have been associated with the LIS through mapping of moraines which have been associated with the retreating of the Saginaw Lobe of the LIS (Zumberge, 1960; Farrand and Bell, 1982) or its readvance (Kozlowski, 1999). A simplified version of the Farrand and Bell (1982) 1:500,000 scale map is in Appendix A.

Data availability

The state of Michigan has moderate bedrock topography data availability, and little morphological analysis done on the features. Due to the focus and timing of the work done, several key types of data are not easily accessible. These data-sets were not able to be located during the remit of this project, though it may be that some data is available on these features. Table 3.4 outlines the main data sources found for the region.

Analogue potential

The Michigan CGBLs have been determined as not currently being a viable candidate to take forward as an analogue site for the NSF. The features are less studied and do not appear to be on the same scale as the NSF features and they do not have evidence on how deeply they incise into bedrock, along with the region's low availability of high resolution bedrock topography data.

Table 3.4: Michigan data availability table.

Data type	Data source	Reference publication
Bedrock Geological map	Digitised bedrock geology 1:500,000 scale	Michigan Department of Natural Resources Land and Minerals Services Division. Resource Mapping and Aerial Photography
Sedimentary Geological map	Quaternary Geology of Southern Michigan 1:500,000 scale	Zorn (2017), Farrand and Bell (1982)
Seismic stratigraphy	No seismic stratigraphy found	-
Sedimentary core logs	No cores found	-
Ice extent maps	-	Margold et al. (2015)
Regional Surface DEM	United States Interagency Elevation Inventory USGS Lidar Point Cloud	USGS (2018)
Regional Bedrock topography DEM	USGS Map of Bedrock Topography	Soller and Garrity (2018)

3.3.1.3 *Glacier National Park, Montana*

Introduction

The Glacier National Park region contains 762 lakes (National Park Services) of which Lake McDonald is the largest CGBL in the area. The area is located on what was the southern margin of the Cordilleran Ice Sheet (CIS), under the then Flathead Lobe (Gerald, 1986). The focus of this section is Lake McDonald, due to the availability of seismic stratigraphy and bedrock interpretation data available through work undertaken by Mullins et al. (1991). The area around Lake McDonald exhibits several large normal and thrust faults (Whipple, 1992) but the lake itself does not appear to be structurally controlled. It is instead recorded as being orthogonal to all the large geological structures in the region, including the Flathead Fault (Mullins et al., 1991). The region is recorded by Alden (1953), Gerald (1986), and Carrara et al. (1986) to have been last glaciated during the CIS at ~15 ka BP (Smith, 2004).

Topographic setting

Lake McDonald is located in a foreland of the Rocky Mountains, with the north-eastern end of the lake starting at the southern end of the U-shaped outlet valley between Stanton Mountain and Mt Brown (Fig.3.16). The southern end of the lake is located at the foot of the Apgar Mountains to the west and the Belton Hills to the east. The east and west banks of the lakes are flanked by gently sloping valley walls that rise up to the level of the surrounding plateau (Carrara, 1990).

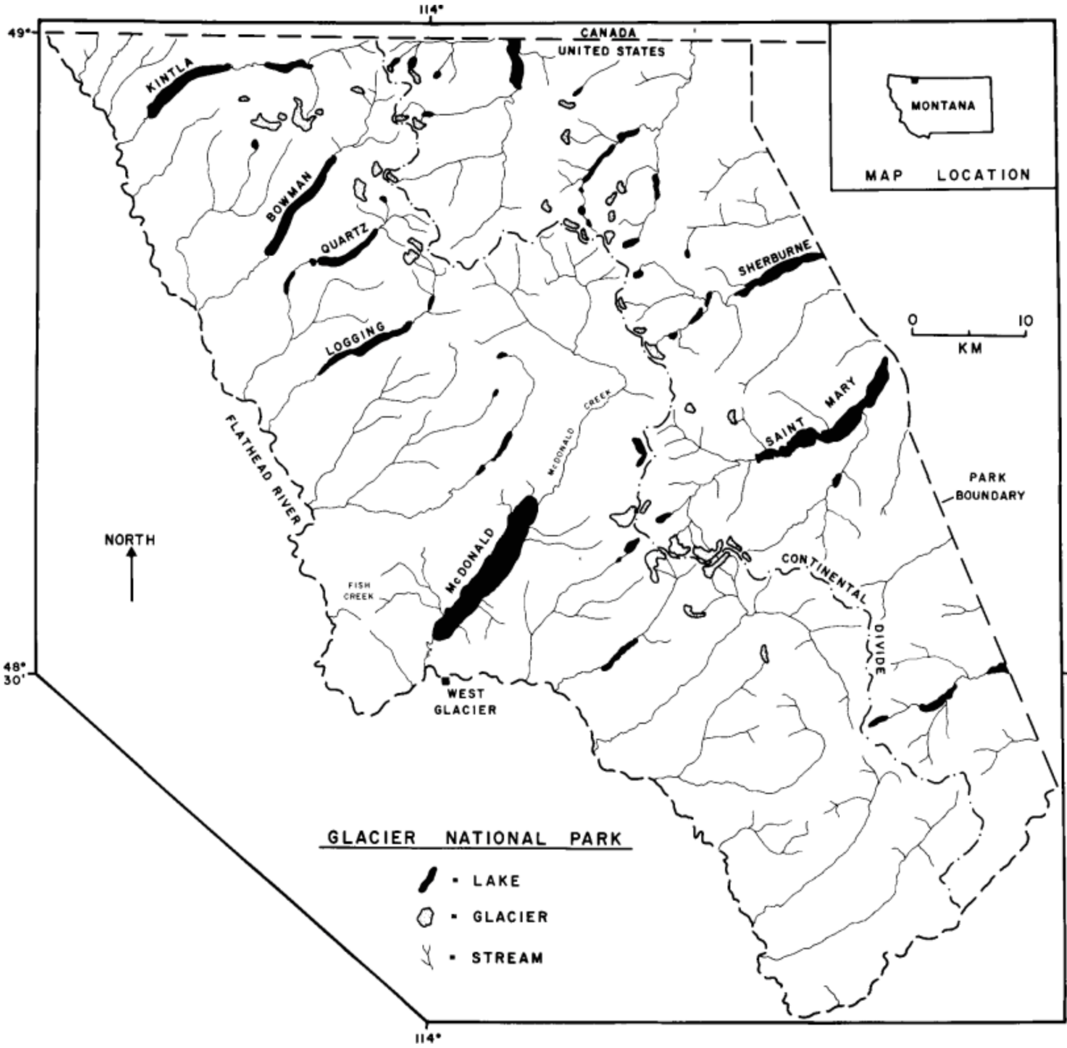

Figure 3.16: Map of location and names of major lakes, glaciers, and streams created from the 1968 U.S.G.S. topographic sheet N4813 (Scale 1:00 000). Figure from Mullins et al. (1991).

Bedrock geology

The geological maps (Fig. 3.17) produced by Whipple (1992) and Carrara (1990) show that the foreland of the Rocky Mountains is covered by a layer of glacial till, and small landslide and alluvium deposits. Whipple (1992) interpreted cross-section of the valley, just to the north of Lake McDonald, shows that the lake is located over a syncline within a graben with the Flathead Fault and Wolf Gun Thrust Fault to the northeast and the Nyack Fault to the southwest. The syncline is made up of Middle Proterozoic Belt Supergroup formations. The Belt Supergroup is reported to be made up of Purcell lavas, and Gabbroic sills and dykes. The Greyson, Spokane and Snowslip formations are described as being made up of reddish-brown and greenish-gray argillites and siltites, with some quartzite. The Empire formation is a transitional unit approximately 375 m thick between the aforementioned Greyson, Spokane and Snowslip formations and the Altyn, Helena, and Shepard formations which are made up of different carbonate units (Ross, 1959; Mudge, 1977; Whipple, 1992).

The region surrounding Lake McDonald is shown to have significant normal and thrust faulting. The recorded faults are all perpendicular to the direction of ice flow and erosion. The largest named faults in the areas are the Blacktail/ Flathead Fault, the Nyack Fault, and the South Fork Fault (Whipple, 1992; Ross, 1959). The area also has several large anticlines and synclines recorded in the regional geological map, with the largest being the Flathead Anticline (Whipple, 1992; Ross, 1959).

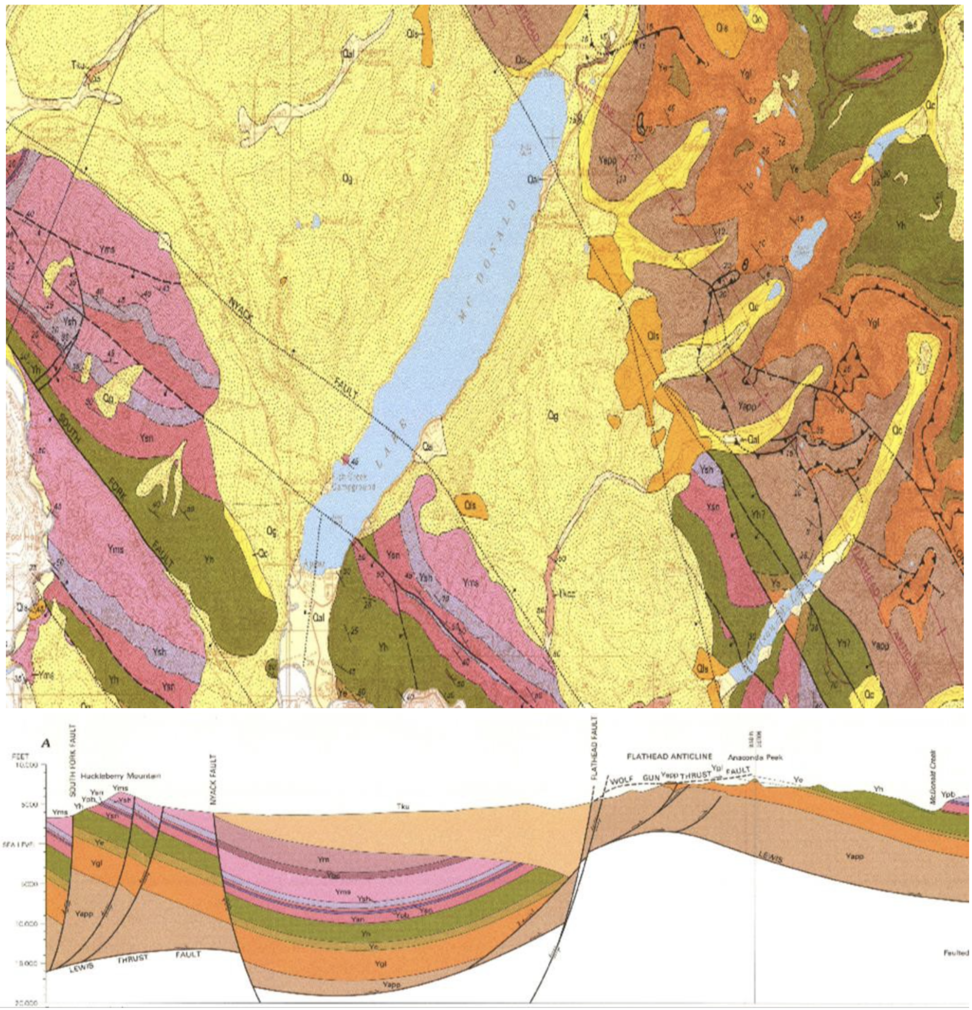

Figure 3.17: Geological map of the area around Lake McDonald and selected portion of geological cross-section that is located northwest of Lake McDonald. Cross-section shows Lake McDonald being located in Quaternary sedimentary deposits that overly folded rocks of the Middle Proterozoic Belt Supergroup. Map extract from Geologic map of Glacier National Park, Montana (1:100,000). See full map in Appendix A for descriptions of each geological unit and location of geological cross-section.

Published morphologies

Lake McDonald's length is just over 15 km, its maximum width ~2 km, and its maximum bedrock depth is 279 m below lake level and occurs near its midpoint. High resolution seismic stratigraphy was captured by Mullins et al. (1991). Mullins describes the bedrock cross profile as a complex V-shaped morphology (Figs. 3.18 and 3.19), with a narrow erosional thalweg along the central axis of the lake. Despite portions of the bedrock being obscured by zones of acoustic impenetrability, larger sections of the bedrock surface and stratigraphy of the lake infill have been successfully resolved (Fig.3.20). Due to the limitations of the techniques used in the collection of the seismic stratigraphy profiles, both the northern and southern ends of the lake have no data. This is due to shallow, nutrient-rich eutrophic water resulting in areas of acoustic impenetrability.

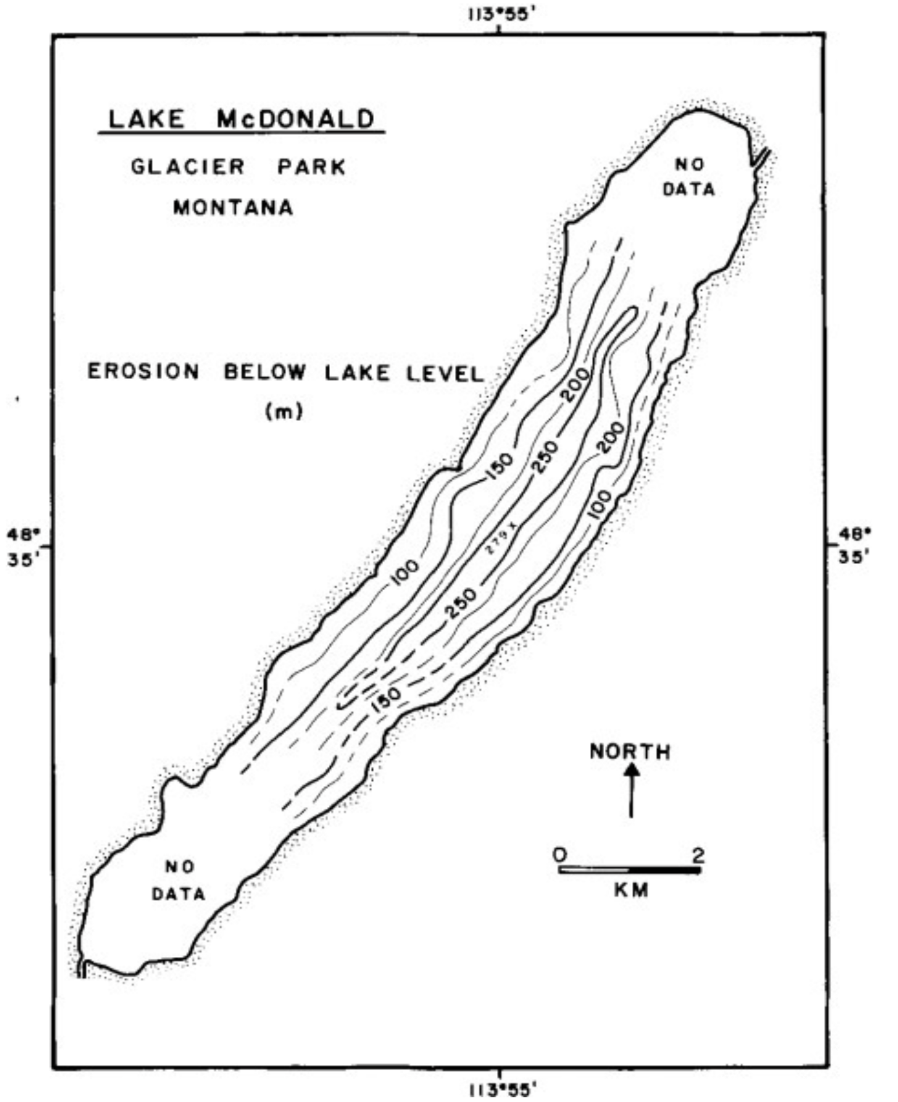

Figure 3.18: Contour map of erosion below lake level (depth to bedrock) for Lake McDonald. Maximum value (X) of 279 m is near lake midpoint. No data available from the ends of the lake due to acoustic impenetrability. Figure from Mullins et al. (1991).

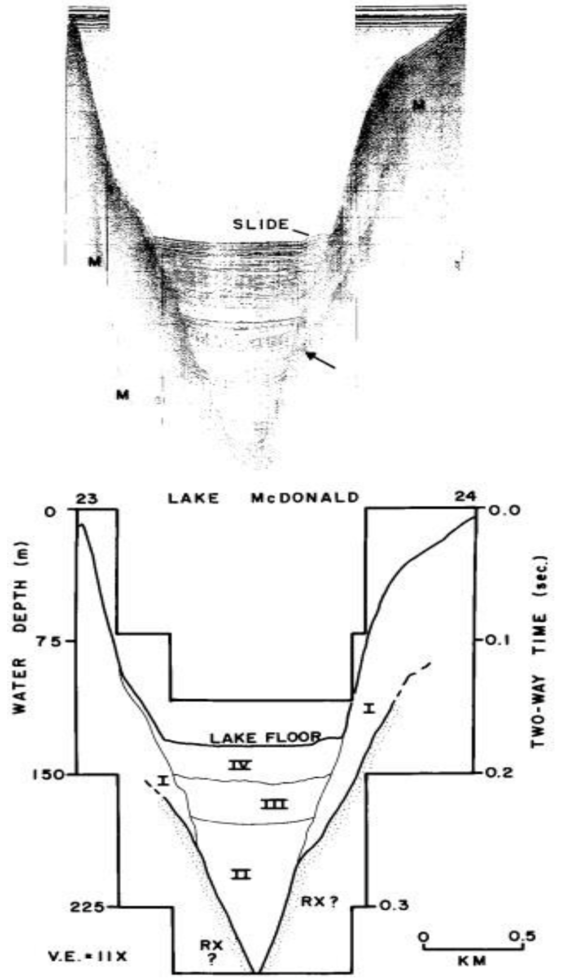

Figure 3.19: Photograph and interpretation of seismic reflection profile from Lake McDonald. The interpretation highlights the stratigraphic relationships between each of the units and the bedrock topography. Water depth scale assumes a constant velocity of 1.5 km s^{-1}. M: multiple reflection. Figure from Mullins et al. (1991).

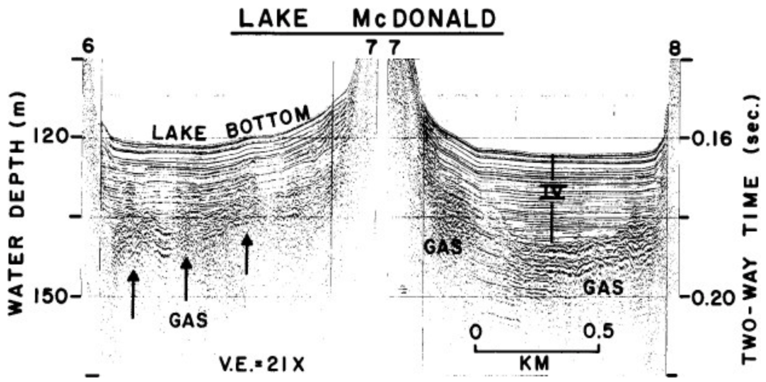

Figure 3.20: Annotated photographs of the axial portions of seismic profiles illustrating acoustically impenetrable zones in the southwest portion of Lake McDonald, indicated by the black arrows, marked gas. Water depth scale assumes a constant velocity of 1.5 km s^{-1}; V.E: vertical exaggeration. Figure from Mullins et al. (1991).

Sediment infill

The sedimentary geology and lakebed stratigraphy is well described by Whipple (1992) and Mullins et al. (1991). The broad regional sedimentary geology of the plateau in which Lake McDonald is situated is dominated by a thick layer of glacial till, which thickens towards the northeast, and small landslide and alluvium deposits (Whipple, 1992; Mullins et al., 1991). Mullins et al. (1991) report the lake infill to be made up of four main stratigraphic units.

Unit I, which is the oldest, is characterised by chaotic seismic facies. The unit is recorded as having a maximum thickness of 113 m, and generally thickens towards the valley margins and is generally absent from the main axis of the valley. The style and type of seismic reflectors, in conjunction with the local onshore deposits, have meant that this unit has been interpreted by Mullins et al. (1991) as being part of the lateral moraine debris, as seen along the lake shores (Boulton and Eyles, 1979). The lack of the debris layer in the central part of the valley, in conjunction with the valley morphology, has been interpreted by Mullins et al. (1991) as being evidence of strong subglacial meltwater flushing and erosion, which would have transported the debris away and produced the more V shaped morphology (Gustavson and Boothroyd, 1987; Vivian, 1970; Hooke et al., 1985). Mullins et al. (1991) also use the work previously done by Walder and Hallet (1979) to strengthen this argument, who recorded bed forms in the bedrock produced by pressurised subglacial meltwater elsewhere in Glacier National Park.

Unit II is described by Mullins as being the oldest of the three units that crosscut Unit I. Unit II is up to 105 m thick. The unit produces sub-sequences of continuous, parallel high-amplitude reflectors that sit on top of transparent zones. The seismic reflectors of Unit II have been interpreted as being typical of glaciolacustrine silt and sand deposits deposited during glacial retreat. Mullins et al. (1991) suggest that the main source of the sediment would be from large volumes of meltwater transported down McDonald Creek.

Unit III has a maximum thickness of 34 m, and has a characteristic seismic reflectance profile of a lowermost transparent zone that grades upwards into continuous parallel reflectors. There is a zone of more chaotic reflectors in the southwest, which have been interpreted as being slope failure slide deposits. Similar to Unit II, the unit has been interpreted as being made up of glaciolacustrine silts and fine sands (Ashley, 1975; Hsu and Kelts, 1984). These deposits have been interpreted as being deposited rapidly in thick massive beds as a result of enhanced meltwater discharge during glacial retreat.

Finally, Unit IV is the youngest of the seismic units with a maximum thickness of 23 m. The seismic profile of this unit is described by Mullins et al. (1991) as being continuous, parallel, high-frequency, high-amplitude reflections that distinctly onlap the other units. The units have been interpreted as having a high likelihood of being post-glacial deposits occurring while the glacier retreated further up-valley and the continued sedimentation regime that continued up until time of study (1991).

Data availability

Lake McDonald and the surrounding region has been extensively studied over the last several decades and so has relatively good data availability. However, due to the time at which the seismic data was collected, only printed diagrams exist, not raw seismic data. The large-scale morphological mapping of Lake McDonald was undertaken by Mullins et al. (1991) with only the published data from these studies retrievable. The table below outlines the main data sources found for the lake and surrounding region.

Analogue potential

Lake McDonald, Glacier National Park has been determined to not be a suitable analogue site for northern Switzerland due to the ends of the feature having no bedrock topography data, and the feature being isolated from any other well mapped features in the region. However, if more high-quality data was to be made available, the site may be a suitable analogue for a future study.

Table 3.5: Glacier National Park data availability table

Data type	Data source	Reference publication
Bedrock Geological map	Map of Glacier National Park, Montana (Scale 1:100 000) Reconnaissance Geological Map and Sections of Glacier National Park, North-western Montana (Scale 1:125 000)	Whipple (1992), Ross (1959)
Sedimentary Geological map	Surficial Geologic Map of Glacier National Park, Montana (Scale 1:100 000)	Carrara (1990)
Seismic stratigraphy	-	Mullins et al. (1991)
Sedimentary core logs	No cores found	-
Ice extent maps	-	Locke (1995), Smith (2004)
Regional Surface DEM	United States Interagency Elevation Inventory (Topographic Lidar), Southern margin of the Lake USGS Topo Map Vector Data (Vector) (Extent 7.5x7.5 minute) USGS NED 1/3 arc-second n49w114 1x1 degree ArcGrid 2017 USGS NED Original Product Resolution MT GlacierNP 2016	-
Regional Bedrock topography DEM	USGS Map of Bedrock Topography	Soller and Garrity (2018)

3.3.2 *Canada, British Columbia*

3.3.2.1 *Okanagan Lake*

Introduction

The southern half of British Columbia is made up of an interior plateau that is aligned in an eastward orientation towards the interior highlands of the Columbia Mountains. There are several CGBLs incised into the plateau and interior highlands, which have been associated with the westward flow of ice streams (Eyles et al., 1991).

The Okanagan Valley and Lake has been studied by several authors (Eyles et al., 1991; Vanderburgh and Roberts, 1996; Shaw, 1977; Fulton and Smith, 1978), so data on the bedrock-sediment interface morphology and stratigraphy have been collected for both the lake and northern section of the valley. The stratigraphic work undertaken for the Okanagan region has been interpreted to suggest that multiple glaciations have occurred since the last interglacial period at 125 ka BP (Eyles et al., 1991). The glaciation of the Okanagan valley has been interpreted to have been caused by a large ice stream, which terminated in a piedmont style lobe on the Columbia Plateau ~15.5 ka, with ice retreating to present day Lake Okanagan by ~12 ka (Clague, 1981; Booth, 1987). The region is reported as being ice-free by approximately 10 ka (Fulton, 1969; Fulton, 1984).

Topographic setting

Okanagan Lake is located in an area of foreland topography within the Thompson plateau, which reaches a maximum height of 1,617 m a.s.l (Fig.3.21). The Okanagan valley is located 2000 m below the rim of the surrounding plateau, and is bounded by low lying hills. The valley runs in a general north-south orientation, with the northern section of the valley completely infilled with a range of fluvial and lacustrine sediments. The hills surrounding the valley reach a maximum height range of 1,200-1,800 m a.s.l. (Google Earth, 2018). The orientation and magnitude of the topography is highly affected by the local geology and regional faulting.

Bedrock geology

The bedrock geology is recorded by Nasmith (1962) who describes how it is strongly influenced by the 350 km long Okanagan shear zone. Shuswap Lake, Okanagan Lake, and Kalamalka Lake are located within the zone of influence of the Okanagan shear zone (Brown and Murray, 1987). The large fault which runs in a north-south orientation bounds Omineca Crystalline Belt rocks to the east, and rocks of the Intermontane Belt to the west.

The Intermontane Belt formations comprise columnar jointed volcanic rocks of the Thompson plateau, which are underlain by Carboniferous to Triassic metasedimentary and metavolcanic units. The Omineca Crystalline Belt is made up of Eocene cover volcanic rocks of the Okanagan Highlands, dipping westward under Okanagan Lake

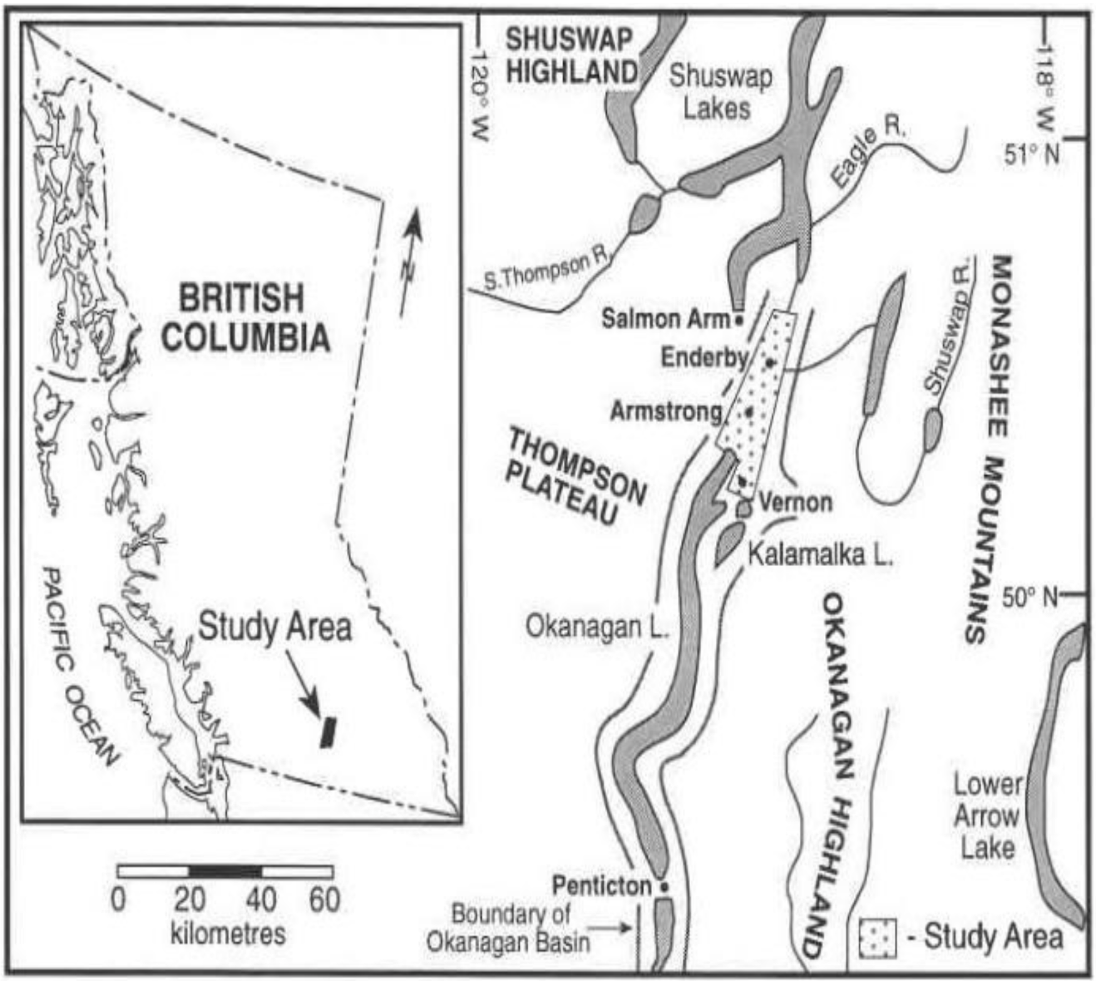

Figure 3.21: Location of sedimentary basin data in the northern Okanagan valley, south-central British Columbia. Figure from Vanderburgh and Roberts (1996).

overlying gneissic of the Okanagan Metamorphic and Plutonic complex (Nasmith, 1962). All of the bedrock units have been highly fractured during regional orogeny and tectonic unroofing prior to the Eocene (Nasmith, 1962).

Published morphologies

Okanagan lake is reported by Eyles et al. (1991) as being ~108 km long, >5 km wide, and reaching maximum bedrock depths of 450 m, 509 m, 564 m, 642 m below lake level (b.l.l.) in its four nested low points. The lake is shown to bifurcate at its northern headward end (Fig. 3.22).

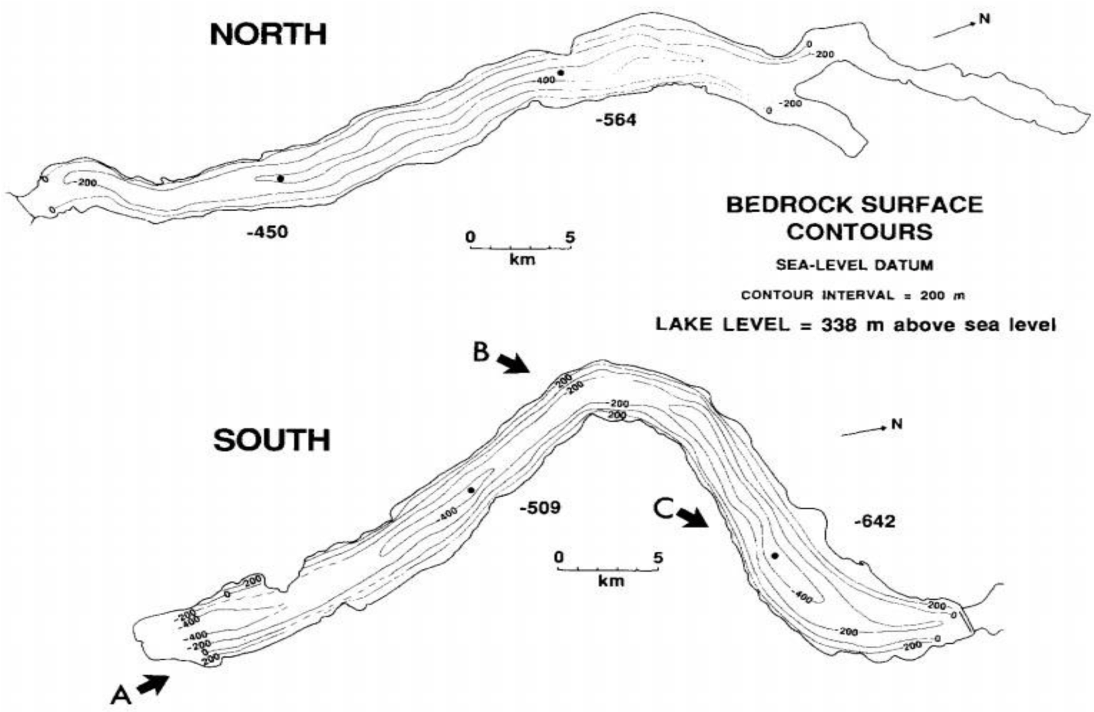

Figure 3.22: Bedrock surface contour map produced from seismic profiles. Figure from Eyles et al. (1991).

Sediment geology and infill

The Quaternary sedimentary fill of the Okanagan Valley and lake has been recorded as consisting of up to four distinct stratigraphic units, ranging in age from Pre-Early Wisconsin to the Holocene (10 ka) (Fulton, 1969). The Pre-Early Wisconsin age is inferred through correlation with other sediments in the region (Eyles et al., 1991). The units of Pre-Early Wisconsin are dominated by till and gravels, as well as some valley-side alluvial fans. The Mid-Late Wisconsin units are dominated by silts/glaciolacustrine silts (and valley-side alluvial fans). The Late Wisconsin-Holocene units consist of fluvial deposits (Eyles et al., 1991; Vanderburgh and Roberts, 1996).

Vanderburgh and Roberts (1996) use the sedimentary stratigraphy to propose four main periods of deposition preserved in the stratigraphy of the northern section of the Okanagan Valley. These are an initial period of subglacial fluvial deposition during glaciation, followed by the formation of a proglacial lake during glacial retreat depositing the glaciolacustrine sediments. This was followed by the infilling of the lake through deposition of glaciolacustrine sediments and fan deposits. The final stage of deposition recorded in the stratigraphy is that of the latest and current fluvial deposition of channel deposits associated with the present river in the valley (Vanderburgh and Roberts, 1996).

Data availability

Okanagan Lake and its surrounding region has been studied in several different contexts over the last several decades (including glaciological, ecological and geological), and has good bedrock morphological and geological data availability. Due to the time at which the majority of the data was collected, only printed diagrams exist, not raw data. The table below outlines the main data sources found for the lake and the region.

Table 3.6: Okanagan Lake data availability table.

Data type	Data source	Reference publication
Bedrock Geological map	Geological Map of British Columbia (Scale 1″:20mile)	Little (1962)
Sedimentary Geological map	Superficial materials of Canada (1:5,000,000 scale)	Fulton (1995)
Seismic stratigraphy	-	Eyles et al. (1991), Vanderburgh and Roberts (1996)
Sedimentary core logs	-	Vanderburgh and Roberts (1996)
Glacial feature and Ice extent maps	Geological Survey of Canada, (1968). Glacial Map of Canada. Map 1253A, scale 1:5 million	Church et al. (2010), Prest et al. (1968)
Regional Surface DEM	Shuttle Radar Topography Mission (SRTM) (30 m resolution)	USGS (2004)
Regional Bedrock topography DEM	No bedrock DEM found	-

Analogue potential

Okanagan Lake has been determined as being a good analogue site, if used in conjunction with other features in the same region of British Columbia, to take forward for further analysis. The feature shows similar morphology and scale to that of the NSF, as well as having similar deposition of sediment infill. The features also have good bedrock topography data sets and sedimentary infill data available to allow for further morphological analysis.

3.3.2.2 *Kalamalka Lake*

Introduction

Kalamalka Lake is located 5 km to the east of Okanagan Lake, and has a north-northeast- south- southwest orientation. Kalamalka Lake is ~16 km long, 2-3 km wide, and has a maximum bedrock depth of 417 m, with a pronounced bifurcation at the NNE end. The lake's sedimentary infill reaches a maximum thickness of 272 m. The bedrock morphology and sedimentary stratigraphy has been investigated by MacAulay and Hobson (1972), Fulton (1972) and Mullins et al. (1990).

Topographic setting

See Okanagan Lake section (Section 3.2.2.1).

Bedrock geology

The bedrock geology of the lake and surrounding area is reported by Mullins et al. (1990) as being part of the Shuswap Metamorphic complex. The complex is made up of Precambrian, Paleozoic and Mesozoic plutonic, volcanic and sedimentary rocks which underwent metamorphism during convergent tectonics. Previous work on the region has suggested that Kalamalka Lake, similar to Okanagan Lake, has a strong structural control on its location (Ross, 1981; Okulitch, 1984). Mullins et al. (1990) go on to state that this structurally controlled preferential erosion would have initially been undertaken by the regional fluvial drainage network.

Previous morphologies

The previous bedrock morphological work undertaken by Mullins et al. (1990) shows that Kalamalka Lake has two nested overdeepenings, reaching maximum bedrock depths of 417 m and 296 m below lake level. The bedrock mapping also indicates another much smaller nested overdeepening in the most northerly bifurcation (located at the headward end of the feature), of a maximum bedrock depth of 100 m below lake level. The seismic profiles and bedrock maps produced by Mullins et al. (1990) seem to indicate that the cross-valley profile is more V-shaped than U-shaped. Mullins et al. (1990) propose that the overdeepening was formed due to fast flowing ice transporting large volumes of sediment that preferentially eroded this specific area due to a pre-existing structurally controlled fluvial valley (Fig.3.23).

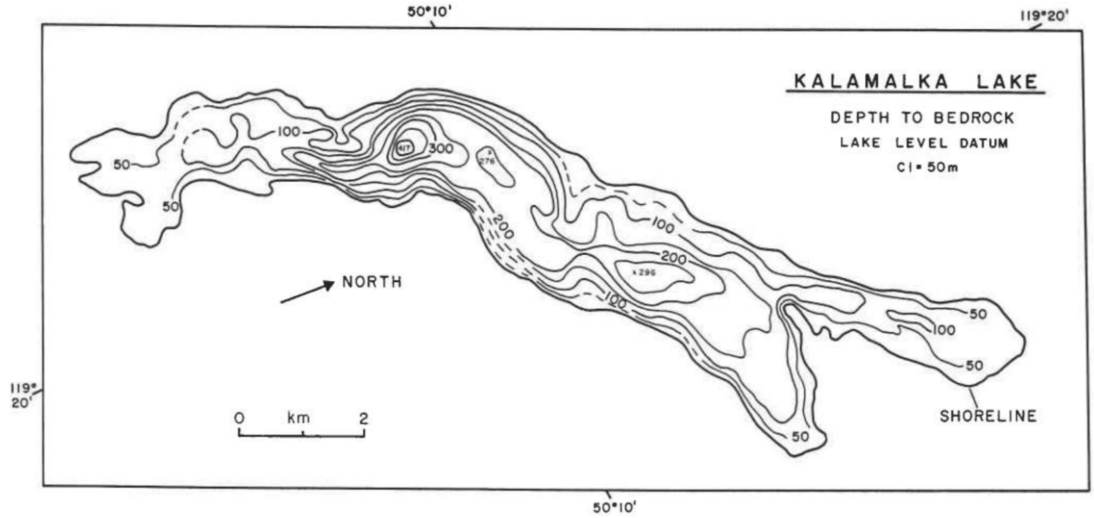

Figure 3.23: Bedrock topography map produced from seismic profiles. Lake level is used as datum (~391 m). Maximum bedrock depressions extend as much as 417 m below lake level (26 m b.s.l.). Figure from Mullins et al. (1990).

Sediment infill

Mullins et al. (1990) have interpreted the seismic reflectors of the sedimentary units in the lake. The thin upper sedimentary unit has been interpreted to be a water-saturated unit of rhythmic glaciolacustrine silt deposited during deglaciation. The middle 272 m thick sedimentary unit has been interpreted as being till, and the final bottom sedimentary unit has been interpreted as being a water- saturated unit of laminated, rhythmically bedded silts and clays, ripple laminated sand and pebbly sands, and boulder gravel deposited during glacial advance. Mullins et al. (1990) made these interpretations in conjunction with data collected by Fulton and Smith (1978) for the Kamloops Lake Drift.

The sedimentary and surface geology of the area of Kalamalka Lake and surrounding area was mapped by Nasmith (1962) and Fulton (1965), who reported that it consisted of rock outcrops with patches of drumlinised till on the uplands, and lacustrine deposits. These deposits have been associated with a complex history of ice-dammed lake formation during deglaciation.

Data availability

There have been few relevant studies, and due to the age of these, available data on lake morphology is likely only in printed form. The table below outlines the main data types and sources found for the lake and the region.

Table 3.7: Kalamalka Lake data availability table.

Data type	Data source	Reference publication
Bedrock Geological map	Geological Map of British Columbia (Scale 1":20 mile)	Little (1962)
Sedimentary Geological map	-	Fulton (1995), Nasmith (1962)
Seismic stratigraphy	-	Mullins et al. (1990)
Sedimentary core logs	No cores found	-
Glacial feature and Ice extent maps	Geological Survey of Canada, (1968). Glacial Map of Canada. Map 1253A, scale 1:5 million	Church et al. (2010), Prest et al. (1968)
Regional Surface DEM	Shuttle Radar Topography Mission (SRTM) (30 m resolution)	USGS (2004)
Regional Bedrock topography DEM	No bedrock DEM found	-

Analogue potential

Kalamalka Lake has been determined as being a good analogue site when analysed in conjunction with Okanagan Lake and other features in British Columbia, due to its similar morphology, and the availability of good bedrock topography data set.

3.3.2.3 *Shuswap Lake*

Introduction

Shuswap Lake is located in southern British Columbia (51°00'00"N 119°00'55"W) ~200 km north of the USA-Canada border (Eyles and Mullins, 1997). The lake is made of two main basins that run in a northeast-southwest orientation, and are joined approximately in the middle, producing a rough overall "X" shape morphology. The two lake basins are each ~60 km long, with the basins reaching a maximum width of ~3 km, and the maximum bedrock depth of each of the basins being recorded as 643 m (Shuswap lake) and 551 m (Salmon arm) b.l.l.. The lake morphology and seismic stratigraphy has been studied by Eyles and Mullins (1997), the regional geology and sedimentary cover has been mapped by the British Columbian Geological Survey (BCGS), as well as being studied by Okulitch (1989); Brown and Murray (1987); Erdmer and Cui (2009).

The regional tectonics of the area have been studied by Brown and Murray (1987), MacAulay and Hobson (1972), Vanderburgh and Roberts (1996), Okulitch (1989), and Erdmer and Cui (2009), who found that the valley incised into the Shuswap Highlands has a strong structural component. Thus the lake is located in the northern end of a structurally-controlled valley system that extends southwards through the North Okanagan Valley, through Okanagan Lake and past the border of the USA. The lake and the surrounding area are therefore significantly faulted. However, the geological maps of the area do not show any faults parallel with the main direction of the two lake arms.

The climatic setting of the previous glaciations has been investigated by Alley (1976a), Alley (1976b), who reports that the region of the Shuswap Highlands shows evidence of four main Holocene glacial advances, the oldest being between 4-5 ka BP, then 2.3 ka BP and 3.2 ka BP, with the youngest being reported as occurring "at some time in the last several centuries" (Duford and Osborn, 1978). Eyles and Mullins (1997) suggest that the sedimentary deposits were laid down in an ice-frontal lake during the late Wisconsin deglaciation approximately 10 ka BP.

Duford and Osborn (1978) found evidence of an additional two Holocene glacial advances (the younger being the Raft Mountain Advance, and the older being the Dunn Peak advance). The oldest Dunn Peak advance has been proposed as potentially correlating with an Early Holocene advance, evidence of which has been noted in other areas of the Canadian Rockies and northern American Rockies. (Duford and Osborn, 1978).

Topographic setting

Shuswap Lake is located, similar to Okanagan Lake and Kalamalka Lake, in the foreland of the Columbia Mountains, and the Shuswap and Okanagan Highlands. The lakes occupy the low points in two valleys that start in the Columbia Mountains and is orientated southwest through the Shuswap and Okanagan Highlands into the Thompson Plateau. The valley sides reach maximum heights of ~2,000 m in the north of the lake and ~1,600 m in the south. The location of the lake basins in the surrounding topography has been influenced by the presence of large-scale faults in the region (Nesje and Whillans, 1994; Okulitch, 1979; Okulitch, 1989).

Bedrock geology

The bedrock geology of the surrounding area of Shuswap Lake has been mapped by the BCGS, as well as being studied by Okulitch (1989); Brown and Murray (1987); and Erdmer and Cui (2009). The bedrock is recorded by the BCGS as being made up of intrusive rocks of the middle to late Jurassic and volcanic rocks of the late Tertiary in the northeast. The surrounding area of the central part of the lake is mostly made up of metamorphic rocks of Mesozoic, Paleozoic and Late Proterozoic age. There are also extensive sedimentary deposits recorded in the east, west and south from the lower Paleozoic and upper Proterozoic (Cui et al., 2017). The metamorphic rock is reported to be part of the Shuswap complex which was formed during the accretion of Mesozoic terrains across the western margin of the North American Plate (Eyles and Mullins, 1997; Okulitch, 1989).

Published morphologies

The bedrock morphology of Shuswap Lake has been imaged during a high-resolution, single- channel seismic reflection investigation by Eyles and Mullins (1997), and shows that the two subparallel basins are each ~60 km long and up to a maximum of 3 km wide in the south-eastern leg. The seismics record a maximum bedrock depth of ~643 m b.l.l. The basin cross-sections have not been measured quantitatively, but are shown by Eyles and Mullins to be more V-shaped than U-shaped. This is explained by Eyles and Mullins (1997) as being due to the valley being eroded by both ice and melt water, and that the melt water played a major role in the erosion of the basins along the tectonically weakened valleys.

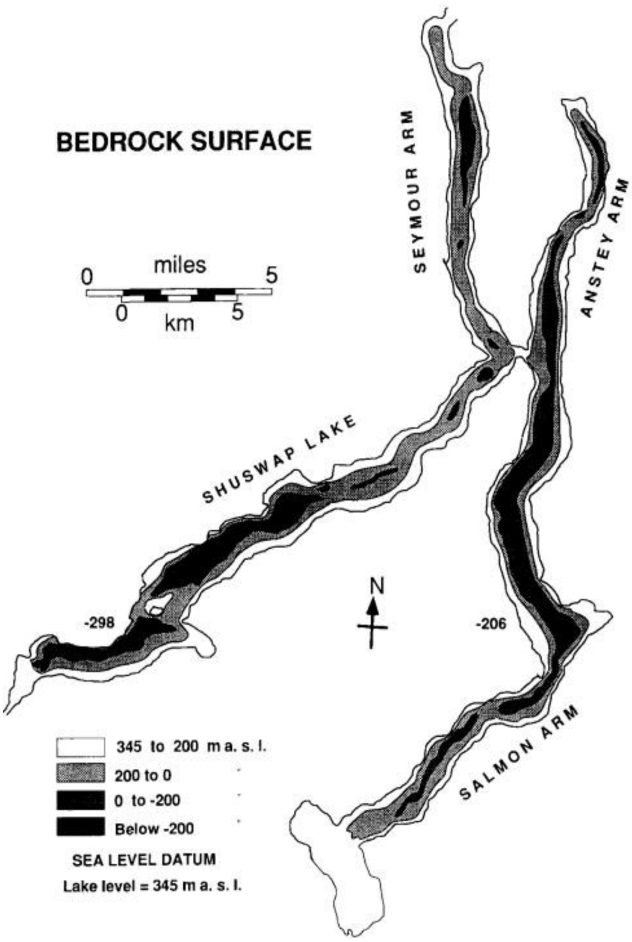

Figure 3.24: Bedrock surface topography map. Figure from Eyles and Mullins (1997).

Sediment infill

Eyles and Mullins (1997) have recorded the sedimentary stratigraphy of Shuswap Lake through a high-resolution, single-channel seismic reflection investigation using a bolt airgun source.

The sedimentary infill has been split into three distinct seismic units. The sediment infill has been recorded as reaching five main local maximum thicknesses of up to 329 m, 403 m, 454 m, and 600 m (Eyles and Mullins, 1997). The sedimentary units have not been dated by any direct method, however dates have been inferred from correlation of the sedimentary units with dated sediments of the South Thompson Valley immediately west of Shuswap Lake, which is stated to be late Wisconsin in age, approximately 14.2 ka-2.3 ka BP (date measured using thermoluminescence dating by Berger (1985)).

Seismic-Stratigraphy Sequence (SSS) I (oldest)

The seismic reflector of this unit is described by Eyles and Mullins (1997) as having a generally flat lying upper surface, and is recorded as lying directly on top of bedrock, and overlain by the following two units. The unit has been recorded as having a varying thickness and distribution. The unit has been recorded as continuous in the Anstey Arm and the Salmon Arm, but restricted to the deep bedrock sub-basins in the Seymour Arm and Shuswap Lake. The unit is characterised by a chaotic seismic profile. A distinct unconformable relationship is recorded between SSS I and SSS II to the north of Copper Island.

The sediments of SSS I have been interpreted by Eyles and Mullins (1997) as having a strong likelihood of being ice-contact glaciolacustrine deposits made up of deformed and differentially compacted silts, sands and gravels. The chaotic nature of the deposits suggests rapid dumping and slumping of debris at or under a retreating ice margin.

Seismic-Stratigraphy Sequence (SSS) II

The SSS II unit has been recorded by Eyles and Mullins (1997) as onlapping both SSS I and bedrock on the side slopes of the basins. The SSS II has been described by Eyles and Mullins (1997) as being characterised by a planar upper surface, with a distinct down-basin slope in several parts of the lake basin. It also has a well-stratified seismic profile with continuous high-frequency reflections, and massive reflection-free seismic zones. The seismic profiles of SSS II have been interpreted by Eyles and Mullins (1997) as being characteristic of glaciolacustrine sands and silts deposited by density currents from a point source (such as a fan delta).

Seismic-Stratigraphy Sequence (SSS) III (youngest)

The SSS III has been described by Eyles and Mullins (1997) as a very well-defined unit with closely spaced, and very high-frequency, parallel continuous seismic reflectors. The unit seems to fill the topographic lows in the underlying SSS II and is only found in areas of water depth greater than 10 m. The seismic reflectors of SSS III have been interpreted as being characteristic of laminated postglacial silts which are seen in similar settings elsewhere in British Columbia.

Data availability

Shuswap Lake has moderate to good morphological and geologic data availability. Due to the time that the seismic data was collected it has only been possible to obtain published diagrams, and not the raw data. The table below outlines the main data sources found for the lake and the region.

Table 3.8: Shuswap Lake data availability table.

Data type	Data source	Reference publication
Bedrock Geological map	Geological Map of British Columbia (Scale 1″:20 mile)	Little (1962)
Sedimentary Geological map	No Sedimentary Geological map found	-
Seismic stratigraphy	-	Eyles and Mullins (1997)
Sedimentary core logs	No cores found	-
Glacial feature and Ice extent maps	Geological Survey of Canada, (1968). Glacial Map of Canada. Map 1253A, scale 1:5 million	Church et al. (2010), Prest et al. (1968)
Regional Surface DEM	Shuttle Radar Topography Mission (SRTM) (30 m resolution)	USGS (2004)
Regional Bedrock topography DEM	No bedrock DEM found	-

Analogue potential

Shuswap Lake has been determined as being a good analogue site due to its topographic and climatic setting, interesting morphology and scale; however, due to the lack of high-quality bedrock topography data, set crosssectional and long profile geomorphological analysis is not possible to a high enough quality. Therefore, the Shuswap Lake feature should not be taken forward for further study as part of this work.

3.3.3 *New Zealand*

3.3.3.1 *Southern Alps*

Introduction

There are several large overdeepened lake basins present in the foreland of the Southern Alps on the southern island of New Zealand (Fig.3.25). Their scales, spatial locations and distribution, and areal extents have been reported to show strong similarities to those of the NSF (Fitzsimons and Veit, 2001).

Previous work undertaken by Fitzsimons and Veit (2001), Upton and Osterberg (2007), Alexander et al. (2014), Barrell (2011), Irwin (1970), Irwin (1973), Irwin (1978), Warren and Kirkbride (1998), Warren and Kirkbride (2003), Carter and Lane (1996), Brodie and Irwin (1970), and Lowe and Green (1992) has shown that the New Zealand Southern Alps are comparable to the Eurasian Alps due to the high alpine topography, piedmont lobe mountain glaciation during the Quaternary, and large glacial lakes. However, Fitzsimons and Veit (2001) also point out several differences, the main one being that the mega scale lithology and overall orogenic structures present in the Southern Alps are more simplistic due to the orogeny being derived from only one type of source: the New Zealand Geosyncline. Further, uplift and denudation rates in the Southern Alps are orders of magnitude greater than that of the European Alps. The former is due to the tectonic setting, while the latter is due to the orientation of the Southern Alps in relation to the westerly winds, and the proximity of the Pacific Ocean (Fitzsimons and Veit, 2001).

A great many of the foreland lake basins, including Lake Tekapo, Lake Godley, Lake Maud, Lake Hooker, Lake Ohau, Lake Coleridge and Lake Te Anau, have been the subject of published studies (Upton and Osterberg, 2007; Barrell, 2011; Irwin, 1970; Irwin, 1973; Irwin, 1978; Warren and Kirkbride, 1998; Warren and Kirkbride, 2003; Carter and Lane, 1996; Brodie and Irwin, 1970; Lowe and Green, 1992), with bathymetric data being abundant. Significant time was spent investigating what seismic data was available for the different overdeepenings in the Southern Alps foreland, but no relevant data was found. This lack of seismic data was corroborated through personal communication with David Barrell of New Zealand's Geological Survey (GNS).

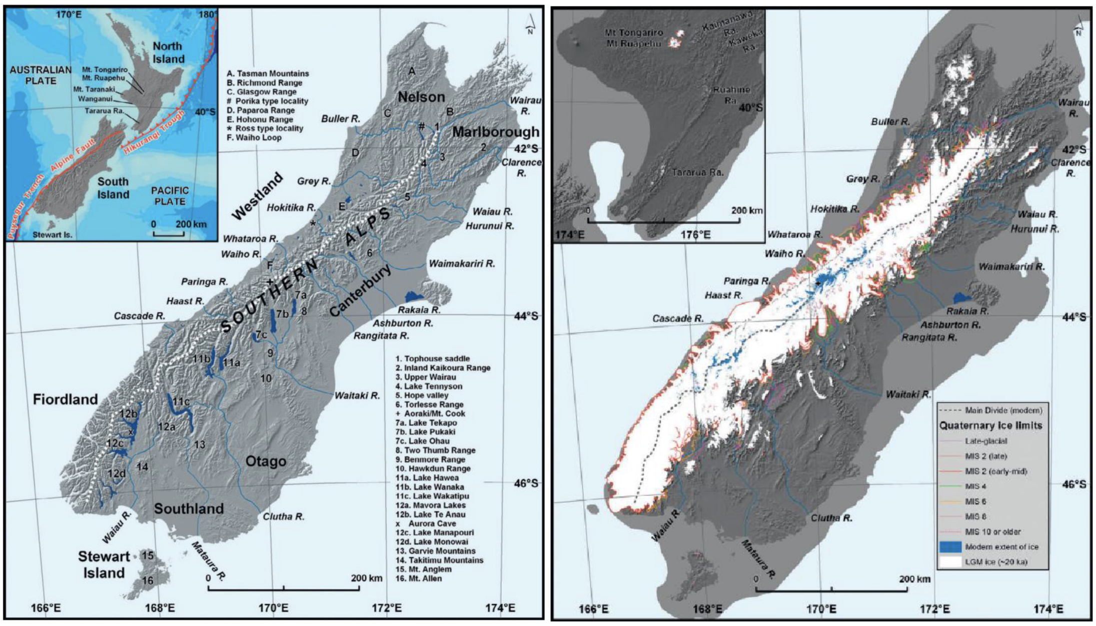

Figure 3.25: Map showing geographic location of the largest lakes in New Zealand (left), and map of mapped Quaternary ice limits for New Zealand (right). Figures from Barrell (2011).

Topographic setting

All of the above overdeepened glacial features are pro-alpine, and located in the foreland of the Southern Alps and Fjordland region of the southern island of New Zealand. The tectonic and topographic context of the lakes is therefore similar to that of the NSF. However, none are located entirely on the foreland, with the majority located mainly within the higher topography and extending onto the foreland for only a short distance (Fig.3.25).

Bedrock geology

The underlying geology of the southern island of New Zealand can be split into greywacke, Otago schists, old volcanic arc and related sediments, and Tuhua rocks (Fitzsimons and Veit, 2001)(Fig.3.26). The rocks of the southern island record evidence of three major tectonic orogenic events: the Tuhua (Devonian to Carboniferous), the Rangitata (Cretaceous) and the Kaikoura (Cenozoic till present) events. The major faults associated with the orogeny of the Southern Alps all trend southwest-northeast parallel with the mountain range (Fitzsimons and Veit, 2001). Extensive geological mapping has taken place across the whole of New Zealand by the GNS and can be accessed for free at a scale of 1:250,000 for both the north and south islands (GNS Science Geological Map 1 - Geological Map of New Zealand 1:250 000). After a preliminary review of the published CGBL locations in relation to the geological data, it is noted that the location of CGBL formation does not appear to have a lithological control. However, the location and orientation of the major CGBLs does appear to have a structural control. All the large CGBLs appear to either show influence by the large normal and thrust faults parallel to the direction of compression or by the smaller faults that form perpendicular to the main direction of compression (GNS Science Geological Map 1 - Geological Map of New Zealand 1:250 000).

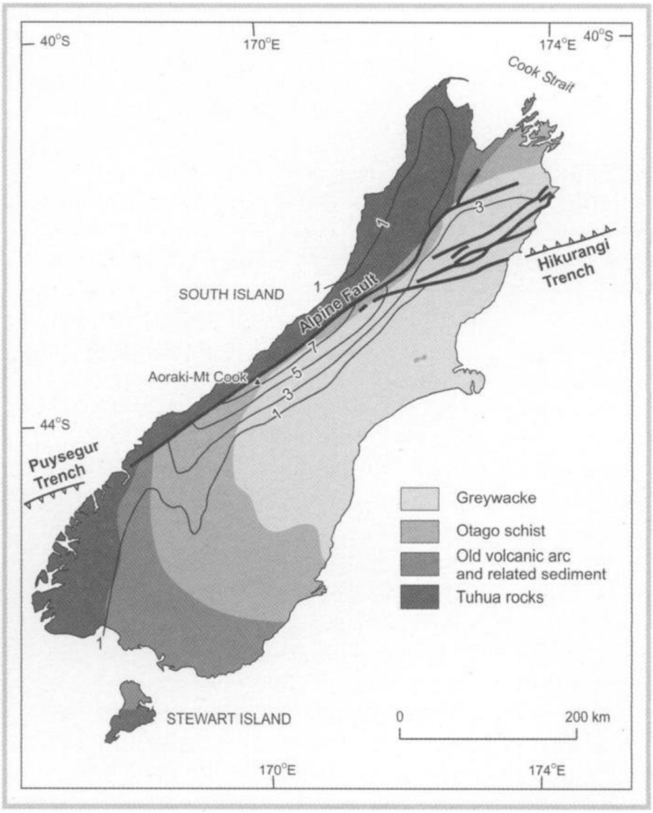

Figure 3.26: Map of New Zealand's southern island's simplified geology, from Fitzsimons and Veit (2001).

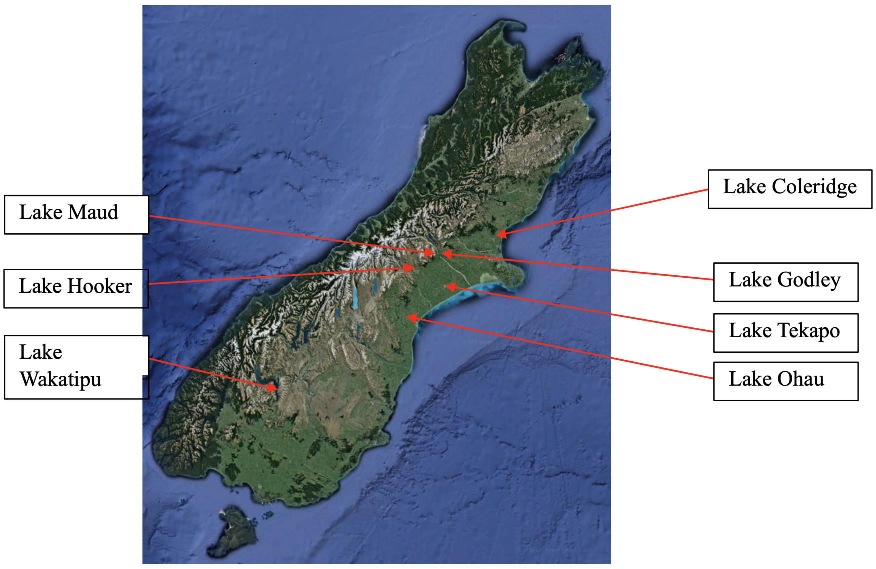

Figure 3.27: Map of locations of published morphologies.

Published morphologies

Lake Tekapo

The previous work undertaken by Irwin (1973) and Irwin (1978) reports that Lake Tekapo is a glacially overdeepened lake located to the east of the Southern Alps on the South Island in New Zealand. The lake is approximately 27 km long and has a maximum width of 6 km, and an average of 3.5 km. The lake generally tapers towards the southern end. The overall surface area of the lake is recorded as 87 km^2. The lakes cross profile is described as having steep sides of about 90 m, and a relatively flat bottom (Figs. 3.27, 3.28, and 3.29).

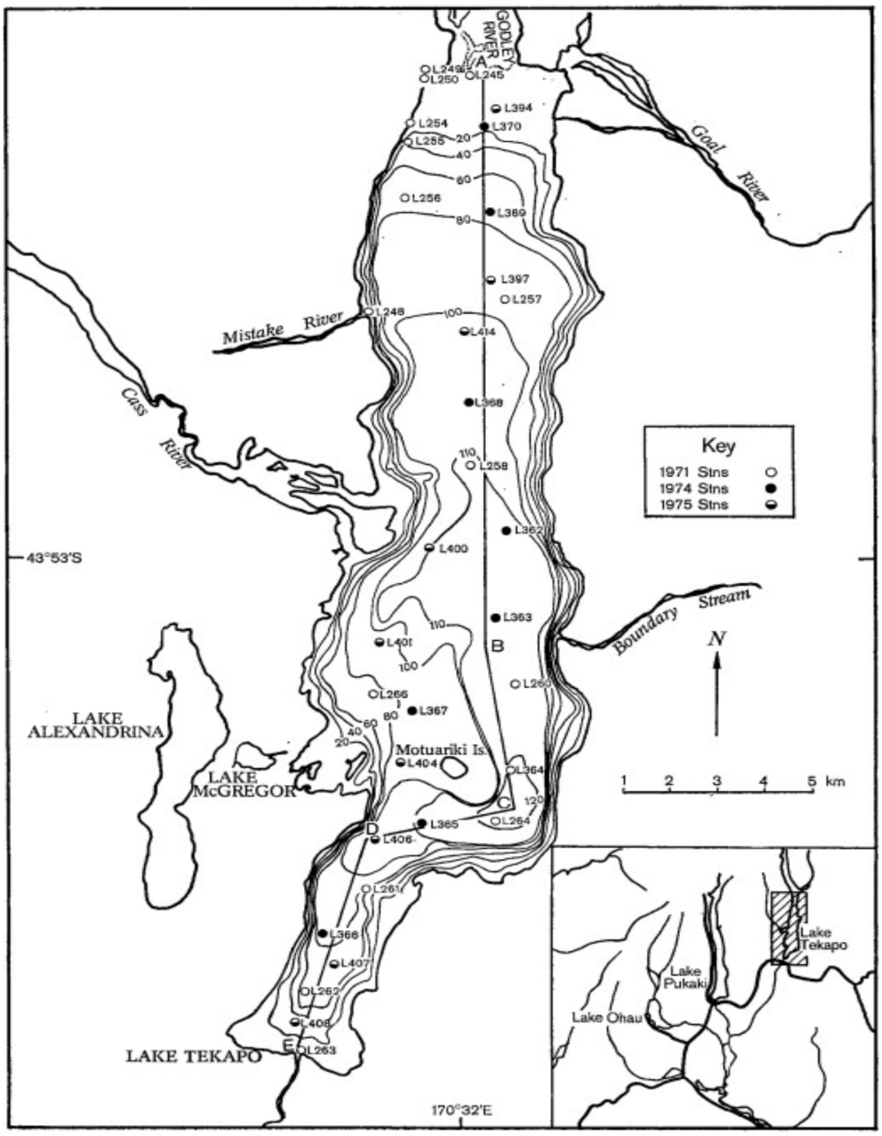

Figure 3.28: Sketched bathymetric map of Lake Tekapo from Irwin (1978) using measurements published by Irwin (1973).

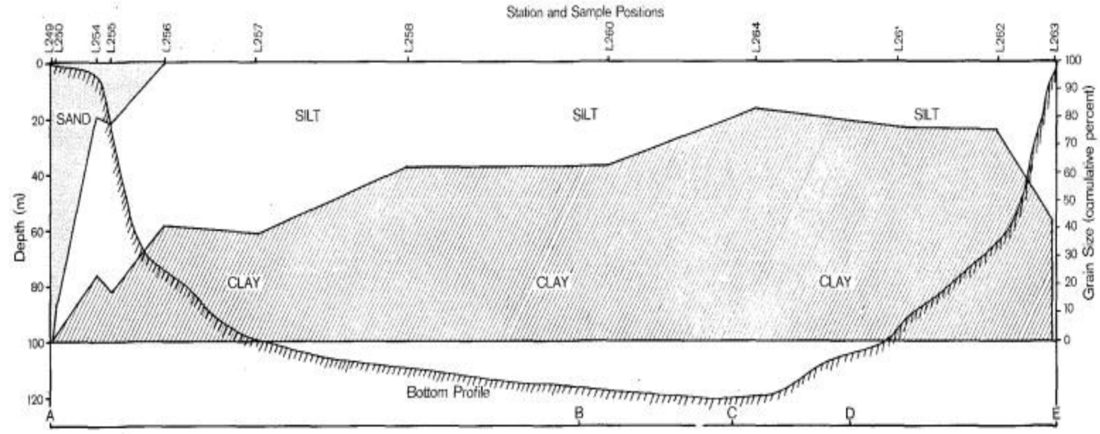

Figure 3.29: Schematic longitudinal profile of bathymetry and lake sediments in Lake Tekapo, 1971 (profile A to E shown in 3.28). Figure shows the weight distribution of particle size alone profile A to E in Irwin (1978). Figure from Irwin (1978).

Lake Godley, Lake Maud and Lake Hooker

Lake Godley, Lake Maud and Lake Hooker have been studied by Warren and Kirkbride (1998),Warren and Kirkbride (2003), and are recorded as being all relatively small glacially overdeepened lakes located in the Southern Alps, on the South Island of New Zealand. All three of the lakes are relatively small in comparison to the other potential analogues, and have only relatively recently become ice free in the last 50–60 years (Warren and Kirkbride, 1998; Kirkbride, 1993). The lakes have bathymetric data collected (Warren and Kirkbride, 1998) but no published bedrock morphology maps have been found.

Lake Ohau

Lake Ohau, located in the central eastern section of the Southern Alps (44°14′40″S 16°951′19″E) has had its bathymetry mapped by Irwin (1970). The mapping only covers the bathymetry of the lake and does not measure the depth to bedrock. The lake is recorded as being ~18.6 km in length with the lake curving slightly to the east in the southern section. The lake has a maximum width of ~5 km, and a water depth of 129 m.

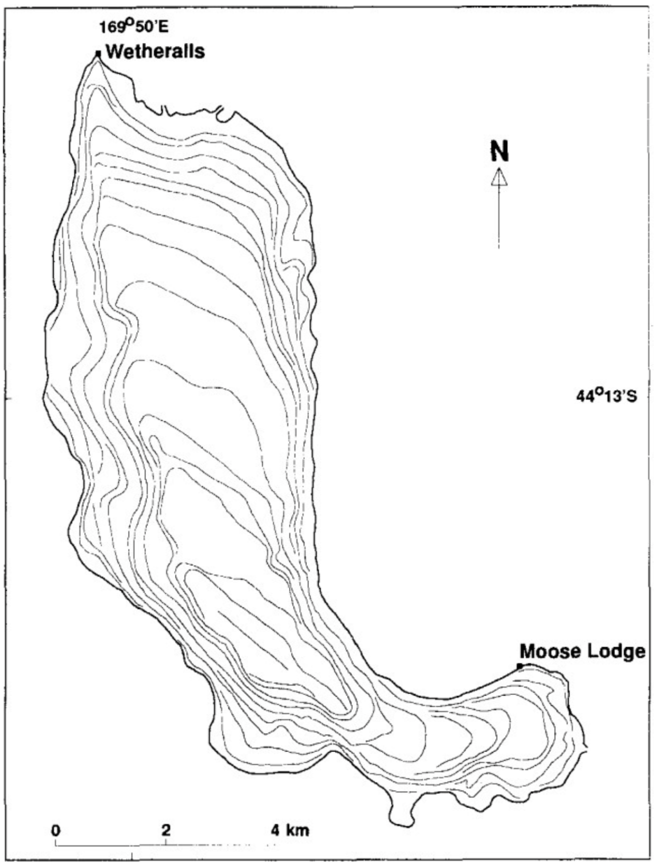

Figure 3.30: Bathymetric map of Lake Ohau, with irregular contour intervals selected to best show the measured bathymetry. Figure from Carter and Lane (1996) originally measured by Irwin in (1970).

Lake Coleridge

The depth of Lake Coleridge, located above the Rakaia Gorge in Canterbury in the Southern Alps (43°17′42″S 171°29′57″E) has been measured by Flain (1970). The measurements only cover the bathymetry of the lake and do not measure the depth to bedrock. The lake is recorded as being ~17.5 km in length, it has a maximum width of ~3.5 km, and a maximum water depth of 200 m.

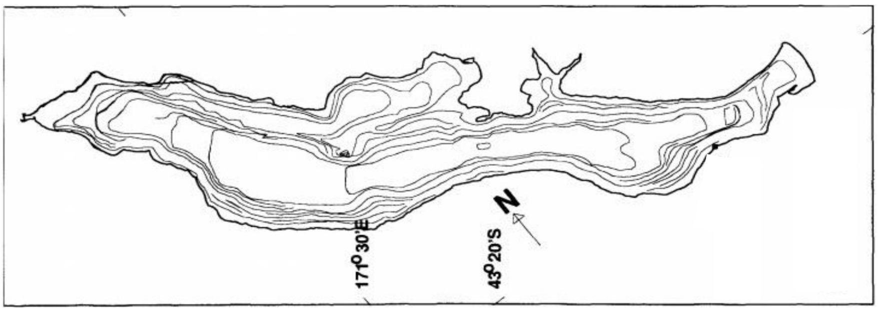

Figure 3.31: Bathymetric map of Lake Coleridge, with irregular contour intervals selected to best show the measured bathymetry. Figure from Carter and Lane (1996) originally measured by Flain in (1970).

Lake Te Anau

Lake Te Anau, located in the southwest of the South Island of New Zealand (45°15′20″S 167°45′19″E) has been measured by Irwin (1971). The lake has a much more irregular shape than the other lakes as it is formed by the confluence of four different glacial valleys. The measurements only cover the bathymetry of the lake and do not measure the depth to bedrock. The lake is recorded as being ~60 km in length. The lake has a maximum width of ~7 km not including the length of the tributary arms, and a maximum water depth of 425 m.

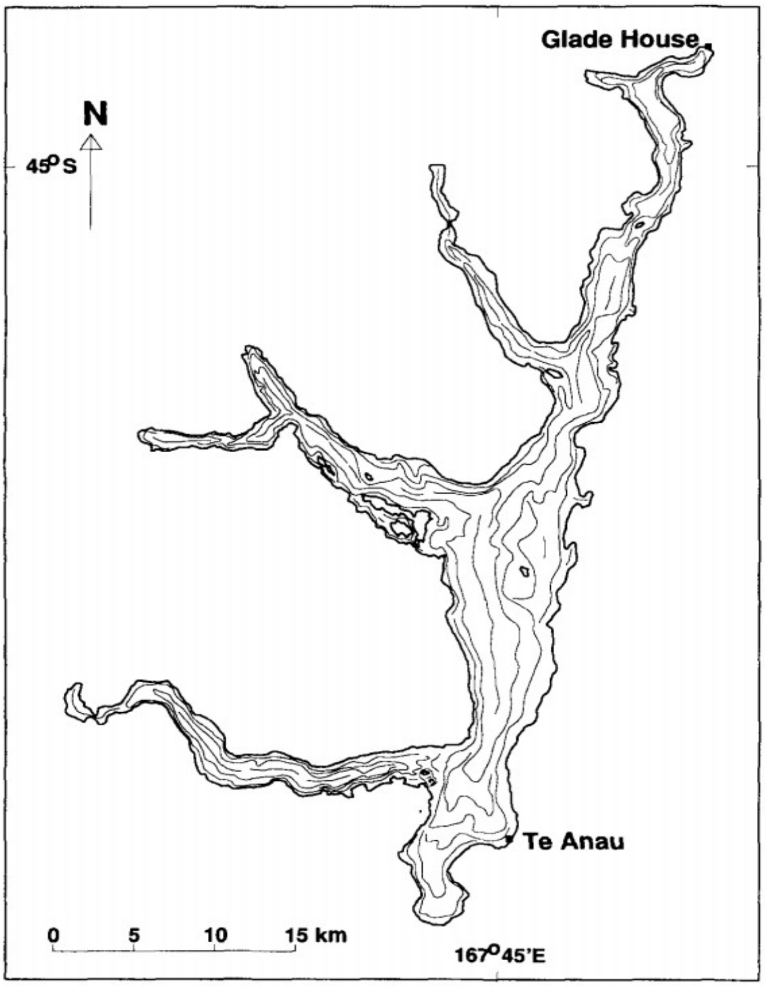

Figure 3.32: Bathymetric map of Lake Te Anau, with irregular contour intervals selected to best show the measured bathymetry. Figure from Carter and Lane (1996) originally measured by Irwin in (1971).

Data availability

No bedrock topography data sets were found, or seismic stratigraphy data sets that could be used to study the underlying bedrock morphologies of these lakes and sedimentary basins. However, surface topography DEM data is available (Land Information New Zealand DEM, 2012). There have been some geological data found consisting of boreholes, and large-scale surface mapping, as well as extensive bathymetric data sets on a large number of the glacial lakes. The table below outlines the main data sources found for the different lakes, and the rest of the southern island of New Zealand.

Analogue potential

The Southern Alps of New Zealand has been determined to not be a current viable option as an analogue region for the NSF. This is due to the lack of bedrock topography data sets for morphological analysis, but if more data were collected, the region has good analogue potential. The Southern Alps of New Zealand has a similar foreland setting to that of northern Switzerland, and the possible CGBL features have a similar scale, and appear to incise into bedrock.

Table 3.9: New Zealand data availability table.

Data type	Data source	Reference publication
Bedrock Geological map	Geological 1:250,000 scale maps	GNS
Sedimentary Geological map	Geological 1:250,000 scale maps	GNS
Seismic stratigraphy	No seismic stratigraphy found	-
Sedimentary core logs	No cores found	-
Bathymetric measurements	Varying scale maps	Irwin (1973), Irwin (1970), Flain (1970), Irwin (1971), Lowe and Green (1992)
Ice extent maps	-	Barrell (2011)
Regional Surface DEM	8 m DEM	Land Information New Zealand DEM (2012)
Regional Bedrock topography DEM	No bedrock DEM	-

3.3.4 *Greenland*

3.3.4.1 *Greenland*

Introduction

Overdeepenings in Greenland have been mapped by Patton et al. (2016b) using the terrestrial subglacial topography dataset produced by Bamber et al. (2013) merged with the International Bathymetric Chart of the Arctic Ocean dataset for the offshore areas of the marine shelf (Jakobsson et al., 2012). Patton et al. (2016b) measured 3948 individual subglacial overdeepenings, though overdeepening number and distribution was notably influenced by bed data quality. This was highlighted by the largest density of overdeepenings being measured in the Jakobshavn Isbrae catchment, an area that has been mapped at a much higher resolution. Some inaccuracies in mapping likely exist in certain fjord regions where bed elevations have been corrected by hand by Bamber et al. (2013). Patton et al. (2016b) observed the deepest overdeepenings to be predominantly in the high-elevation East Greenland mountain range.

The automated method of overdeepening identification and extraction used by Patton et al. (2016b) has meant that no depressions below their quality control criteria are present in their results (<2.5 km wide, <5 km long, and <40 m deep).

Topographic setting

Greenland has a wide range of topographic settings ranging from large tectonic basins under the centre of the Greenland ice sheet, large-scale mountain ranges in the southern and eastern margins of the ice sheet, with some areas of elevated topography also in the northwest, and finally foreland style setting on what is now the marine shelf on the eastern side of Greenland, shown in Figure 3.33.

Bedrock geology

The geology of Greenland has proved difficult to study in the past due to most of the large island being covered by the Greenland Ice Sheet. Using work undertaken by the Geological Survey of Denmark and Greenland (GEUS), as well as published work by White et al. (2016) and St-Onge et al. (2009) a general overview of the geological setting has been put together.

The geology has been extensively mapped by GEUS and has been shown to cover a wide range of lithologies, including crystalline rocks of the Precambrian shield, Proterozoic and Phanerozoic sedimentary rocks and metamorphic rocks of the Ellesmerian (low grade metamorphic amphibolite facies), and Caledonian fold belt (pelitic, semipelitic and quartzitic metamorphosed at amphibolite facies), and Palaeogene basalts and intrusions (Henriksen et al., 2009; White et al., 2016).

The bedrock interior of Greenland has been mapped by subjecting sand-sized ice-rafted debris from known glacial catchments to analysis of Pb-isotope compositions of feldspars and ^{40}Ar/^{39}Ar ages of hornblendes by White et al. (2016) (Fig.3.35).

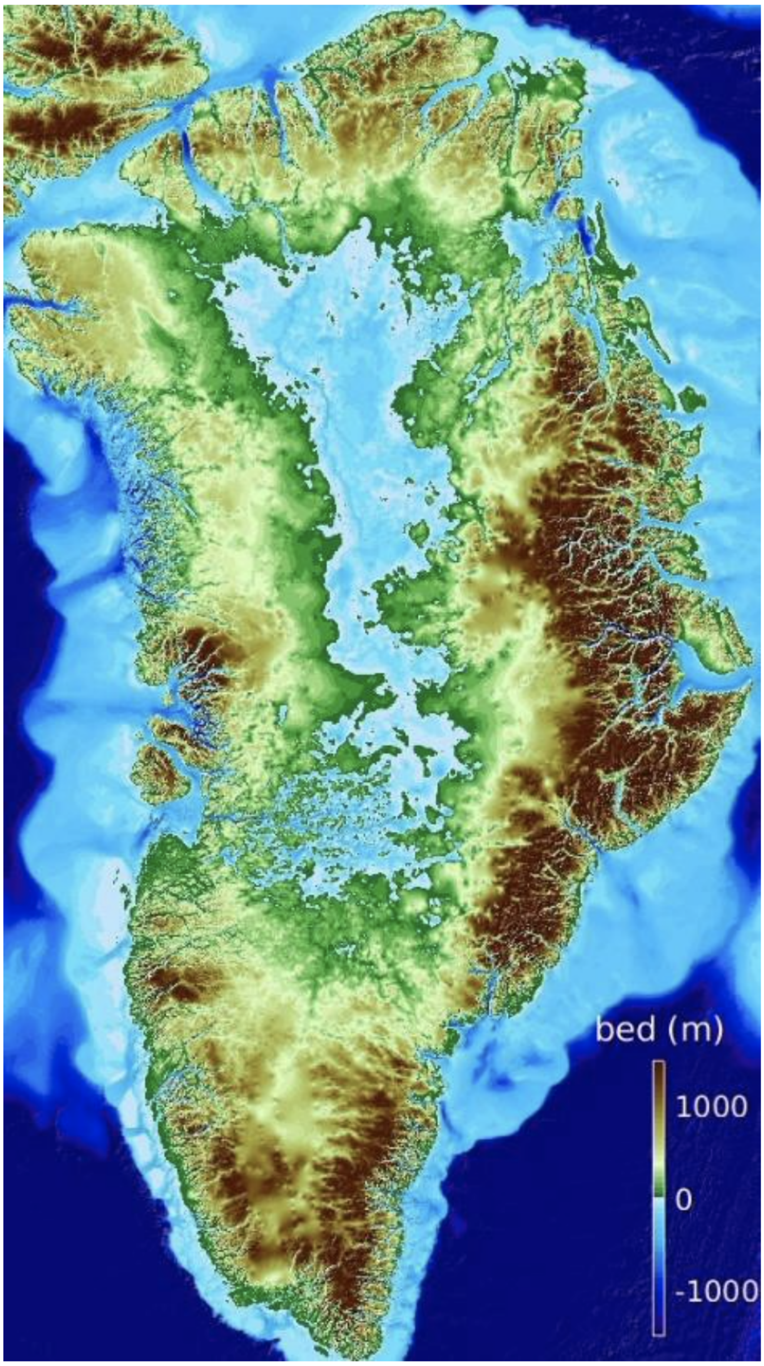

Figure 3.33: Map of Greenland bed topography produced by Morlighem et al. (2017).

Several large ice-free areas have been extensively mapped by the GEUS (https://eng.geus.dk/mineral-resources/greenland-and-geoscience-maps/geological-mapping). These maps are split into three main groups according to year of publication: 2000, 1985-1999, and 1967-

1984. The maps are at 1:100,000 scale and generally cover the west, southwest, central east and a small portion of the north.

Comparing the locations of the mapped overdeepenings by Patton et al. (2016b) (Fig.3.35) and the limited geologic maps obtained, there doesn't appear to be any strong correlation between lithology and the location of the overdeepenings. Due to the majority of Greenland being covered in ice, it is also unclear if there is any large structural control on the locations and orientations of the mapped overdeepenings. However, due to the filtering of the features during mapping by Patton et al. (2016b), features with strong structural control on morphology would most likely not be shown, as they would not pass the different morphology-based filtering processes used in producing the data.

The sedimentary cover and infill of the mapped overdeepened features has not been determined due to the large number of the features, and the difficulties associated with the geographic settings of the features either located under the ice sheet or on the marine shelf.

Published morphologies

The morphologies of the overdeepenings present under the current Greenland Ice Sheet have been summarised by Patton et al. (2016b), and are shown in the table below (3.10). The method used did not attempt to discriminate between overdeepenings and tunnel valleys (the criteria are described by Patton et al. (2015)).

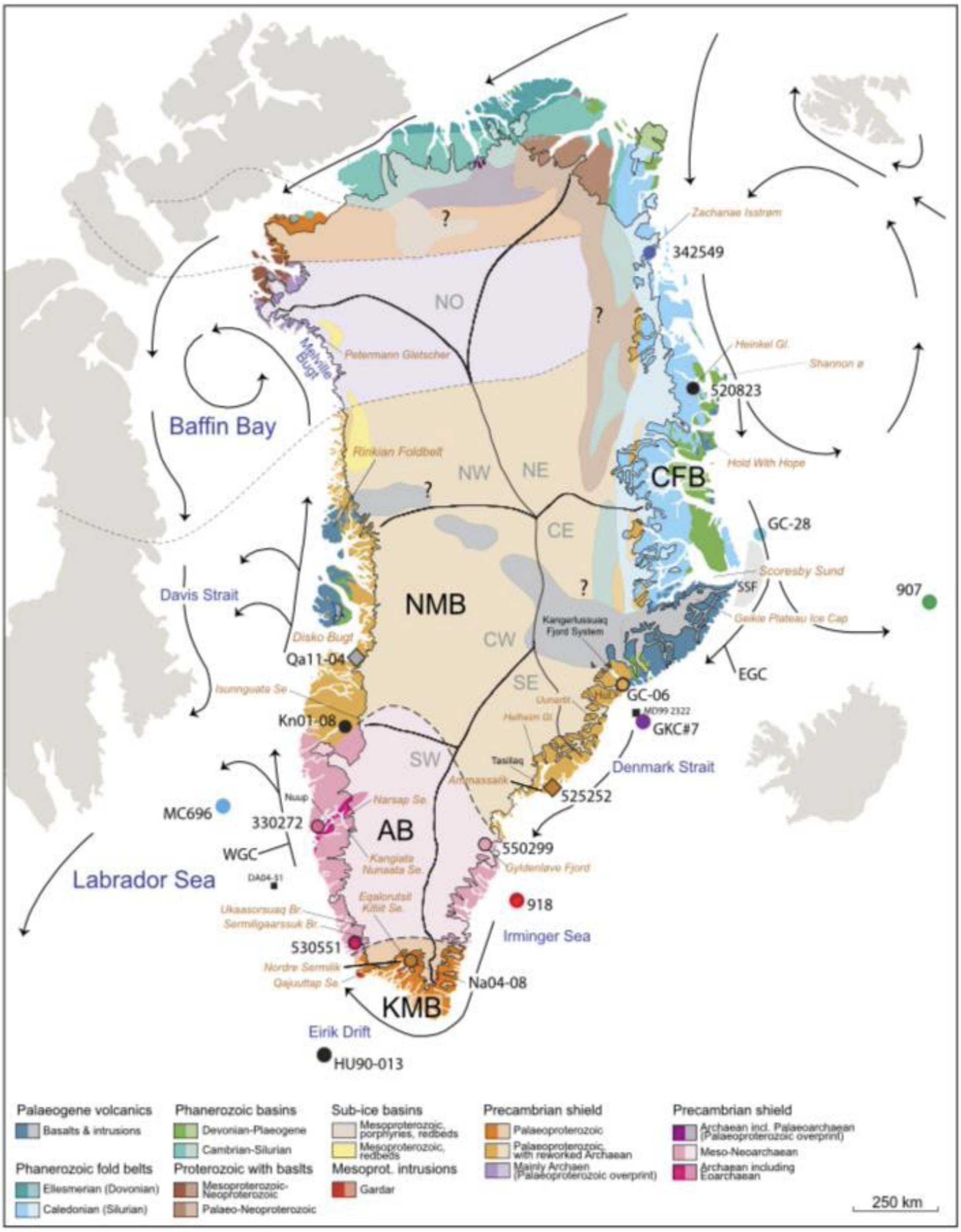

Figure 3.34: Geological map of Greenland with interpretation of sub-ice bedrock geology from White et al. (2016), modified from Dawes (2009).

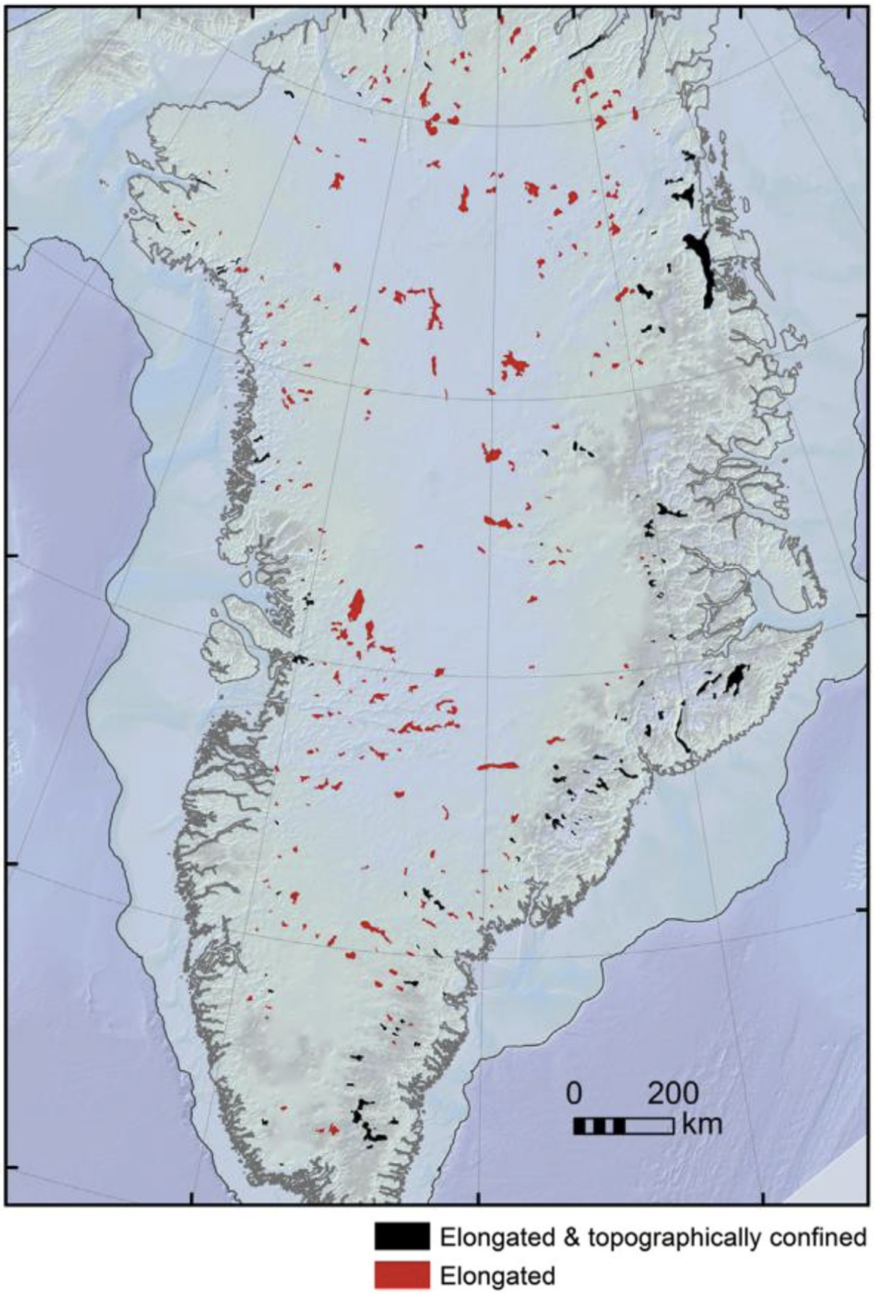

Figure 3.35: Map of locations of overdeepening used in the metric dataset (Table 3.10). Black polygons are overdeepenings that have been classified as topographically confined (i.e. those depressions where the mean relief within a small (20 km) buffer of the depression perimeter exceeds 500 m) Figure from Patton et al. (2016b).

Table 3.10: Greenland overdeepening morphometries measured by Patton et al. (2016b). The mapped overdeepenings are divided into elongated, and elongated and topographically confined. σ = standard deviation.

	Greenland		
	Mean	Median	σ
Depth to Sediment (m)			
Elongated	227	173	±195
Elongated and topographically confined	360	296	±249
Length (km)			
Elongated	22.2	17.1	±16.5
Elongated and topographically confined	24.5	16.8	±21.1
Width (km)			
Elongated	5.6	4.9	±3.2
Elongated and topographically confined	5.6	5.0	±3.4
Elongation ratio			
Elongated	4.05	3.43	±2.15
Elongated and topographically confined	4.40	3.70	±2.74
Lip elevation (m a.s.l.)			
Elongated	359	250	±469
Elongated and topographically confined	649	600	±569
Surface Area (km^2)			
Elongated	138	74	±241
Elongated and topographically confined	161	73	±349
Adverse-slope Length (km)			
Elongated	12.5	9.2	±9.5
Elongated and topographically confined	13.8	9.6	±11.8
Mean adverse-slope gradient			
Elongated	0.023	0.017	±0.023
Elongated and topographically confined	0.036	0.030	±0.030
Asymmetry (%)			
Elongated	-20.3	-22.0	±36.0
Elongated and topographically confined	-22.3	-21.6	±37.8
Adverse slope to surface slope relation			
Elongated	-3.64	-2.51	±3.43
Elongated and topographically confined	-3.69	-2.17	±4.20

σ = Standard deviation

Data availability

The spatial coverage of the bed topography is good for the Bamber et al. (2013) dataset and the newer improved dataset of Morlighem et al. (2017). Other datasets for smaller areas (not listed) also exist, which includes seismic and radar lines. For the purpose of this report, only the datasets that are most relevant for the study of the Greenland CGBLs have been cited. The table below outlines the main data sources found for the CGBLs and the surrounding areas.

Table 3.11: Greenland data availability table.

Data type	Data source	Reference publication
Bedrock Geological map	-	GEUS (2018), White et al. (2016), St-Onge et al. (2009)
Sedimentary Geological map	No sedimentary map found	-
Seismic stratigraphy	IceBridge Radar	-
Sedimentary core logs	No cores found	-
Ice extent maps	Greenland Ice Mapping Project (GIMP) DEM	-
Regional Surface DEM	ArcticDEM	-
Regional Bedrock topography DEM	BedMachineV3 (150 m resolution) GAP bed surface DEM (250– 500 m resolution) IceBridge Radar	Morlighem et al. (2017), Bamber et al. (2013)

Analogue potential

The CGBLs of Greenland show very good potential as a modern analogue of the NSF despite of the lack of active mountain ranges. The features located in Greenland are on the same scale as the NSF CGBLs, have similar morphologies, incise deeply into the underlying bedrock, and are forming under similar conditions to those that would have potentially been in place during the formation of the NSF CGBLs. Therefore, further insight into the formation of the NSF CGBLs can be gained by looking at the Greenland features that most closely match the NSF setting and morphology. However, due to the resolution of the available data sets (100s of meters) the large spatial area covered by the data sets, and the time constraints of the semi-automated mapping methods used in this thesis, it is not possible to take advantage of these bedrock topography DEMs. Therefore, Greenland as a single study region cannot be used for further analysis in this work.

3.3.4.2 *Humboldt Glacier*

Introduction

Humboldt Glacier is located in the northwest of Greenland. Livingstone et al. (2017) identified an extensive subglacial channel network of possible palaeofluvial or subglacial meltwater origin.

Topographic setting

The glacier is marine terminating and is located between two areas of elevated bedrock (Fig.3.36). The glacier is part of an ice stream that drains a catchment to the southeast, with the ice building up in the northern part of the central Greenland depression and flowing through the area of lower elevation (as shown in Fig.3.36).

Bedrock geology

The bedrock geology has been poorly mapped in the Humboldt Glacier region, with St-Onge et al. (2009), White et al. (2016), and Henriksen et al. (2009) describing the bedrock in the area as potentially being part of the Inglefield and Ellesmere metamorphic (low grade metamorphic amphibolite facies) and sedimentary rocks.

Published Morphologies

The northern section of the Humboldt is reported to be made up of a 15 km-wide trough, with adverse slopes reaching depths (unknown if sediment or bedrock) greater than 300 m b.s.l. and extending ~50 km inland from the ice margin (Livingstone et al., 2017). Livingstone et al. (2017) report that upvalley of the large troughs, the subglacial hydrology is developed into a dendritic and sinuous channel network (Fig.3.36), with the channels reaching as deep as 400 m, and 7 km in width, and with a width-to-height ratio of <5 consistent with V-shaped valleys (Fig.3.37).

The southern section of the Humboldt Glacier is much shallower, being reported as only reaching maximum bed depths (unknown if sediment or bedrock) of 220 m b.s.l. (Livingstone et al., 2017). The bed is also reported to not have any adverse slopes in this section, and dips across the ice flow (flowing to the northwest) towards the north. Livingstone et al. (2017) also reports the presence of a number of roughly linear channels, parallel with ice flow and oblique with bed slope, in the bed in the south of the glacier. The parallel channels reach up to 80 km long, and increase in size: 65 km inland of the ice margin, the channels are 1.5-2.5 km wide and <352 m deep; 10 km from the ice margin, their size increases to 2-4 km wide and <400 m deep. The channels have a ~5 km spacing and have a V-shaped cross profile (Livingstone et al., 2017). Figure 3.36 shows the location of the troughs and channels, and Figure 3.37 shows the cross profile of the large troughs.

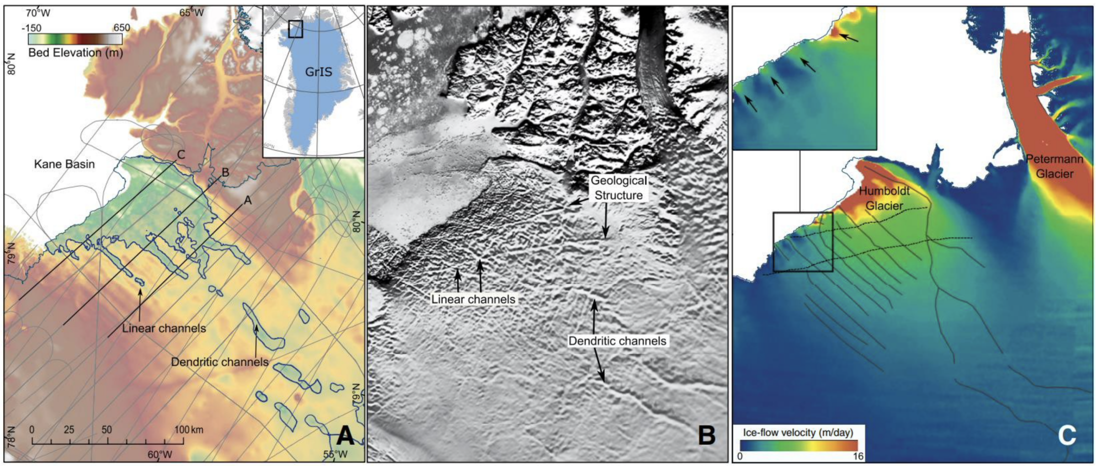

Figure 3.36: Mass-conservation bed DEM (Morlighem et al., 2017) of Humboldt Glacier with radio-echo sounding flight lines (left). Moderate-Resolution Imaging Spectroradiometer (MODIS) Mosaic of Humboldt Glacier (Haran et al., 2015) (centre). Ice velocity structure of Humboldt Glacier catchment (Joughin et al., 2010) (right). Figure from Livingstone et al. (2017).

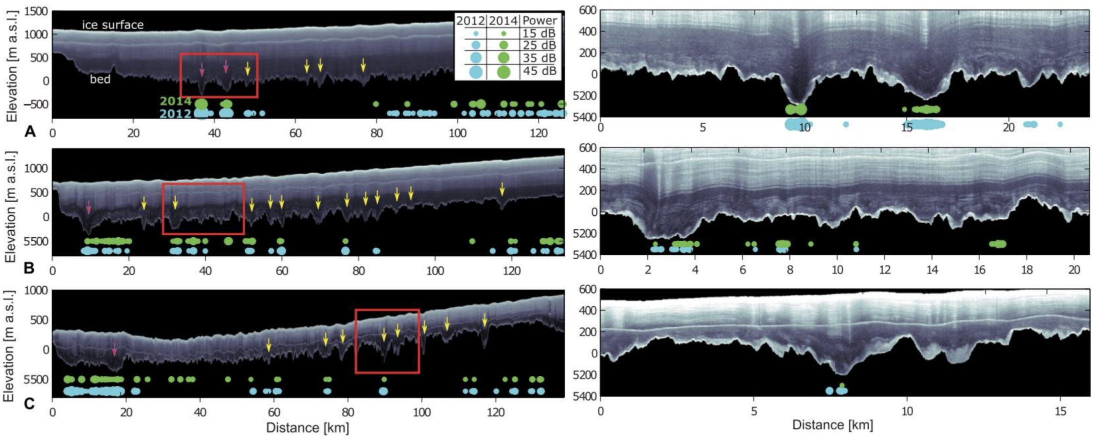

Figure 3.37: Ice penetrating radargram profiles running across paleofluvial and subglacial channels at three locations on Humboldt Glacier. Figure shows the general morphology of the features, and the high resolution and data quality. Figure from Livingstone et al. (2017).

Additional data on Greenland's bed topography is available through the BedMachine v3 data set (Morlighem et al., 2017), which covers the whole of Greenland and the Greenland coast at a 150 m horizontal resolution.

Data availability

The data availability for Humboldt Glacier is not as extensive as other areas due to the area being covered by ice and so limiting the types of studies able to be undertaken, combined with its remote location. The table below outlines the primary data sets that have been retrieved as part of this project.

Table 3.12: Humboldt Glacier, Greenland data availability table.

Data type	Data source	Reference publication
Bedrock Geological map	-	White et al. (2016), St-Onge et al. (2009)
Sedimentary Geological map	No sedimentary map found	-
Seismic stratigraphy	Ice penetrating radargram	Livingstone et al. (2017)
Sedimentary core logs	No cores found	-
Ice extent maps	Greenland Ice Mapping Project (GIMP) DEM	National Snow and Ice Data Center
Regional Surface DEM	ArcticDEM	-
Regional Bedrock topography DEM	BedMachineV3 (150 m resolution) Greenland Analogue Project	Livingstone et al. (2017), Morlighem et al. (2017), Lindbäck et al. (2014)

Analogue potential

The Humboldt glacier CGBLs have been determined as being a good modern example of tunnel valleys and subglacial meltwater erosion, and a good analogue of the NSF CGBLs. Its cross-sectional morphology shows comparable bedrock incision depths and feature widths, with the feature cross-sections being mapped to a very high resolution. The Humboldt glacier features are therefore determined to be a good example of bedrock incised CGBL features and suitable for further morphological analysis in conjunction with other sites.

3.3.5 *Antarctica*

Introduction

The recent work by Patton et al. (2016b) found 9905 overdeepenings across the continent of Antarctica, and features in several areas are potential analogues for features on the NSF. These features are generally located on the foreland of the Transantarctic Mountains and on the continental shelf close to the coastline.

The dataset used by Patton et al. (2016b) was the 1 km-resolution Bedmap2 bed topography dataset produced by Fretwell et al. (2013). Appropriate to the resolution of the bed data, the automated method of overdeepening identification used by Patton et al. (2016b) included quality control criteria that excluded depressions smaller than 2.5 km wide, 5 km long, or 40 m deep.

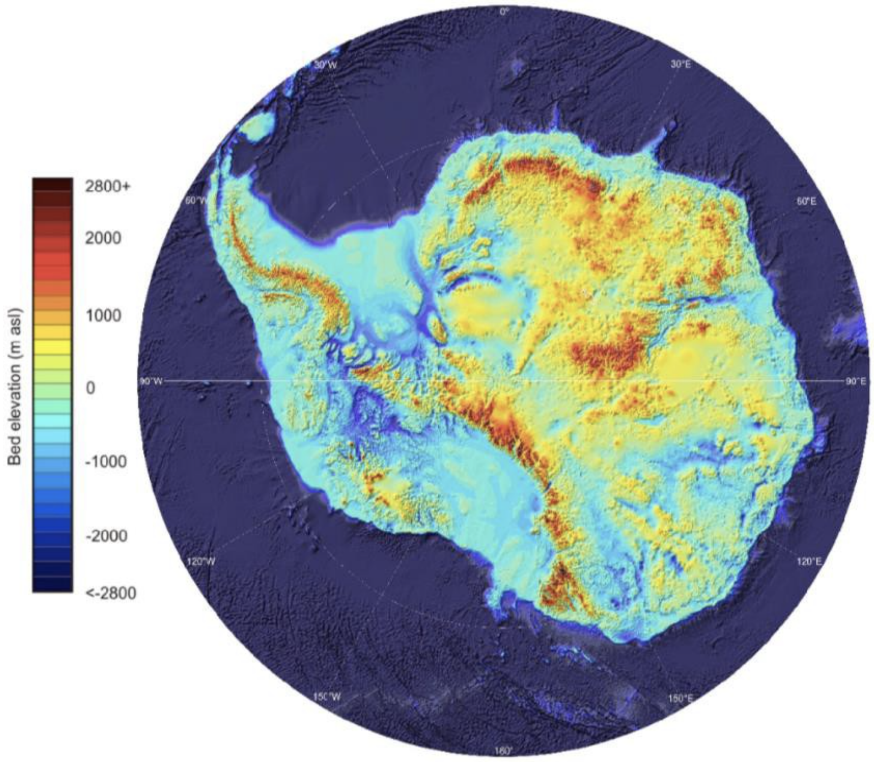

Figure 3.38: Bed topography map of Antarctica from Bedmap2 (Fretwell et al., 2013)

Topographic setting

The general topography of Antarctica can be split between the western Antarctic Peninsula and the larger eastern Antarctic continental land mass (Fig. 3.38). The west of Antarctica is made up of several smaller regions of higher bed topography, in an archipelago type topography, under the ice sheet, including the Antarctic Peninsula and the Vinson Massif in the Northwest, and an area of high ground at the margin of the continent at 120°W, beside the area of low topography occupied by the Pine Island and Thwaites outlet glaciers. The east of Antarctica has large areas of consistent high ground in its centre and north made up of the Gamburtsev Mountains under Dome Fuji, the Shackleton Range, and the Fimbulheimen and Thorshavnheine ranges in Dronning Maud Land. The bed topography under Dome C is shown to be much more undulating with far fewer areas of high elevation. The two areas are separated by the Transantarctic Mountains. The continent of Antarctica is also surrounded by a significant continental shelf (Fretwell et al., 2013),(Antarctica and the Arctic, British Antarctic Survey (BAS) 1:10,000,000).

Bedrock geology

The bedrock geology of the Antarctic continent is poorly understood due to the majority of the continent being covered by ice. However, significant work has been undertaken to study the areas near and at the margin of the ice sheet, as well as the sedimentary geology of the marine shelf (Craddock, 1970). The work that has been done has shown that the continent is comprised of a wide verity of lithology and has undergone a wide range of tectonic events (Craddock, 1970).

Published morphologies

The morphology of overdeepenings present under the Antarctic ice sheet has been summarised by Patton et al. (2016b), who used the BedMap2 data set (Fretwell et al., 2013) and the automated methodology put forward by Patton et al. (2015) to measure the morphometries of 9905 subglacial overdeepenings. The reported overdeepenings were filtered down to this number, and so does not include all overdeepened depressions present under the ice mass. Table 3.13 is from Patton et al. (2016b) and shows the measured morphometries.

Table 3.13: Antarctic overdeepening morphometries measured by Patton et al. (2016b). 'σ' = standard deviation. Depths unknown if bedrock or sediment.

	Antarctic		
	Mean	Median	σ
Depth (m)			
Elongated	222	169	$\pm$178
Elongated and topographically confined	290	233	$\pm$206
Length (km)			
Elongated	52.3	22.5	$\pm$340.2
Elongated and topographically confined	63.6	22.3	$\pm$481.4
Width (km)			
Elongated	8.5	6.8	$\pm$6.3
Elongated and topographically confined	8.0	6.4	$\pm$6.8
Elongation ratio			
Elongated	4.43	3.36	$\pm$8.77
Elongated and topographically confined	4.92	3.41	$\pm$12.10
Lip elevation (m a.s.l.)			
Elongated	-105	-150	$\pm$672
Elongated and topographically confined	81	0	$\pm$669
Surface Area (km^2)			
Elongated	468	140	$\pm$1584
Elongated and topographically confined	469	135	$\pm$1931
Adverse-slope Length (km)			
Elongated	25.6	11.2	$\pm$97.7
Elongated and topographically confined	26.9	10.4	$\pm$110.7
Mean adverse-slope gradient			
Elongated	0.018	0.013	$\pm$0.019
Elongated and topographically confined	0.024	0.018	$\pm$0.022
Asymmetry (%)			
Elongated	-14.6	-20.7	$\pm$40.6
Elongated and topographically confined	-14.5	-18.8	$\pm$40.8
Adverse slope to surface slope relation			
Elongated	-4.23	-3.02	$\pm$3.85
Elongated and topographically confined	-4.55	-3.20	$\pm$4.04

σ = Standard deviation

Data availability

The data availability for the continent of Antarctica is extensive and covers an extremely wide range of areas at varying resolution, and wide range of climatic time periods. For the purpose of this report only the datasets that are most relevant for the study of the Antarctic CGBLs have been cited. The table below (Table 3.13) outlines the main data sources found for the CGBLs and the surrounding areas.

Table 3.14: Antarctica data availability table.

Data type	Data source	Reference publication
Bedrock Geological map	Geologic Map	
of Antarctica		
(1:10,000,000 scale)	Craddock (1970)	
Sedimentary Geological map	No sedimentary map found	-
Seismic stratigraphy	IceBridge Radar	-
Sedimentary core logs	No cores found	-
Ice extent maps	-	Anderson et al. (2002), Bentley et al. (2014)
Regional Surface DEM	The Reference Elevation Model of Antarctica (8m spatial resolution)	Howat et al. (2019)
Regional Bedrock topography DEM	Bedmap2 (1:10,000,000 scale)	Fretwell et al. (2013)

Analogue potential

The CGBLs of Antarctica show very good potential as a modern analogue of the NSF. The features located in Antarctica have a wide range of sizes but there is a significant number that share a similar scale and morphology to those of the NSF CGBLs. The features are also found in a range of different topographic settings and areas of topographic confinement similar to that of the NSF. In addition to areas of analogue with the NSF, the area of Pine Island Glacier and the Dry Valleys has been determined to have been formed by subglacial meltwater, and would be a good region of study as a group of end member erosional features formed by subglacial meltwater. However, the region of Antarctica has similar issues to Greenland with regards to further analysis as part of this work. The available DEM resolution is quite coarse (1:10,000,000 scale) in comparison to that of the NSF, and the previous works by Patton et al. (2016b) have shown that a more automated mapping and analytical approach would be required to analysis the features to a high enough quality for comparison with the rest of the chosen study sites as well as the NSF features. Therefore, Antarctica as a single study region will not be taken forward for further analysis. However, the area of Pine Island Glacier and the Dry Valleys will be further investigated as an end-member example of subglacial fluvial erosion.

3.4 ADDITIONAL POTENTIAL ANALOGUE REGIONS

The following section highlights additional areas that may contain analogue sites that, due to time constraints, were not fully investigated.

3.4.1 *European Tunnel Valleys*

There is additional extensive literature on potential analogue tunnel valleys in Europe. However, these features have not been discussed here as they predominantly occur in sediments, with no features found that incise to comparable depths into bedrock. These features have been extensively studied with good data coverage, and the associated literature is shown in Table A.1 in the Appendix A. The features are reported to be, on average, several kilometres in length, with some reaching over 150 km long, and have widths ranging from hundreds of meters to up to 6 km. The incision depths of the tunnel valleys have been recorded mostly being less than 500 m in depth into soft sediment. (Stumm, 2010; Kehew et al., 2012).

3.4.2 *South America (Peru)*

A significant amount of work has been done on the overdeepenings in the Peruvian Andes due to their potential implications for future freshwater resources (Haeberli et al., 2016; Colonia et al., 2017). The work has focused on the high mountain overdeepenings and valley overdeepenings, with little work being undertaken on any of the CGBLs present in the foreland. In spite of the overdeepenings not being located in the same setting as the NSF CGBLs, the available data on these features may provide useful insight into whether overdeepenings and tunnel valleys are distinct phenomena or part of a spectrum of phenomena (Haeberli et al., 2016). However, due to time constraints, further investigation of the data availability, and suitability of the region as an analogue for the NSF, has not been able to be achieved.

3.5 STUDY SITE SELECTION

The data that has been chosen to take forward, for analysis as study sites, are the regions of northern Switzerland, the Finger Lakes (USA), Humboldt glacier (Greenland), and the British Columbian lakes of Okanagan and Kalamalaka (Canada). The Finger Lakes were chosen as the strongest analogue to the features of northern Switzerland. The published cross-sections and bedrock topographic maps show the features of the region seem to have similar morphologies, and are of a compatible scale with the features, reaching depths and widths of 442 m and 5.6 km respectively (Mullins and Hinchey, 1989; Mullins et al., 1996). The published works show that the region has a larger number of lithological units, but are comparable due to their sedimentary nature (Rickard and Fisher, 1970a).The features in the region are incised deeply into the underlying bedrock, and are found in a similar foreland-like topographic setting, which has been recorded as having similar past climatic conditions during formation (however, under an ice sheet not a piedmont lobe) (Yager et al., 2001). The Finger Lakes also have very good data availability, specifically the bedrock topography and sedimentary infill data required for the proposed morphological analysis. The Humboldt glacier CGBLs and British Columbian Okanagan and Kalamalka Lakes were chosen to be taken forward for morphological analysis as they showed morphological similarities with the features of northern Switzerland (with depths of up to 400 m and widths of 7 km), and varying similarities in regional setting as proposed climatic formation conditions (Livingstone et al., 2017). The Humboldt glacier CGBLs were chosen to be taken forward as they a good modern example of bedrock incised tunnel valleys and subglacial meltwater erosion. The region is not as good an analogue for the region of northern Switzerland as the Finger Lakes. However, the features' cross-profiles have been mapped to a very high resolution and the features are reported as being bedrock incised tunnel valleys, while the British Columbian features of Okanagan Lake and Kalamalka Lake are described as "fiord lakes" formed from glacial erosion in a foreland setting. When compared in conjunction with each other, the two features show similar morphology and scale to that of the NSF (reaching depths of up to 642 m below lake level (b.l.l.) and widths of >5 km wide), as well as having similar deposition of sediment infill (Eyles et al., 1991; Vanderburgh and Roberts, 1996; Shaw, 1977; Fulton and Smith, 1978). The features also have good bedrock topography datasets and sedimentary infill data.

3.6 END MEMBER SELECTION

The selection of end member locations was undertaken to identify locations that had likely seen a single type of dominant erosion during formation. The end member types of erosion that were selected for comparison with the study site locations were, glacial erosion (ice erosion), subaerial fluvial erosion (i.e. erosion by non pressurised water), and subglacial fluvial erosion (e.i. subglacial meltwater erosion including pressurised water). Six end members of erosion were selected, three using morphometrics calculated using the methods discussed in chapter 4 (the mountain valleys near Anchorage, Alaska, the valleys of the western side of the Hawaiian Island of Kauai, and the Labyrinth Dry Valleys, Antarctica), and three using published morphological measurements from valleys in New Zealand, the Tian Shan Mountains in China, and the bedrock channels on the Antarctic inner continental shelves (Augustinus, 1992; Li et al., 2001; Kirkham et al., 2020).

The large U-shaped valleys near Anchorage, Alaska were chosen as the examples of end member glacial erosion due to their strong U-shaped morphology, strong consensus in the literature of the ranges formation through dominant glacial erosion (Spotila and Buscher, 2004; Briner and Kaufman, 2008), and high topographic data availability (Porter et al., 2018). The main factor that was taken into consideration against this site as an end member of erosion was the recorded high uplift rate of the Alaska range, however the potential influence of this on the resulting valley morphology was reduced by taking a large number of cross-sectional measurements from a wide geographic area along the full lengths of the valley profiles.

The Hawaiian Island of Kauai was chosen as the example end member of subaerial fluvial erosion due to the age of formation of the island and global latitude (McDougall, 1979), and high topographic data availability. Both of these factors mean that the island cannot have been effected by glacial erosion. The valleys present on the island are therefore the result of subaerial erosion. A potential challenge of the use of Kauai as an end member of erosion is that the valley contains limited examples of bedrock geology due to its style of formation. Preliminary cross sectional analysis suggests that the underlying igneous bedrock geology has a minor effect on the resulting cross sectional morphology, with the effect of the bedrock geology also being mitigated by sampling across the whole western side of the island to capture as much variation in geology as possible.

The final chosen example end member of subglacial fluvial erosion was the Labyrinth Dry Valleys. The Dry Valleys were selected as they have high quality topographic data availability, and are proposed to have been formed by catastrophic outburst flooding (Denton and Sugden, 2005; Lewis et al., 2006; Kehew et al., 2012). The understanding of the formation of the Dry Valleys has developed over time with a fluvial origin being proposed for many years (Shaw and Healy, 1977; Armstrong, 1978), but they are now believed to have formed by catastrophic flooding (Denton and Sugden, 2005; Lewis et al., 2006). Additional supportive evidence of subglacial flooding has been shown in works such as Margerison et al. (2005), who performed cosmogenic dating on boulders in deposits from the Coombs Hills.

The authors identified the deposits as flood deposits and the dating suggests that there has been been minimal erosion in the area since the mid-Miocene. This dating shows there has been minimal erosion of the feature since the flooding in the mid-Miocene. The smaller cross sectional sampling size of the Dry Valleys have been supplemented by the 2700 published cross sectional morphometrics of the fluvial bedrock channels of the Antarctic inner continental shelves to help reduce influence of local factors and selection bias (Kirkham et al., 2020).

4

4. DATA PREPROCESSING

4.1 INTRODUCTION

This chapter describes the work done to achieve objective 2 (described in chapter 1 section 1.3.2) through the development and implementation of different preprocessing methods aimed to produce comparable data formats (Digital Elevation Models, DEMs) for each of the different published data formats for the chosen CGBL study sites and erosional end-member sites. Critically, each of the chosen sites requires differing levels of preprocessing to convert the published data sets into usable DEMs that can be used as part of further morphological cross- and long-profile analysis.

The chapter first covers the different levels of preprocessing required for the creation of DEMs for the CGBL study sites that either did not have a published DEM or for sites that required the creation of a higher quality DEM from multiple data sources. It then covers the mapping of CGBL features for each of the study site regions, before describing the methods used for creation of cross- and long-profiles used for morphological analyses in chapters 5 and 6. The methods described in this chapter build on previously implemented automated and semi-automated mapping of CGBL features (e.g. Patton et al., 2015; Patton et al., 2016b).

4.2 DEM AVAILABILITY AND RESOLUTION

Available bed topography data for each of the ten different CGBL study sites and end-members differed in terms of collection method and resolution (Table 4.1). Notably, some datasets represented bedrock surface models, whereas others were sediment surface models. Further, for some, digital data were not available, meaning data needed to be manually digitised to produce a Digital Elevation Model (DEM) of the bedrock surface, and for one site, data availability was so limited it precluded DEM creation. The sites with existing digital data of the bedrock or sediment surface includes northern Switzerland, Alaska, Hawaii, and Labyrinth Dry Valleys (Table 4.1). The sites requiring manual digitisation were the Finger Lakes and British Columbia features, for which the original seismic reflection data (Mullins et al., 1990; Eyles et al., 1991; Mullins et al., 1996) no longer exists. Finally, data from the Humboldt region consisted only of isolated airborne radar lines (Livingstone et al., 2017).

Manual digitisation and DEM creation, where required, was conducted as follows. For the Finger Lakes, the Mullins et al. (1996) interpretations of seismic reflection data were hand-digitised (50 m resolution) and merged with Soller and Garrity (2018) 500 m resolution bedrock topography DEM (Fig.4.1). This involved using kriging to combine the higher-resolution manually digitised bedrock and sedimentary-thickness maps of Mullins et al. (1996) with the lower-resolution digital USGS bedrock topography map (Soller and Garrity, 2018) into a continuous DEM covering the whole study area. For the two British Columbian CGBLs, published data were again manually digitised from

Mullins et al. (1990) for Kalamalka lake, and from Eyles et al. (1991) for Okanagan Lake, before each digitised data set were individually combined with the 3-arc-second Shuttle Radar Topography Mission (SRTM) DEM using the same methods shown in the workflow in Figure 4.1 for the Finger Lakes region. Example outputs from the different stages of the methods are shown in Figure 4.2. Figure 4.2f show examples of the long- and cross-profiles produced using this methodology and highlights how the resulting long-profile smoothness is affected by the density of contours available along feature. Therefore, each long-profile is manually inspected to determine if it is of high enough quality for use in analysis of feature aspects such as angle of normal and adverse slopes.

The DEMs obtained and produced by the above methods varied in resolution (maximum resolution: 8 m, minimum resolution: 500 m) and data quality. However, all dataset resolutions were below the scale (in terms of width, for example) of the CGBLs present in each region, meaning that that there would be enough pixel resolution per feature to resolve basic cross- and long-profile morphology required for the planned analysis. Nonetheless, for the Finger Lakes region, large variation in available resolution of source data led to the features in this region being subdivided into high- and low-quality features in subsequent analyses (Chapters 5 to 6). High-quality features could be digitised directly from the seismic lines, whereas low-quality features used data derived only from the 500 m bedrock DEM of Soller and Garrity (2018). For the Humboldt region, radar line spatial resolution was 150 m, which was more than sufficient for analysis (Chapter 5) of 1-dimensional feature cross-profiles directly from the flight lines.

Table 4.1: Table of CGBL features and data sources

Location	Reported Feature type	Number of Features/valleys	Data format	Morphometric calculated by	Resolution	Reference publication
Northern Switzerland	Overdeepening	11	25 m Bedrock topography DEM	Gilgannon et al. 2021	25 m	Pietsch and Jordan (2014)
British Columbia	Overdeepening	2	Seismic reflection data	Gilgannon et al. 2021	90 m - 50 m	Eyles et al. (1991), Vanderburgh and Roberts (1996), Mullins et al. (1990)
Finger Lakes, USA	Tunnel valley	16	Seismic reflection data, and bedrock topography DEM	Gilgannon et al. 2021	500 - 50 m	Mullins and Hinchey (1989), Mullins et al. (1996), Soller and Garrity (2018)
Humboldt Glacier, Greenland	Tunnel valley	Unknown	Airborne radio echo sounding	Livingstone et al., (2017)	150 m	Livingstone et al. (2017)
Alaska	Glacial U-shaped valley	11	32 m Surface topography	Gilgannon et al. 2021	32 m	Porter et al. (2018)
Hawaii	Fluvial V-shaped valley	68	10 m Surface topography DEM	Gilgannon et al. 2021	10 m	USGS EROS Data Center, 1999
Labyrinth Dry Valleys, Antarctica	Subglacial meltwater	20	8 m surface topography DEM	Gilgannon et al. 2021	8 m	Howat et al. (2019), Denton and Sugden (2005)
Inner continental shelves, Antartica	Subglacial meltwater	2700	Table	Kirkham et al., 2020	-	Kirkham et al. (2020)
China	Glacial U-shaped valley	49	Table	Li et al. 2001	-	Li et al. (2001)
New Zealand	Glacial U-shaped valley	>75	Table	Augustinus, 1992	-	Augustinus (1992)

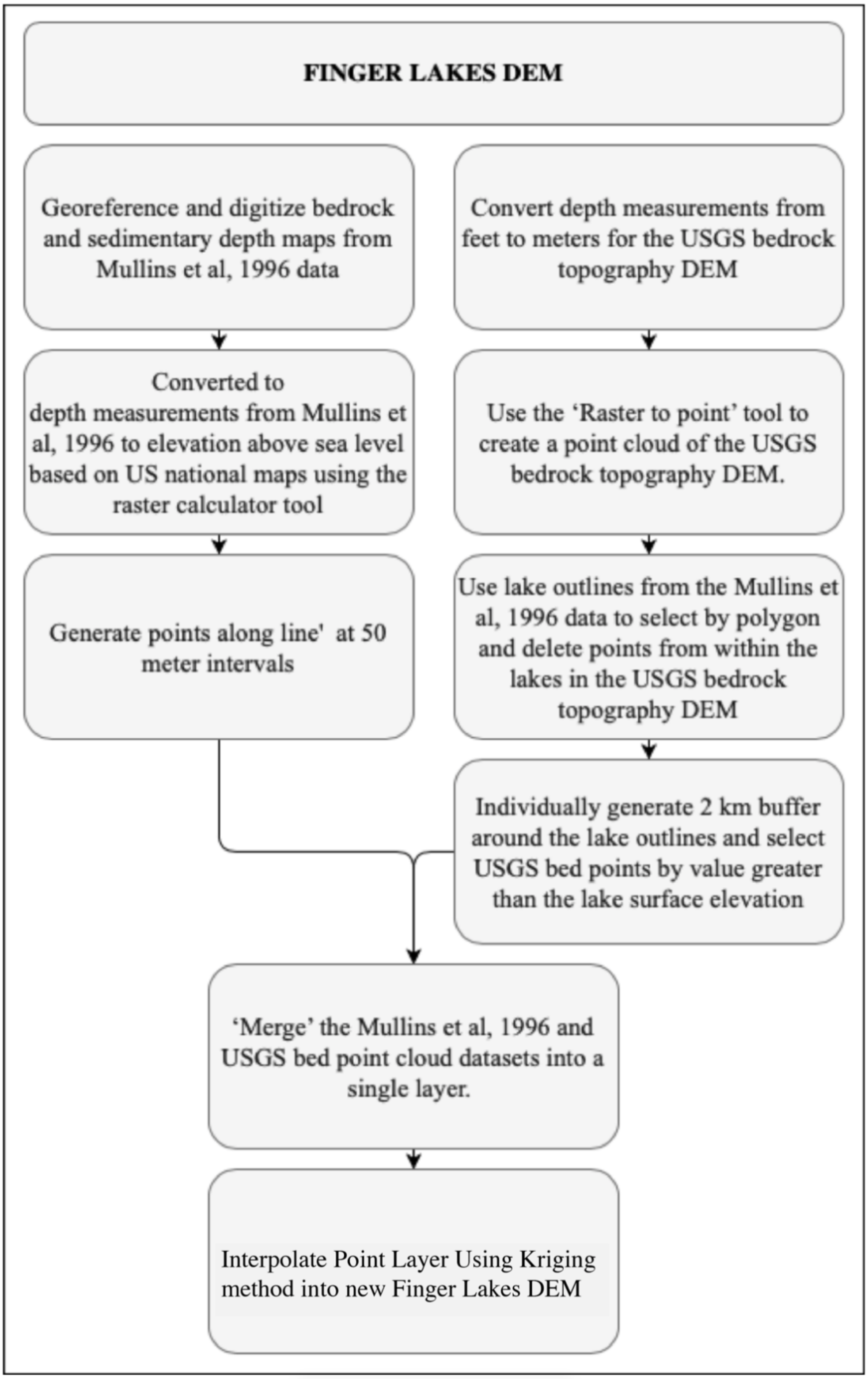

Figure 4.1: Workflow chart showing steps taken in the creation of the Finger Lakes DEM using data from Mullins et al. (1996) and the USGS bedrock topography map.

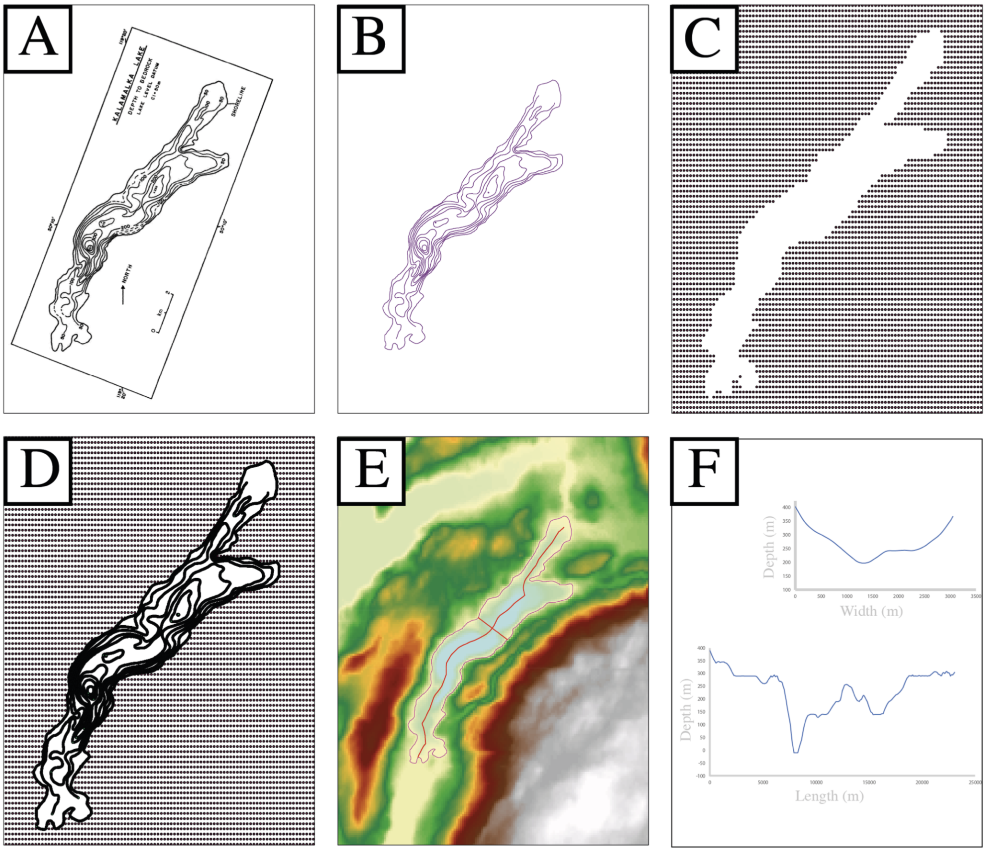

Figure 4.2: Example images from selected stages of the DEM creation. Examples taken from the creation of the Kalamalka Lake CGBL DEM. A) Image of georeferenced published bedrock topography map by Mullins et al. (1990) georeferenced to shore outlines identified in SRTM imagery. B) depth contour polylines hand digitised from the georeferenced Mullins et al. (1990) bedrock topography map, which were converted to point at 50 m intervals along each contour. C) point cloud generated from SRTM raster with the Kalamalka lake area removed using a shoreline polyline. D) the merged point clouds of the SRTM data and hand digitised Kalamalka bedrock topography map. E) the resulting DEM from the interpolated point layer using the Kriging method for the Kalamalka lake region (red lines shows the outline of the original published bedrock topography map, and the example long- and cross-profile shown in F), F) example cross-section showing profile smoothness and resolution resulting from the implemented methodology.

4.3 FEATURE MAPPING

The mapping of CGBL features for all of the chosen study site regions, except for Humboldt Glacier (due to a lack of a high-quality bedrock DEM and only ice penetrating radar traces), were processed using the same workflow in ArcGIS (Fig.4.3). This workflow used hydrological tools in ArcMap 10.7 to identify potential CGBL features by filling closed-basins in the bedrock- (or sediment-) surface DEMs, resulting in the location of the topographical closed CGBL basins producing areas of ~0 degrees surface slope. The resulting areas of 0 degrees slope were identified as CGBL basins using the raster calculator, and then were filtered to remove features < 3 km^2. The filter was chosen to remove features below acceptable spatial resolution for further morphological analysis, which means features less than 4 pixels in size for Switzerland and 1 pixel for the Finger Lakes (in the high-quality areas covered by the digitised data), with the spatial resolution of the DEMs of the study areas of Switzerland and the Finger Lakes being 25 m and 50 m respectively. The feature and cross profiles of the features of Humboldt Glacier were manually mapped directly from ice penetrating radar lines published by Livingstone et al. (2017).

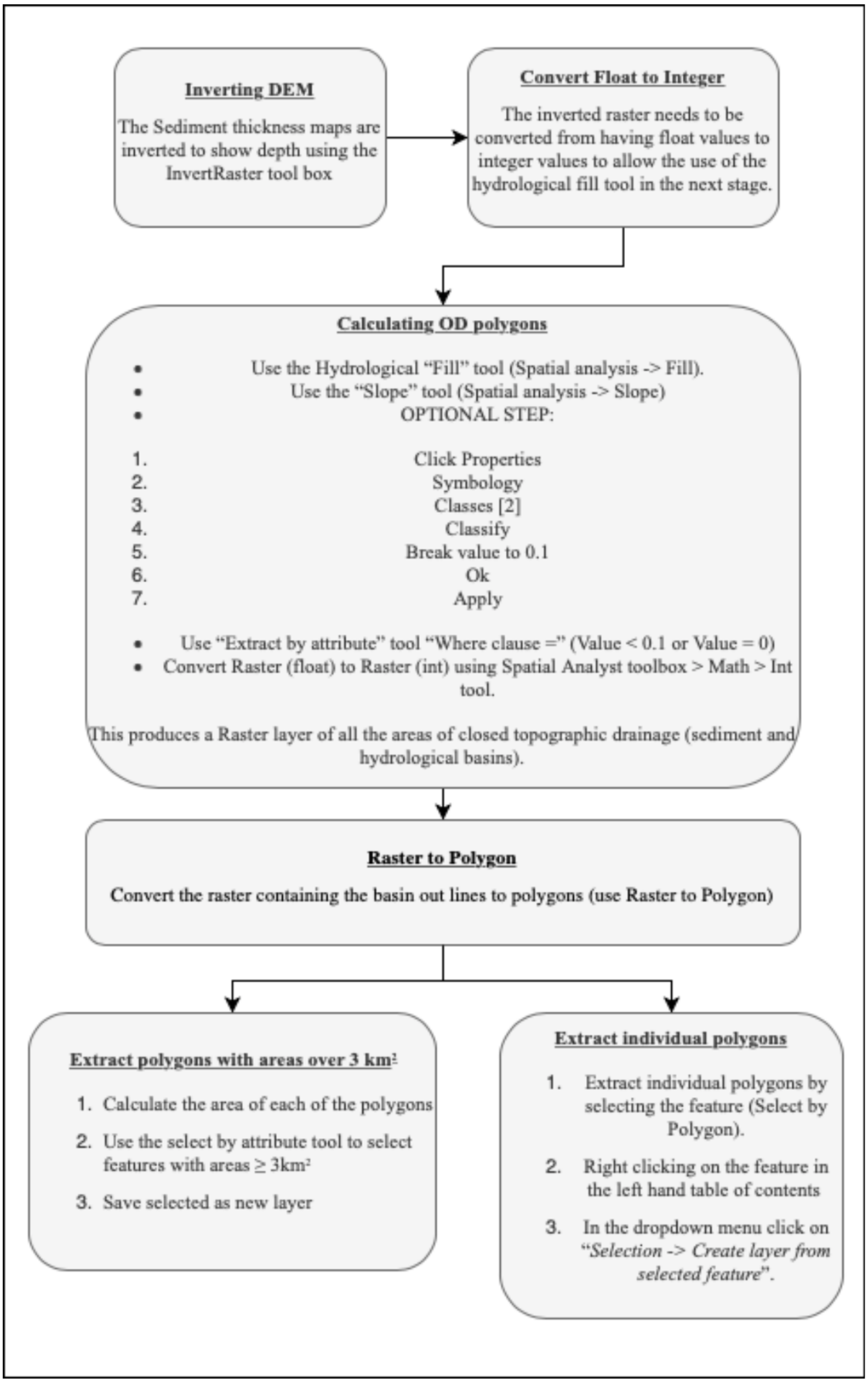

Figure 4.3: Workflow chart showing steps taken in the mapping of CGBL feature in the northern Swiss, Finger Lakes, and British Columbia study regions.

4.4 FEATURE LONG- AND CROSS-PROFILE EXTRACTION

4.4.1 *Centreline creation*

After the location and spatial extent of the CGBLs in each region were mapped, feature polygon centrelines were calculated to allow for the creation of cross-profiles and long-profiles. The term "long-profile" is used in this thesis to refer to the line of deepest erosion along a feature, from inflow to outflow points (Fig.4.4), which differ from feature polygon centrelines which simply follow the geographic central line along features. The long-profiles of deepest erosion were calculated to allow for the accurate measurement of the location and angles of the normal and adverse slopes present in each feature. Additionally, the calculation of the long-profiles allowed the accurate assignment of the location of changes in depth in relation to changes in cross-sectional morphology, similarly to the methods used by Patton et al. (2016b).

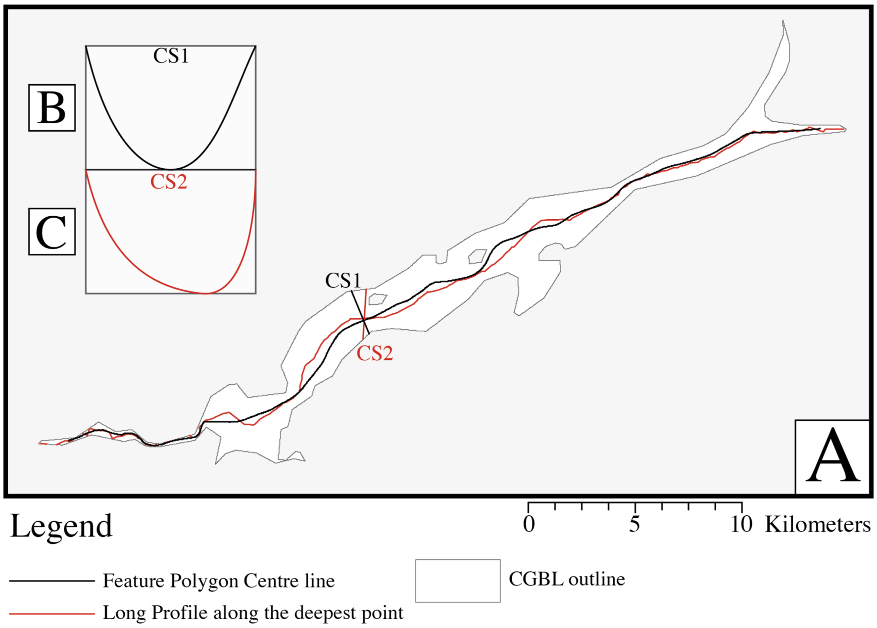

Figure 4.4: Figure showing differences between feature polygon centrelines and long-profiles and how cross-sections from each may be affected. A) Outline of feature 6 from northern Switzerland, and the locations of the feature centreline (black) and long-profile (red) as well as the location of theoretical cross-sections. B) Theoretical cross-section morphology using feature polygon centreline during creation shown in black. C) Theoretical cross-section morphology using long-profile during creation shown in red.

Figures 4.5 shows the workflow for the creation of the study site feature centrelines. The centrelines were calculated to allow for the calculation of cross-profiles orientated perpendicular to the feature sides, reducing the level of cross-profile distortion that occurred when using the line of deepest erosion (Fig.4.4). The centrelines were calculated in ArcMap 10.7 using the Skeleton tool designed for finding the centrelines of network data sets such as roads. The outputs were then trimmed of any branching lines produced at feature widenings, such as tributaries (example shown in Fig.4.6).

The centrelines for the end members of erosion were calculated differently to CGBL features because the end member valleys are not closed basins. End member features were mapped using the hydrological flow accumulation tool in ArcMap 10.7 to find the location of valley centres along which ice and water would flow under gravity, and manual selection of the flow paths that traversed valleys that did not show strong signs of external modification (i.e, due to presence of large landslides or lakes).

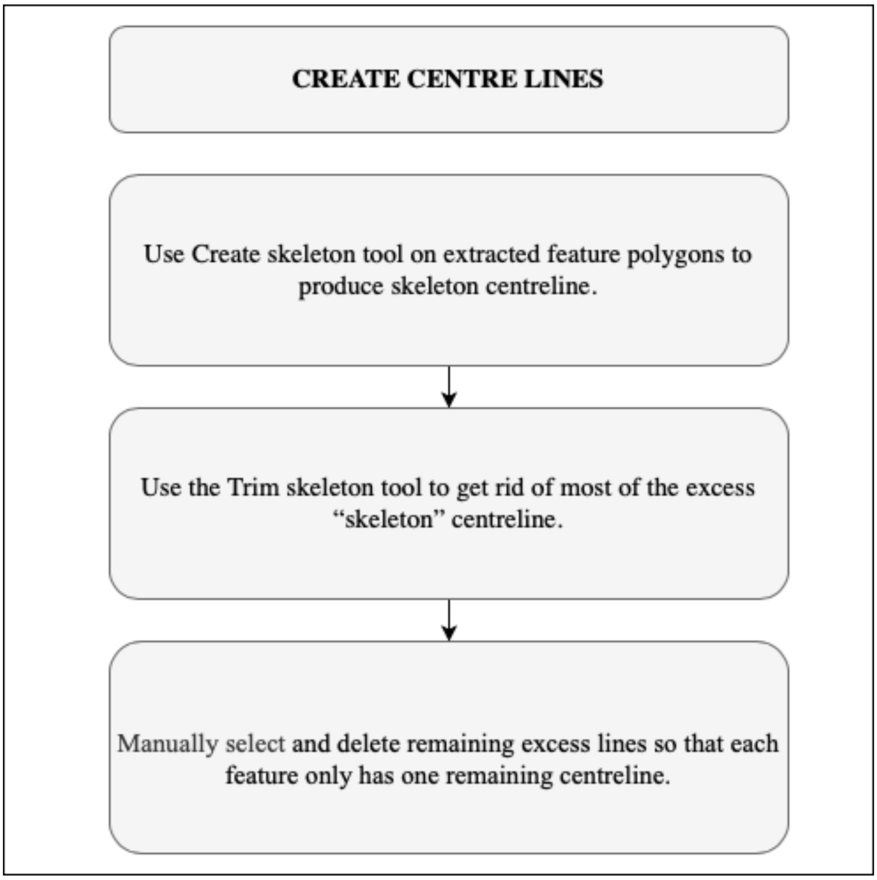

Figure 4.5: Workflow chart showing steps taken in the mapping of the centrelines of CGBL features in the northern Swiss, Finger Lakes, and British Columbia study regions.

4.4.2 *Cross-profile creation*

Following the creation of the centrelines for each of the features, cross-profiles for all the CGBL and erosional end-member features were calculated at a spacing of 100 m to capture large scale morphological changes while still producing a computationally manageable data set. The cross-profiles located at tributary features and bifurcations were manually selected and deleted due to the complex morphologies of cross-sections at these localities, which are difficult to measure with the V-index MATLAB code (Zimmer and Gabet, 2018) (see Fig. 4.7 and Section 5.3 for description of the V-index and *b*-exponent methods). Additionally, due to the semi-automated nature of the production of cross-profiles, many of these had to be manually clipped to polygon edges. This was due to variations in feature width sometimes overlapping with the spacing between different branches of the same feature, or smaller features located near to larger ones (see Fig.4.8). Cross-profiles for the Alaskan end-member region were manually selected due to the available computational processing capacity and time requirements of automatic detection over the ~600 km^2 study area.

4.4.3 *Long-profile creation*

The long-profiles for each of the CGBL features were calculated using the Zonal Statistics tool, in ArcMap, on the cross-profile data sets produced in the above stage of pre-processing. This was done to find the location of the deepest point of each cross-profile (locations outputted as point data). The resulting point data was then converted into polylines showing the paths of deepest erosion in each feature, i.e. the long-profiles of each feature (See Fig. 4.9 for workflow). Figure 4.10 shows through three schematic cross-profiles how the location of the deepest point in a cross-profile (represented by the green cross in figure 4.10) can vary from the geographic centre of the cross-profile (represented by the red cross in figure 4.10).

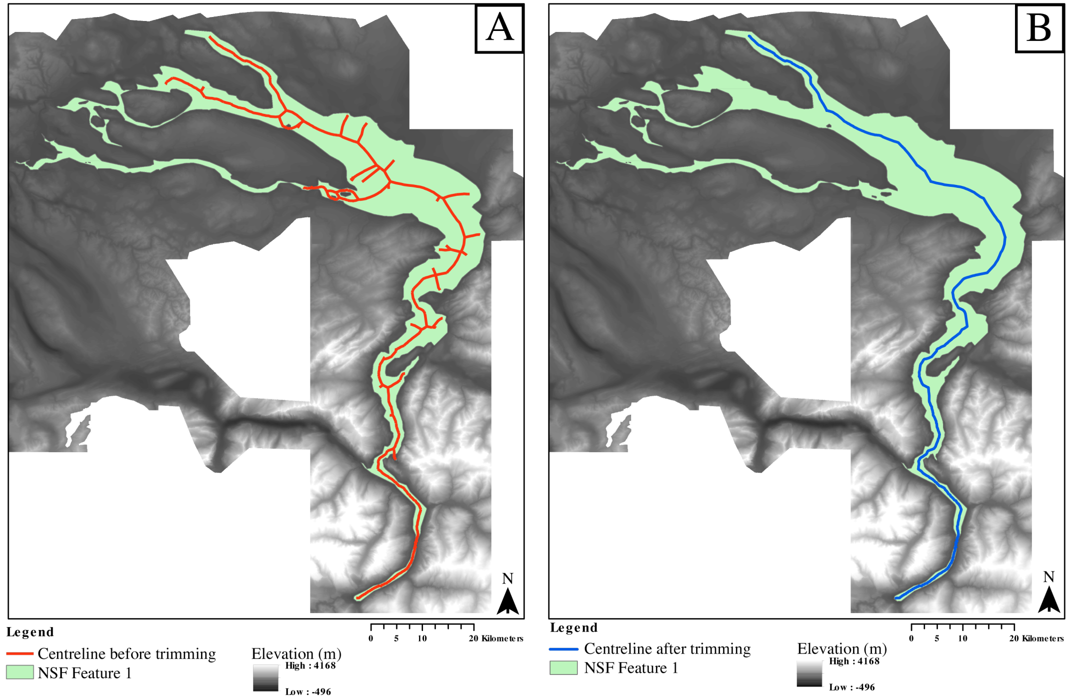

Figure 4.6: Example figure for northern Switzerland feature 1 centreline creation and trimming of tributary lines. A) Map showing centrelines with tributary (red line) lines before trimming. B) Map showing centrelines (blue line) without tributary lines after trimming. Feature 1 area is shown in green. Topographic elevation of bedrock DEM shown in grey scale.

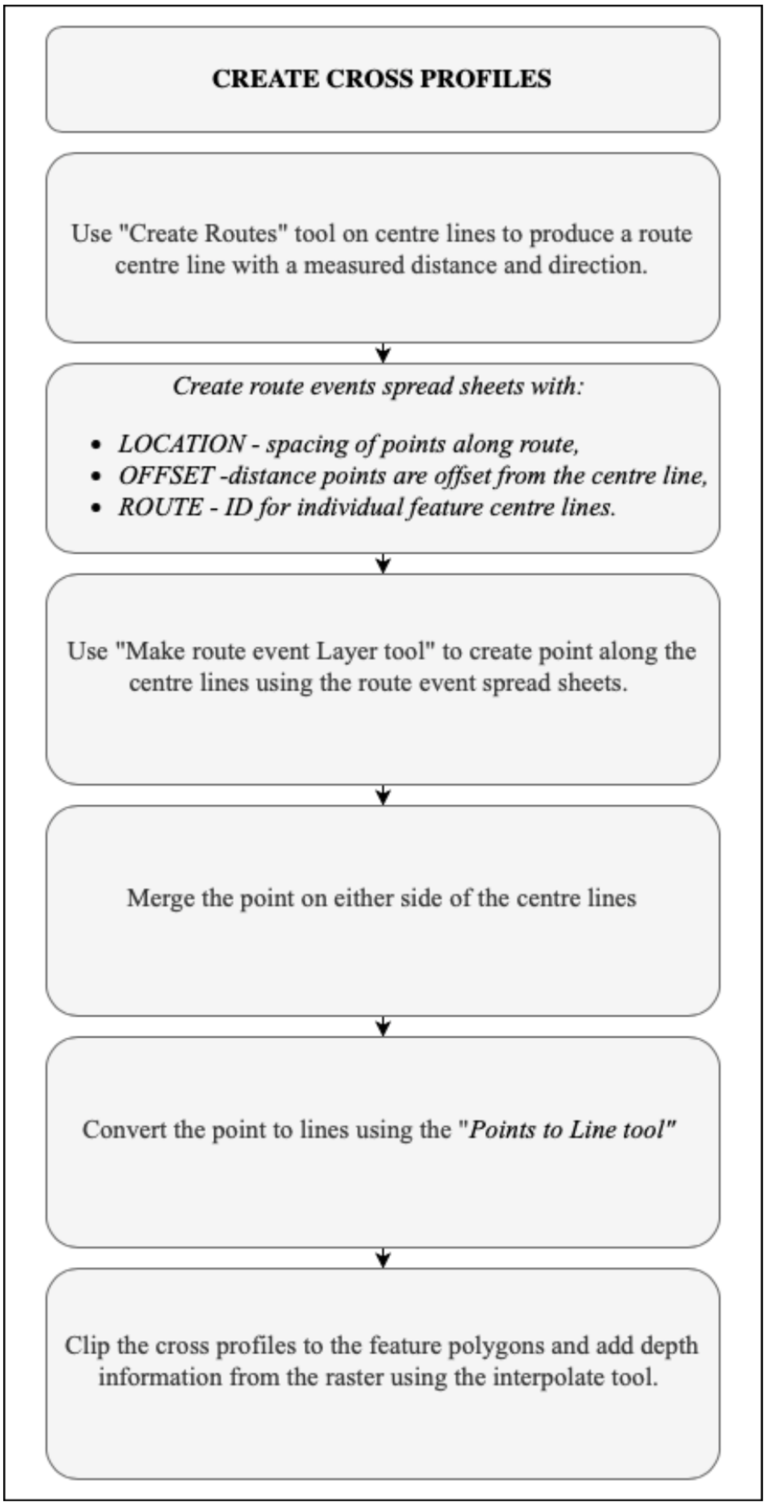

Figure 4.7: Workflow chart showing steps taken in the mapping of cross-profiles at 100 m intervals for CGBL features in the northern Swiss, Finger Lakes, and British Columbia study regions, as well as end member study sites.

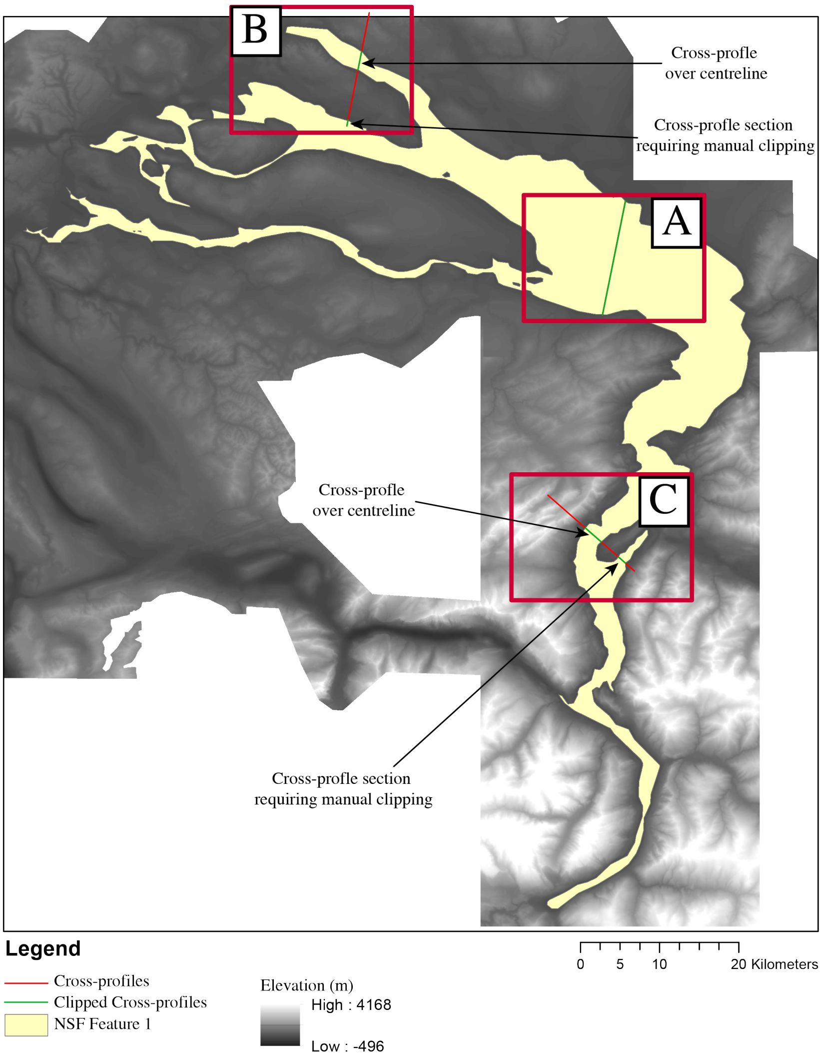

Figure 4.8: Schematic diagram showing locations where cross sections would require manual clipping to edges of feature polygons.

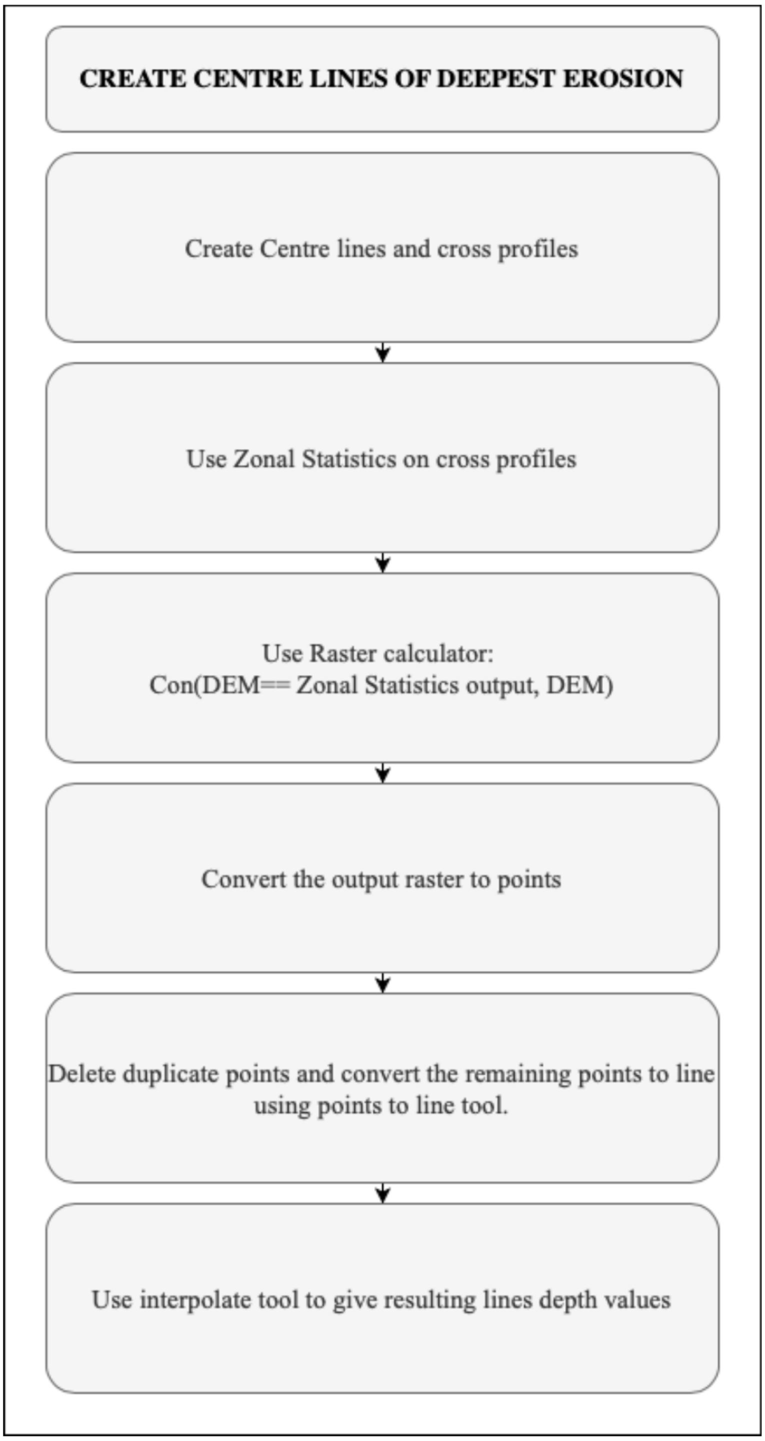

Figure 4.9: Workflow chart showing steps taken in the mapping line of deepest erosion along the long-profile of CGBL features in the northern Swiss, Finger Lakes, and British Columbia study regions.

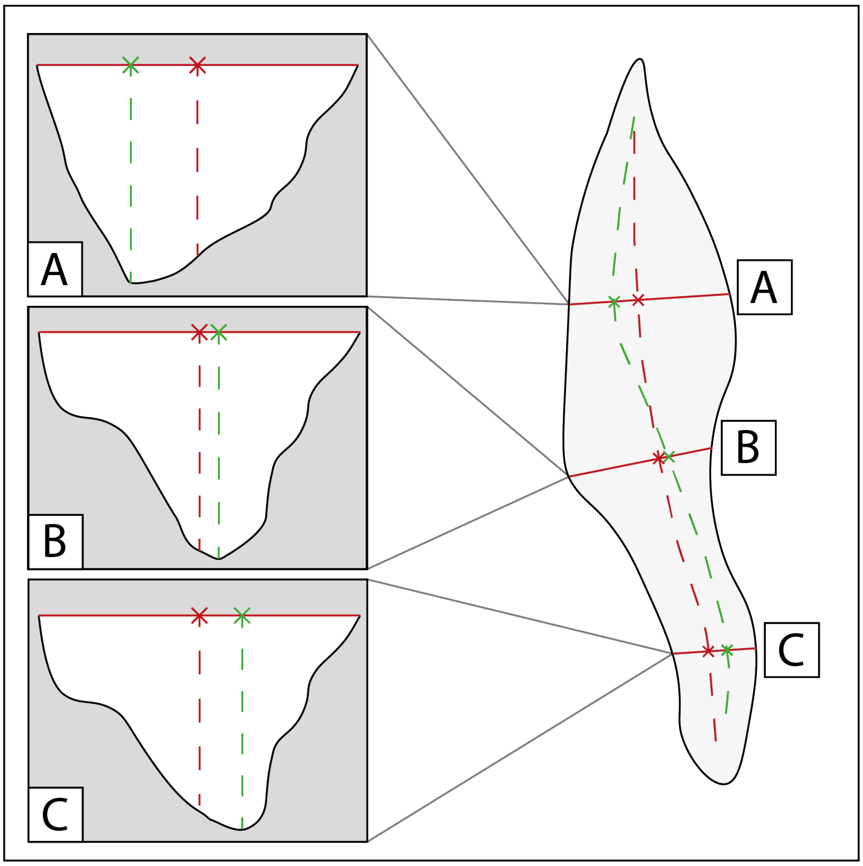

Figure 4.10: Schematic diagram showing how the location of the deepest point in a cross-profile can vary from the geographic centre of the cross-profile, highlighting how the Zonal statistics method calculates the location of the deepest points at each cross-profile.

4.4.4 *Identification of foreland and alpine boundary*

The foreland/alpine boundary was mapped to be at the break in slope at the 1000 m above sea level mark (Fig. 4.11). This was decided on as the location of the boundary after inspecting several elevation profile lines manually placed across the northern Swiss study region (example Fig. 4.12). Figure 4.13 shows how the alpine/foreland boundary cross cuts several of the identified CGBL features. The cross sections calculated for these features will be sub divided into foreland cross-sections and alpine cross-sections as part of the morphological analysis in the following chapters (Chapters 5 and 6).

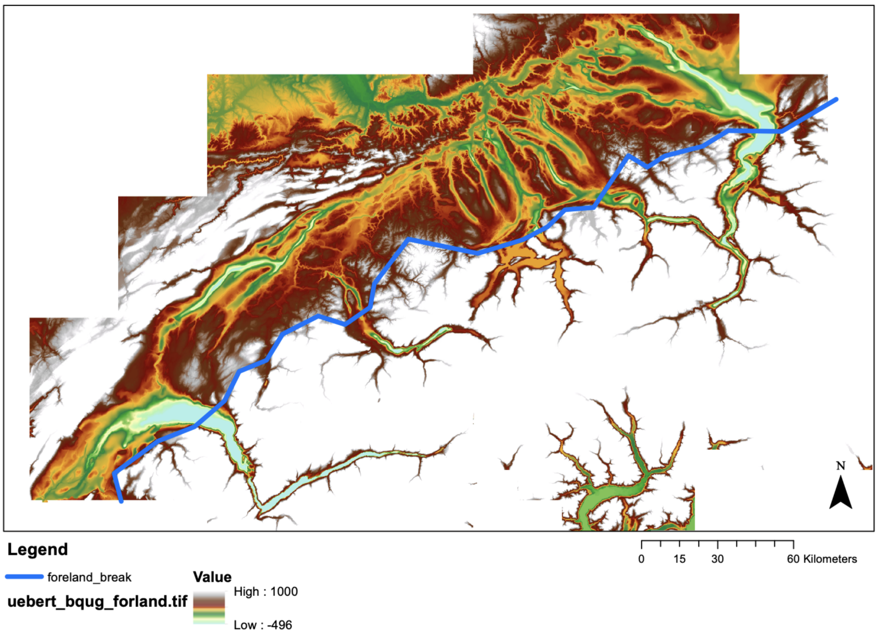

Figure 4.11: Location of alpine foreland boundary in relation to 1000 m elevation line in the region of northern Switzerland

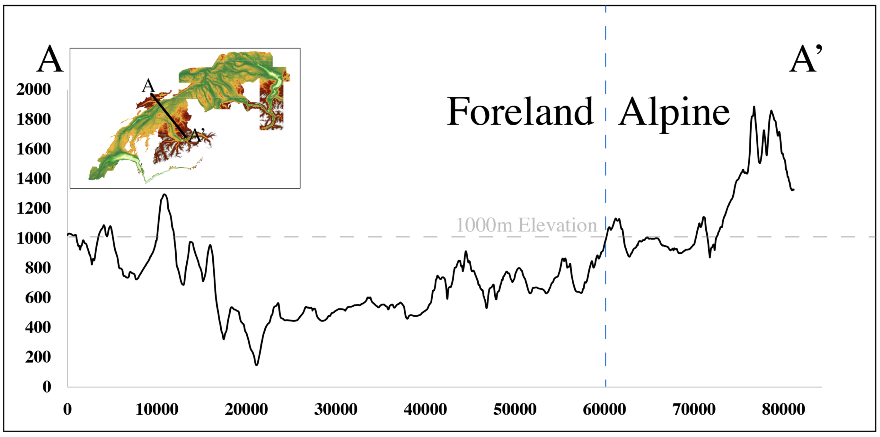

Figure 4.12: Example elevation profile line manually placed across the study site of northern Switzerland

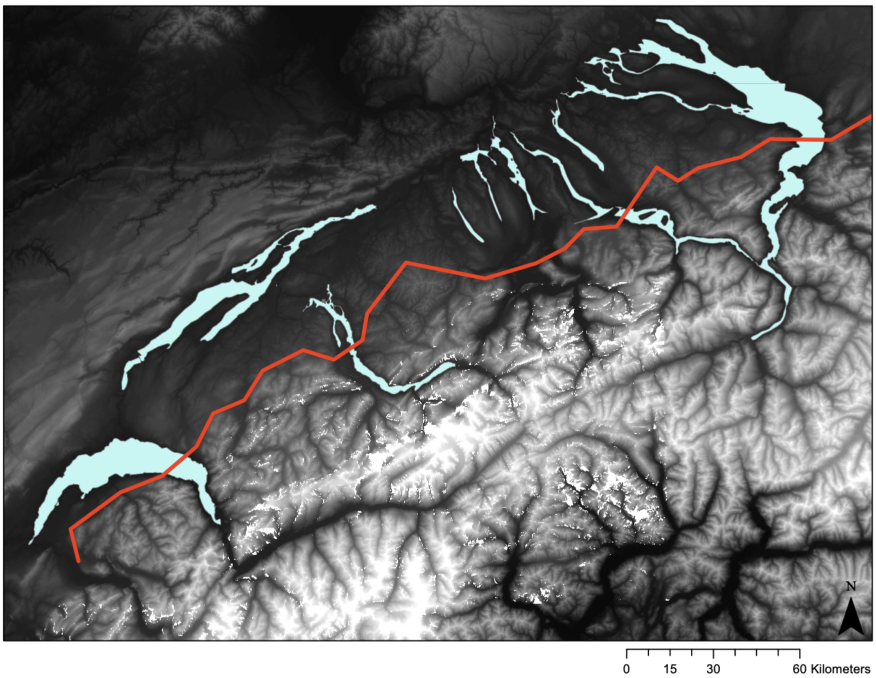

Figure 4.13: Location of alpine-foreland boundary in relation to CGBL features

Part III

MORPHOLOGICAL ANALYSIS

5

CROSS-SECTIONAL FORM OF BEDROCK OVERDEEPENINGS AND TUNNEL VALLEYS IN FORELAND SETTINGS: THE CONTRIBUTION OF SUBGLACIAL FLUVIAL VERSUS GLACIAL EROSION

5.1 INTRODUCTION

Glacially sculpted foreland settings commonly host overdeepened valley sections that incise into bedrock and penetrate deeper than the fluvial base level (Cook and Swift, 2012; Kehew et al., 2012; Patton et al., 2016b) (Fig.5.1a). Despite the ubiquity of these features their formation is still poorly understood. This difficulty arises, in part, because it has not been clearly established if the morphology of these features can reveal any information about which processes were active during the incision into the landscape. In the most general of terms, it remains an open question if glacial or subglacial fluvial erosional processes are the dominant erosive process involved in their formation and development. It is important to resolve this and understand how overdeepened valley sections form, as their occurrence and evolution is suspected to influence subglacial meltwater drainage transitivity (e.g. Creyts and Clarke, 2010), sediment transport (e.g. Swift et al., 2018) and ultimately even large scale ice sheet geometry and flow (e.g. Schoof, 2007).

There are two descriptive definitions of valley sections that are overdeepened into bedrock, overdeepenings and tunnel valleys, but they are not clearly linked to specific formation processes. An overdeepening is defined as a large-scale (10^1-10^2 m deep and 10^2-10^4 m long) closed-basin feature (Linton, 1963; Cook and Swift, 2012),whereas a tunnel valley is defined as an elongated depression (10^2-10^3 m wide and 10^2-10^4 m long), that can be straight or anastomosing, with an undulating bed profile incised into bedrock or sediment (Ó Cofaigh, 1996; Kehew et al., 2012; Livingstone and Clark, 2016). In the literature, both of these types of bedrock overdeepenings have been variously ascribed to glacial erosion by abrasion and quarrying (Harbor, 1989; Cook and Swift, 2012) or – more often in the case of tunnel valleys – subglacial meltwater erosion (Ó Cofaigh, 1996; Kehew et al., 2012). For example, the overdeepened bedrock features of the Finger Lakes region of the USA (Fig.5.1b) have been interpreted to have been incised by meltwater erosion and are referred to as tunnel valleys (Mullins and Hinchey, 1989). In contrast, similar-scale bedrock features in northern Switzerland (Fig.5.1c) have been classed as overdeepenings and interpreted to have been formed via glacial erosion (Preusser et al., 2010) and/or subglacial meltwater erosion (Dürst Stucki and Schlunegger, 2013). From this alone, it is clear that some other tests or criteria are needed to better link the descriptions of overdeepened valley morphologies to processes.

A convenient starting point for this, would be to consider the similarity of the morphology of overdeepened valleys to the morphology of valleys formed by known processes. This can be achieved by quantifying valley cross-profiles and comparing them to one another. Such analyses have not been widely applied to overdeepened features associated with foreland settings (although see Kirkham et al. (2020); Magrani et al. (2020)) but are routinely used elsewhere to decipher valley origin (e.g. Svensson, 1959; Augustinus, 1995; Brook et al., 2004). Previous analyses have shown that valleys of glacial origin have a characteristic U-shaped cross-profile form that is distinct from the V-shape exhibited by valleys formed by subaerial fluvial incision (Hirano and Aniya, 1988; Montgomery, 2002). The U-shaped glacial morphologies are considered to result from the distributed erosional forces between the ice and its valley sides and bed (Harbor, 1995), while V-shaped fluvial morphologies are caused by gravity driven vertical incision focused on the valley floor (Schumm and Ethridge, 1994) (Fig.5.2). This would seem to suggest that glacial and subglacial fluvial erosional processes will leave distinctly different morphological signatures, and hence the shapes of valleys may help indicate the formation processes active in overdeepened valleys.

This chapter aims to elucidate the relative importance of subglacial fluvial versus glacial erosion in the formation of bedrock overdeepenings in foreland settings through comparison of the cross-profile form. The cross-profiles of bedrock overdeepenings are compared with cross-profiles from a variety of valleys of known process origin that can be considered as characteristic 'end-members' for purely glacial, fluvial or subglacial-fluvial formation (Augustinus, 1992; Seidl et al., 1994; Li et al., 2001; Briner and Kaufman, 2008; Kirkham et al., 2020).

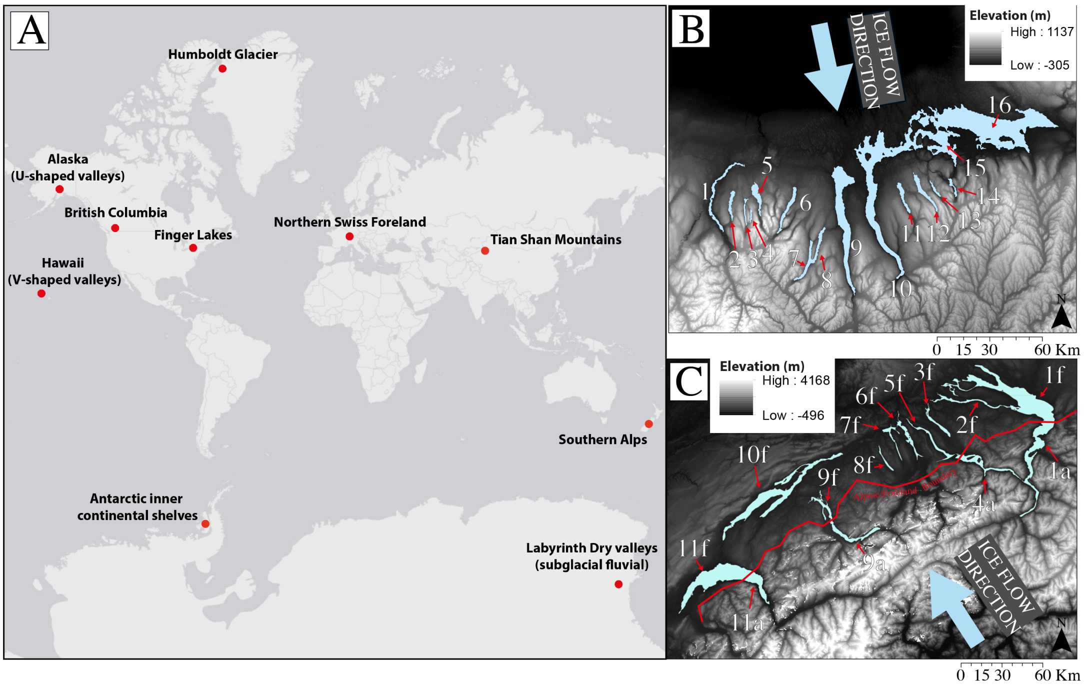

Figure 5.1: Location map. (A) Red dots show locations of CGBL sites, and end-members of erosion. (B) Location of identified CGBL features in the Finger Lakes region, USA shown in blue. The direction of ice flow during last glaciation is indicated by a blue arrow. (C) Locations of identified CGBL features in northern Switzerland shown in blue, location of foreland/alpine boundary shown in red, and direction of ice flow during last glaciation in blue.

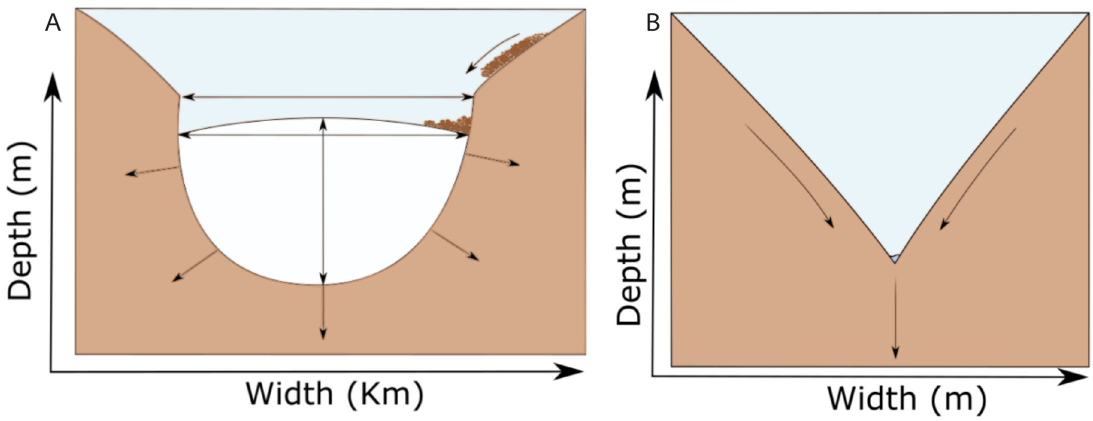

Figure 5.2: Schematic diagram of glacial and subaerial valley erosion and the resultant valley cross-profiles. (A) Distributed glacial erosion by buttressing glacial ice on valley walls and floor and subglacial meltwater. Section (A) also shows the stabilising effect of the glacial ice on valley walls preventing slope failure below the trim line. (B) Focused vertical incision by fluvial erosion at valley base with gravity driven slope failure and erosion of valley sides.

5.2 STUDY SITES

5.2.1 *Channel-like glacial-erosional bedrock landform (CGBL)*

The CGBL study sites that were selected for morphological analysis include northern Switzerland, the Finger Lakes, Humboldt Glacier, and the British Columbian lakes of Okanagan and Kalamalaka (Fig.5.1). The rationales for site selection are discussed in chapter 3.

5.2.2 *End members of erosion*

The location of erosional end-member sites (Fig.5.1) were selected based on the specific types of erosion. This included 523 cross sections from glacially eroded U-shaped valleys near Anchorage, Alaska (Briner and Kaufman, 2008); 49 published U-shaped glacial cross-sections from the Tian Shan Mountains, China (Li et al., 2001); the published mean value for 5 glaciated regions in the southern Alps, New Zealand with a minimum of 15 cross-sections per region (Augustinus, 1992); 1,508 cross-sections from subaerial fluvially eroded V-shaped valleys calculated from the western slopes of the Hawaiian Island of Kauai (Seidl et al., 1994); 218 example cross-sections of catastrophic subglacial fluvial morphology from the Labyrinth dry valleys, Antarctica (Denton and Sugden, 2005), and the mean values of over 2700 subglacial fluvial bedrock channels on the Antarctic inner continental shelves (Kirkham et al., 2020), (see Table 4.1).

5.3 METHODS

5.3.1 *Cross-sectional analysis*

Analyses of glacial valley cross-section form have been applied widely (e.g. McGee, 1894; Svensson, 1959; Hirano and Aniya, 1988; Harbor, 1995; Zimmer and Gabet, 2018) and have focused on quantifying observable differences in form with respect to that of subaerial fluvial valley systems (Fig. 5.2). Svensson (1959) was the first to quantify the 'U-shapedness' of a valley by comparing the shape of the valley to a parabolic curve (Fig. 5.3). This approach relies on fitting a power law function to the valley profile of the form:

$$Y = ax^b \tag{5.1}$$

Where x and Y are the horizontal and vertical distances from the point of deepest erosion on the cross section respectively and the b-exponent indicates the parabolic nature of the curve. The b-exponent is calculated using equation 5.2 (Svensson, 1959), and the a-coefficient is calculated using equation 5.3 (Svensson, 1959). The value of the b-exponent and a-coefficient are calculated using:

$$b = \frac{\Sigma X \Sigma Y - n\Sigma YX}{(\Sigma X)^2 - n\Sigma X^2} \tag{5.2}$$

$$loga = \frac{\Sigma X \Sigma XY - n\Sigma Y \Sigma X^2}{(\Sigma X)^2 - n\Sigma X^2} \tag{5.3}$$

Where Y is the log of the vertical component and X is the log of the horizontal component.

To provide even better discrimination between glacial and fluvial valley forms the b-exponent has typically been plotted in conjunction with the Form Ratio (Fr) (Graf, 1970; Hirano and Aniya, 1988; Kirkham et al., 2020). The latter is calculated for each cross-section using:

$$Fr = \frac{D}{W} \tag{5.4}$$

Where D is the depth from the lip of the CGBL to the deepest point in the cross-section and W is the CGBL cross-section's maximum width (see Fig.5.3).

The power law function does have some issues. For example, the curve fitting approach can be applied to only one side of the valley at a time and the necessary logarithmic transformation of the cross-section data means the fit favours points that are closer to the valley centre (Wheeler, 1984; Harbor and Wheeler, 1992; Pattyn and Van Huele, 1998). An alternative V-index approach has therefore been developed (Zimmer and Gabet, 2018) that quantifies the difference in cross-sectional area between

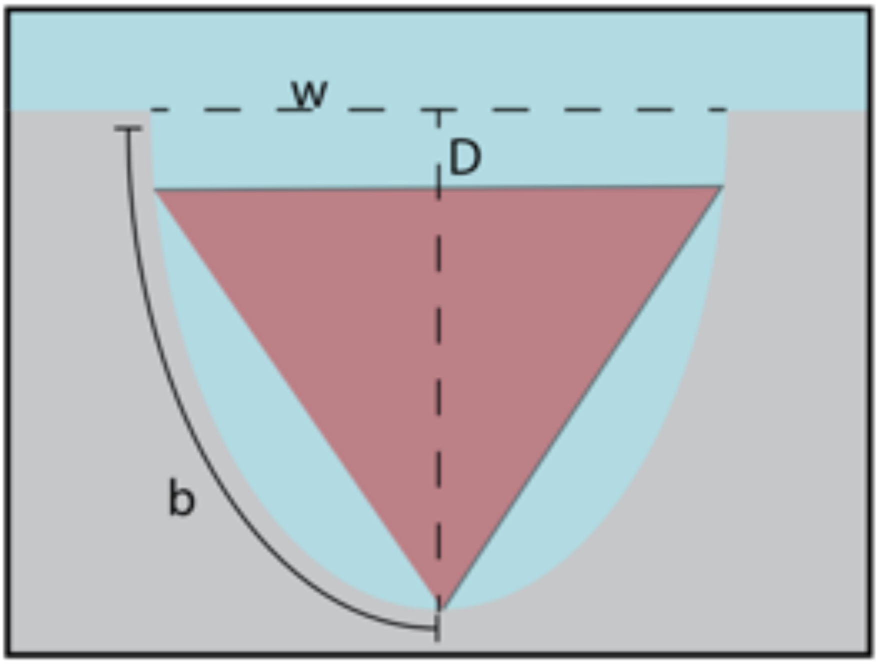

Figure 5.3: Schematic valley cross-section showing the dimensions each metric records. Grey area shows bedrock location. W = width of valley cross section from the top of the valley sides. D = depth of valley. b = exponential nature of feature side slope. Red triangle shows idealised V used to calculate the V-index (difference between idealised V and real-world cross-section).

that of the actual valley and that of a 'pure V-shaped' valley of identical width and depth (Fig.5.3). A valley with convex sides will return a negative V-index value, while a valley with concave sides will return a positive value (Fig.5.4). A perfect V-shaped valley will return a value of 0.

In this study, the *b*-exponent was calculated for both the left and right sides of each cross section using an adapted MATLAB script developed by Zimmer and Gabet (2018) to derive a mean *b*-exponent for the cross-section as a whole. The *b*-exponent typically ranges from just under 1 to upper extremes of over 5 (Graf, 1970; Hirano and Aniya, 1988). The same MATLAB script was then used to calculate the V-index for each of the cross sections. Both the *b* and V-index values were calculated to explore the utility of each method, and in particular, whether particular shapes are better represented with certain methods.

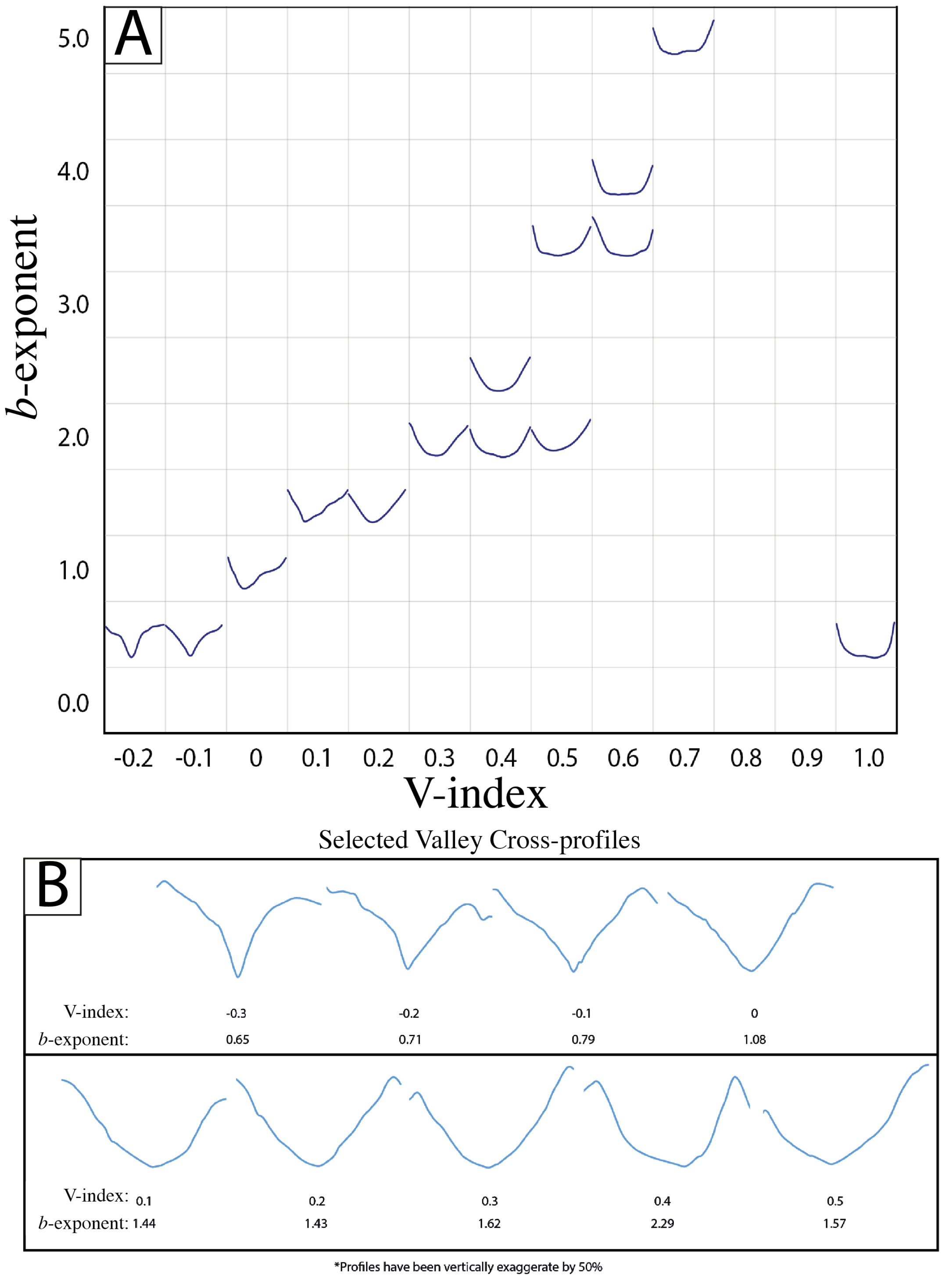

Figure 5.4: Example cross-profiles and associated measured mean b values and V-index values. A) Example *b* vs V-index plot showing real world cross-sections and their measured *b*-exponent vales and V-index values. The cross-sections were taken from features in northern Switzerland and the Finger Lakes. B) Example cross-profile and associated measured mean *b*-exponent and V-index values. Profiles extracted from example erosional end-members.

5.3.2 *Feature morphology averaging*

To obtain *b*-exponents and V-index values for each individual CGBL, geometric mean and peak kernel density estimation (KDE) values were calculated for all cross-sections per feature. The peaks in the two-dimensional (2D) KDE surface show the central points of the clusters in the populations, and therefore represent the relationships in the data best (Fig. 5.5). However, for ease of comparison with existing morphometrics in the literature, both results are presented. KDE surfaces were calculated in a set of Python scripts that implement functions from the SciPy and Numpy libraries for all CGBLs of interest and the highest value points (peaks) were extracted to represent the average values per feature.

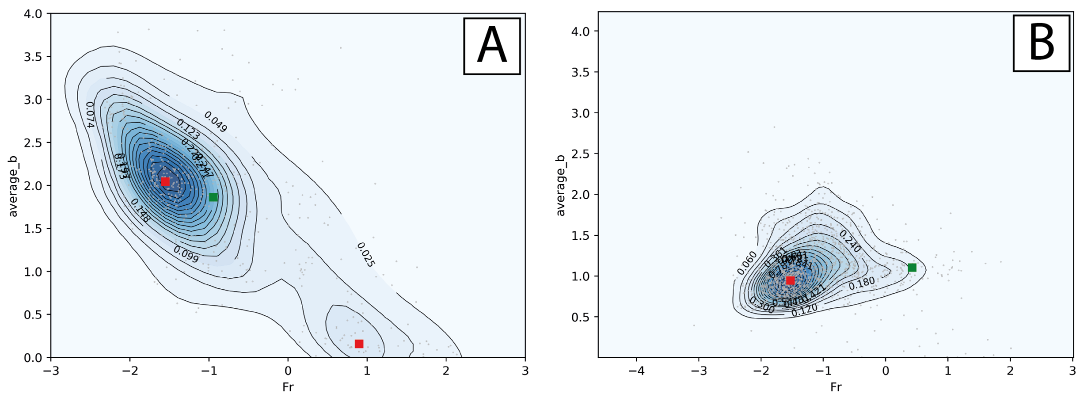

Figure 5.5: Example 2D KDE surfaces for the end-member cross-sections. A) Alaska b/Fr relationship. B) Hawaii b/Fr relationship. The red boxes show the location of peaks in the 2D KDE field. The green box shows the location of the calculated mean value. The contour lines show the clustering of the points in the 2D KDE field, with the grey dots showing individual cross-section values. Note how the 2D KDE does a better job of identifying the centre of the distribution, and is therefore more representative than the mean.

5.4 RESULTS

5.4.1 *CGBL width and depth*

The northern Switzerland alpine CGBLs have maximum bedrock depths of 280-450 m and maximum widths of 2.9-5.9 km. The high-quality Finger Lake CGBLs are comparable in scale to those of northern Switzerland, with maximum bedrock depths of 110-300 m and maximum widths of 1.0-8.6 km, while the lower quality data generally shows a shift towards shallower CGBLs with maximum depths of 20-200 m and widths of 1.63-14.14 km (Fig.5.6a). The foreland CGBLs of northern Switzerland have maximum depths of 70-320 m and widths of 1.3-11.3 km (Fig.5.6b). The CGBL sites of British Columbia and Greenland also display similar widths and depths; Lake Okanagan is the larger CGBL with a depth of 280 m and width of 2.98 km, and Kalamalaka the smaller feature, with a depth of 75 m and width of 1.26 km. While the Alaskan U-shaped valleys are wider than CGBLs, the subaerial and subglacial fluvial end-members of Hawaii and the Labyrinth, respectively, are much narrower (Fig.5.6c).

CGBLs in the foreland of northern Switzerland show a general positive trend between depth and width (Fig.5.6b).

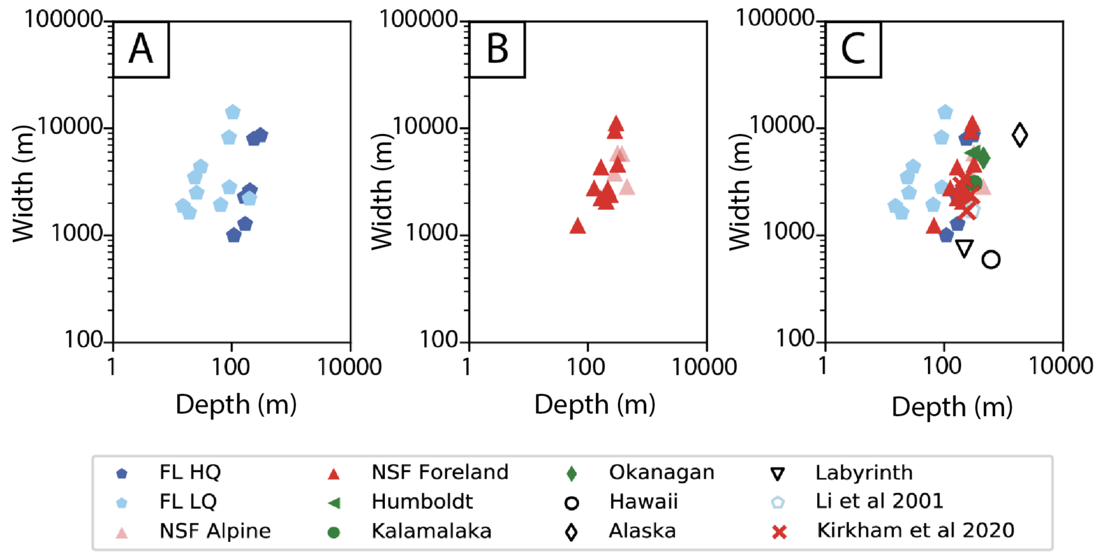

Figure 5.6: Loglog scatter plots of feature maximum depth against maximum width. NSF = Northern Switzerland. FL = Finger Lakes. LQ = Low Quality; HQ = High Quality. The maximum depths and widths of features from Augustinus (1992) were not reported.

5.4.2 *CGBL Morphology*

5.4.2.1 *Mean morphometric values (variations in morphology)*

In general, the mean V-index, *b*-exponent and form ratio of CGBLs in northern Switzerland show little variation with the exception of foreland feature 11F (Fig.5.7 and Table 5.1). The alpine features of northern Switzerland have mean V-index values that range from 0.25 - 0.34, *b*-exponents that range from 1.40 - 1.90, and form ratios of 0.15 - 1.42. The foreland features of the northern Switzerland study area have mean V-index values of 0.18 - 0.39 and *b*-exponents and form ratios of 1.25 -1.87 and 0.04 - 0.46 respectively. This is comparable with the high-quality Finger Lakes data. In contrast, the low-quality Finger Lakes data exhibits large variation in b and form ratio values (Fig. 5.7). The Alaskan U-shaped valleys have higher mean V-index values, but similar b and form ratio values to the Labyrinth features. The Hawaiian fluvial end-member has notably lower mean b, and V-index values than the other end-members of erosion. The mean *b*-exponent and form ratio of the Tian Shan Mountains, China are reported as 1.87 and 0.23 (Li et al., 2001). The mean *b*-exponent and form ratio of the Southern Alps, New Zealand are reported as 1.16-2.14 and 0.14-0.23 respectively (Augustinus, 1992). The mean *b*-exponent and form ratio of the subglacial fluvial bedrock channels of the Antarctic inner continental shelves are reported as 1.1-1.3 and 0.11-0.14 respectively (Kirkham et al., 2020).

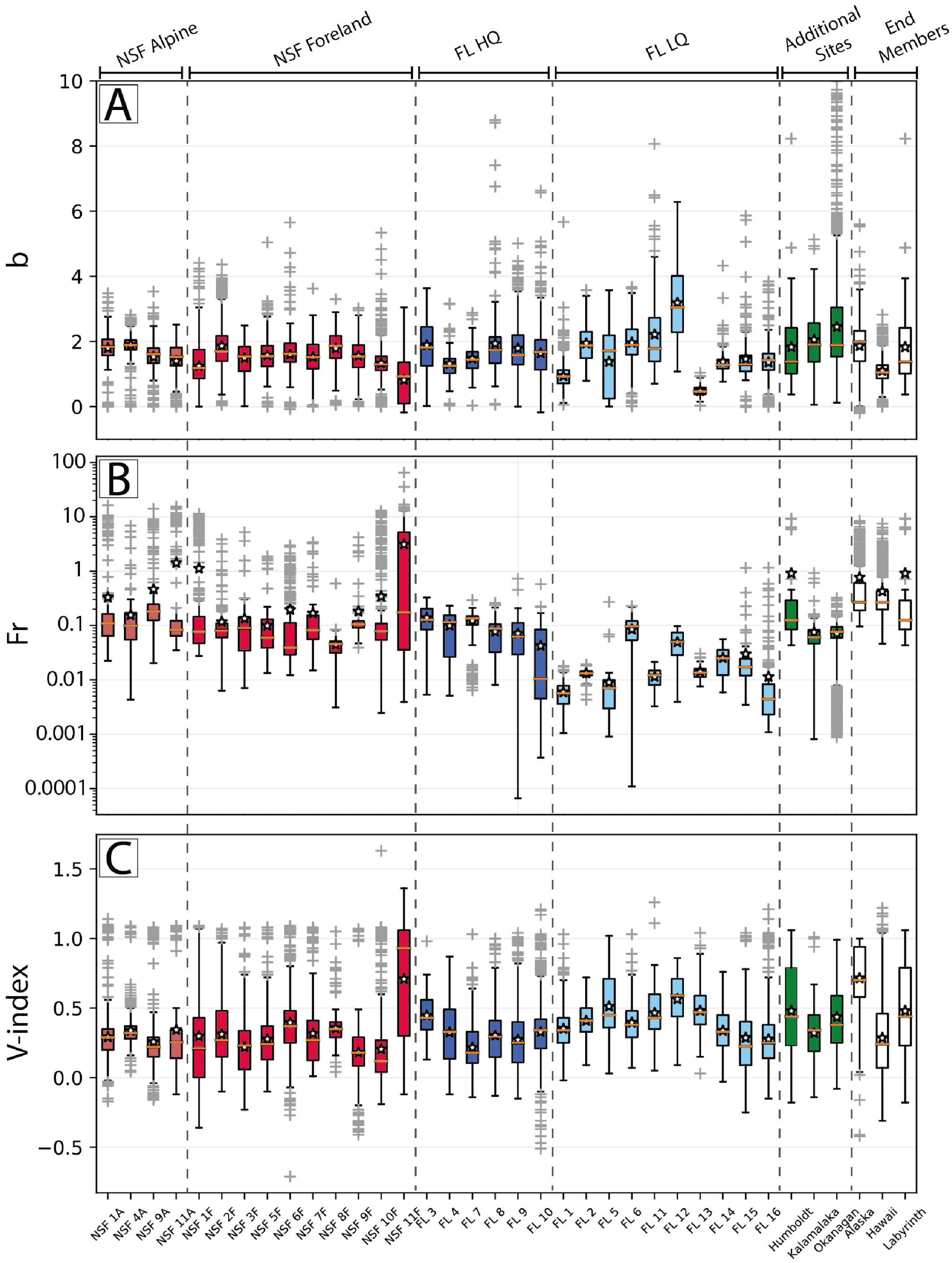

Figure 5.7: Box plots of the *b*-exponent (A), form ratio (Fr) (B) and V-index (C) for each CGBL. Each box represents the quartiles for each CGBL with the box colour indicating the data set: northern Switzerland (NSF) Alpine (brown); northern Switzerland (NSF) Foreland (red); Finger Lakes (FL) Low quality (LQ) (light blue); Finger Lakes (FL) high quality (HQ) (dark blue); Humboldt glacier (green); Kalamalaka (green); Okanagan (green); Alaska (white); Hawaii (white); Labyrinth (white). The star marker shows the mean value of each feature. The horizontal red line represents the features median value. The whiskers show the extent of non-outlier data points per feature, with the outlier data points shown by cross marks (+).

5.4.2.2 *KDE Values: mean b values and form ratio*

The following section reports the peak KDE *b*-exponent and form ratio values of the CGBL study sites and the end-members of erosion. Similar to the mean values reported above, which were provided for easier comparison with previously published works, the values represent an average value per feature. However, Figure 5.5 shows that the peak KDE is more representative of the data in bivariate space, and so are used in this chapter to explore the average values of the CGBLs and end-members of erosion.

The peak KDE mean *b*-exponent for the subaerial fluvial and glacial erosional end members show distinct morphologies with a peak KDE mean *b*-exponent of 0.94, and form ratio of 0.22, and peak KDE mean *b*-exponent of 2.04 and a peak KDE form ratio of 0.23, respectively (Fig.5.8a). The *b*-exponent and form ratios for two published glacial erosional end-members are presented in Fig. 5.8b, with the glacial valleys of New Zealand displaying mean *b*-exponents and form ratios ranging from 1.16 - 2.14, and 0.14 - 0.23 respectively (Augustinus, 1992), and individual valley cross-sections from glacial valleys of the Tian Shan Mountains, China have *b*-exponents of 1.94 - 4.08, and form ratios of 0.13 - 0.32 (Li et al., 2001). The positioning of the Tian Shan Mountain cross-sections correlate strongly with the data envelope of the Alaskan glacial valleys, and only partially with the New Zealand valleys presented by Augustinus (1992). The subglacial fluvial channels of the Labyrinth, Antarctica, were calculated from the mean *b*-exponent and display a peak KDE mean *b*-exponent of 1.48 and peak KDE form ratio of 0.15 (Fig. 5.8a). This correlates well with the bedrock meltwater channels on the inner continental shelves of Antarctica recorded by Kirkham et al. (2020), which have mean *b*-exponents ranging from 1.1 - 1.3 and form ratios of 0.11 - 0.14, well within the 66% data buffer zone shown in Figure 5.8a.

The peak mean *b*-exponents identified by the KDE analysis for northern Switzerland CGBLs range between 0.99 - 2.11 for the foreland and 1.57 - 2.00 for the alpine valleys (Fig. 5.8c). The corresponding peak form ratio varies between 0.09 - 0.21 for the alpine features, and 0.03 - 0.15 for the foreland features (Fig. 5.8c). The peak KDE *b*-exponents and form ratios of the alpine feature mostly correlate well with the data envelope of the glacial erosional end-member, while the b/Fr of the foreland features fall mostly in the range of the subglacial fluvial end-member data envelope. The peak KDE mean *b*-exponents for the two Finger Lakes data sets range from 1.17 - 2.26 for the high-quality data, and 1.24 - 2.34 for the low-quality data (Fig. 5.8c). The form ratios for the high-quality features range between 0.05 - 0.15, and between 0.01 - 0.38 for the low-quality features (Fig. 5.8c). These *b*-exponent and form ratio values for both the high-quality and low-quality Finger Lake features fall within the ranges of all three erosional end-member data envelopes, and show no strong correlation with any one in particular. The British Columbian CGBLs of lakes Okanagan and Kalamalaka have recorded peak KDE mean *b*-exponents of 1.72 - 1.74 and peak KDE form ratios of 0.08 - 0.07 respectively (Fig. 5.8c), falling in the overlapping areas of the glacial and subglacial fluvial end-member data envelopes. Humboldt Glacier in Northern Greenland has a peak KDE b value of 1.20, and a peak KDE form ratio of 0.08 (Fig.

5.8c), falling between the data envelopes of both the subglacial and subaerial fluvial end-members.

Table 5.1: Cross-section morphometrics

Region	Feature	Width (max)	Width (KDE)	Depth (max)	Depth (KDE)	V-index (mean)	V-index (std)	Average b (mean)	Average b (std)	Form Ratio (mean)	Form Ratio (std)
NS	1a	5885	1256	313	144	0.29	0.18	1.80	0.48	0.33	1.28
NS	1f	9531	3767	282	259	0.30	0.41	1.25	0.74	1.12	2.82
NS	2f	2411	821	238	63	0.31	0.22	1.87	0.72	0.12	0.25
NS	3f	2233	1006	163	129	0.22	0.21	1.49	0.48	0.13	0.36
NS	4a	3838	1331	277	242	0.34	0.12	1.90	0.37	0.15	0.44
NS	5f	2742	459	215	26	0.28	0.20	1.58	0.50	0.10	0.17
NS	6f	2781	1024	126	34	0.39	0.27	1.60	0.69	0.19	0.41
NS	7f	4372	679	165	40	0.32	0.26	1.52	0.54	0.17	0.40
NS	8f	1244	1162	67	55	0.35	0.13	1.79	0.55	0.04	0.04
NS	9a	2870	1547	453	371	0.25	0.24	1.53	0.49	0.46	1.38
NS	9f	2091	1509	202	162	0.18	0.25	1.56	0.56	0.18	0.43
NS	10f	4635	1839	316	180	0.20	0.28	1.33	0.53	0.34	1.37
NS	11a	5814	3416	372	271	0.34	0.34	1.40	0.64	1.42	3.40
NS	11f	11304	713	297	17	0.26	0.24	1.53	0.49	0.46	1.38
FL	1	1883	806	15	3.32	0.34	0.15	0.93	0.46	0.01	0.002
FL	2	2492	1489	25	19.31	0.41	0.13	1.88	0.61	0.01	0.002
FL	3	1279	632	167	112	0.43	0.15	1.82	0.77	0.13	0.09
FL	4	1002	635	108	94	0.33	0.24	1.25	0.53	0.12	0.07
FL	5	4382	791	29	2.26	0.45	0.23	1.72	1.05	0.01	0.02
FL	6	2207	1359	198	167	0.38	0.14	1.90	0.70	0.10	0.05
FL	7	2627	1199	202	169	0.18	0.19	1.44	0.41	0.13	0.05
FL	8	2285	1130	164	111	0.30	0.24	1.74	1.12	0.09	0.06
FL	9	8621	2298	303	153	0.25	0.23	1.58	0.76	0.06	0.06
FL	10	7978	1574	235	178	0.34	0.23	1.67	0.77	0.01	0.05
FL	11	3485	1299	23	18	0.43	0.18	1.78	1.26	0.01	0.0
FL	12	2812	1030	91	84	0.59	0.18	3.05	1.22	0.05	0.03
FL	13	1629	827	19	13	0.47	0.18	1.40	0.52	0.01	0.0
FL	14	1929	649	64	17	0.33	0.16	1.28	0.48	0.03	0.01
FL	15	8220	2525	89	53	0.22	0.26	1.30	0.82	0.02	0.09
FL	16	14146	10447	104	23	0.25	0.22	1.42	0.54	0.01	0.06
BC	Okan	5284	2979	457	283	0.34	0.19	1.91	0.94	0.06	0.09
BC	Kala	3066	1261	319	75	0.38	0.22	1.88	1.69	0.08	0.04
HU	All	5917	1985	293	201	0.38	0.34	1.74	1.08	0.87	2.27
HA	All	596	468	616	90	0.24	0.29	1.05	0.35	0.27	0.55
AL	All	8700	4803	1883	1151	0.71	0.22	1.86	0.91	0.77	1.25
LA	All	750	222	217	31	0.44	0.35	1.38	1.39	0.13	2.24

NS = Northern Swizterland
FL = Finger Lakes
BC = British Columbia
HU = Humboldt
HA = Hawaii
AL = Alaska
LA = Labyrinth

5.4.2.3 *KDE Values: V-index*

The peak KDE V-index is plotted against the *b*-exponent (Fig. 5.9), to visualise the changes in feature cross-sectional morphology independent of feature maturity (i.e. depth and width as a proxy for age). The below section reports the V-index values per feature, with the *b*-exponent values reported in the section above.

The peak KDE V-index (Fig. 5.9) of the end-members of erosion generally lie on or near the expected threshold of 0 for subaerial fluvial systems (Hawaii = 0.05), and >0.25 for purely glacial erosion (Alaska = 0.58) (Zimmer and Gabet, 2018). The end member for large-scale subglacial meltwater erosion, the Labyrinth, has a peak KDE value of 0.18, which plots in the middle between the glacial (U-shape) and subaerial fluvial (V-shape) end-members examples, although the spread of data (shown by the 66% data envelopes) overlaps strongly with the subaerial fluvial data in both the x (V-index) and y (*b*-exponent) directions (Fig. 5.9).

The peak KDE V-index values for all of the CGBLs generally fall within the envelope of subglacial fluvial erosion (grey bubble shown in Fig. 5.9), and therefore lie between the subaerial fluvial (V-shaped) and glacial (U-shaped) end members. The peak KDE V-index calculated for northern Switzerland ranges between 0.18 - 0.31 for the alpine cross sections and -0.04 - 0.38 for the foreland, while the peak KDE V-index values of 0.16 - 0.39 and 0.53 - 0.11, for the high-quality and low-quality Finger Lakes data, respectively. The Okanagan and Kalamalaka lakes have peak KDE V-index values of 0.27 and 0.29 respectively, and the Humboldt CGBLs have a recorded peak KDE V-index of 0.16. Overall, Fig. 5.9 reveals a strong positive relationship between the results of the *b*-exponent and V-index methods (r2 = 0.5 and p-value = <0.05).

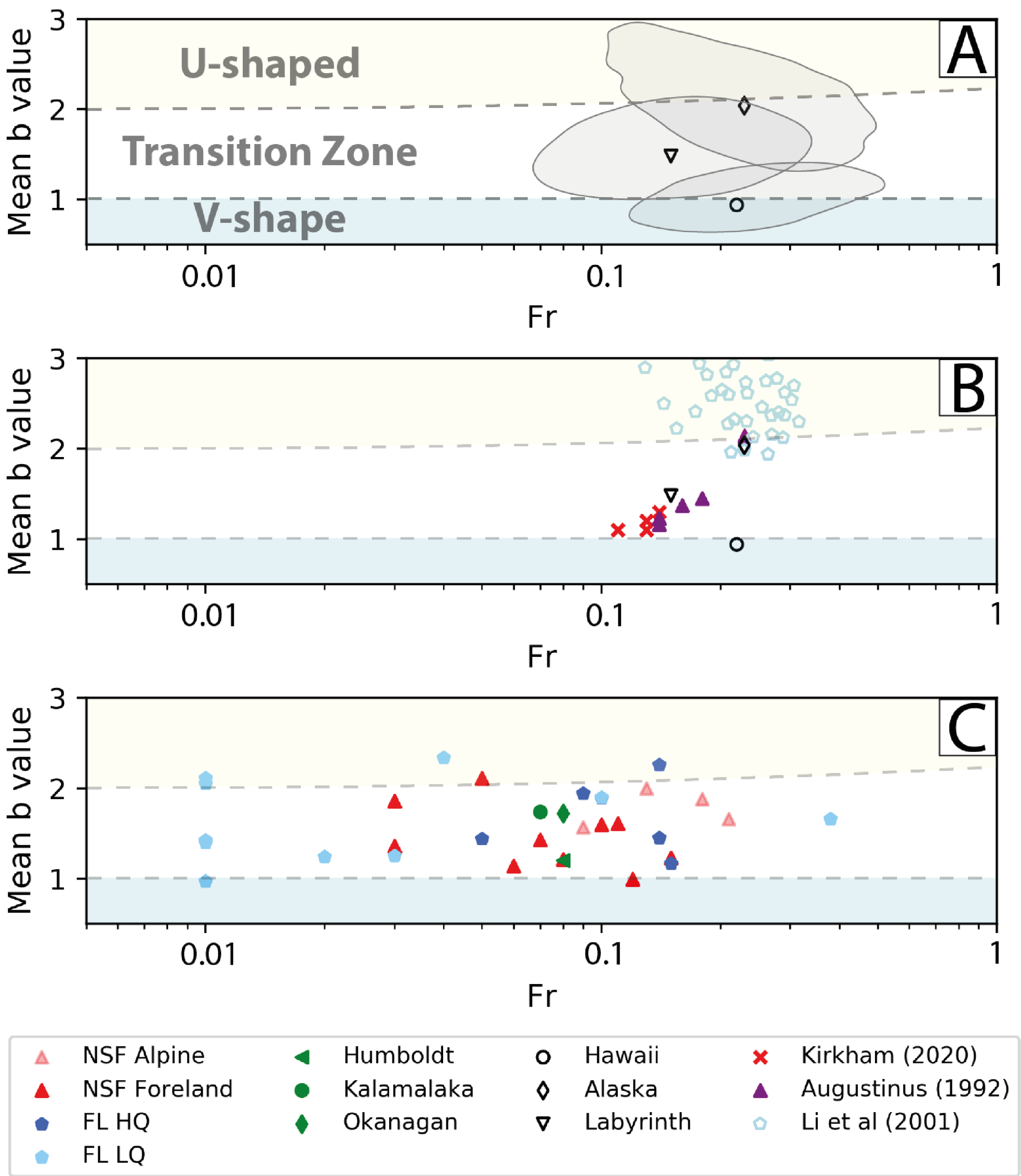

Figure 5.8: Scatter plots of b/Fr relationships from the peak mean KDE (for calculated sites) and reported b/Fr for previously published sites. (A) Peak KDE values of erosional end-member sites Alaska, Hawaii, and Labyrinth. The grey bubbles with solid grey lines indicate the location of 66% of measurements for each of the three end-member sites. (B) b/Fr data extracted from Augustinus (1992) showing mean values for 5 regions in New Zealand Southern Alps, Li et al (2001) showing mean b/Fr values for individual valley cross sections in Tian Shan Mountains, China, and Kirkham et al. (2020) showing mean values for meltwater channels in 4 regions across the Antarctic inner continental shelf, and the peak KDE values for the Hawaii, Alaska, and Labyrinth regions. (C) CGBL study sites. *b*-exponent indicative of pure glacial and fluvial signals are indicated by dashed lines, with positions of lines taken from Hirano and Aniya (1988) for comparison.

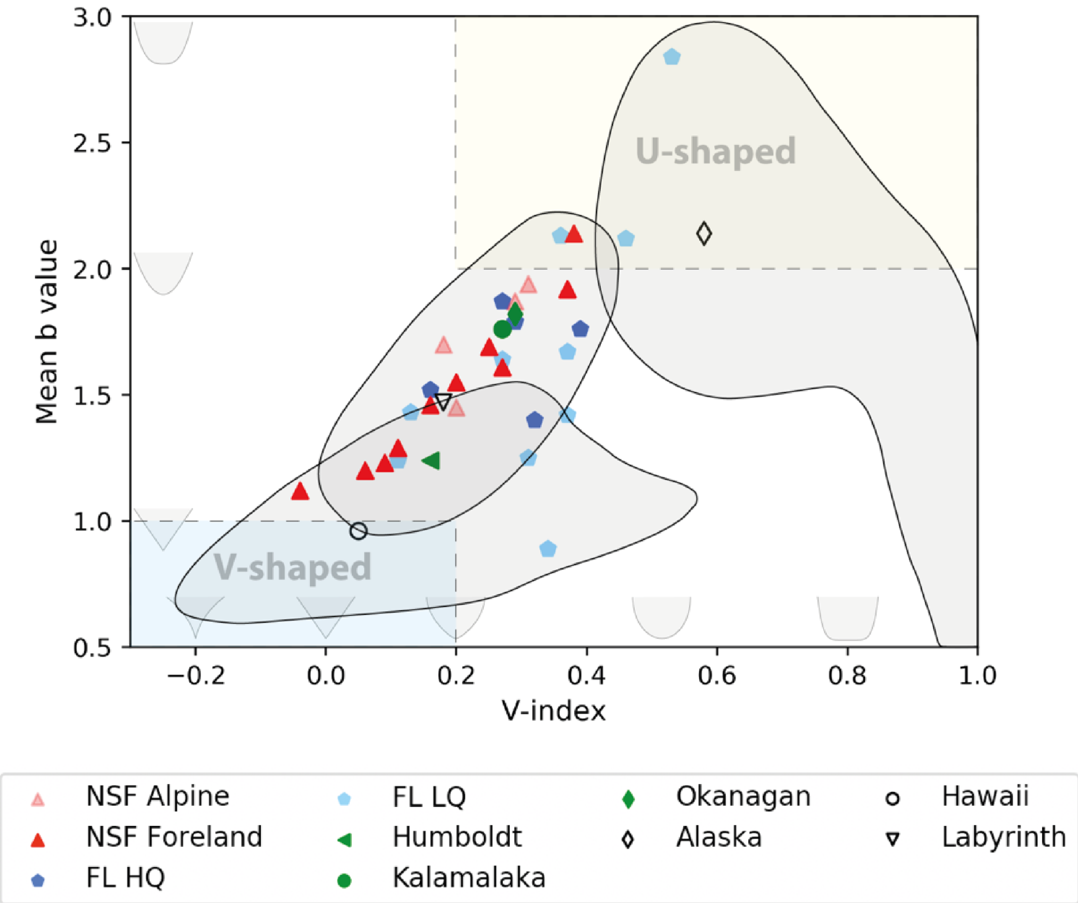

Figure 5.9: Scatter plots of peak KDE mean *b*-exponent against peak KDE V-index values for CGBL study sites and example end-members of erosion. Shaded silhouettes with dashed lines show idealised cross-sectional morphologies for given *b*-exponent and V-index values, with the light blue box displaying the expected zone of purely subaerial fluvial erosion and the yellow box displaying the expected zone of purely glacial erosion (Hirano and Aniya, 1988; Zimmer and Gabet, 2018). The grey bubbles with the solid grey lines indicate the location envelope of 66% of the data for the end-member sites of Alaska (purely glacial), Hawaii (subaerial fluvial), and the Labyrinth (subglacial fluvial). The long tail of the purely glacial data envelope is due to the *b*-exponent method not easily resolving very box shaped cross-sections resulting in extremely low *b*-exponents. This issue does not appear to be a problem when plotting b/Fr due to the data points not clustering around a single Fr value, and so not effecting the 66% data envelope. This issue is not translated to the V-index method, which calculates more reliable high V-index values expected with such morphologies.

5.5 DISCUSSION

Distinct morphological differences between glacial and fluvial erosion, first proposed by McGee (1894) and then others (Svensson, 1959; Hirano and Aniya, 1988; Harbor, 1995; Zimmer and Gabet, 2018), are clearly evident in both the *b*-exponent versus form ratio and *b*-exponent versus V-index plots (Figs.5.8 and 5.9). These relationships are shown in the locations of the peak KDE values and 66% data envelopes for our glacial and fluvial end members, which show little overlap in either relationships (Figs. 5.8 and 5.9). In addition, these data are roughly consistent with previously established *b*-exponent and V-index 'thresholds', indicative of strong glacial ($b \geq 2$, $V > 0.25$) and fluvial erosion ($b \leq 1$, $V < 0.25$) (Hirano and Aniya, 1988; Zimmer and Gabet, 2018), with the V-index threshold values conforming slightly better with the presented end-member data than the *b*-exponent thresholds. This is more clearly shown when comparing the averaged values and the data envelopes shown in Figures 5.8 and 5.9, where the data envelopes of the b/Fr values (Fig. 5.8) have significant overlaps in both the x (Fr) and y (*b*-exponent) directions, while the *b*/V-index relationships (Fig. 5.9) show a much clearer distinction between the 66% data envelopes of the glacial and two fluvial end members of erosion, with only slight overlap between the 66% data location envelops of all three end-members of erosion, in both b and V-index values.

The end-member 66% data location envelope for glacial erosion shows a strong correlation with the b/Fr values published for the U-shaped valleys in the Tian Shan Mountains, China (Li et al., 2001), and the same is true for the mean *b*/Fr values for meltwater channels across the Antarctic inner continental shelf (Kirkham et al., 2020) and the fluvial end-members (subaerial and subglacial). This strong correlation, however, does not hold for the published mean *b*/Fr data for U-shaped valleys of the Southern Alps in New Zealand (Augustinus, 1992), with all but one value plotting in the fluvial end member envelopes. This lack of correlation may be due to the limited number of cross-sections used for the calculation of each region in New Zealand (minimum 5 cross-sections), the potential variations in formation age of the features measured in conjunction with the wide variety of bedrock geologies, affecting the ability of the glacial valleys to maintain the classical U-shaped morphology, due to some geologies having low Rock Mass Strengths (RMS), as discussed by Augustinus (1992).

Despite being described as both tunnel valleys (e.g. Mullins and Hinchey, 1989; Mullins et al., 1996) and overdeepenings (e.g. Eyles et al., 1991; Vanderburgh and Roberts, 1996; Mullins et al., 1990; Dürst Stucki and Schlunegger, 2013), CGBLs display very similar morphologies (Figs. 5.6-5.9). All of the CGBL features show morphological relationships in *b*/Fr and V-index/*b* that fall mostly between the glacial and subaerial fluvial erosion envelopes, and overlap strongly with the subglacial fluvial examples (Figs. 5.8-5.9). The CGBL features of Northern Switzerland and the Finger Lakes display a wide range of morphologies, including valleys that plot within the purely fluvial and glacial ranges for both the *b*/Fr and *b*/V-index. The variations in cross-sectional morphologies may be due to the wide range of feature sizes seen in both regions, or could relate to the compounding influences of variations in other factors such as geology, topographic confinement, and style or timing of glaciation. Both the alpine and foreland regions of northern Switzerland are shown to have cross-sectional morphologies between the expected fluvial ($b \leq 1$ and V-index < 0.2) and glacial ($b \geq 1$ and V-index > 0.2) values (Hirano and Aniya, 1988; Zimmer and Gabet, 2018), with the alpine features clustering between *b*-exponents of 1.5 and 2. The foreland features, however, exhibit a much wider ranging of b and form ratio values, going from extremely U-shaped ($b > 2$), similar to b values of the glacial end member (Alaska), to V-shaped ($b < 1$), similar to the subaerial fluvial end member of Hawaii. The mean b and form ratio values of the high-quality Finger Lakes data sit in a similar range to those of northern Switzerland (Fig 5.8c). The b values from the low-quality Finger Lakes data also show similar ranges in b values to the high-quality Finger Lakes data, with just one value dropping below the expected fluvial b value of 1. However, the low-quality data show a much greater range of form ratio values and are typically much lower than other CGBLs or end-members (Fig. 5.8) This lower form ratio is interpreted to be caused by the USGS bedrock surface DEM (Soller and Garrity, 2018) used in the creation of the Finger Lakes DEM not capturing the full depth of the features, and so producing a shallower depth compared to width ratio (form ratio). This difference in depth is seen when the location of the high-quality features are compared with the USGS bedrock DEM and the bedrock maps published by Mullins et al. (1996). The peak KDE V-index/*b* and *b*/Fr value distributions show a trend towards strongly U-shaped for British Columbia features, and V-shaped for Humboldt. The study sites of the Humboldt and British Columbia lakes all fall within a similar envelope to the CGBLs in northern Switzerland and the Finger Lakes. However, the Humboldt features are notably more V-shaped than the CGBLs, but still above the *b* value expected for purely fluvial signals, and in the same range as the subglacial fluvial envelope. This lack of correlation of feature morphologies in CGBLs with either end-member of glacial or subaerial fluvial erosion is also seen in the V-index/*b* value relationships presented in Figure 5.9.

The relationship between the width and depth components of the form ratio and CGBL morphologies (*b*-exponent and V-index) was investigated further to explore how different erosional processes interact during the development of CGBLs, assuming size is a rough proxy for feature age. The glacial erosion end-members are characteristically the deepest and widest CGBLs (peak KDE depth = 1136 m, and width = 5027 m), with the subaerial and subglacial fluvial end-members of erosion characterised by much shallower and narrower features (peak KDE depths = 77 m and 36 m, and widths = 471 m and 267 m for subaerial fluvial and subglacial fluvial respectively). The study site CGBL features have peak KDE depths and widths of intermediate values (Figs. 5.10 and 5.11) between those of the purely glacial and fluvial end members, although the low-quality Finger Lakes CGBLs are much shallower than the high-quality data.

Previous works have proposed several expected trends in maturity (development) of glacial valleys (Hirano and Aniya, 1988) related to the widening or deepening of valleys and the styles of glaciation. The trends proposed by Hirano and Aniya (1988) stated that pre-glacial valleys would evolve from their V-shaped fluvial valley morphology towards more U-shaped glacial morphology, with the amount of change in morphology related to the length of glacial occupation. The proposed trends by Hirano and Aniya (1988) rely on an assumption of development of features from a preglacial fluvial feature. The trace of these preglacial features would likely be hard to see due to CGBL feature being eroded below fluvial base level, but would be expected to result in complex morphologies including changes in valley cross-section angles (e.g. inset valleys), which are not seen in any of the CGBLs (Fig. 5.12). The use of form and morphology trends as a tool for interpreting feature maturity in such a direct way have been shown to be highly dependent on the influence of several other external factors, including underlying bedrock erodibility and structure (discussed further in chapter 6), as well as the timing and extent of glaciations (Augustinus, 1992; Harbor, 1995; Brook et al., 2004; Swift et al., 2008), which lie outwith the scope of this chapter and thesis.

The *b*-exponents and V-index of the Finger Lake CGBLs show no perceivable trend with depth or width, while northern Switzerland features show a slight trend to stronger V-shaped morphologies (lower *b*-exponents and V-index values) with increasing peak KDE depth and width. The trend of development in the features of northern Switzerland appears to be the opposite of that seen in the erosional end-members of Alaska and Hawaii (i.e., more U-shaped glacial valleys are associated with widening and deepening) (Hirano and Aniya, 1988; Augustinus, 1992; Harbor, 1995; Brook et al., 2004; Swift et al., 2008).

Increased widening and deepening with V-shaped-ness, seen in the features of northern Switzerland, are interpreted to indicate that as the features grow to sizes similar to the glacial end-member, they are increasingly influenced by compounding factors. The increasing V-shape-ness is not thought to be simply increased influence of subglacial fluvial erosion, as this would be expected to result in a skew towards deepening of the features, and not widening, with the formation of features such as slot gorges in the base of the CGBLs (Dürst Stucki et al., 2012; Jansen et al., 2014). Therefore, the increased V-shape-ness of the northern Swiss features may be a result of a combination of factors. The first potential factor of influence may be increased meltwater erosion due to focusing of meltwater flow with feature development (Kessler et al., 2008; Herman et al., 2015). The second explanation for the observed changes in cross-sectional morphology with depth may be due to factors such as the rock mass strength (RMS) of the incised bedrock (Augustinus, 1992). The latter may be a key component, due to the bedrock of the foreland of northern Switzerland consisting of Molasse (shales, sandstones and conglomerates) as well as some limestone and dolostone units, which are classified as highly erodible by Kühni and Pfiffner (2001). The highly erodible nature of the foreland bedrock geology in northern Switzerland is likely to mean the units have lower RMS, and so may not be able to maintain the traditional U-shaped morphology for extended periods of time (Augustinus, 1992; Kühni and Pfiffner, 2001). See chapter 6 for further discussion of these points. The lack of any strong trend between feature size and average morphology (*b*-exponent and V-index) makes it difficult to untangle the question of feature development/maturity using size as a proxy for age or feature maturity.

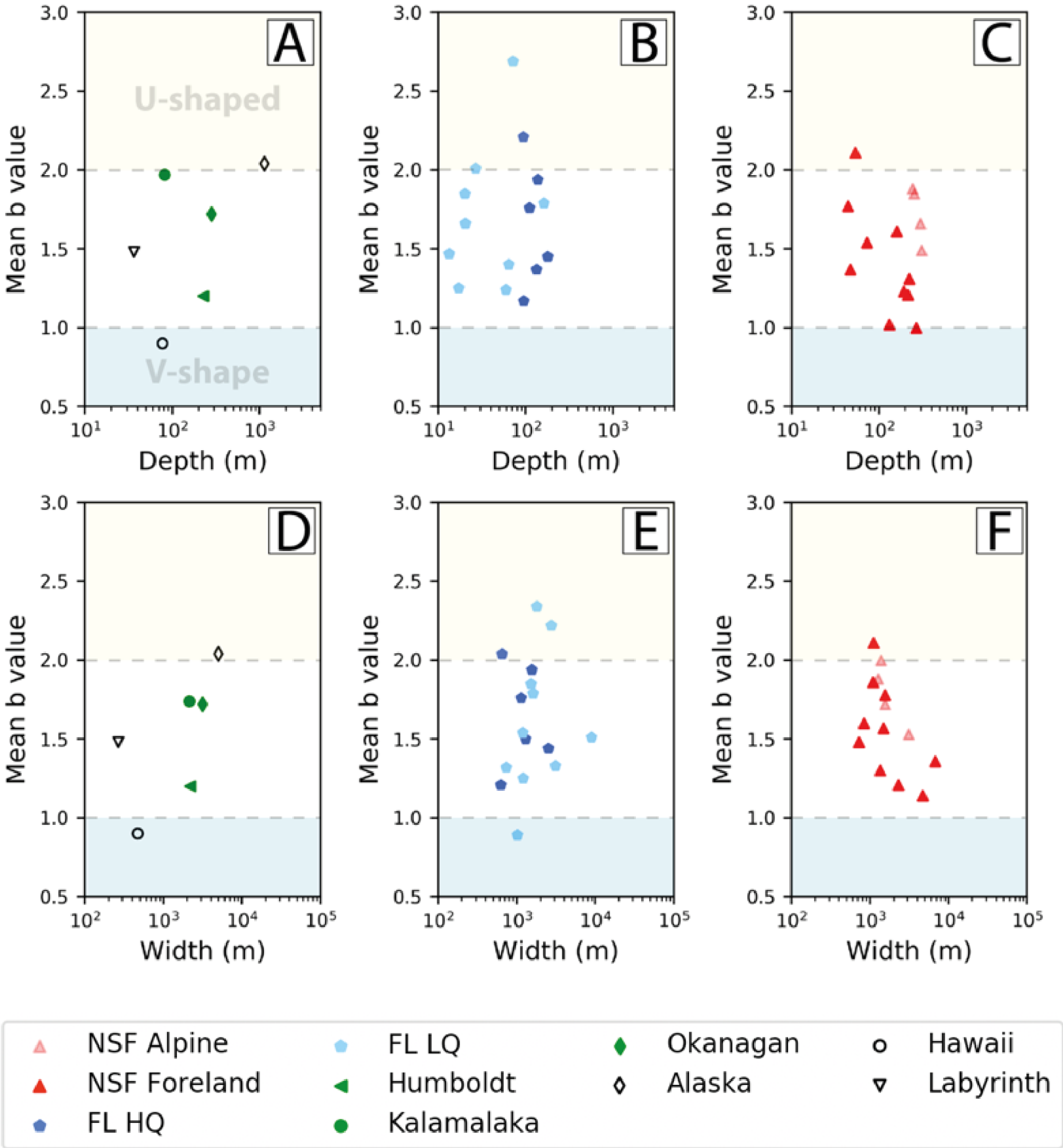

Figure 5.10: Scatter plots of peak KDE mean *b*-exponents against peak KDE width and peak KDE depth. (A) Peak KDE mean *b*-exponents against peak KDE depth for CGBL study sites of the Humboldt and British Columbian lakes, and end-members of erosion. (B) Peak KDE mean *b*-exponents against peak KDE depth for Finger Lakes features. (C) Peak KDE mean *b*-exponents against peak KDE depth for northern Switzerland features. (D) Peak KDE mean *b*-exponents against peak KDE width for CGBL study sites of the Humboldt and British Columbian lakes, and end-members of erosion. (E) Peak KDE mean *b*-exponents against peak KDE width for Finger Lakes features. (F) Peak KDE mean *b*-exponents against peak KDE width for northern Switzerland features. Dashed lines indicate published mean *b*-exponents thresholds for glacial (*b*-exponents ≥ 2) and subaerial fluvial (*b*-exponents ≤ 1) cross-sectional morphology (Hirano and Aniya, 1988; Harbor, 1995).

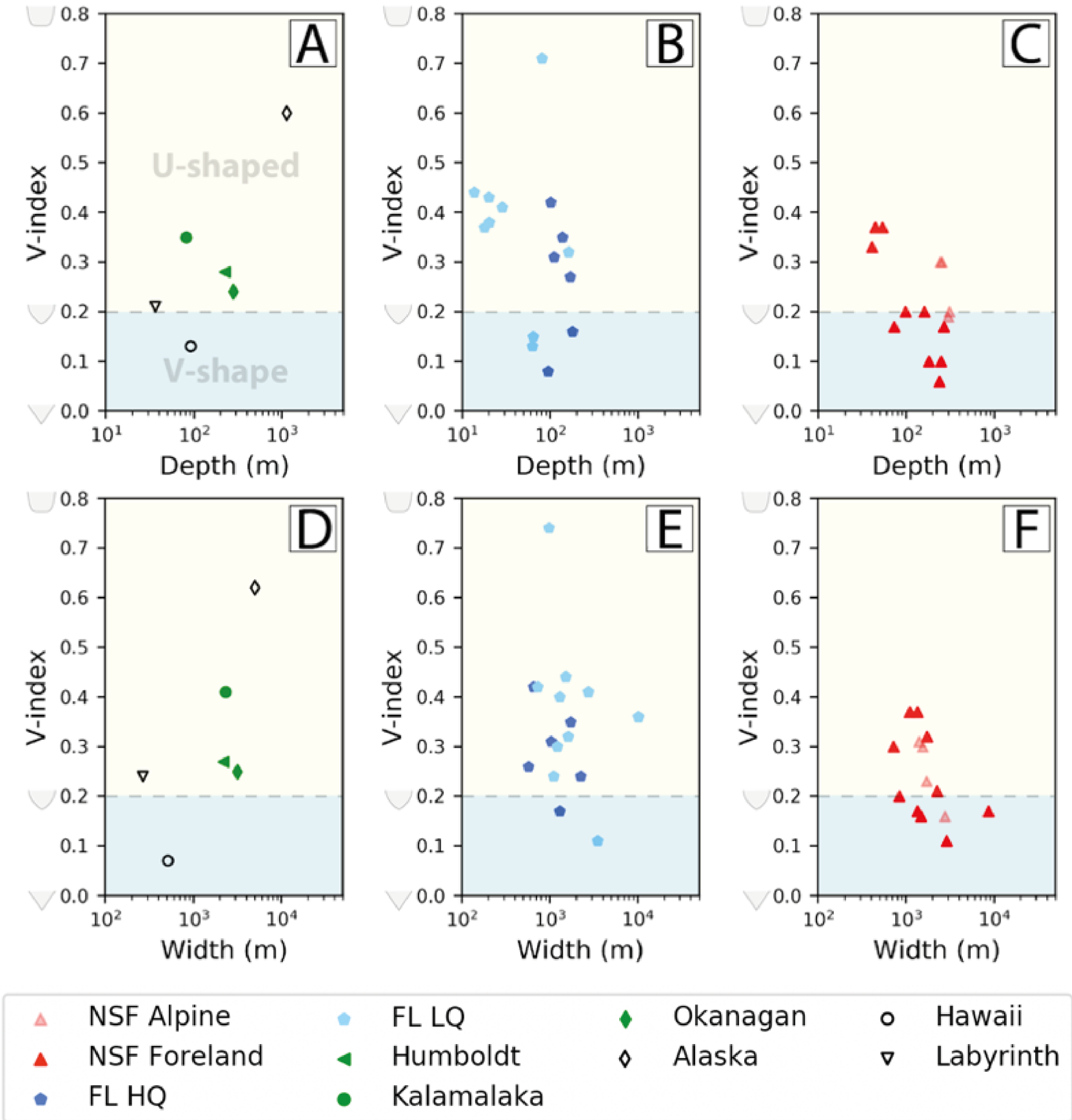

Figure 5.11: Scatter plots of peak KDE V-index against peak KDE width and peak KDE depth. (A) Peak KDE V-index against peak KDE depth for CGBL study sites of the Humboldt and British Columbian lakes, and end-members of erosion. (B) Peak KDE V-index against peak KDE depth for Finger Lakes features. (C) Peak KDE V-index against peak KDE depth for northern Switzerland features. (D) Peak KDE V-index against peak KDE width for CGBL study sites of the Humboldt and British Columbian lakes, and end-members of erosion. (E) Peak KDE V-index against peak KDE width Finger Lakes features. (F) Peak KDE V-index against peak KDE width for northern Switzerland features. Dashed lines indicate published V-index thresholds for glacial (V-index $\geq$0.2) and subaerial fluvial (V-index $\leq$0.2) cross-sectional morphology (Hirano and Aniya, 1988; Harbor, 1995).

The variable cross-sectional form of CGBL sites shows a strong relationship with the Labyrinth subglacial fluvial end member 66% data envelope, that formed by catastrophic meltwater drainage (Lewis et al., 2006) and the meltwater channels recorded by Kirkham et al. (2020), which fall between established values representative of end-member glacial and subaerial fluvial erosion processes (Hirano and Aniya, 1988). This overlap may indicate a distinct class of landform characterised by strong hydrological conditioning of glacial erosion processes, which might be expected in a subglacial environment dominated by temperate warm-based conditions and single or recurrent large magnitude subglacial flood activity, for example due to subglacial (Lewis et al., 2006) or supraglacial lake drainages (Alley et al., 2005; Greenwood et al., 2016) or diurnal meltwater inputs (Boulton et al., 2007; Smith et al., 2021). However, despite the shape of the CGBL features showing a strong relationship with the Labyrinth end member, the typical widths and depths of the CGBL features are much larger than the fluvial end-members of erosion. The difference in geometry in conjunction with the morphologies of the CGBLs may be an indication of a mixed signal of glacial and fluvial erosion.

This mixed erosional signal (i.e. fluvial and glacial) may be due to the strong dependency of subglacial erosion on subglacial water discharge (e.g. Alley et al., 2019); increased meltwater accumulation causes faster ice flow speeds through CGBL features resulting in greater glacial erosion, further incising the features, which in turn results in the increased focusing of subglacial meltwater through the features (Kessler et al., 2008; Herman et al., 2015). This feedback loop of incision focusing meltwater, which in turn increases incision, would be limited by ice-bed decoupling during high meltwater flow, which would cause reduced erosion (Lesemann et al., 2010). Additionally, the mixed signal may be the result of repeated but separate episodes of subglacial fluvial and glacial erosion (Dürst Stucki and Schlunegger, 2013). It is unclear if such cycling is linked with fluctuations in surface melt inputs or specific development stages of the ice mass. However, no strong morphological evidence has been seen for or against this style of development in the analysis undertaken as part of this chapter.

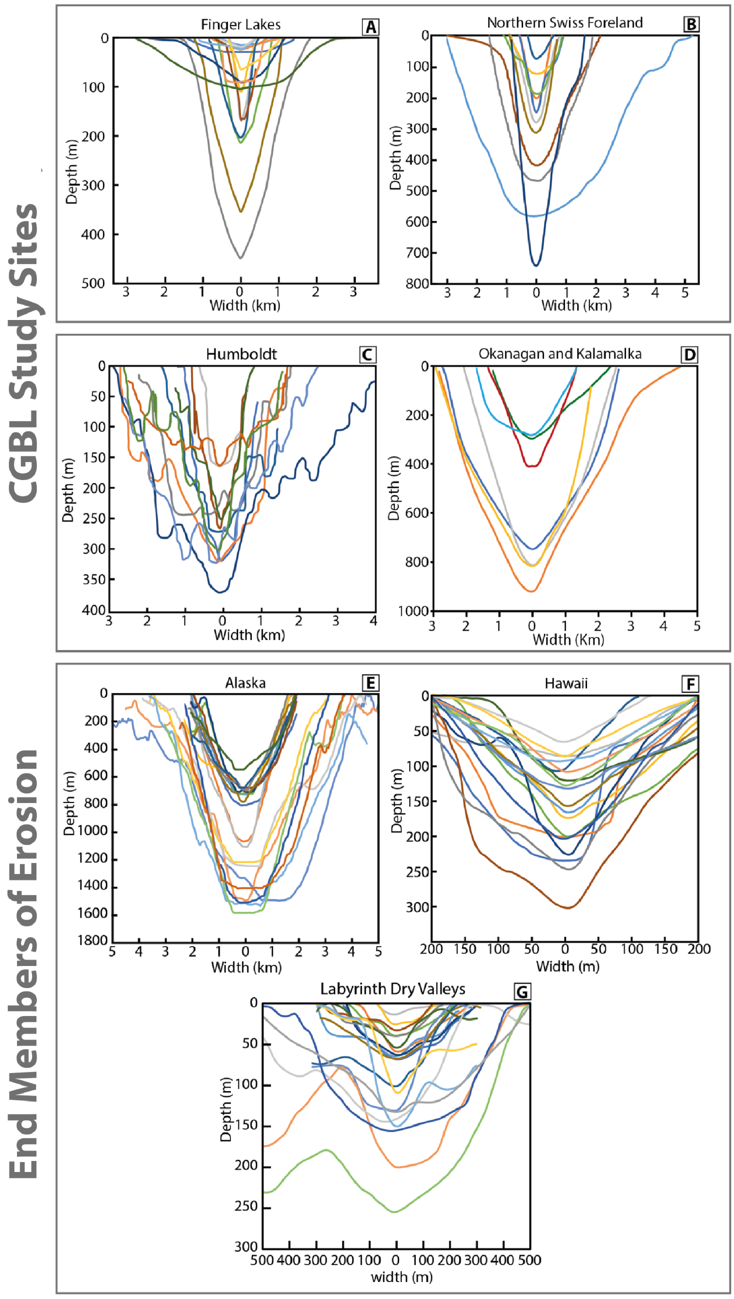

Figure 5.12: Example cross-profiles of study sites, additional comparison sites, and erosional end members. Cross-profiles for the study and additional sites were selected at points of deepest erosion per feature, with the exception of Humboldt due to lack of longitudinal data, allowing identification of feature continuity between cross-profiles. Example cross-profiles for end members of erosion were selected at approximate locations of deepest erosion per CGBL with an even spatial spread across identified CGBLs. Cross-profiles are coloured to allow easy identification and visualisation of individual profiles.

5.6 SUMMARY

Overall, these results demonstrate that CGBLs, despite previously being described as separate features (e.g. tunnel valleys and overdeepenings), have similar averaged cross-sectional morphologies, and when compared with end-members of erosion, fall between the subaerial and purely glacial morphologies, and strongly within the subglacial fluvial end member. This lack of clear morphological differences between CGBLs brings into question the use of distinct genetic nomenclature, and suggests that a single term (such as Channel-like Glacioerosional Bedrock Landforms) that does not imply genetic interpretation and covers the full spectrum of processes involved in the formation of all CGBL type features should be used to discuss the features, and a more specific name could be assigned where dominant erosional processes are known (such as tunnel valleys and overdeepenings).

Any model of the formation and development of CGBL features needs to be able to explain the range in morphologies shown in the CGBLs of the four study regions, and the general tendency of larger CGBLs in northern Switzerland to be more V-shaped. The large spread of the data between V-shaped and U-shaped morphologies suggests that the features are eroded by both glacial and fluvial erosion, and that additional factors including the erodibility of the underlying bedrock (RMS, Augustinus (1992)) and changes in topography confinement may play a significant role in affecting the resulting feature morphologies. The exact proportions and timings of the different types of erosion cannot be calculated using the data presented in this chapter. As the features grow in depth (using depth as a proxy for age) they may, in some cases, increasingly act as conduits for subglacial fluvial meltwater pathways, although this relationship is only apparent in northern Switzerland.

6

VARIATION IN MORPHOLOGY ALONG PROFILE FORM OF BEDROCK OVERDEEPENINGS AND TUNNEL VALLEYS IN FORELAND SETTINGS: THE CHANGING CONTRIBUTION OF FLUVIAL VERSUS GLACIAL EROSION

6.1 INTRODUCTION

The aim of this chapter is to present the results of the analysis of CGBL cross-sectional morphological changes within features, and address how and why these changes occur along features. This work was done to answer research objective 4, as such changes in morphology along the length of a CGBL may indicate the influence of various factors on feature formation and development; such as erodibility of bedrock lithology (RMS); geological faulting; topographic confinement; and angle of feature slopes. An example of how feature morphology is affected by such factors comes from Swift et al. (2008) who showed that changes in the East Greenland fjord region were due to changes in bedrock hardness. By these means, this chapter hopes to address research questions 3 and 4, as mentioned in chapter 1, regarding erosional processes, geology and topography, and what role these play in determining the present-day morphology.

The previous chapters of this thesis discussed in depth the proposed formation and development of CGBL features, as well as how these features have been studied in the past (Ó Cofaigh, 1996; Kehew et al., 2012; Cook and Swift, 2012; Livingstone and Clark, 2016). Chapter 5 specifically uses an analysis of four main study regions to compare the average morphologies of each feature and region against example end-members of the main types of erosion: glacial, subaerial fluvial and subglacial fluvial. This work, presented in chapter 5, enhances the scientific community's understanding of such glacially eroded landforms: features which were previously considered to have been formed by distinct erosional processes were actually found to have overlapping but diverse morphological forms. As such, features which were previously considered to be taxonomically independent, i.e. overdeepenings and tunnel valleys, can be thought of as part of a spectrum containing many different morphologies.

The results presented in chapter 5, based on analysis of typical cross-section form, suggest a mixed formation process involving both glacial and subglacial fluvial erosion. However, the there is still further diagnostic morphological information related to process that could be gained from the variations in form in the selected CGBL features. For example, CGBLs can be found to straddle different geological regional contexts that contain rocks of various compositions, metamorphic histories, and hence erodibility, and likely intersect several populations of tectonic structures that possess different anisotropies, like fractures, faults or folds. To this point, while the method used in Chapter 5 provides an indication of the dominant erosional forces that affected a feature, it cannot provide insight into how these forces may have interacted or changed within features, where one force may have dominated over another nor how local geometrical complexity may have influenced morphology. It is the purpose of this chapter to investigate, and untangle, this issue of local variability along a feature as it is likely to have an important role to play in the formation and development of CGBLs.

This chapter focuses on long-profile variability of features in the NSF and FL regions because these have the best available data (see Chapter 3). The lakes and basins of the foreland of northern Switzerland have previously been described as overdeepenings (Dürst Stucki and Schlunegger, 2013), whilst the basins of the Finger Lakes region of New York State, USA have typically been described as tunnel valleys (Mullins and Hinchey, 1989; Mullins et al., 1996). Both regions have been described in detail in Chapter 3, and have been studied extensively with good coverage in published topographical and geological maps (Rickard and Fisher, 1970a; Mullins et al., 1996; Kühni and Pfiffner, 2001)(Federal Office of Topography swisstopo, 2005). Thus, data of suitably high resolution is available to permit further detailed analysis of changes along features. Moreover, as the features of NSF and the FL have average cross-sectional morphologies that range between or overlap with the glacial, subaerial fluvial and subglacial fluvial end-members of Chapter 5, a detailed study of each feature's changing morphology will hopefully allow for a deconvolution of where an erosional force was most influential. Alongside this, the comparison of the two regions also allows for the investigation of the role of ice flow direction in relation to topographic confinement; paleao-ice flow was from the topographically confined alpine valleys to the unconfined foreland in northern Switzerland, while the opposite occurs in the Finger Lakes, with palaeo-ice flow into the more confined Allegheny Plateau from the Erie-Ontario Lowlands.

Changes in cross-sectional morphology along the long-profile of CGBLs in the northern Switzerland and Finger Lakes regions are explored in this chapter, specifically in the context of variability in geology, topographic confinement, and erosional process. It is hypothesised that the dominant erosion process, and thus cross-section form, might be affected by bedslope (i.e. whether the CGBL long-profile is sloping in a normal or adverse direction (Alley et al., 2003; Cook and Swift, 2012; Werder, 2016)), by the joining of tributary valleys, and by changes in bed erodibility. Specifically, cross-profile morphology along each CGBL feature is plotted with respect to the locations of: normal and adverse slopes; changes in topographic confinement; tributary valleys or valley junctions; and major geological features (bedrock lithology and faulting).

6.2 METHOD

6.2.1 *Morphometric methods*

The semi-automated methods used to preprocess the DEM data of the Finger Lakes and northern Switzerland are described in Chapter 4. Long-profiles for each CGBL were calculated along the path of deepest erosion in ArcGIS using a route-finding algorithm and cross-sections extracted at 100 m intervals, as described in Chapter 4 section 4.4. The methods for calculating morphometrics (b-Fr, and V-index) every 100 m at cross-profiles along CGBLs are described in Chapter 5 section 5.3.

6.2.2 *Qualitative analysis of long-profile change in form*

The changes in *b*-exponent and V-index were plotted against changes in depth, width, and form ratio along the long-profiles of the 11 CGBLs of northern Switzerland and 16 CGBLs of the Finger Lakes (Figs.6.5 and 6.6 and Figs. B.1, B.2, B.3, and B.4 in the appendix B). This was done to qualitatively identify relationships between variations in cross-sectional morphology and feature depth and width, which allowed for preliminary identification of patterns for further analysis.

6.2.3 *Quantitative analysis of variation in long-profile form*

To gain a fuller understanding of the distribution of the different morphological relationships of the CGBLs of northern Switzerland and the Finger Lakes, relationships between depth, width, form ratio, *b*-exponent, and V-index have been plotted for all of the cross-sections in each region (Figs. 6.7 and 6.8). For each of the plots linear regression was performed and the resulting r^2 values plotted along with the trend lines for relationships with an r^2 value of over 0.05.

6.2.4 *Statistical analysis of relationships between form metrics*

To investigate the relationship between distributions of morphometrics within features and to identify simple correlations between key factors, linear regressions were carried out (Tables 6.1 and 6.2). Linear regression has been undertaken on a per feature basis, focusing on the key scalar factors of depth, width, and form ratio, as well as the results of the two methods of cross-sectional morphological analysis, the b-exponent and V-index.

6.2.5 *Hypothesis testing: controls on long-profile and cross-profile form*

6.2.5.1 *Normal and adverse slopes*

The locations of normal and adverse slopes (Fig. 6.2) were calculated using a Python script which implements a peak finding algorithm (Scipy, 2020) to find the peaks and troughs associated with the start and end of normal and adverse slopes for the features in the northern Swiss study area. The peak finding algorithm identifies the locations of prominent peaks and troughs from the vertical difference between the points along the profile (Fig. 6.2). The peak/trough is determined when the difference is equal to or greater than a given prominence. Several different peak prominences were tested, with the final prominence value chosen as 40 m. 40 m was chosen for this grid size to capture the detail of the feature, while eliminating the noise found at smaller scales. The long-profiles of each of the features were then resampled from the 25 m resolution extracted from ArcMap 10.7 to 100 m resolution and normal and adverse slopes categorised (Fig. 6.2) to allow for comparison with the cross-sectional morphological data calculated using the V-index code (Zimmer and Gabet, 2018). The method was predicted to produce several normal and adverse slope segments per feature from visual inspection. These nested basins are additionally predicted in features such as overdeepenings, and have been previously described as containing numerous sub-basins or “nested-basins” (Cook and Swift, 2012). Tunnel valleys have also been described as having “undulating bed forms” which may contain adverse and normal slopes (Kehew et al., 2012). The angles of the slopes were then calculated for each point along the slope using the derivative between each point and converting into degrees. The long-profiles of the Finger Lakes were not of high enough quality to extract meaningful slope angles from, and so the Finger Lakes were not analysed as part of the normal and adverse slope analysis.

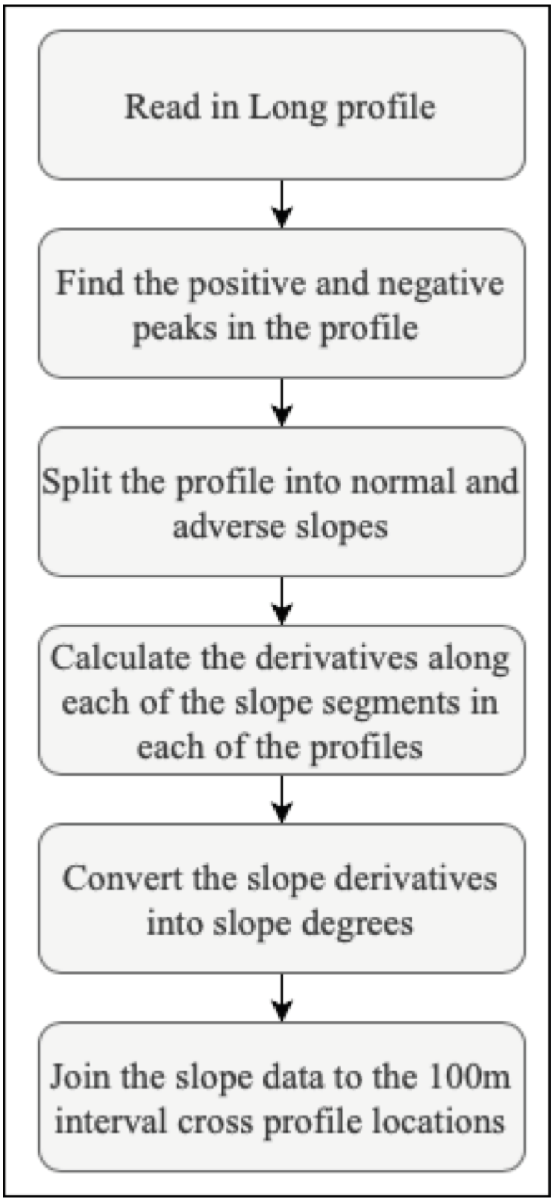

Figure 6.1: Workflow chart showing steps taken in the identifying normal and adverse slopes in line of deepest erosion in CGBL features in northern Switzerland.

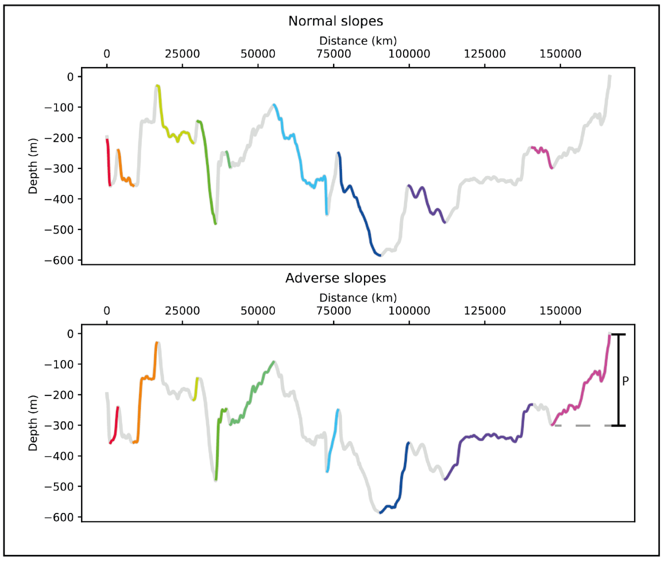

Figure 6.2: Example of how normal and adverse slopes were categorised. The slopes are colour coded to relate an adverse and normal slope to each other and therefore a sub-basin in the CGBL feature. P shows peak prominence.

6.2.5.2 *Topographic confinement*

The topographic confinement of each feature in northern Switzerland and the Finger Lakes were calculated in ArcGIS. This involved producing 5 km buffers for points spaced at 1 km intervals along the line of deepest erosion, and using zonal statistics to calculate standard deviation of the bedrock elevation for each buffered area as a proxy for topographic confinement (see Fig.6.3).

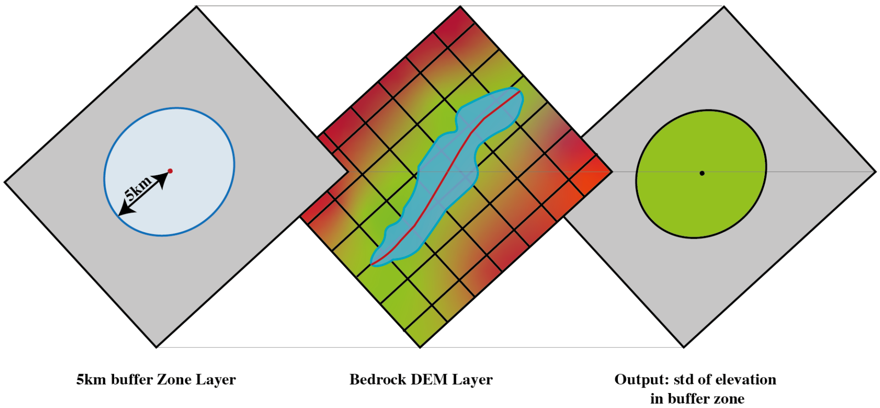

Figure 6.3: Schematic diagram showing how topographic confinement is calculated for each point along the centre lines of each of the CGBL features. Figure adapted from ArcGIS documentation for Zonal Statistics.

6.2.5.3 *Tributary valleys*

The locations of tributary valleys were determined by eye for each of the CGBLs in northern Switzerland and the Finger Lakes. This involved projecting the estimated centre point for the tributary valleys to meet the long profile line of the trunk CGBL. The human error in choice of angle of projection of a tributary valley can influence whether the valley is interpreted as intercepting with a particular sub-basin feature or if it is not, the magnitude of which cannot be easily calculated. Therefore, only broad trends of association between the location of tributary valleys and sub-basin locations are reported in this chapter.

6.2.5.4 *Geology / bedrock erodibility*

Changes in geology and bedrock erodibility were identified through visual inspection of published geological and erodibility maps, where available, of the two study sites of Norther Switzerland (Geological Map of Switzerland 1:500,000 (Federal Office of Topography swisstopo, 2005), (Kühni and Pfiffner, 2001) and the Finger Lakes (Rickard and Fisher, 1970a). The region of northern Switzerland has both geological and erodibility maps available, and so the relative erodibility of the bedrock units published by Kühni and Pfiffner (2001) have been used for the investigation of the effect of underlying geology on feature scale and morphology. The region of the Finger Lakes did not have any bedrock erodibility maps or published bedrock RMS measurements available, so the comparison of the influences of changes in bedrock lithology has been undertaken using only the boundaries of the different formations and groups mapped by Rickard and Fisher (1970a).

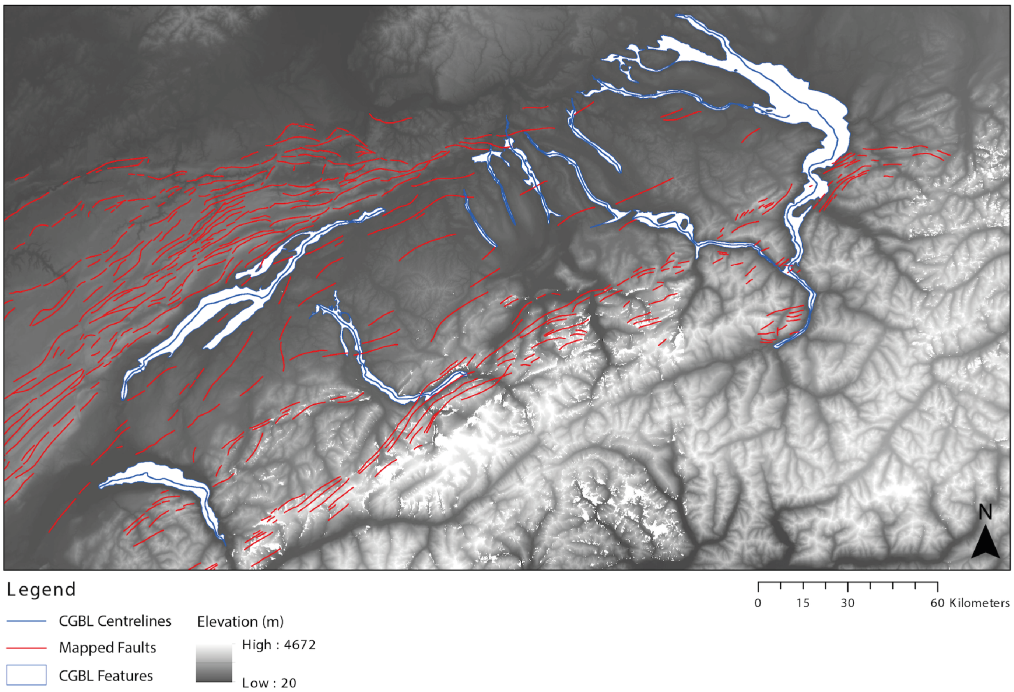

Figure 6.4: Map showing location of published mapped geological faults in northern Switzerland and CGBL features. Faults mapped by the Federal Office of Topography swisstopo (2005)

Figure 6.4 shows the location of the published mapped large-scale geological faults present in the study area of northern Switzerland (Federal Office of Topography swisstopo, 2005). The number of intercepts of the faults with the centrelines of the CGBL features were used to determine the influence of geological faulting on sub-basin formation within CGBL features. Because the CGBLs are buried either by sediment or water, making mapping of geological structures difficult, faults that were mapped within 10 km of the centrelines of the features were projected into the feature. The region of the Finger Lakes was not analysed for the influence of geological faulting on CGBL development as Rickard and Fisher (1970a) showed no normal or thrust faults present within the Finger Lakes study region.

6.2.6 *Statistical analyses*

6.2.6.1 *Linear regressions*

Linear regression analysis was undertaken for all of the bi-variant relationships investigated as part of the analysis of this chapter. This was done to quantify potential trends seen in the data between different variables. The trend lines were plotted in the figures where the r^2 values were over 0.05. Log and exponential regression analysis was undertaken to investigate the relationship between the b-exponent and the V-index, however due to the scatter of the data, no significant improvement over the linear regression was noted.

6.2.6.2 *Kolmogorov–Smirnov test*

The Kolmogrov-Smirnov statistical test was used to check similarity between distributions of V-index values of all normal and adverse slopes of northern Switzerland. The Kolmogorov–Smirnov test was chosen because it does not assume a normal distribution of the compared data and is non-parametric.

6.3 RESULTS

6.3.1 *Initial description of long-profile variation in form*

The location of the point of deepest erosion of features in the NSF (Fig. 6.5) appear to vary between features, with several of the features having the deepest point near the inflow (features 5, 9, 10, and 11) while others erode more deeply closer to the feature outflow (feature 2,3, and 7) or middle (feature 4). This variation in location of deepest erosion is not seen as strongly in the long-profile of the features of the Finger Lakes, where the features seem to have more uniform patterns of erosion, with the features eroding more deeply either near the middle (features 4, 6, and 13) or closer to the outflow end (features 3, 9, 10, and 16). The variations in location of increased erosion between the features of northern Switzerland and the Finger Lakes is also seen in the presence of nested basins (see examples in feature 1 in Fig. 6.5 and feature 9 in Fig. 6.6). The long-profiles of the northern Swiss features show many large nested basins, while the features of the Finger Lakes show very few nested basins (features 6 and 9).

The change in both the b-exponent and V-index along the profiles appears not to be random (i.e., scattered), but appears to show trends of increasing and decreasing values along long-profiles from feature inflow to outflow, although with significant variation in morphology along features (Fig.6.5 and 6.6). The changes in cross-sectional morphology down features show potential correlation between changes in topography (Fig. 6.5 F1, F9, and F11), in the form of changes in depth and width of features (Fig. 6.5 F5 and Fig. 6.6 F4, F9, and F10; and Fig. B.1 F1 in the appendix), and the location of tributary valleys (Fig. 6.5 F7, F10, and F11). It is noted that the ends of the features do show some random variations which might be due to the cross-sections becoming very shallow or developing cross-profiles that are too complex for the semi-automated method. The ordered nature of the changes in morphology along features are investigated and quantified in the following section of this chapter.

6.3.2 *General morphometrics of CGBLs per region*

Figures 6.7a shows that CGBLs of northern Switzerland have a strong trend of increasing width with increasing depth up to a depth of ~350 m and width of 4 km, before changing into a much wider trend. This may be better represented by two trends, with a significant population widening up to 16 km without deepening, and another population deepening up to 800 m but with limited widening. This potential bimodal distribution of cross-sectional morphologies is seen more strongly in the features of the Finger Lakes (Fig 6.8a).

The CGBLs of northern Switzerland show a weak but statistically significant trend of increasing V-index with depth and width (r^2 values of 0.11 and 0.15 respectively, with p-values < 0.05) (Figs. 6.7d-e). The trend of increasing V-index with width and depth is also potentially seen in the morphologies of the Finger Lakes feature, specifically the V-index/depth ($r^2 = 0.05$; $p < 0.05$) (Fig 6.8d). This trend, positive or negative, is not seen strongly in the b vs depth and width relationships for northern Switzerland ($r^2 = 0.03$; $p < 0.05$) (Figs. 6.7b-c). However, the corresponding b/depth relationships of the Finger Lakes (Fig. 6.7b) show a trend of increasing b-exponent with depth up to 25 m, after which the relationship seems to break down. The relationships of b with width (Fig 6.7c and 6.8c) and the form ratio (Fig. 6.7f and 6.8f) do not show strong trends, with only the b/Fr of the Finger Lakes showing the potential of a trend to lower b values with lower Fr values.

The b/V-index relationships of both regions show that the two methods for measuring feature cross-sectional morphologies match quite well, with figures 6.7g and 6.8g showing a strong trend with increasing b-exponent and increasing V-index, but at high V-indexes the populations becomes bimodal with V-index values remaining high but b-exponent values being much lower.

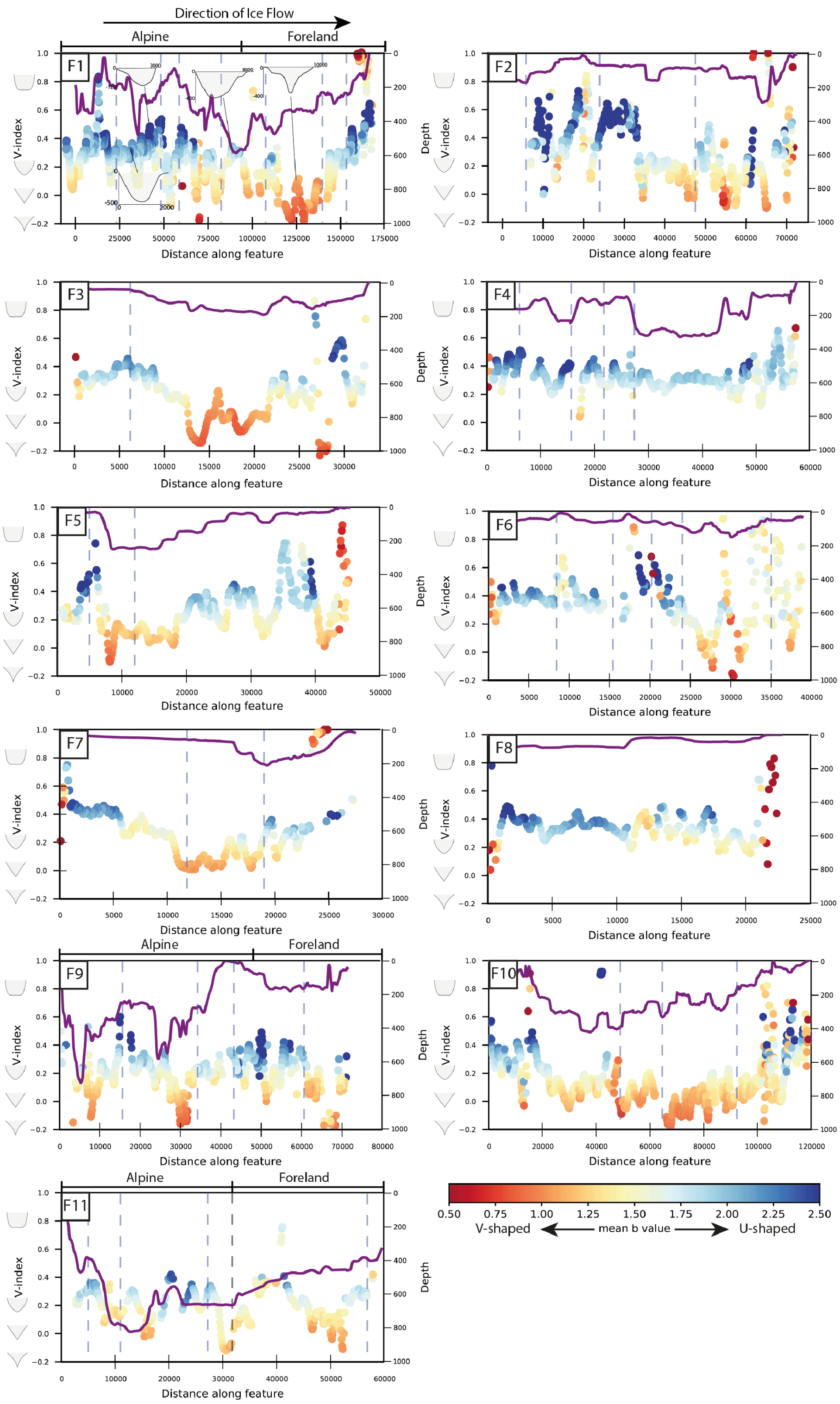

Figure 6.5: Long-profiles of the features of northern Switzerland showing the line of deepest erosion (purple), the location of tributary valleys (dashed blue lines), location of the boundary between the alpine and foreland regions, and the V-index and b-exponents of each CGBL. The scatter plots of the V-index data are colour coded to its corresponding b-exponent value.

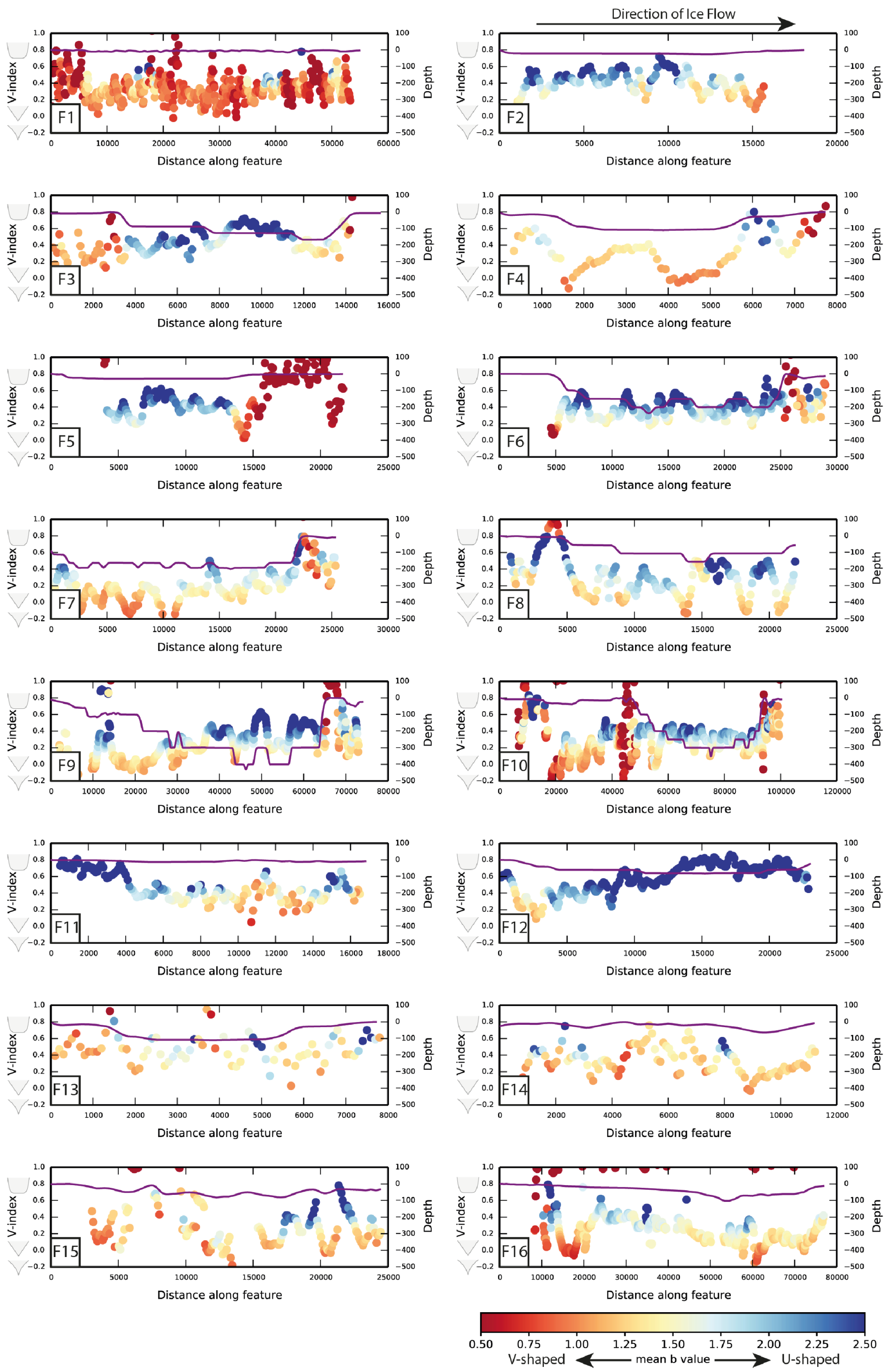

Figure 6.6: Long-profiles of the features of the Finger Lakes showing the line of deepest erosion (purple), and the V-index and b-exponents of each feature. The scatter plots of the V-index data are colour coded to its corresponding b-exponent value.

6.3.3 *Statistical morphological trend within features*

Tables 6.1 and 6.2 reveal that 53% of plotted relationships show moderate (r^2 between 0.05 and <0.5) linear trends, and only 7.4% show more significant linear trends (r^2 >0.5). These data do not seem to show a strong linear correlation for any of the features, except for the b-exponent vs V-index (right column of tables 6.1 and 6.2). The exceptions in the b-exponent vs V-index appear to be seen in features that contain a high number of shallow cross-sections, either due to the small nature of the feature, such as NSF 8 and FL 13, or the undulating nature of the feature, for example FL 15 and 16. All of the plotted relationships for the CGBLs of both regions show a wide range of r^2 values, with most values being of low to moderate range. The two largest CGBLs in the Finger Lakes (F9 and F10) display the least correlation, while the two largest features in northern Switzerland (F1 and F10) show much higher correlation than other Swiss features. This lack of correlation in the Finger Lake features F9 and F10 may be due to the higher number of data points measured in the features, compared to smaller features such as FL 5, which shows a much simpler morphology with no real evidence of nested basins and only crosses a few geological boundaries. The high number of moderate correlations (r^2 values) suggest that the relationships between the different metrics may be more complex and contain both single linear trends and multiple distinct linear trends, as seen previously in the general distributions (shown in Figs. 6.7 and 6.8).

Table 6.1: r^2 values of morphological relationships for each of the CGBL features of northern Switzerland (see Fig. 5.1 for spatial location). The cells are colour coded according to the strength of the relationship, shown by the r^2 value. Green: r^2 > 0.5, Yellow: r^2 = 0.5 - 0.1. Orange: r^2 = 0.1 - 0.05 Red: r^2 < 0.005.

Features	Depth Vs Width	Depth Vs b exponent	Depth Vs V-index	Width Vs b exponent	Width Vs V-index	Fr Vs b exponent	Fr Vs V-index	b exponent Vs V-index
NSF 1	0.274	0.140	0.275	0.192	0.333	0.0004	0.122	0.297
NSF 2	0.131	0.040	0.095	0.006	0.076	0.069	0.017	0.331
NSF 3	0.028	0.465	0.442	0.008	0.000013	0.011	0.006	0.772
NSF 4	0.022	0.022	0.075	0.245	0.013	0.023	0.044	0.245
NSF 5	0.191	0.181	0.389	0.00003	0.199	0.227	0.197	0.240
NSF 6	0.115	0.046	0.084	0.149	0.052	0.031	0.234	0.147
NSF 7	0.123	0.013	0.005	0.069	0.061	0.119	0.048	0.052
NSF 8	0.744	0.468	0.016	0.598	0.008	0.262	0.055	0.009
NSF 9	0.009	0.088	0.048	0.013	0.000009	0.036	0.023	0.764
NSF 10	0.518	0.121	0.225	0.034	0.116	0.117	0.103	0.459
NSF 11	0.141	0.016	0.044	0.021	0.076	0.002	0.003	0.504

Table 6.2: r^2 values of morphological relationships for each of the CGBL features of the Finger Lakes. The cells are colour coded according to the strength of the relationship, shown by the r^2 value. Green: $r^2 > 0.5$, Yellow: $r^2 = 0.5 - 0.1$, Orange: $^2 = 0.1 - 0.05$ Red: $r^2 < 0.005$

Features	Depth Vs Width	Depth Vs b exponent	Depth Vs V-index	Width Vs b exponent	Width Vs V-index	Fr Vs b exponent	Fr Vs V-index	b exponent Vs V-index
FL 1	0.269	0.499	0.118	0.263	0.037	0.163	0.065	0.008
FL 2	0.322	0.068	0.068	0.084	0.006	0.001	0.028	0.688
FL 3	0.043	0.298	0.049	0.004	0.115	0.215	0.045	0.232
FL 4	0.020	0.030	0.506	0.114	0.244	0.015	0.278	0.085
FL 5	0.755	0.810	0.242	0.700	0.355	0.0002	0.020	0.234
FL 6	0.189	0.160	0.077	0.062	0.243	0.181	0.007	0.095
FL 7	0.312	0.0009	0.493	0.012	0.328	0.003	0.224	0.188
FL 8	0.184	0.060	0.271	0.005	0.020	0.028	0.067	0.191
FL 9	0.013	0.099	0.002	0.091	0.384	0.091	0.066	0.197
FL 10	0.081	0.076	0.015	0.0003	0.082	0.024	0.0009	0.080
FL 11	0.0001	0.226	0.264	0.349	0.131	0.430	0.276	0.501
FL 12	0.168	0.242	0.226	0.417	0.607	0.466	0.607	0.777
FL 13	0.234	0.092	0.138	0.093	0.0002	0.0001	0.106	0.003
FL 14	0.166	0.011	0.367	0.031	0.143	0.029	0.066	0.246
FL 15	0.251	0.003	0.046	0.012	0.105	0.050	0.133	0.036
FL 16	0.040	0.001	0.126	0.145	0.098	0.077	0.105	0.0006

6.3.4 *Normal and adverse slopes*

Figure 6.9 shows the relationship between the cross-sectional morphology of the normal and adverse slopes and the corresponding slope angle for all the features of northern Switzerland. Figure 6.9c and 6.9f shows that normal and adverse slopes in the northern Switzerland CGBLs are typically low angled, with the normal slope peaking at 0.22 degrees and the adverse slope at -0.30 degrees. Both the normal and adverse slope histograms (Fig. 6.9c and 6.9f) show distribution tails in either the positive (adverse) or negative (normal) directions revealing smaller populations of steeper slopes.

The V-index distribution of the normal and adverse slopes are shown in Figure 6.9a and 6.9d, which show peak KDE V-indexes of 0.24 for the normal slopes and 0.30 for the adverse slopes. The differences in V-index distributions are also seen in the locations of sub peaks in the two histograms. Both the normal and adverse slopes have slight V-index peaks between 0.8–1.0 (Fig. 6.9b and 6.9e). The other noticeable peak in the V-index distribution is seen at ~0.1 on the adverse slope.

The frequency distribution histograms of the V-index were statistically tested to determine the significance of the differences in the distribution shapes. The resulting p value of < 0.001 from the Kolmogorov–Smirnov test shows that the difference in the distribution of the V-index values for the normal and adverse slopes are statistically significant.

6.3.5 *Changes in Topographic Confinement*

The topographic confinement of CGBLs is shown in Figure 6.10. In northern Switzerland, former ice flow within the CGBLs would have been from a high confinement zone into a low confinement zone of the foreland. This is in contrast to CGBLs of the Finger Lakes, where the trend would have been from low topographic confinement of the plateau edge into the higher confinement of the Allegheny Plateau.

Figures 6.11 and 6.12 show the relationships between confinement and the metrics of depth, width, form ratio and cross-sectional morphology (V-index) in northern Switzerland (Figs. 6.11) and the Finger Lakes (Fig. 6.12). In northern Switzerland the CGBLs do not fit a simple single population linear trend. There is a slight positive association between lower topographic confinement (< 200 m) and wider CGBLs, up to 16 km (Fig 6.11a). This slight positive trend is also seen in Fig. 6.11b where CGBL depth increases with confinement, from <50 m to ~200 m confinement, showing increasing depths of up to ~350 m. These trends are not seen in the cross-sectional morphology, which cluster around 0.25 V-index, although there is greater variation in morphology below 200 m confinement. As the CGBLs of northern Switzerland cross from an alpine into a foreland setting, the measurements were reproduced just for the foreland setting to determine if there was clearer relationship where the CGBLs were less topographically confined, however, no change to the relationships were observed.

The CGBLs of the Finger Lakes region show a negative trend between CGBL width and local topographic confinement (r^2 = 0.13; p-value =< 0.05)(Fig. 6.12a), although there is a bimodal distribution with CGBLs in high confinement only reaching widths of ~4 km, compared to the regions of low confinement that reach widths of up to 12 km. There are strong positive relationships between increasing confinement and CGBL depth (r^2 = 0.58; p-value = < 0.05) (Fig. 6.12b) and between confinement and CGBL form ratio (r^2 = 0.38; p-value =<0.05) (Fig. 6.12c). However, there is no clear relationship between the level of confinement and cross-sectional morphology (Fig. 6.12d).

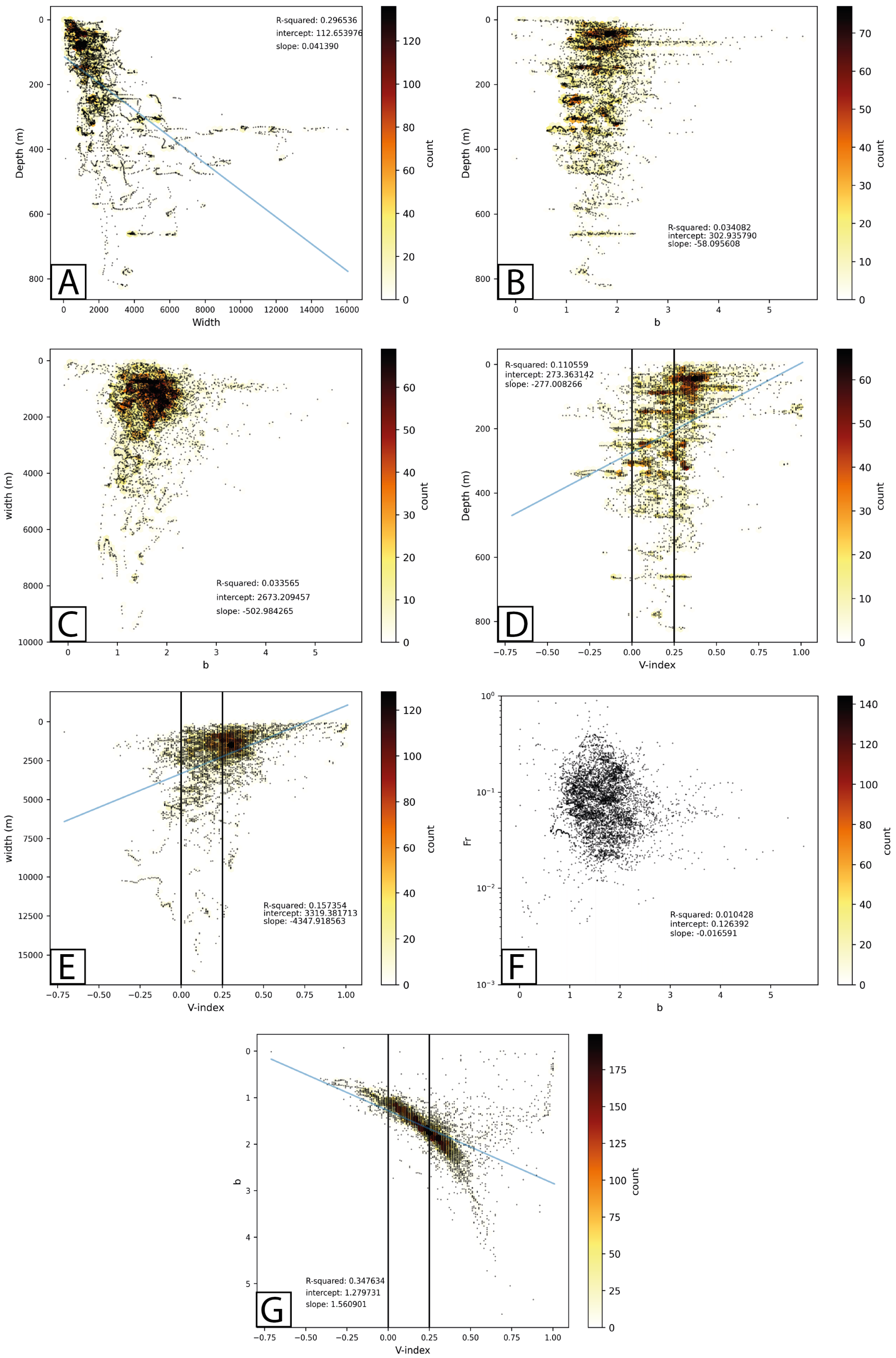

Figure 6.7: Scatter plot hexbin for morphometric relationships present in the CGBL features of northern Switzerland. The hexbins have a bin size of 50 and are colour-coded for point counts in each bin as well as having each of the points plotted. A) plot of cross-sectional depth vs width, B) plot of cross-sectional depth vs b-exponent, C) plot of cross-sectional width vs b-exponent, D) plot of cross-sectional depth vs V-index, E) plot of V-index vs width, F) plot of b-exponent vs form ratio, G) plot of b-exponent vs V-index. The vertical lines in D, E, G show the theoretical thresholds for a perfect V-shaped crossprofile (V-index = 0) and the the published threshold for U-shaped glacial valleys (V-index $\geq$ 0.25). The blue trend lines were plotted in the figures where the r^2 values were over 0.05.

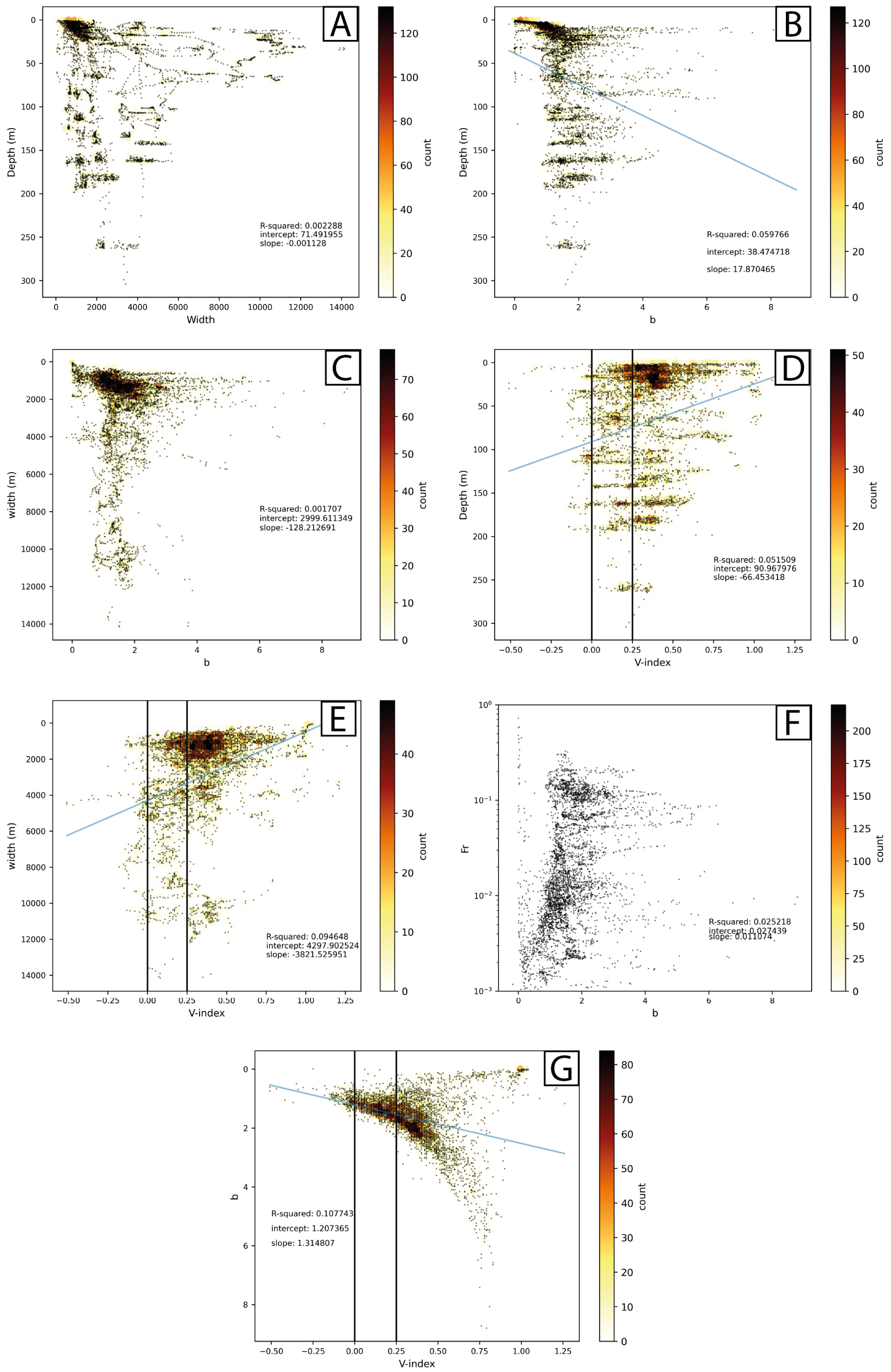

Figure 6.8: Scatter plot hexbin for morphometric relationships present in the Finger Lake CGBL features. The hexbins have a bin size of 50 and are colour-coded for point counts in each bin as well as having each of the points plotted. A) plot of cross-sectional depth vs width, B) plot of cross sectional Depth vs b-exponent, C) plot of cross sectional width vs b-exponent, D) plot of cross sectional depth vs V-index, E) plot of V-index vs width, F) plot of b-exponent vs form ratio, G) plot of b-exponent vs V-index. The vertical lines in D, E, G show the theoretical thresholds for a perfect V-shaped crossprofile (V-index = 0) and the the published threshold for U-shaped glacial valleys (V-index $\geq$ 0.25). The blue trend lines were plotted in the figures where the r^2 values were over 0.05.

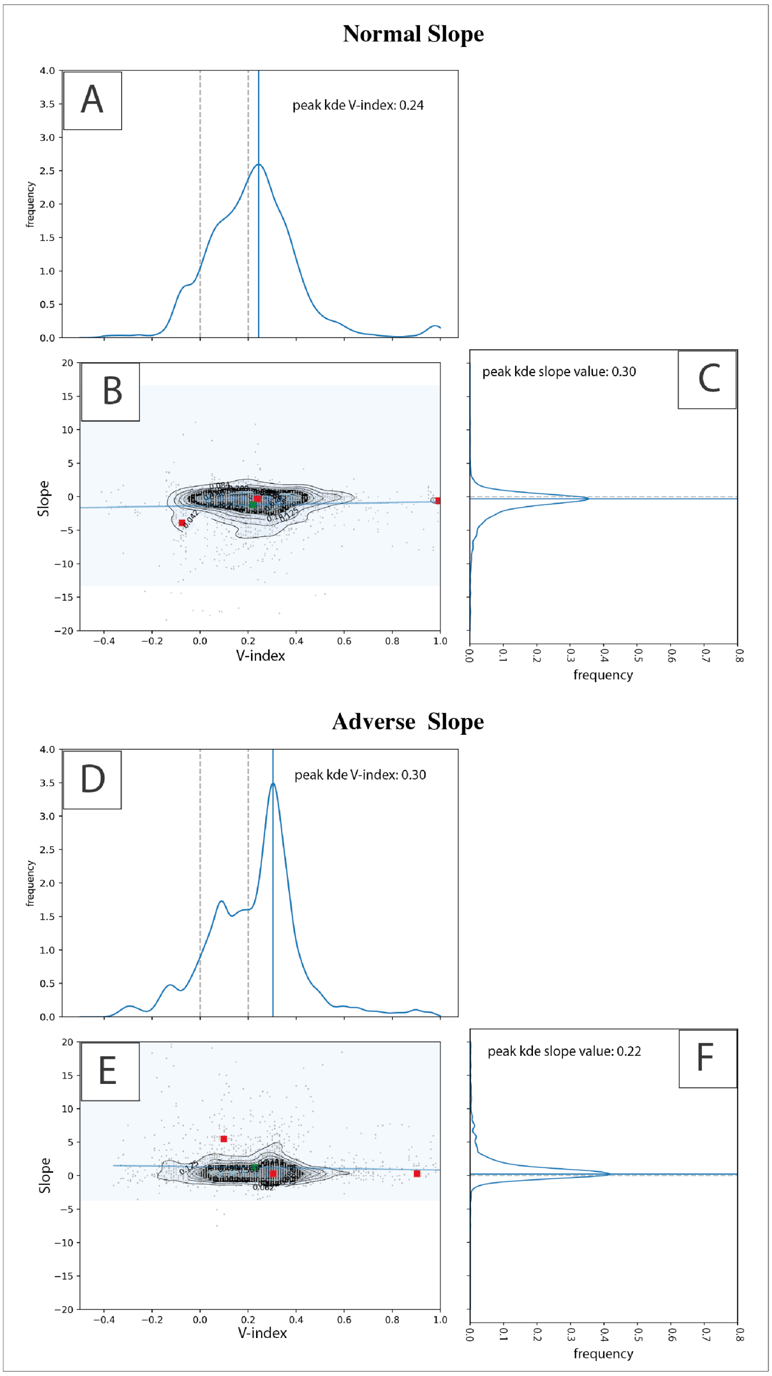

Figure 6.9: Slope angle frequency distribution graphs for all normal and adverse slopes of the features in northern Switzerland. A) histogram of the distribution of V-index values on normal slopes with the grey dashed lines showing the V-index values for a perfect V-shape (0.0) and the transition to U-shaped (0.25), and the blue line showing the location of the highest peak value in the distribution. B) scatter plot with point density contours for V-index vs slope (°) with the red boxes showing the location of peaks in the KDE field for normal slopes and the blue line showing the liner trend line. C) histogram of the distribution of slope angles on normal slopes with the blue line showing 0°. D) histogram of the distribution of V-index values on adverse slopes with the grey dashed lines showing V-index values for a prefect V-shape (0.0) and the transition to U-shaped (0.25), and the blue line showing the location of the highest peak value in the distribution. E) scatter plot with point density contours for V-index vs slope (°) with the red boxes showing the location of peaks in the KDE field for adverse slopes and the blue line showing the liner trend line. F) histogram of the distribution of slope angles on adverse slopes with the blue line showing 0°.

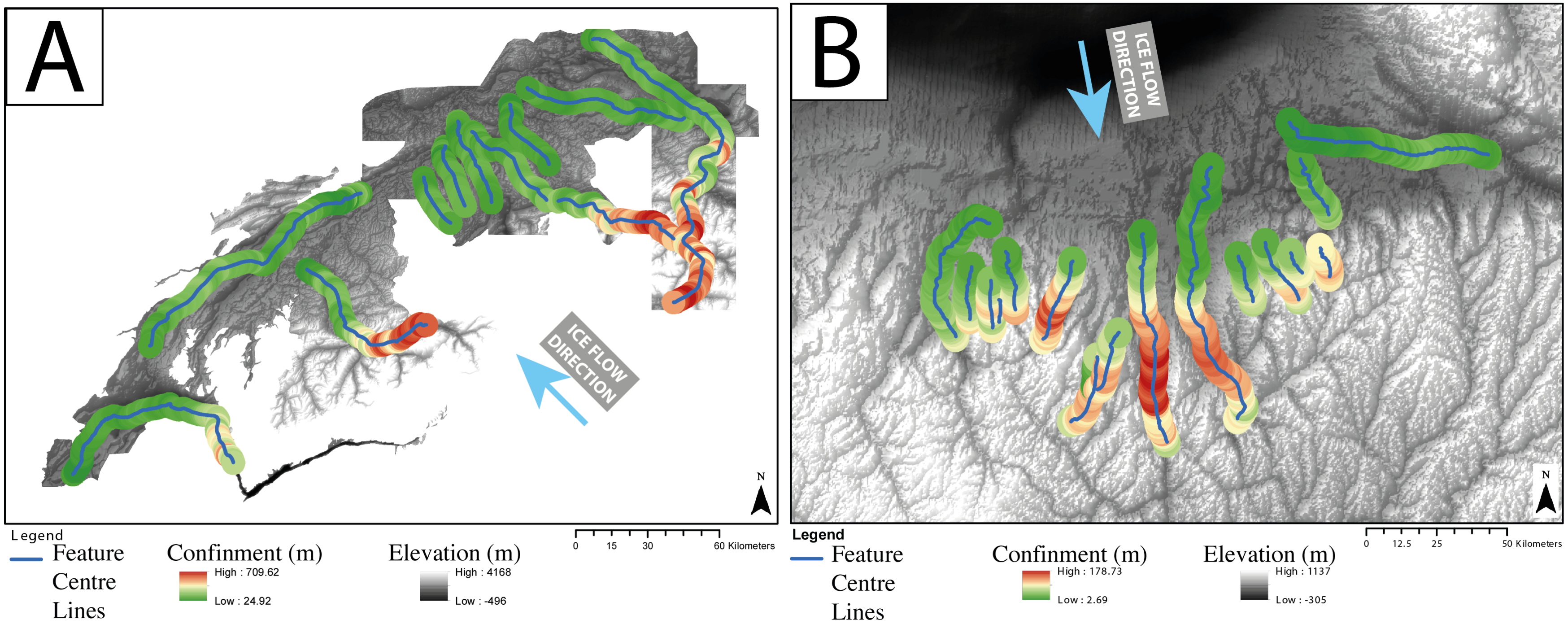

Figure 6.10: Changes in confinement for CGBLs of northern Switzerland and the Finger Lakes. A) Confinement for northern Switzerland (green is low confinement and red is high confinement), B) Confinement for the Finger Lakes (green is low confinement and red is high confinement).

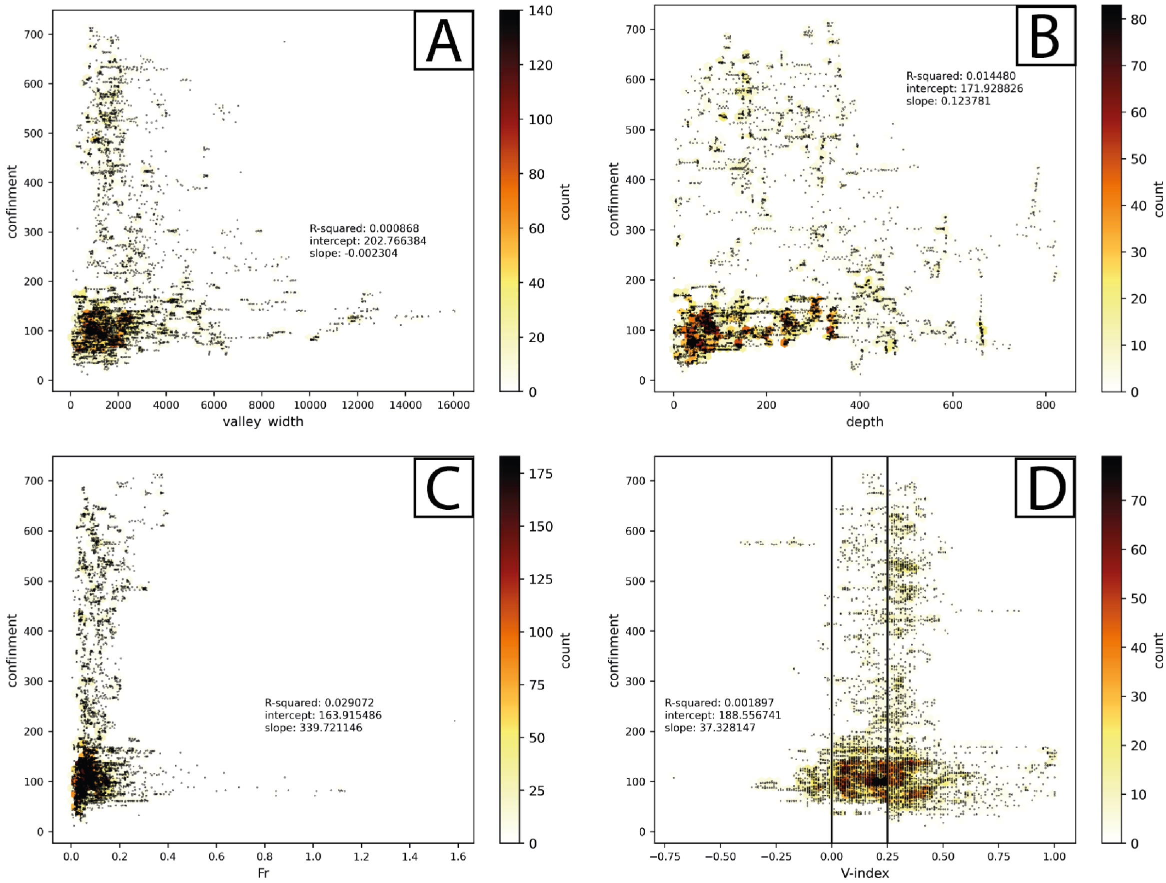

Figure 6.11: Scatter plot hexbins of topographic confinement for the northern Switzerland. A) hexbin scatter plot of width vs confinement, B) hexbin scatter plot of depth vs confinement, C) hexbin scatter plot of form ratio vs confinement, D) hexbin scatter plot of V-index vs confinement. Hexbins are colour coded according to the frequency of points in each 50 hexbin. The vertical lines in D show the theoretical thresholds for a perfect V-shaped cross profile (V-index = 0) and the published threshold for U-shaped glacial valleys (V-index $\geq$ 0.25). The blue trend lines were plotted in the figures where the r^2 values were over 0.05.

6.3.6 *Tributary valleys*

The locations of tributary valleys (shown by dashed blue lines in Fig 6.4) exhibit a moderate qualitative association with the location of nested CGBL features in northern Switzerland. The location of tributary valleys shows some correlation with the deepest location of 5 of the features of northern Switzerland (F4, F5, F7, F10, and F11), as well as the locations of changes in normal slope angle (including F3). However, not all projected intercepts show a strong correlation, with F6 and F1 exhibiting wider variation in distance between the location of tributary valleys and sub basin locations. This lack of correlation may partly be due to higher error associated with the chosen projection angles (as discussed in the methods section 2.5.3).

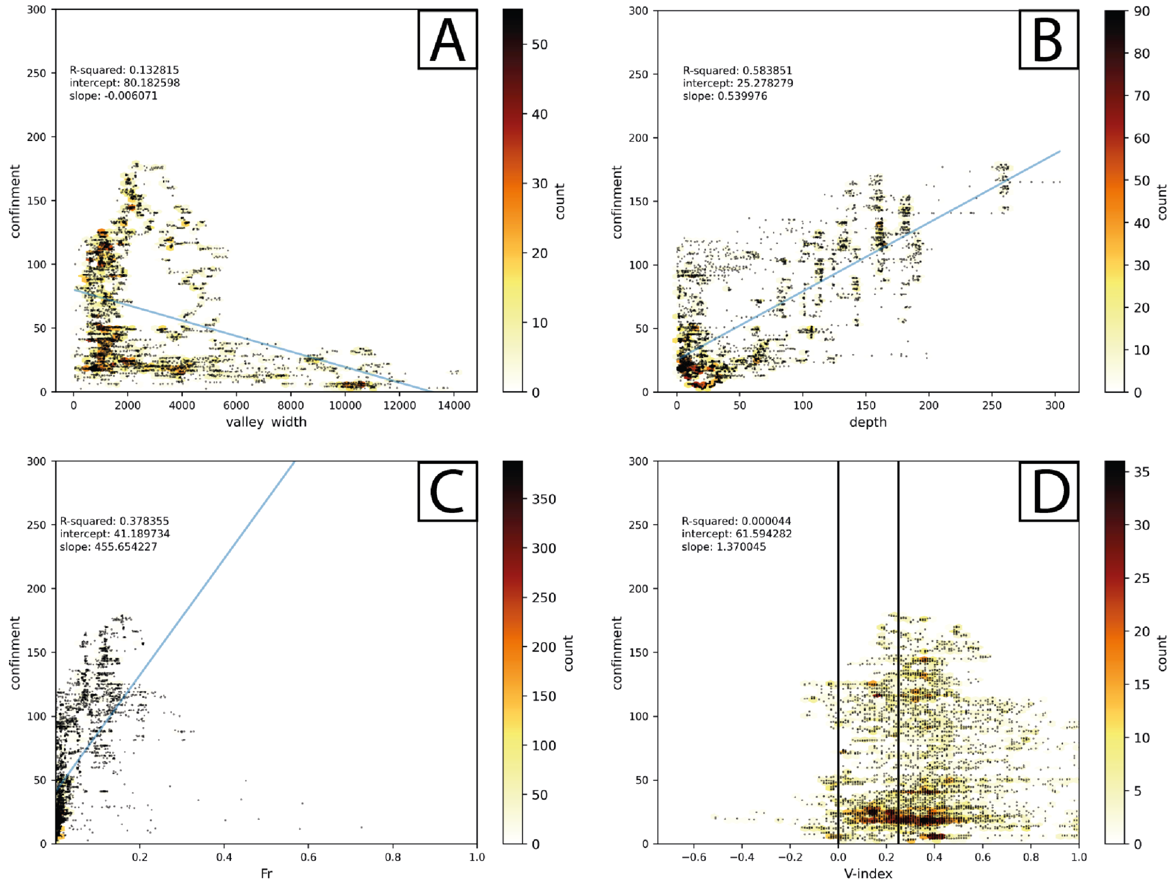

Figure 6.12: Scatter plot hexbin of topographic confinement for Finger Lakes. A) hexbin scatter plot of width vs confinement, B) hexbin scatter plot of depth vs confinement, C) hexbin scatter plot of form ratio vs confinement, D) hexbin scatter plot of V-index vs confinement. Hexbins are colour coded according to frequency of points in each 50 hexbin. The vertical lines in D show the theoretical thresholds for a perfect V-shaped cross profile (V-index = 0) and the published threshold for U-shaped glacial valleys (V-index $\geq$ 0.25). The blue trend lines were plotted in the figures where the r^2 values were over 0.05.

6.3.7 *Lithology*

The effects of variations in lithology are shown in Figures 6.14 and 6.15. Only northern Switzerland has available published erodibility values, so the interpretation of the influence of lithology in the Finger Lakes is based purely on geological units (Table. 6.3).

Figure 6.14 shows the effect of lithology on CGBL width and depth, and the b-exponent and form ratio for each CGBL in the Finger Lakes. The Finger Lakes region has 15 distinct lithological formations and groups mapped by Rickard and Fisher (1970a). These units comprise of shales, siltstones, limestones, Cherty Limestones, sandstones, hematite, and conglomerate (Fig. 6.13 and Table. 6.3). To increase the significance of any trends seen between lithologies and reduce the likely effect of small local anomalies associated with individual features, Figure 6.14 shows the relationships of lithological units that are crosscut by at least 4 distinct features. The depth and width relationships in Figure 6.14a show strong clustering of values around peak KDE values, with the clusters plotting along a weak linear trend of increasing depth with width. This trend is seen in all the lithological units, except for T3 (Onondaga Limestone), with r^2 of >0.05 and p-values ranging from 0.02 to 0.08. Figure 6.14b shows the two different b/Fr relationships for the different lithologies in the Finger Lakes. The first is a very weak linear trend with the b-exponent values increasing with increasing form ratio (T3, T4, and T9, T10) (r^2 values ranging between 0.23 and 0.06 and p-values <0.05). In the second, morphological values appear to cluster around a given value (T5,T6, T7, and T11) and show no significant linear trend (r^2 values < 0.05).

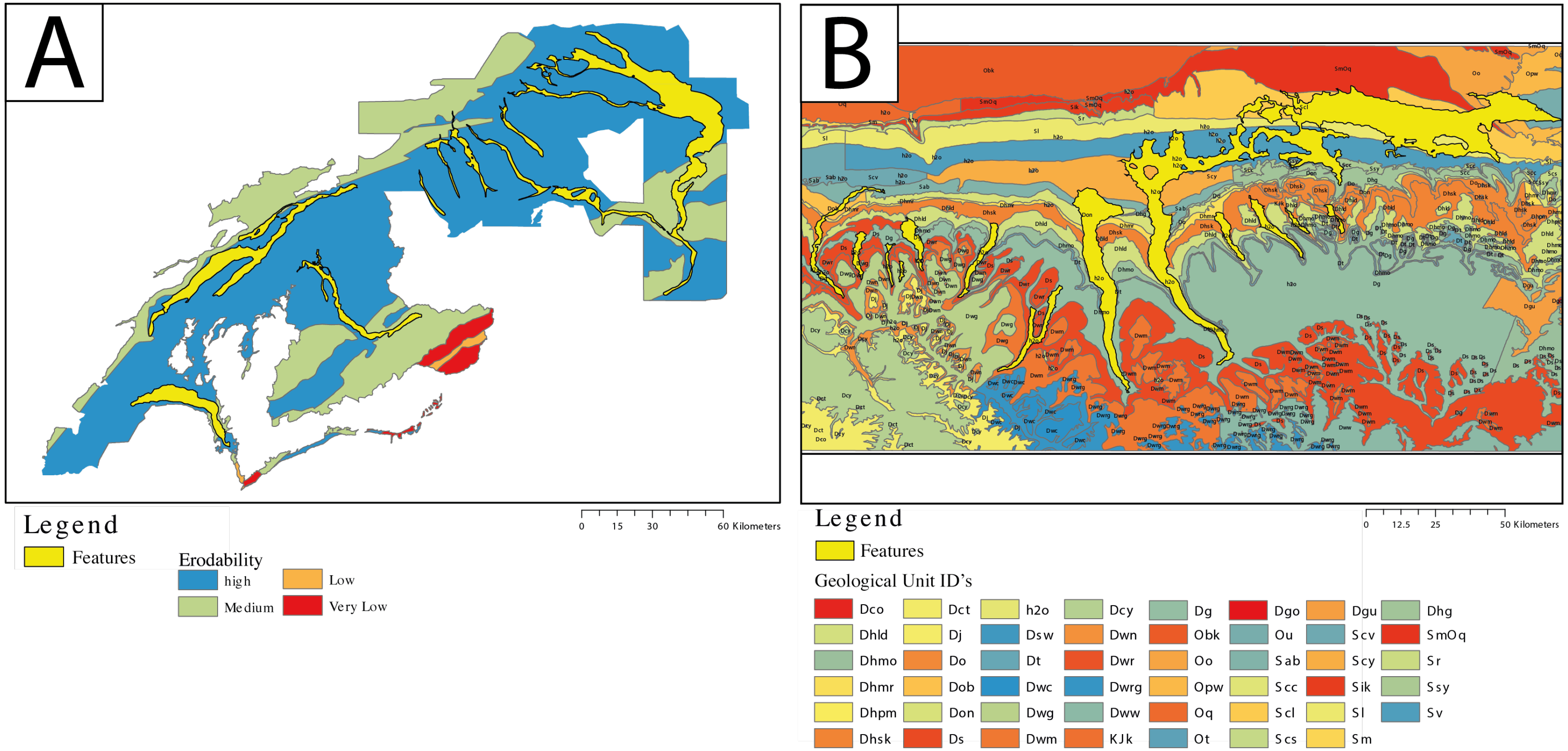

Figure 6.13: Changes in geology maps for CGBLs of northern Switzerland and the Finger Lakes. A) Erodibility map modified from Kühni and Pfiffner (2001) for northern Switzerland (Blue= High, Green = Medium, Orange = Low, Red = Very Low), B) geological map modified from Rickard and Fisher (1970) for the Finger Lakes (colour-coded by geological unit. See Rickard and Fisher (1970) and Table 6.3 for unit descriptions).

Table 6.3: Mapped geological units, formations and groups crosscut by CGBLs in the Finger Lakes region. Formation thicknesses are the thickness reported for each geological formation in which the lithological unit is mapped, and therefore is likely thinner than stated.

Figure ID	Geological Unit ID	Geological formation	Lithologies	Formation thickness
T1	Sv	Vernon Formation	Shale, and Dolostone	210 -300 m
T2	Scy	Camillus and Syracuse Formation	Shale, Dolostone, gypsum, and salt	210 -300 m
T3	Don	Onondaga Limestone	Limestone, Cherty Limestone, and Sandstone	23 - 45 m
T4	Dhmr	Marcellus Formation	Shale, Limestone	180 - 460 m
T5	Dhsk	Skaneateles Formation	Shale, Limestone, and Sandstone	180 - 460 m
T6	Dhld	Ludlowville Formation	Shale, Limestone, and Sandstone	180 - 460 m
T7	Dhmo	Moscow Formation	Shale, Limestone	180 - 460 m
T8	Dt	Tully Limestone	Limestone	60 - 300 m
T9	Dg	Genesee Group	Shale, Limestone, Siltstone	60 - 300 m
T10	Ds	Sonyea Group	Shales, Siltstones	60 - 300 m
T11	Dwm	West Falls Group	Shales, Siltstones	340 - 490 m
T12	Scl	Clinton Group	Sandstone, Hematite, Shale, and Conglomerate	40 - 100 m
T13	SmOq	Medina Group and Queenston Formation	Sandstone, Shale, and Siltstone	0 - 270 m
T14	Opw	Pulaski and Whetstone Gulf Formation	Siltstone and Shale	210 - 270 m
T15	Ou	Trenton Group	Shale	30 - 90 m

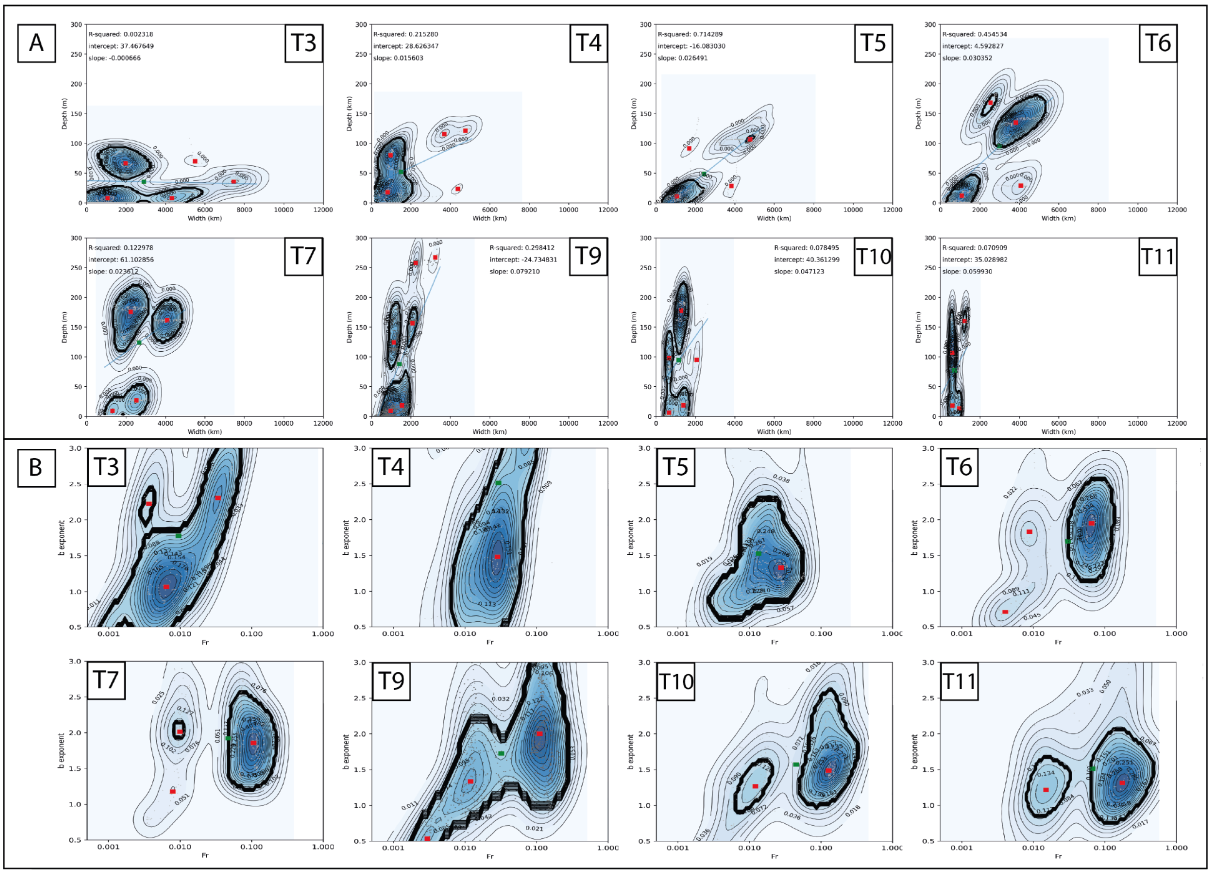

Figure 6.14: Contoured KDE scatter plots for the Finger Lakes for scale (depth and width) and cross-sectional morphology by underlying lithology. A) plots of depth vs width B) plots of b/Fr. Only lithologies that crosscut a minimum of 4 features have been shown in this figure. The blue trend lines were plotted in the figures where the r^2 values were over 0.05.

Figure 6.15 shows the effect of differences in bedrock erodibility on CGBLs in northern Switzerland. The CGBLs of northern Switzerland region cross two of the classified erodibilities: highly erodible (T1) and moderately erodible (T2) (Table 6.4). Figure 6.15a and 6.15b shows that both the CGBLs present in T1 and T2 show strong correlation with increasing depth and width (r^2 of 0.3 and 0.5, with p-values of <0.05 and 0.08 respectively), with the more erodible T1 lithologies having a large frequency of cross-sections with depths around 400 m that reach much greater widths (up to 16051 m wide) than those in the T2 lithologies. Both the T1 and T2 lithologies contain cross-sections that reach significant depths of >700 m, with the deepest cross-sections being found in the softer T1 lithologies. Figure 6.15c and 6.15d shows that there is significant overlap in cross-sectional morphologies present in both classifications, with the less erodible T2 units recording mostly U-shaped morphologies within the 1.5-2 b-exponent value range, and the softer T1 units recording a much wider spread of cross-sectional morphologies, ranging from very V-shaped b-exponent of 1 to highly U-shaped values of $b > 2$.

Table 6.4: Table showing mapped geological erodibility groups crosscut by CGBLs in northern Switzerland.

Geological Unit ID	Erodability	Lithologies
T1	Highly erodible	"Molasse (shales, sandstones and conglomerates); Fine grained sediments of the Penninic and Helvetic flysch units; Sandstones, shales, and Slates interlayer by limestone and dolostone of the Bündnerschiefer Volcanicalstic units."
T2	Moderately erodible	Mesozoic carbonates of the Helvetic, Penninic, Austroalpine and Southalpine units.

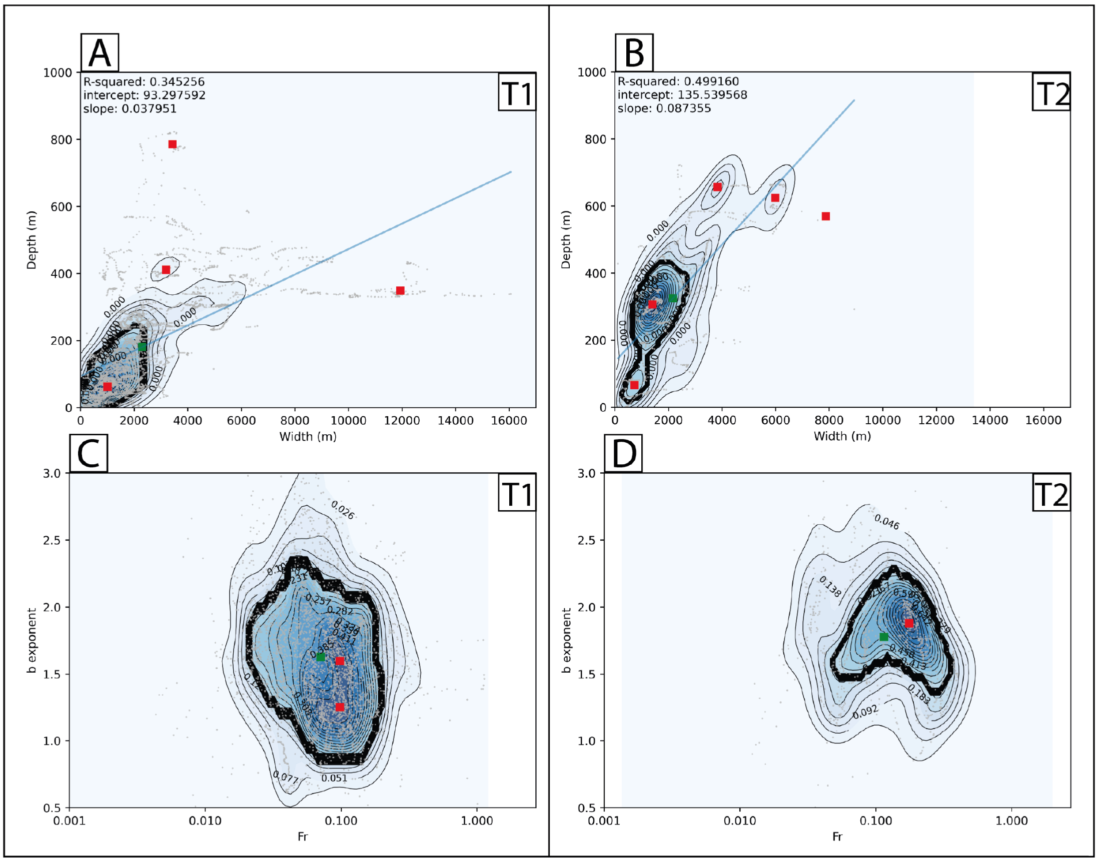

Figure 6.15: Contoured KDE scatter plot for northern Switzerland for scale (depth and width) and cross-sectional morphology divided by erodibility of underlying lithology. A) plots of depth vs width B) plots of b/Fr. The blue trend lines were plotted in the figures where the r^2 values were over 0.05.

6.3.8 *Inferred faults vs sub-basins*

The relationship between regions of faulting and the location and number of nested sub-basins is shown in Figure 6.16. It reveals a strong positive relationship (r^2 value: 0.597) between number of faults within 10 km of features and the number of nested basins, although this is based on limited data (n=8).

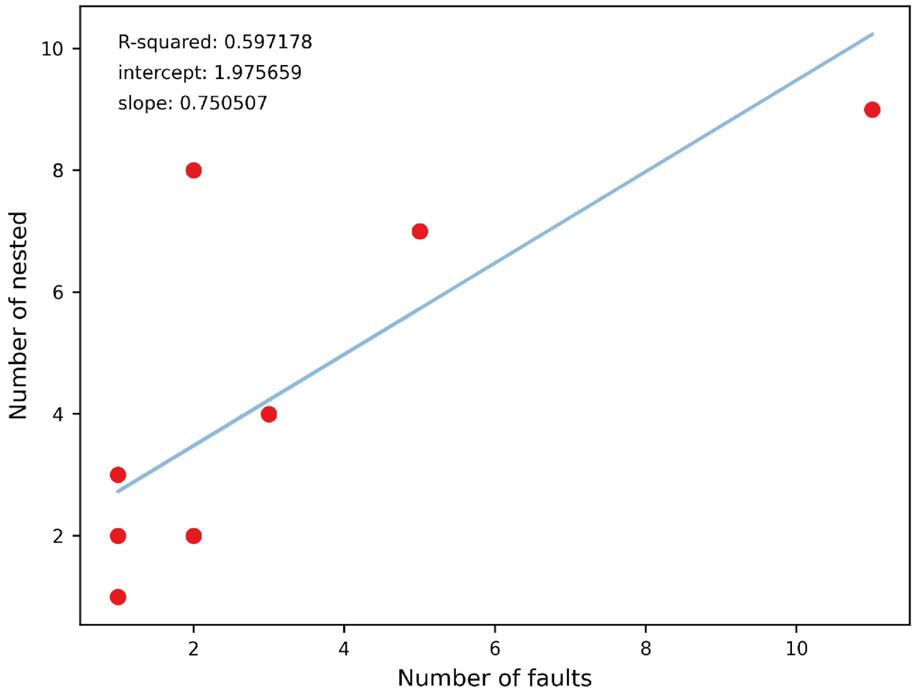

Figure 6.16: Scatter plot for northern Switzerland for number of mapped faults within 10 km buffer of features against number of nested basins present in features. Blue line shows linear trend line.

6.4 DISCUSSION

This chapter has aimed to investigate the relationship between changes in cross-sectional morphology along the long-profile of CGBLs in the northern Switzerland and Finger Lakes regions, specifically focusing on the effect of variations in geology, topographic confinement, and potentially active erosional processes. The following section aims to discuss the potential glaciological implications of the presented results on CGBL feature formation and development. The following section has therefore been subdivided into a discussion of the general qualitative observed variations within feature, and a focused discussion of each of the hypothesised factors. The key discussion points have then been summarised in the following section, describing how each of the factors may affect the location of changes in morphology, specifically in the feature of northern Switzerland and the Finger Lakes. The discussion of how these results may affect the different previously proposed formation hypothesis will be discussed in the following discussion chapter.

6.4.1 *General CGBL morphology*

The differences in location of deepest erosion, in both the features of northern Switzerland and the Finger Lakes (shown in Figs. 6.5 and 6.6), is thought to be strongly influenced by the surrounding regional topography, which may focus the erosive potential of the ice and melt water through topographic confinement of these flows. At the same time, the locations and number of nested sub-basins may be related to the underlying bedrock lithologies and the geological structures present. The relation of both of these points to geology and topographic confinement are discussed later.

The variations in morphology are also seen in the cross-profiles along feature in both the features of northern Switzerland and the Finger Lake features. The changes in cross-sectional morphology (b-exponent and V-index) seem to occur due to influencing factors either within the feature or related to changes in the regional context due to the non-random nature of the variations. The causes of the variations in locations of the point of deepest erosion and nested basins, as well as cross-sectional morphology are discussed in the following sections.

6.4.2 *Variability due to specific influences*

6.4.2.1 *Relationship between key morphological variables*

Depth vs Width

The depth/width relationships seen in the features of the northern Switzerland and the Finger Lakes show similar trends (Figs. 6.7a and 6.8a). The bimodal trends are likely due to the influence of regional context such as topographic confinement and geology. Numerical modelling work done by Kessler et al. (2008) shows that the local topography can act as a containing force, focusing both glacial and subglacial meltwater erosion, increasing depth of incision and limiting growth of feature width. Similar to the topography, the erodibility of the underlying bedrock is likely a factor in the resulting depths and widths of features, with this influence being shown by Swift et al. (2008). These influences are discussed later in the following subsections.

Depth and width vs V-index and b-exponent

In both the Finger Lakes and the features of northern Switzerland, a trend of increasing V-shape is noted with increasing depth and decreasing width, when compared to the cross-sectional V-index values of all the features (Figs. 6.7d, e and 6.8d, e). However, this trend is not seen to significant values when compared to the b-exponent values of the same features in either the Finger Lakes or northern Switzerland. This lack of trend may be due to the variations in how each method calculates the cross-sectional morphology, and how well they each handle more extreme morphologies (i.e. more box shaped or convex cross-sections).

b-exponent vs V-index

This variation in b-exponent and V-index measurements are shown in figures 6.7g and 6.8g. The figures show a very strong positive trend between each method, but that there is significant scatter between the resultant measured values for each method of measurement for cross-sections with very high V-index values and low b-exponent values (discussed further in chapter 7 section 5.2). As mentioned in the previous subsection above, these differences in the measured morphologies are believed to have resulted from the two methods different approaches to calculating cross-sectional morphology. The potential effects of the limitations of each of the methods are discussed further in the next chapter (chapter 7).

6.4.2.2 *Hypothesis testing*

Adverse and normal slopes

The first main factor of influence is the slope angles of both the normal and adverse slopes, shown in figure 6.9 for the features of northern Switzerland. The figure (6.9) shows the total distribution of all normal and adverse slopes for all the features of northern Switzerland, and shows similar peak KDE values (0.22° and -0.3°) for both of the normal and adverse slopes, with each appearing to have tails in the distribution curves at higher value angles in either the negative (normal) or positive (adverse) direction. The similarity in peak KDE slope angle suggests that the features overall are being formed by erosional processes that occur at both the inflow and outflow ends of the features, with the "tail" of higher angle values potentially resulting from the normal and adverse slopes present in features that are located at or near abrupt changes in geology or perpendicular to ice flow geological faults. Figure 6.2 shows how a single feature can contain several normal and adverse slopes with a wide variety of slope angles, however, the lack of a stronger overall trend towards steeper normal slope angles present in the total distribution of normal slopes suggest that glacial quarrying does not play as strong a role in CGBL formation as proposed by Hooke (1991).

The normal and adverse slopes of the features of northern Switzerland show fewer similarities when looking at differences in the distributions of cross-sectional morphology (Fig. 6.9a and 6.9d). It is clear that there are differences between the two slope types, with the distribution of V-index along the normal slopes (Fig 6.9a) showing a very straight forward bell curve shape, and a much more complex V-index distribution curve for the values of the adverse slopes. As described in the results section, adverse slopes produce two main distinct peaks in the cross-section morphology, suggesting a shift in feature morphology towards more U-shaped cross-profiles on these slopes (i.e., higher V-index).

These variations in cross-sectional morphology between the normal and adverse slope may relate to changes in subglacial hydrological pathways from the normal slopes to the adverse slopes, with changes in cross-sectional morphology resulting from changes from channelised to distributed pathways, which potentially reduces meltwater velocities. Figure 6.17 schematically shows how, in a CGBL sub-basin, the cross-sectional morphology may change due to several factors including; how subglacial channels may produce more efficient pathways with greater activity on normal slopes (flowing with gravity Fig. 6.17 b and c), and that as the subglacial hydrology reaches the adverse slopes they may divert to more optimal hydrological routes (either through englacial pathways or pathways that do not route along paths of deepest erosion), or lose hydrological power climbing the adverse slopes, resulting in deposition of sediment, reducing the availability of subglacial meltwater to incise into bedrock base of the features resulting in a greater influence of glacial erosion, such as glacial scouring and plucking along the base and sides of the features (Alley et al., 2003; Cook and Swift, 2012; Werder, 2016) (Fig. 6.17c and d).

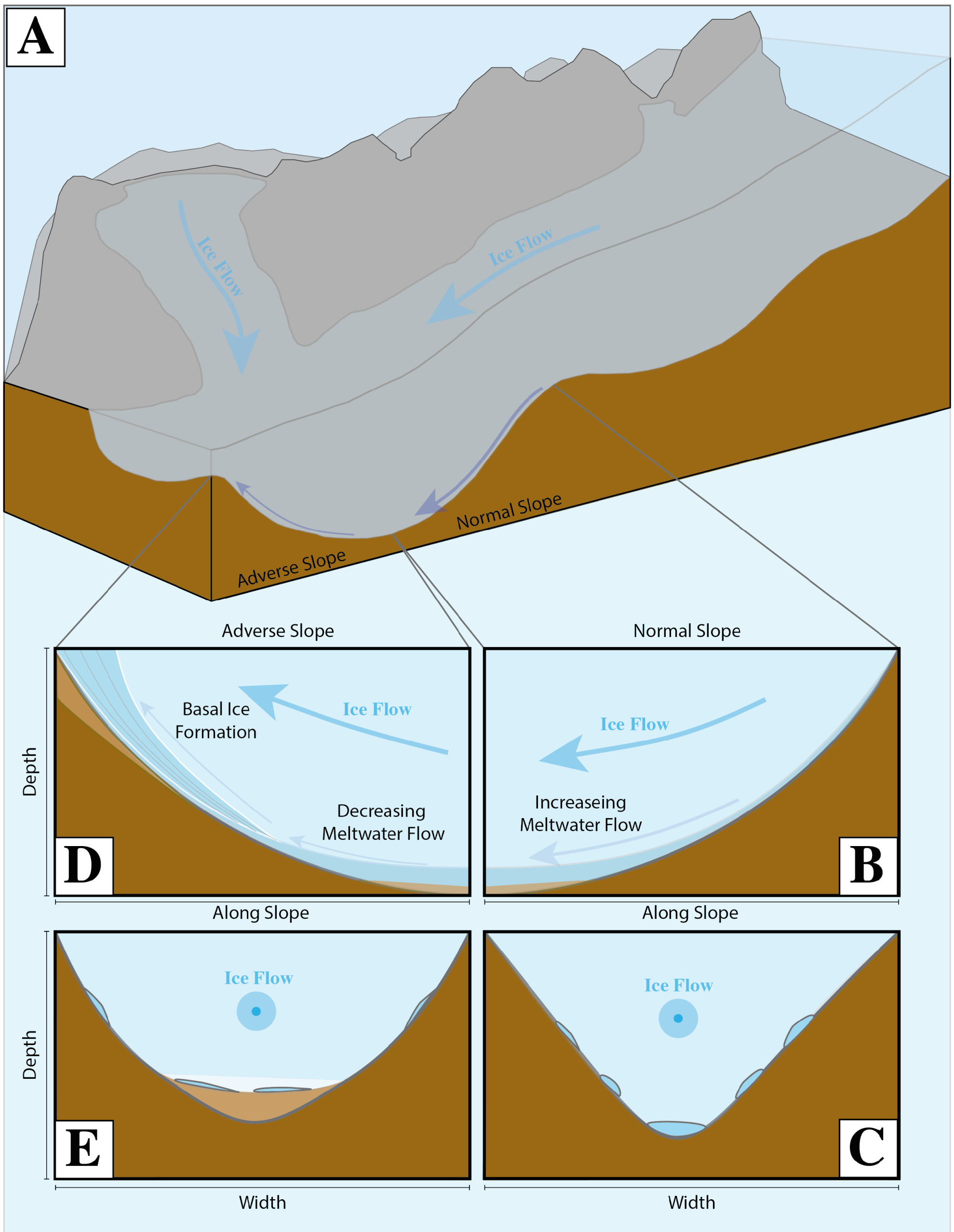

Figure 6.17: Schematic diagram normal and adverse slopes of a theoretical CGBL feature formed in an alpine setting. A) shows the location of the normal and adverse slopes in a sub-basin of the CGBL feature. B) Long-profile view of normal slope showing the increasing rate of meltwater flow down slope as the flow is focused from the more distributed up-glacier catchment. C) Cross-profile view of normal slope schematically showing the well-developed subglacial hydrological pathways formed on the normal slope. D) Long-profile view of adverse slope schematically showing the decreasing levels of meltwater pathways on the adverse slope due to increased distribution of flow and englacial routing of flow, and the increased formation of basal ice as slopes start to reach the supercooling threshold. E) cross-profile view of adverse slope schematically showing the lower number of open channelised subglacial hydrological pathways on the adverse slope, and the increased deposition of sediments at the ice/bed interface.

Confinement

The next factor of influence discussed in this chapter is that of topographic confinement. The topographic confinement maps (Fig. 6.10) show that the features of northern Switzerland and the Finger Lakes developed in opposing contexts with regard to the relation of ice flow direction to topography. The features of northern Switzerland developed from the highly confined valleys of the Swiss alpines into the much lower lying less confined Swiss foreland, in contrast to the features of the Finger Lakes where the ice flow was from low lying land into the higher confinement of the Allegheny Plateau.

Figures 6.11a and 6.11b show slight agreement with the hypothesis that the depths and widths of the features of northern Switzerland were influenced by the relative confinement of the surrounding topography. Figure 6.11a suggests that this relationship may be a bimodal distribution, in which the features formed in areas with confinement values higher than 200 m have limited width development, of up to ~4 km, and that features below the 200 m confinement level develop much greater widths of up to ~16 km. Figure 6.11b similarly shows a relationship between depth and confinement, with the depth of the feature increasing with confinement up to about 350 m deep and confinement values of 200m. However, at values higher than 200 m confinement the trend appears to completely disappear. A positive relationship is seen in the Fr confinement figure (Fig 6.11c) but not the cross-sectional morphology (6.11d).

To test the influence of the high confinement areas of the alpine valleys of the feature development and signal strength of the perceived trends, only the features present in the foreland were plotted up (Appendix, Fig. B.5). Both the bimodal trend of the widths and the unimodal trend of the depths presented more strongly in the foreland figure, as well as the lack of a trend in the cross-section morphology to increasing confinement. Similar analysis of the widths, depths, Fr and cross-sectional morphology were undertaken for the features of the Finger Lakes (Fig. 6.12). Both the bimodal distribution of the widths with regards to confinement, and the strong correlation of increasing depth with confinement, were seen in the Finger Lakes, matching the results of the features of northern Switzerland. The similarity continued with a lack of any trend between cross-sectional morphology (V-index) and confinement being found.

The findings of the analysis of topographic confinement suggest that the relative topography of the surrounding area has a significant impact on the development of the width and depth of a CGBL feature, but that it has no statistically significant impact on the resulting cross-sectional morphology, and therefore processes present during formation. Figure 6.18 schematically shows how CGBL feature development changes with changes in topographic confinement.

Locations of tributary valleys

The location of tributary valleys shows some correlation with the locations of nested basins within features and the location of the deepest points, specifically in the region of northern Switzerland. This correlation between tributary confluences and CGBL incision agrees strongly with work done by Holtedahl (1967); Frey et al. (2010); Cook and Swift (2012); Lloyd (2015); Haeberli et al. (2016); Linsbauer et al. (2016), who demonstrated the link between the location of tributary junctions with the location of overdeepenings due to the increased ice flow. The magnitude of the influence of the different tributary valleys is not possible to determine without knowing the approximate size of each tributary and therefore an estimate of the additional ice flow at the junction points, which is beyond the scope of this work. Additionally, due to the uncertainty surrounding the projection error between the tributary features and the centre of the CGBL features, it is also difficult to determine the influence that individual tributaries have had on the locations of nested features and increased erosion. Figure 6.18 schematically shows how tributaries may influence increased incision along CGBL features through increasing rate and volume of ice flow.

Geology

Lithology

The relative strength of the weak linear trend seen in the depth and width graphs (Fig. 6.14a) for the different lithologies of the Finger Lakes , and the positive trends in depth/width seen in the features of northern Switzerland, suggest that the underlying bedrock erodibility (RMS) might have a key role in determining how features develop in respect to depth and width. Previous work by Swift et al. (2008), showed that the erodibility of the bedrock can result in changes in valley widths and depths. Swift et al. (2008) showed that the more erodible bedrocks produced wider and shallower valleys, while the more difficult to erode harder bedrocks produced narrower, deeper valleys. This result correlates well with the depth and width relationships seen in northern Switzerland, and is strongest when looking at the linear regression lines of the two bedrock types (Fig. 6.15). The T1 trend line has a much shallower slope, resulting from the data flattening off in favour of widening instead of deepening (Fig. 6.15a), which is contrasted with the T2 trend line with has a much steeper slope, due to the preference of deepening and not widening of the features (Fig. 6.15b). The hardness of the bedrock will have acted as a feedback loop affecting feature development, that would have also been highly affected by the influence of the regional topography resulting from the orogeny of the Alps and tectonic faulting associated with said uplift. This faulting would further affect the erodibility of the bedrock resulting in higher erodibility of the bedrock along the fault lines/zones (as seen in Lloyd (2015)).

The comparison between variation between bedrock lithologies (erodibility) and resulting cross-sectional morphology do not show clear trends, with the two geological units of northern Switzerland showing significant overlap and clustering around singular points (Fig. 6.15c and d). While the lithological units of the Finger Lakes (shown in Fig. 6.14b) show two different b/Fr relationships, a weak linear trend with increasing b-exponent and no linear trend is apparent, but with strong clustering around single points. This lack of either a linear trend or distinct clustering of features suggest that the feature cross-sectional morphologies are related more to the type of erosive processes occurring than the variations in bedrock erodibility. Nonetheless, the difference in spread of b/Fr values seen in the softer T1 bedrock of northern Switzerland, in comparison with its less erodible T2 counterpart, also may suggest that, as Augustinus (1992) suggested, weaker bedrock produces more V-shaped morphologies, simply due to the bedrock not being able to maintain the traditional U-shaped morphology. However, it may also be influenced by variations in meltwater availability which could affect the resultant feature cross-sectional morphologies.

Faulting

The influence of faulting on the development of CGBLs has been extensively shown in previous works (Lloyd, 2015), however the majority of these works have focused on either CGBLs forming along (parallel) fault lines or simply in conjunction with general faulting. Figure 6.16 shows a strong correlation with the number of inferred perpendicular faults with the number of nested basins per feature. This correlation suggests that the faults produce localised areas of weakness within the bedrock which is exploited by the erosive processes during CGBL formation and development (Fig. 6.18 schematically shows how this might work). The orientation of the faults in relation to ice flow would therefore affect the resulting long-profile morphology. This would result in faulting oriented parallel with ice flow causing easier incision along a feature, while perpendicular faulting would result in features with multiple sub-basins associated with the changes in weaker (faulted) bedrock and harder (un-faulted) bedrock. As such, it follows that more pronounced erosion is seen at the locations of perpendicular faults, compared to potential sub-basin formation related to changes in lithology, as the fault acts as an unconformity within the bedrock.

6.5 SUMMARY

The findings of this chapter suggest that the changes in cross-sectional morphology and bed profile for the features of northern Switzerland and the Finger Lakes are strongly interlinked between changes in bed profile and regional contextual factors. The work has shown that the angles of the bed slope are related to significant changes in cross-sectional morphology, that may suggest that they are affecting the relative dominance of glacial and fluvial erosion, with glacial erosion potentially becoming more dominant on adverse slopes due to the potential lowering of hydrological potential and the influence of the supercooling threshold. All the regional contexts investigated as part of this chapter have been shown to have influence on each other, and result in potential positive and negative feedback loops. Changes in topographic confinement of the features has been shown to be of importance in feature development, especially in feeding back into the development of the depth and width of features, with the higher confinement areas focusing erosion downwards and limiting feature widening. The location of tributary valleys and features have been shown to potentially have some influence on the location of sub-basins and the location of increased incision. The last factor of regional context, lithology and geological faulting, has been shown to have mixed influence of the features of northern Switzerland and the Finger Lakes. The changes in lithology have been shown to have an influence of the scale of the features, i.e. the width and depth, but not really on the cross-sectional morphologies, while the density of regional faults perpendicular to the long-profiles of the features shows a strong correlation with the number of sub-basins found with each given feature. This influence of regional faulting highlights how regional contextual factors can drastically alter how CGBL features potentially form and develop over time, with the Finger Lakes features showing a different long-profile formation in comparison to the features of northern Switzerland.

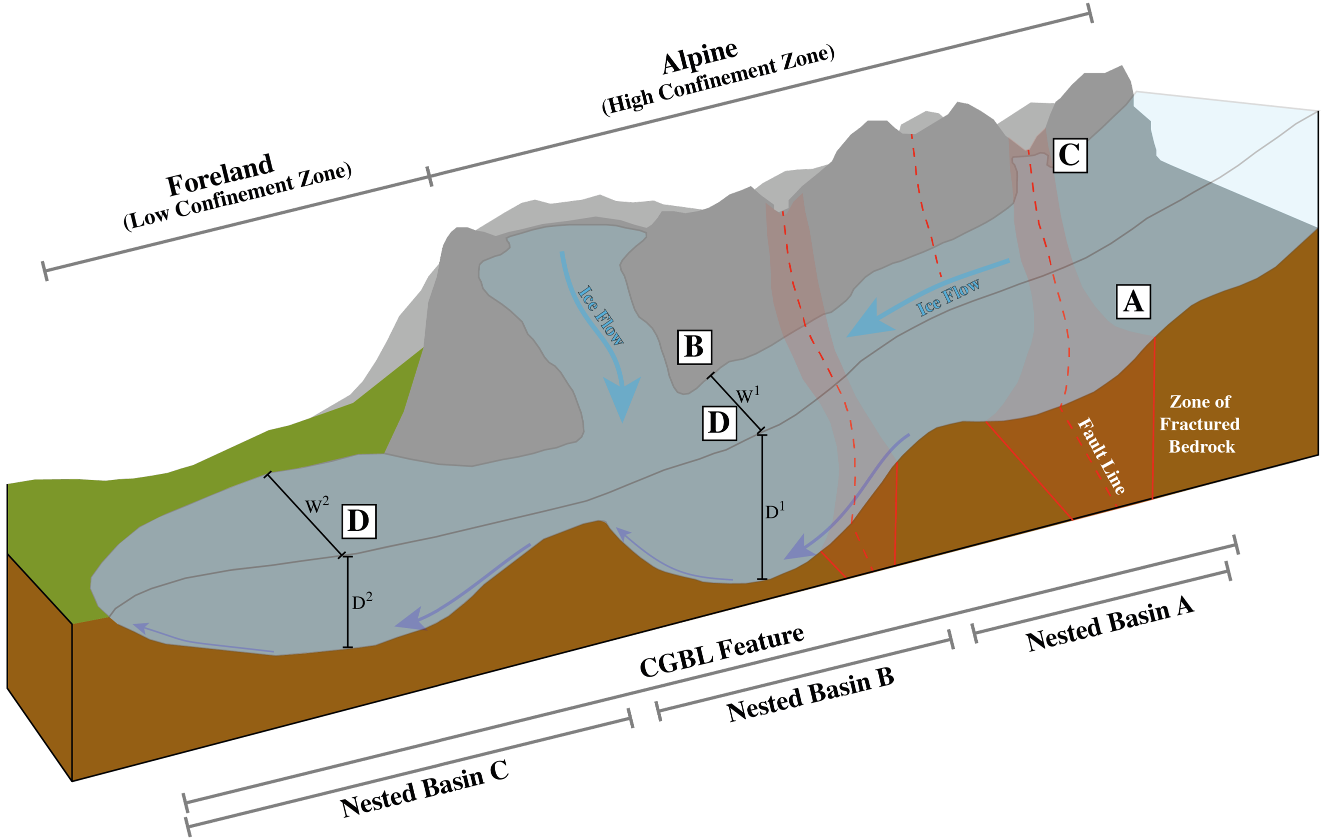

Figure 6.18: Schematic diagram of a theoretical CGBL feature formed across an alpine and foreland setting. A)The location of geological faults (dashed red lines) cross cutting the feature and associated zones of weakened bedrock promote the formation of sub-basins (Nested Basin A); B) the potential influences of tributary features on the locations of sub-basin formation (Nested Basin B). C) shows how geological faults can be associated with tributary features. D) show the changes in depth and width associated with levels of confinement (i.e. Alpine by W1 and D1, or Foreland by W2 and D2). Ice flow directions are indicated by light blue arrows and meltwater pathways are indicated by purple arrows.

Part IV

DISCUSSION AND CONCLUSION

7 DISCUSSION

7.1 INTRODUCTION

The following chapter discusses the findings of Chapters 3 to 6 in terms of their contribution to understanding CGBL formation in foreland settings, specifically relating to the findings to the research objectives outlined in chapter 1 (O1,O3, and O4). The limitations of the findings are also discussed and recommendations for future work are proposed.

The chapter has been split into four main sections. First, a review of the findings of the three main results chapter are presented. This is then followed by the discussion of how well previous formation hypotheses fit with the presented morphological findings, and proposes potential updates to the previous proposed models of formation to better match with the morphological findings. The third section then discusses the potential wider implications of the morphological findings and any formation hypotheses, and the last section summarises the chapter, discussing the limitations of the presented work.

7.2 OVERVIEW OF RESULTS

7.2.1 *Global synthesis*

Chapter 3 presents the findings of an extensive review of the available literature on feature that met the author's definition of a *channelised glacioerosional bedrock landform* (CGBL). The chapter shows that there are over 13,900 identified bedrock CGBLs in many foreland or foreland-like landscapes which were previously and/or are currently glaciated. Specifically, the chapter focuses on features located in Switzerland, The United States of America, New Zealand, Greenland, and Antarctica, as well as outlining publications of CGBL features identified in other regions of the world.

The review highlights how, for many of these sites, there is limited availability of high-quality bedrock topography data, which would allow for further detailed morphological analysis of these features. The most available datasets are either coarse resolution datasets that cover very large areas, such as the published Greenland and Antarctica data sets of BedMachine v3 (Morlighem et al., 2017), and BedMachine Antarctica and Bedmap2 (Fretwell et al., 2013; Morlighem et al., 2020) (which were uses as part of Patton et al. (2016b) to record average CGBL size in Greenland and Antartica as being 22.2 km and 52.3 km in length, 5.6 km and 8.5 km in width and 227 m and 222 m in depth respectively), or they are feature specific datasets that focus on specific features (i.e. Lake McDonald (Mullins et al., 1991) or Okanagan Lake (Eyles et al., 1991)). This is due to the limitations of past and current data collection methods, the features often being; buried under thick ice; thick sediment; or filled with both sediment and water; and therefore the time and cost of collecting high-quality bedrock topography datasets. However, the global review of the available data on CGBL features did show that CGBL features in foreland or foreland-like settings have been recorded to have a range of typical dimensions. Specifically, the CGBL features can reach depths of up to 847 m, widths of 12 km, and the features have a ranged of recorded lengths, with the maximum feature length being recorded as 166 km.

7.2.2 *Average cross-sectional morphology*

The results of the global study, undertaken in chapter 5, show that the CGBL features of the four main study sites (northern Switzerland, the Finger Lakes, the Humboldt Glacier, and the British Columbian lakes), which were previously described as tunnel valleys or overdeepenings, show similar cross-sectional morphologies. The findings showed that CGBL features can range in depth from 20 m to 450 m, with recorded widths of 1.2 km to 14.1 km. The cross-sectional morphologies of the CGBL features are shown to fall across the three chosen erosional end-members, from V-shaped morphologies comparable to those of the subaerial fluvially eroded valleys of the western slopes of the Hawaiian Island of Kauai (b-exponet = 0.94 and V-index = 0.05), to much more U-shaped similar to the glacial eroded valleys of Alaska (b-exponent = 2.04 and V-index = 0.58), with a strong correlation specifically with the subglacial fluvial erosional end-member 66% data envelope. The wide range of averaged cross-sectional morphologies reported in this chapter have been interpreted to represent a mixed erosional signal, suggesting that the studied CGBL features were formed not from a single dominant erosional process but a mix of both glacial ice and subglacial meltwater erosion.

The secondary finding of chapter 5 was the features of northern Switzerland appeared to show an increased V-shaped cross-sectional morphology with depth of features, potentially suggesting the increased influence of subglacial fluvial erosion with development of features. This trend, however, is not present in the other three main study sites, and may actually relate to variations in the underlying bedrock strength.

7.2.3 *Variation of morphology along profile*

The investigation of changes in cross-sectional morphology along CGBL features undertaken as part of chapter 6 focused on the features of northern Switzerland and the Finger Lakes, and specifically focused on changes in the normal and adverse slopes, as well as local contextual changes in the landscape surrounding each CGBL, including changes in topographic (confinement and location of tributary features) and geology (lithology and faulting). The along-profile analysis showed that, within each feature, the cross-sectional morphology can vary significantly, and that the long-profiles can be different between features of the same region and/or comparable regions.

The work showed that regional context plays a key part in the resulting feature morphologies, specifically in relation to the way the surrounding landscape can confine the flow of ice and water (i.e. topographic confinement), and how the underlying bedrock lithologies and geological structures can affect the style of feature development. The findings of chapter 6 show that features have a strong tendency to grow wider in areas of lower topographic confinement, and deeper in confined regions, and that the presence of geological faults perpendicular to ice flow can affect the formation of nested sub-basins within the main CGBL features. This production of sub-basins in turn affects the locations of the formation of normal and adverse slopes within the features, which can potentially result in variations in dominant types of erosion. The findings show changes in cross-sectional morphology between the two types of slopes (normal and adverse), with adverse slopes in the features of northern Switzerland tending to produce more U-shaped cross-sectional morphologies, suggesting either the increased influence of glacial erosion or the decreased influence of subglacial meltwater erosion. These changes in erosional process have been interpreted to potentially be due to decreased hydrological potential, and increased influence of basal ice formation and deposition of transported sediments upslope. The findings of the chapter also suggest that there are no strong correlations between the level of topographic confinement of a CGBL feature, or changes in the lithology of the underlying bedrock, with the resulting cross-sectional morphology of the feature.

7.3 DISCUSSION OF CGBL FORMATION HYPOTHESIS

Throughout the published literature there are several proposed formational hypotheses for CGBL type features (named "overdeepenings" and "tunnel valleys" in the literature). The following section is split into two subsections; the first evaluates how well the previously proposed formation hypotheses conform with the morphological evidence present in the studied CGBLs, focusing specifically on the features of northern Switzerland and the Finger Lakes, due to the high number of features and quality of the bedrock topography datasets; and the second section aims to discuss what an updated formation hypothesis for CGBL feature requires.

7.3.1 *Existing formation hypotheses*

The morphological evidence for and against the four existing formation hypotheses are outlined in Table 7.1. The following section describes in more detail how well the existing formation hypotheses match with the morphological evidence presented in the previous chapter and the model of formation discussed in the previous section.

The mixed signal of the cross-sectional morphology of the four main study regions investigated as part of chapter 5 suggest that the erosional processes involved in the formation and development of features most likely contain both glacial ice and subglacial meltwater, as discussed as part of the proposed model of formation above. These findings in conjunction with the variations in cross-sectional morphology seen along-profile within the features of northern Switzerland and the Finger Lakes (discussed in chapter 6) suggest that previously proposed formation hypotheses may not capture the full picture, or may only address limited settings dependant on regional contextual factors such as style of glaciation, underlying bedrock and geological faulting, and topographic setting.

Table 7.1: Table outlining morphological evidence for and against the existing formation hypotheses.

Time scale	Existing formation hypotheses	Morphological evidence for	Morphological evidence against
Time-transgressive formation	Quarrying dominated erosion	The features in northern Switzerland contain a large number of nested basins that could result from headward glacial erosion, as well as the location of the features deepest point being located between the centre and headward (inflow) ends of most of the features.	The slope analyses of the features of northern Switzerland show similar distributions of slope angle for normal and adverse slope, which would not be expected if quarrying was the dominant formation process. Additionally, the features of the Finger Lakes have deepest points located in the marginward (outflow) ends of most of the features.
Time-transgressive formation	Sapping of deformable weak bedrock	The association of nested features with the number of mapped large-scale faults present in the northern Switzerland features. Additionally, the increased V-shape of the Swiss features with depth.	The lack of strong morphological evidence in the other CGBL study sites.
Time-transgressive formation	Steady state subglacial erosion	The distribution of cross-profile morphologies along normal slopes.	The distribution of cross-profile morphologies on adverse slope indicate that subglacial meltwater erosion may have been more limited along these slopes.
Instantaneous	Catastrophic flooding	The increased V-shape of the Swiss features with depth.	The lack of additional sub-features present in CGBL sites such as slot gorges.

7.3.1.1 *Quarrying dominated erosion*

The main formation hypothesis proposed for glacial erosion into bedrock invokes the physical process of headward erosion through the "quarrying" of fractured bedrock by entrainment of basal ice (as described in chapter 2 section 2.2.1.2) (Hooke, 1991; Iverson, 2012; Patton et al., 2016b). Hooke (1991) invoked this style of formation, hypothesising that the features develop from the joining up of smaller depressions and that the features generally grow headward upvalley by quarrying, with the downvalley erosion limited by the deposition of sediments on the adverse slopes. The features in northern Switzerland show morphological evidence that has been interpreted to suggest that this style of erosion by glacial quarrying may have been present during the formation and development of the Swiss features. The evidence that is invoked by Hooke (1991) and Patton et al. (2016b) for formation by glacial quarrying is the presence of multiple nested basins, which is noted to be present in many of the northern Swiss features, and the location of the deepest points of erosion of many of the features being located between the centre of the features' long-profile and headward (glacial inflow) end of the northern Swiss features.

The potential influence of quarrying as the dominant form of erosion is brought into question by the distribution of cross-sectional morphology along all the normal slopes. The distribution curves of the normal slopes indicate that there must also be extensive erosion by subglacial meltwater due to the high numbers of more V-shaped cross-sections measured. Figure 7.1 shows how quarrying may be taking place on the steeper parts of the normal slopes and that meltwater erosion may be more dominant on the shallower sections, as suggested by the distributions of cross-sectional morphology of normal slopes shown in figure 6.2 and 6.9. However, this distribution of cross-sectional morphologies may also be the result of variations in the rock mass strength of the underlying bedrock, which may result in the bedrock not being able to maintain the steep sides of the traditional U-shaped glacial features. The variations in cross-sectional morphology are not likely due to variations in bedrock geology, as most of the changes between normal and adverse slopes for the features in northern Switzerland occur within single type of bedrock erodibility (an example of this is shown for NSF feature 1 between Fig. 6.2 and 6.13a). This explanation of the higher V-shaped cross-sectional morphologies raises the question, if the cross-sectional morphologies are made more V-shaped due to lower rock mass strengths then why do you see a higher level of U-shaped-ness when looking at the morphology of all the adverse slopes? Additionally, 'if quarrying was the only dominant processes of erosion', the location of the deepest points of erosion would predominately be found in the headward side of the feature long-profile, as proposed by Hooke (1991) and Patton et al. (2016b), but the points of deepest erosion for the CGBLs investigated as part of this thesis are shown to not be located in one particular section, but can be found near the inflow (headward) (Fig. 6.5 F9, F11), middle (Fig. 6.5 F1, F4; and Fig. 6.6 F6), or even outflow sections of the features (Fig. 6.5 F7; Fig. 6.6 F9, F10).

The variations in location of deepest point of erosion along features suggest that the control on its location may be more strongly affected by factors such as topographic confinement and the local structural geology than simply glacial quarrying. This is due to the location of the deepest points broadly correlating with regions of higher confinement (over 200m confinement; Fig. 6.10) with the features of northern Switzerland having greater confinement near the headward (inflow) end of feature as well as a tendency for the deepest point to be located headward, and the features of the Finger Lakes having the areas of higher confinement located in the outflow end of the features as well as the location of deepest erosion predominantly forming in similar areas along features. The location of formation of sub-basins also seems to strongly correlate with the presence of large scale geological structural faulting in the region of northern Switzerland.Therefore, sub-basin formation my not be solely driven by the process of glacial quarrying, evidenced by the lack of sub-basin formation in regions that lack geological faulting such as the Finger Lakes. This is compounded even further by the fact that the peak KDE slope angle of both the normal and adverse slopes of the features of northern Switzerland are extremely similar. It would be expected that if quarrying was the dominant erosional force that the normal slopes would be on average much steeper than those of the adverse slopes.

All of the above points of evidence have been interpreted to suggest that quarrying by glacial ice may be active in many CGBL feature but that the level of influence of this type of erosion is highly dependent on the influence of different regional contexts, such as topographic confinement and bedrock geology. The level of topographic confinement would focus glacial erosion, and the RMS of the underlying bedrock (discussed in chapter 6) and the presence of geological faults would effect the relative dominance of glacial quarrying on feature development.

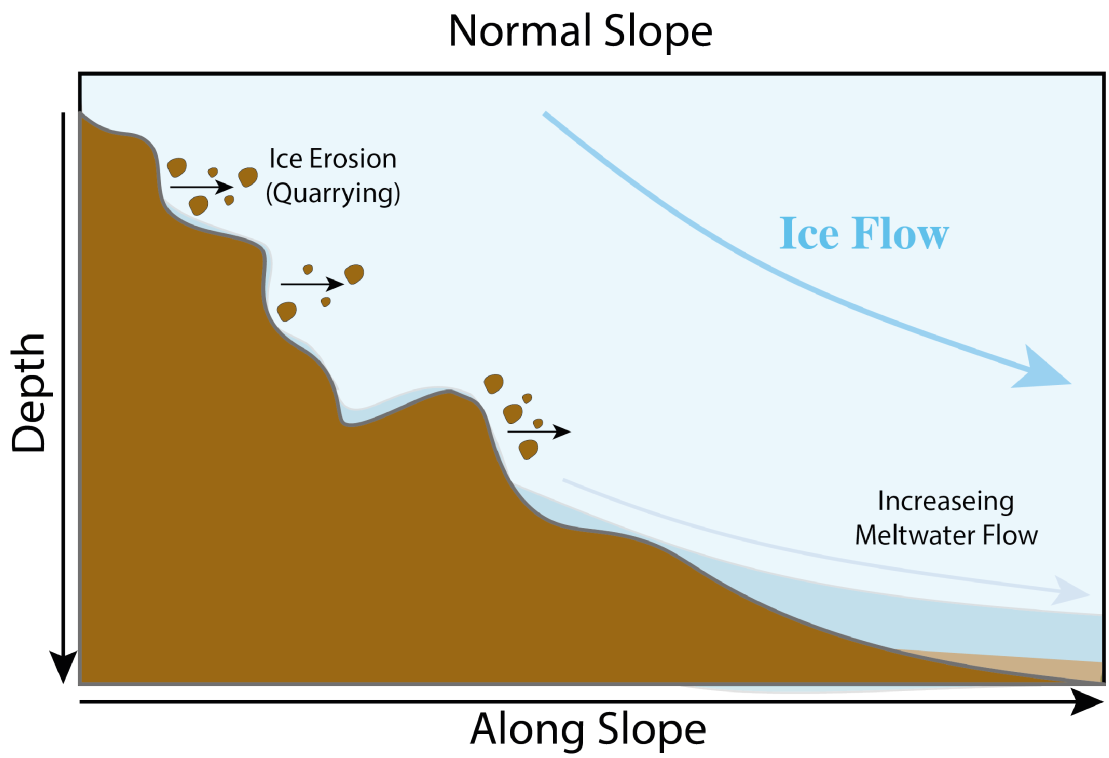

Figure 7.1: Schematic long-profile diagram showing how quarrying may be active on the steeper slopes of the CGBL normal slopes.

7.3.1.2 *Sapping of deformable subglacial sediment or weak bedrock*

The hypothesis for CGBL feature formation and development by deformation of the subglacial sediment and weakened bedrock has had very little morphological evidence to support it found in the features studied as part of this thesis (Boulton and Hindmarsh, 1987; Mullins and Hinchey, 1989; Clayton et al., 1999; Boulton et al., 2009). However, this potential evidence is highly interpretive and so formation of CGBL features by sapping is not believed to be an important formation process, if it is active.

7.3.1.3 *Catastrophic flooding events*

Due to the mixed erosional signal seen in the cross-sectional morphology and the large volumes of subglacial meltwater believed to be required for such large scale incision, the author believes that catastrophic flooding events (previously invoked in CGBL features by Shaw et al. (1989); Huuse and Lykke-Andersen (2000); Jørgensen and Sandersen (2006)) may have been a periodically active erosional process involved in CGBL formation. The strongest morphological evidence for the development of the studied CGBL feature by catastrophic flooding events is the strong overlap between all the CGBL features and features of the Labyrinth dry valleys (the subglacial erosional end-member shown in chapter 5) which are proposed to have been formed by said process. However, if the features were only formed by subglacial catastrophic outburst flood erosion then additional features (i.e. slot gorges) would potentially be expected to be present at the base of at least some of the features, but none of the CGBL features of northern Switzerland, the Finger Lakes, or the lakes of British Columbia show evidence of such sub-features. Figure 7.2 shows how the morphologies of the features may vary from the valley-within-valley morphology seen in other fluvial eroded settings, and if these events happened with enough time between events, the evidence for this increased meltwater incision may be modified or lost by subsequent glacial and steady state meltwater erosion, which may also be affected by the RMS of the incised bedrock resulting in varied levels of preservation of any morphological evidence of the process.

Despite the lack of features such as slot gorges being present in the studied CGBLs, catastrophic outburst flood erosion is believed to have played a significant role in CGBL feature development due to the very strong overlap between all the average cross-sectional morphologies for the CGBL features, and the 66% data envelopes of the labyrinth dry valley features.

7.3.1.4 *Steady state subglacial erosion*

It is highly likely that continuous "steady state" subglacial meltwater erosion is not only active during CGBL formation but active throughout (Alley et al., 1997; Dürst Stucki et al., 2010; Jordan, 2010; Salcher and Wagreich, 2010; Herman et al., 2011). This is due to the continued removal of subglacial sediment required for continued erosion of the features by either ice or water. This style of CGBL formation has been shown to be very important in locations that undergo a fluctuating climate (including fluctuations in meltwater production during summer and winter), which creates periods of time where there is high subglacial melt water pressure and low effective

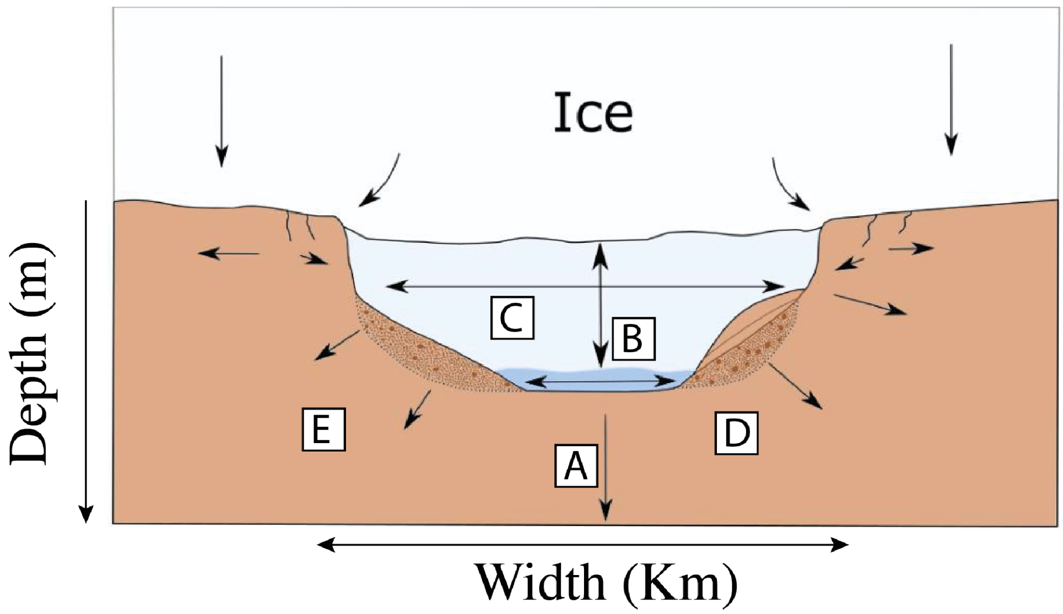

Figure 7.2: Schematic cross-sectional diagram of potential processes active during variations in meltwater flow for bedrock with lower RMS values. A) The primary direction of subglacial fluvial erosion during periods of low flow, B) The range of water depths for flows during low meltwater flow to peak pressurised meltwater flow resulting in maximum subglacial fluvial erosion, C) The width of meltwater flow during peak pressurised subglacial meltwater flow (i.e. during peak meltwater flow and catastrophic outburst floods), D) example slope failure and slumping during periods of low flow with may be transported away during peak flow or during steady-state meltwater erosion, E) Omni-directional erosion during peak pressurised flow.

pressures at the ice bed interface. This in turn increases glacial sliding and erosion (Herman et al., 2011). The work presented by Herman et al. (2011) matches well with the morphological evidence presented in this thesis for several of the Swiss features, however, evidence for this increased meltwater incision in the other CGBL features may have been lost or reduced by subsequent glacial erosion or the incised bedrock not being able to maintain the resulting morphologies due to low RMS. Therefore, due to the feature likely being formed and developed over multiple glacial cycles, a time-transgressive steady state style of erosion is believed to be highly likely, and to have occurred in conjunction with other types of glacial and sub-glacial erosion.

7.3.2 *Proposed broad model of formation*

The previous section has shown that when considering a suitable model for the formation of the CGBLs present in the four main study areas investigated as part of this thesis, there are still some potential gaps in understanding related to CGBL feature formation. The proposed formation hypotheses for overdeepenings and tunnel valleys (described in chapter 2 and discussed above) do not appear to fully account for the wide range of morphologies present in the studied CGBLs. Therefore, the development of an updated formation hypothesis may be required. Such a formation hypothesis would need to take into account not only the erosional processes active during formation and development, but also influence of contextual factors which have the potential to focus feedbacks related to the erosional processes active, and the time scale of which these processes occur (i.e. the effect of features forming over multiple glaciations).

The morphological evidence present for the CGBL features of the four main study areas indicate that the CGBL features have formed by a mix of subglacial fluvial and glacial erosion. Unlike the processes proposed by previous formation hypotheses, the results presented in this thesis suggest that the normal slopes are affected more by subglacial fluvial erosion and that it is actually the adverse slopes that see more glacial erosion on average. Therefore, glacial erosion by quarrying must not be as dominant as previously believed, with this style of erosion potentially limited to the steepest sections of the normal slopes predominantly present in some of the sub-basins. The trend of increasing V-shape seen in the features of northern Switzerland also indicates that the influence of subglacial fluvial erosion increases with feature development (with increasing depth) suggesting that the levels of influence of different erosional processes (glacial and fluvial) vary as the features form.

Unlike previous proposed formation hypotheses, the results of this work suggest that the context in which the CGBL features form have a significant effect on the features' formation and development. The results presented in the previous chapter and discussed above suggest that features that form in areas of higher topographic confinement will grow to greater depths as the erosional processes are focused, with the features' horizontal growth constrained. This is in comparison with feature development in lower confinement areas, where features develop much wider profiles with less focus of erosion vertically.

The work also highlighted that CGBL features may be more likely to form in location of changes in erodibility of the underlying bedrock, such as changes in lithology or areas with a high density of large-scale geological faulting. These areas of higher erodibility of the bedrock would allow for the formation of small basins which could potentially act as nucleation sites for the development of larger CGBL features. If formed in conjunction with higher topographic confinement, they may result in increased incision at these locations due to the feature increasing the local topographic confinement through their own development, producing a positive feedback loop.

The exact proportions and timings of the different types of erosion cannot be calculated using the data presented in this thesis, and would require further analysis using appropriate numerical modelling, in conjunction with other evidence such as borehole stratigraphy, and age dating of bedrock and sediments. However, using feature size and depth as a proxy for age, the results show that the features may go through stages of development which result in changes of dominance of different erosional processes causing the trend towards increased V-shaped cross-sectional profiles seen in the features of northern Switzerland.

Figure 7.3 show a schematic interpretation of how the different glaciological and subglacial erosional processes might interact with one another and be influenced by the changes in normal and adverse slope angle and regional context.

7.3.2.1 *Formation timescales of Switzerland's deepening*

The scale of the features present in all of the CGBL study sites (depths of 20 m to 847 m; widths of 1.2 km to 14.1 km; lengths of up to 166 km) suggest that feature formation likely occurred over multiple glaciations, with the cross- and long-profile morphologies being developed further during each glacial cycle over the previous "inherited" bedrock morphology produced by the previous glaciation, similar to the processes proposed by Kirkham et al. (2020). Infilling and erosion over multiple glacial cycles may also help to explain why the northern Switzerland features show increased V-shape with depth. If feature depth is used as a proxy for feature age, then two possible explanations for the relationship between feature V-shapedness and depth of feature can be proposed. The first is that the features have been influenced over multiple glaciations by glacial ice predominantly in the higher parts of the feature sides and meltwater at the valley base, resulting in the more V-shaped morphologies. Alternatively, the second potential explanation for the increased V-shaped morphologies is a result of those features being formed over a longer period of time in weaker, more erodible bedrock (see Fig. 6.13), with such bedrock not having the rock mass strength to maintain the steep sided traditional U-shaped feature cross-profile, due to fluctuations in lateral shear stresses. The sedimentological evidence of such slope failure may not be present in the features due to erosion and sediment transportation during feature development during subsequent glaciations.

The extensive meltwater pathways required for the first explanation of the increased V-shaped morphology with feature depth seen in the features of northern Switzerland are thought to need to form either during glaciation, or more likely deglaciation, due to the volume of meltwater required (Alley et al., 1997; Dürst Stucki et al., 2010; Jordan, 2010; Salcher and Wagreich, 2010; Herman et al., 2011). This is also mostly confined to or near the base of the features in the form of channelised meltwater networks causing increased fluvial erosion at the base during seasonal meltwater erosion and/or catastrophic flooding events.

As mentioned before, this trend in increasing V-shape with feature depth is not seen in the features of the Finger Lakes. This lack of trend in the Finger Lakes suggests that the changes in cross-sectional morphology may be a result of not only increased meltwater erosion. The three main potential difference between the two regions that were considered in regard to this variation in development were: variations in bedrock lithologies; density of structural geology; and size of features. Fig. 5.6 shows that the features of both regions are formed on comparable scales, which makes it likely that differences in feature scale is not the cause of the lack of the trend. Both the density or presence of large-scale geological structure (faults) and variations in bedrock lithologies (bedrock erodibility) both result in potential variation in the RMS of the bedrock which is likely to affect the ability of features to maintain cross-sectional morphologies. However, figures 6.13 and 6.14 suggest that the variations in bedrock lithologies within each region do not show a significant impact on morphological changes, however it is not possible to easily compare between regions because of the lack of quantification of the RMS of each of the lithologies. While lithologies cannot be compared easily, the lack of mapped large-scale faulting in the region of the Finger Lakes suggests that the bedrock has not been weakened by mechanical stresses in the same way that the features of northern Switzerland have, which may affect the ability of the bedrock to maintain cross-sectional morphologies.

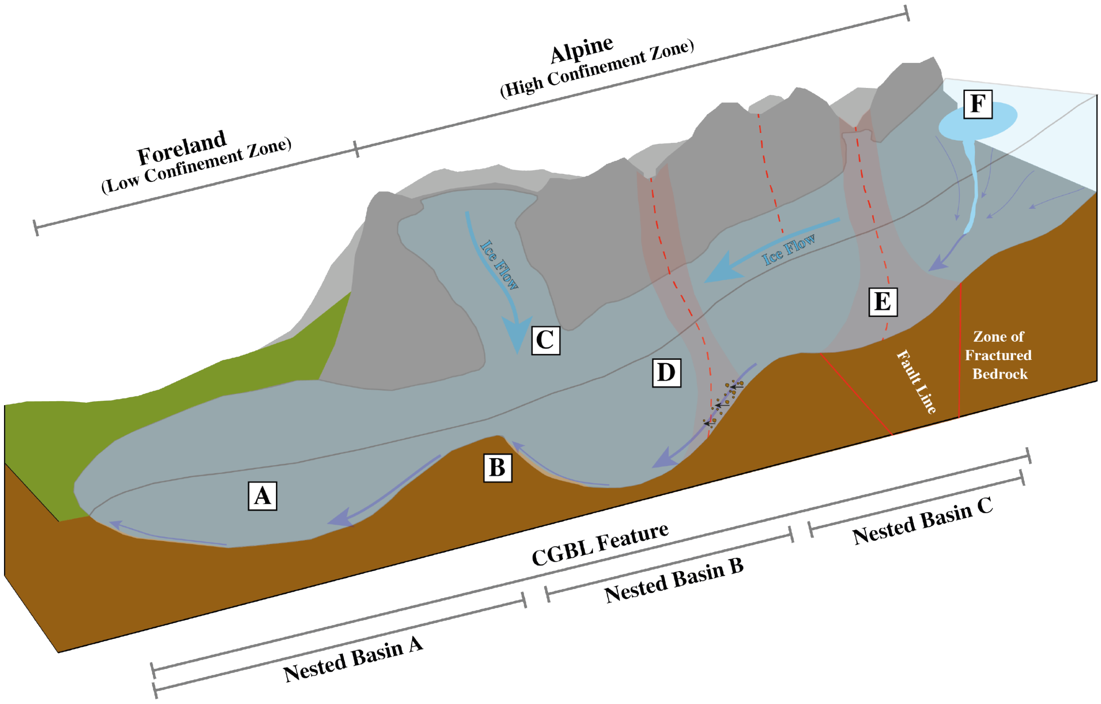

Figure 7.3: Schematic diagram of a theoretical CGBL feature formed across an alpine and foreland setting. A)The section of the CGBL feature in the foreland (lower topographic confinement zone) which trends towards widening more than deepening of features(Nested Basin A); B) The example of the adverse slopes where subglacial meltwater networks decrease, increasing sedimentation and potential basal ice formation resulting in greater influence of glacial erosion(Nested Basin B); C) The increased input of glacial ice and meltwater resulting in increased feature incision (i.e. nested basin formation)(Nested Basin B); D) potential location of glacial erosion (quarrying) along steeper sections of normal slopes (Nested Basin B); E) example location of geological faults (dashed red lines) cross-cutting the feature and associated zones of weakened bedrock, which promote the formation of sub-basins (Nested Basin C); F) example of how large scale catastrophic meltwater events may increase subglacial meltwater erosion.

7.4 WIDER IMPLICATIONS

The implications for the findings presented in this thesis for the understanding of CGBL development, is that the current models of "tunnel valley" (features formed purely from subglacial fluvial erosion) and "overdeepening" (features formed purely from glacial erosion) do not fully capture the complex interconnected glacial and subglacial fluvial processes occurring during the formation of these features. The findings suggest that tunnel valleys and overdeepenings potentially need to be considered as descriptors of types of features that form the end of a spectrum of features, rather than distinct types. This would suggest that the current methods of identifying features (i.e. the amount to which different erosional processes influenced the production of features) needs to be improved, specifically through the greater integration of subglacial hydrology in glacial erosional models (such as implemented by Herman et al. (2011) and Ugelvig et al. (2018)).

The findings of chapters 5 and 6 suggest that the CGBL features grow in a variety of ways during glaciations, and that on average the location of deepest incision is located between the centre and inflow of the features in northern Switzerland, and the centre and outflow for the features of the Finger Lakes. These findings, in conjunction with the noted variations in morphology between the smaller and the larger features, suggest that the features of northern Switzerland will continue to incise most near the inflow ends of the features. This is predicted due to the interpreted influence of the higher confinement of the region in or near to the Alps, focusing feature development down into the bedrock and limiting feature widening, as well as the higher concentration of large-scale faults present at the alpine foreland boundary. This influence of confinement is predicted to also result in the features of the Finger Lakes continuing to incise more in the later part of the CGBL features in the region, if the future glaciations follow past trends with ice flow coming from the north towards the higher Allegheny Plateau. It is difficult to determine how and if the feature will grow laterally in the regions of the Finger Lakes and northern Switzerland. In both situations the outflow growth of the features will be limited by regional contextual factors of geology and topography. In northern Switzerland the features are limited by the higher topography of the Jura mountains and the change in geology with the presence of the harder Jura limestones, and in the Finger Lakes it is the Allegheny Plateau.

Due to the similarities in normal and adverse slope angles measured for the features of northern Switzerland, it is likely that the features will grow with similar rates in both the inflow and outflow direction. However, there is also the possibility that the features will grow more laterally in the regions of higher confinement due to the limiting of ice and meltwater flow (i.e. the erosion is not able to widen the feature and so will result in lengthening the features). If this is the case, then the features of northern Switzerland will likely grow slightly more towards the inflow end of the CGBL features, while the features of the Finger Lakes will develop further into the Allegheny Plateau.

7.5 LIMITATIONS

The findings outlined in the above section and the previous chapters are robust findings, however the above discussion has identified some key limitations of the work. These limitations have not seriously impaired the validity of the results but are important to acknowledge as they may have had an effect on the resultant error of the findings. The following subsection outlines some of the key limitations of the work.

7.5.1 *Data quality for long-profile analysis*

As discussed in chapter 4, the long-profiles produced using the digitisation methodology for non-digital data are not deemed high enough quality for several aspects of the long-profile analysis. This is a result of the lower density of data points (digitised bedrock topography contours) along-profile. This has resulted in the slope analysis being limited to only one of the CGBL study sites (northern Switzerland). This limitation means that the resulting understanding of the effect of normal and adverse slope angles is limited, and therefore, so is any interpretation drawn from these results.

7.5.2 *Is b vs V-index a better way of seeing process trends?*

The comparison of the b and V-index results (Fig. 5.9) show that the two methods produce similar results. This comparison, however, does allow for potential greater insight into the morphology of each cross-section, as both measure morphology in different ways. The use of the V-index rather than the Fr potentially reduces the level of insight into valley development from preglacial fluvial to glacial valleys, such as work done by Hirano and Aniya (1988), Augustinus (1992), and Brook et al. (2004), but focuses on the potential dominant erosional processes involved in feature formation. This is shown well in Fig. 5.9 when looking at the glacial and fluvial end members of erosion, with each of the CGBLs being clearly shown as distinct (as indicated by both the average point values and the 66% data envelopes in grey). This is important for features such as overdeepenings and tunnel valleys, as these features in principle should have limited preglacial signal in the bedrock morphology due to the limited ability of non-pressurised water to erode below the base level and create adverse slope morphologies. However, the comparison does not only show the influence of dominant erosion, but also is affected by the regional context, such as bedrock geology, and topographic confinement. An example of this is shown in Fig. 5.9 were the Alpine CGBLs have higher b values trending towards b = 2 and V-index values above 0.3, indicative of extensive glacial erosion, while those of the northern Switzerland foreland are shown to have a wide variety of values (i.e. morphologies) that range from more U-shaped (0.31) to more V-shaped (0.18). The uses of the V-index against b values can also highlight issues of data quality, such as those seen in the LQ Finger Lakes features which show a wide range in values, on a similar scale to those of the northern Switzerland foreland features, though with less correlation between the b and V-index values and those of idealised features (Fig. 5.9).

A noted limitation of the method as implemented is shown in the 66% data envelope of the glacial end-member of erosion (Fig. 5.9) The envelope shows the long "tail" in data distribution. This distribution is thought to be due to due to the b-exponent method not easily resolving very box-shaped or complex cross-sectional morphologies, resulting in extremely low recorded b-exponents. This issue does not appear to be a problem when plotting b/Fr due to the data points not clustering around a single Fr value, and so not affecting the 66% data envelope, and the issue does not translate to the V-index method, which calculates more reliable high V-index values expected with such morphologies. It is likely that the problem could be corrected with better cross-sectional smoothing and pre-processing methods, but unfortunately due to the limited nature of the PhD project an actionable solution was not developed in time.

7.5.3 *The benefit of using the KDE to see a dominant process*

The results presented in chapters 5 and 6 indicate that the CGBL features of the northern Switzerland and Finger Lakes regions were formed by a mixture of glacial and subglacial fluvial erosion, potentially including catastrophic drainage events, however the work has highlighted the limited one-dimensional nature of using any averaged values for over features that are kilometers long. Chapter 6 shows the wide variety of cross-sectional morphologies present in features that are potentially influenced by multiple erosional processes and variations in several different regional contextual factors, as well as the limited availability of high-quality bedrock topography data for buried CGBL features to fully investigate these variations. The use of averaging methods such as peak KDE (used in chapter 5) allows for the analysis of dominant erosional signatures, on the assumption that the majority of a feature is dominated by a single erosional process for the majority of its formation and development. This assumption is then able to be validated through the further investigation of how morphology changes along features, with work such as that presented in chapter 6.

8 CONCLUSIONS AND FUTURE WORK

8.1 CONCLUSION

This thesis developed an improved semi-automated GIS based approach to analyse changes in long- and cross-profile morphologies to infer changes in dominant erosional processes during formation and development of CGBL features in currently and previously glaciated foreland-like settings. The findings of this thesis have been divided to answer the four main research questions proposed in the thesis (Chapter 1 Section 1.3.1).

8.1.1 *What is the current understanding of CGBL formation and development?*

A significant body of work has been done on the wide variety of CGBL features (*cirque, fjord, overdeepening, trough, tunnel valley, linear incision feature, and inner gorge*), with several formation hypotheses proposed, invoking both glacial (glacial quarrying and abrasion) and subglacial fluvial (sapping of deformable subglacial sediment or weak bedrock; catastrophic flooding events; and steady state subglacial erosion) erosive processes for feature formation into either bedrock or sediments. The synthesis of the literature (presented in chapter 3) identified >13,900s CGBL features cut into bedrock in foreland or foreland-like landscapes which were previously or currently glaciated. CGBL features can reach depths of up to 847 m, widths of 14.1 km and lengths of up to 166 km, and have a wide range of cross-sectional morphologies which are likely to have formed over multiple glaciations. The cross-sectional morphology indicated that the CGBL features of northern Switzerland develop towards a more V-shaped morphology with increased depth, inferring an increasing influence of subglacial meltwater erosion with feature development. This trend in development is not seen in the other studied CGBL sites and so might be influenced by the regional setting (i.e. erodibility of underlying bedrock, topographic confinement, etc.).

8.1.2 *Are overdeepenings and tunnel valleys parts of a continuum of features that can be described as 'CGBLs' or are they distinct phenomena formed by different processes (i.e. glacial versus fluvial)?*

The results of chapters 5 and 6 indicate that both overdeepenings and tunnel valleys are part of a continuum of features formed both by glacial and subglacial fluvial erosion. This is based on the wide range of cross-sectional morphologies, which overlap with the 66% data envelope of the glacial erosional end-member and subaerial fluvial end-member. This overlap is shown in the average b-exponent and V-index values presented in chapter 5, and a similar wide spread of cross-sectional morphometrics are shown in the distributions of all the individual cross-section points for the Finger Lakes and the features of northern Switzerland in chapter 6.

8.1.3 *What can morphological analysis indicate regarding the role of ice (i.e. quarrying and abrasion) and fluvial erosion in relation to CGBLs formation?*

The analysis of the cross-sectional morphologies of the normal and adverse slopes of all the Swiss CGBL features showed greater U-shaped morphologies on the adverse slopes than the normal slopes, indicating that for these features glacial abrasion my play a greater role than glacial quarrying during feature development. Therefore, glacial erosion, such as quarrying, which was proposed by Hooke (1991) to be the dominant process of formation of CGBL features through headward erosion of the normal slopes of CGBL features, has been shown to not be a likely dominant erosional process in the studied CGBL features of northern Switzerland.

The morphological analysis of both the long- and cross-profiles indicate that all of the CGBL features studied as part of this thesis have experienced significant subglacial fluvial erosion, and that subglacial meltwater is a key factor in the development of all CGBL features. The significant overlap with the cross-sectional morphology of the Labyrinth end-member of erosion suggest that the subglacial meltwater erosion may have occurred via catastrophic flooding. This style of erosion may partially explain the increased V-shaped cross-sectional morphology with depth seen in the features of northern Switzerland, however the lack of expected morphological features such as slot gorges suggests that catastrophic drainage was not the sole dominant active erosional process. As discussed in the previous chapter, the evidence of such large-scale erosional processes might not be preserved if the underlying bedrock has a high erodibility (low RMS).

8.1.4 *What role does changes in feature slope (e.g. adverse and normal slope) and regional context (e.g. geology and topography) play in terms of variability in CGBL morphology, both within individual features and between different CGBL features?*

Both the changes in CGBL feature bed slope (normal and adverse) and changes in regional context (including geological structures, topographic confinement, and bedrock lithology) are key factors in both individual CGBL development along feature and between features. The findings of chapter 6 show that the location of normal and adverse slopes correlate with changes in cross-sectional morphologies, indicating that slope angle influences the dominance of erosional processes active along features, with normal slopes showing greater subglacial fluvial (more V-shaped) and adverse slopes greater glacial erosion (more U-shaped). The location of these changes in slope have been shown to be influenced by the location of bedrock geological structures such as large-scale faults and the location of tributary features, with a greater number of sub-basins being found in features intersecting with more large-scale geological faults.

It was also demonstrated that CGBL topographic confinement has a significant impact on how a feature develops in depth and width, with features forming in lower confinement forming wider, shallower features than features formed in regions of higher confinement, which preferentially deepen than widen. The work presented as part of this thesis did not find strong evidence that the studied features were strongly affected by variations in bed lithology due to the lack of quantitative measurements of bedrock RMS.

8.2 future works

The findings of this thesis have highlighted several key areas that would benefit from further work to investigate the erosional processes active during formation and the development of foreland CGBL features, similar to those investigated in this study.

- Numerical modelling to test the relative influence of regional contexts on CGBL feature formation and development, specifically how factors such as topographic confinement, geology, faulting, climate, and timing and glacial extents may affect resulting feature morphologies (similar to the work being undertaken by researchers at the University of Bern and ETH). Recent developments in modelling the influence of different erosional processes means that models now have the complexity to investigate these issues (Beaud et al., 2014; Beaud et al., 2018a; Alley et al., 2019).

- The acquisition and analysis of higher quality bedrock topological data sets for either the Finger Lakes region (similar to the work currently being undertaken at the University of Syracuse) or for one of the other potential analogue sites identified in chapter 3 that currently do not have adequate bedrock topography datasets. Access to such datasets would allow analysis of changes along the long-profiles, which could confirm the trends seen in the changes in adverse and normal slopes.

- Work to better quantify bedrock strength of potential study areas (Finger Lakes, New Zealand features) and its impact on CGBL formation and development. This will likely require field studies to measure rock mass strength.

- Field work to map and date potential sedimentary fan deposits associated with large-scale subglacial meltwater outwash, alongside detailed seismic and dating studies to determine age and whether sedimentary infill is fully flushed out during repeated glacial cycles. This work would allow for the development of a chronology of deposition of outwash sediments and therefore potential timing of erosion and erosion rates. It is not known by the author if any such deposits exist for any of the main study sites.

- The investigation of the potential of developing a method for estimating potential Fr ranges from high-quality data for use with lower quality data in the same region that have undergone similar glaciological conditions. This would allow estimations of depth of features from known feature widths.

Each of these proposed works would help further the work that was undertaken as part of this thesis, and would help the project's commercial partner address their specific research question relating the future development of the northern Swiss foreland CGBL features with the long term security of the proposed nuclear waste storage facilities.

BIBLIOGRAPHY

Alden, W.C. (1953). *Physiography and glacial geology of Western Montana and adjacent areas*. Report 231. USGS. DOI: 10.3133/pp231.

Alexander, D., T. Davies, and J. Shulmeister (2014). "Formation of the Waiho Loop terminal moraine, New Zealand." In: *Journal of Quaternary Science* 29.4, pp. 361–369. DOI: 10.1002/jqs.2707.

Alley, N.F. (1976a). "Post-Pleistocene glaciations in the interior of British Columbia." In: *Programme and Abstracts, Geological Association of Canada* Cordilleran Section, p. 6.

Alley, N.F. (1976b). "The palynology and palaeoclimatic significance of a dated core of Holocene peat, Okanagan Valley, southern British Columbia." In: *Canadian Journal of Earth Sciences* 13.8, pp. 1131–1144. DOI: 10.1139/e76-115.

Alley, R. B., K. M. Cuffey, and L. K. Zoet (2019). "Glacial erosion: status and outlook." In: *Annals of Glaciology* 60.80, pp. 1–13. DOI: 10.1017/aog.2019.38.

Alley, R.B., K.M. Cuffey, E.B. Evenson, J.C. Strasser, D.E. Lawson, and G.J. Larson (1997). "How glaciers entrain and transport basal sediment: Physical constraints." In: *Quaternary Science Reviews* 16.9, pp. 1017–1038. DOI: 10.1016/S0277-3791(97)00034-6.

Alley, R.B., T.K. Dupont, B.R. Parizek, and S. Anandakrishnan (2005). "Access of surface meltwater to beds of sub-freezing glaciers: preliminary insights." In: *Annals of Glaciology* 40, pp. 8–14. DOI: 10.3189/172756405781813483.

Alley, R.B., D.E. Lawson, E.B. Evenson, J.C. Strasser, and G.J. Larson (1998). "Glaciohydraulic supercooling: a freeze-on mechanism to create stratified, debris-rich basal ice: II. Theory." In: *Journal of Glaciology* 44.148, pp. 563–569. DOI: 10.3189/S0022143000002070.

Alley, R.B., D.E. Lawson, G.J. Larson, E.B. Evenson, and G.S. Baker (2003). "Stabilizing feedbacks in glacier-bed erosion." In: *Nature* 424, pp. 758–760. DOI: 10.1038/nature01839.

Amerson, B.E., D.R. Montgomery, and G. Meyer (2008). "Relative size of fluvial and glaciated valleys in central Idaho." In: *Geomorphology* 93.3, pp. 537–547. DOI: 10.1016/j.geomorph.2007.04.001.

Anderson, J.B., S.S. Shipp, A.L. Lowe, J. Smith Wellner, and A.B. Mosola (2002). "The Antarctic Ice Sheet during the Last Glacial Maximum and its subsequent retreat history: a review." In: *Quaternary Science Reviews* 21.1, pp. 49–70. DOI: 10.1016/S0277-3791(01)00083-X.

Anderson, R.S., P. Molnar, and M.A. Kessler (2006). "Features of glacial valley profiles simply explained." In: *Journal of Geophysical Research: Earth Surface* 111.F1. DOI: 10.1029/2005JF000344.

Anderson, W.T., H.T. Mullins, and E. Ito (1997). "Stable isotope record from Seneca Lake, New York: Evidence for a cold paleoclimate following the Younger Dryas." In: *Geology* 25.2, pp. 135–138. DOI: 10.1130/0091-7613(1997)025<0135:SIRFSL>2.3.CO;2.

Armstrong, R.L. (1978). "K-Ar dating: Late Cenozoic McMurdo volcanic group and dry valley glacial history, Victoria Land, Antarctica." In: *New Zealand journal of geology and geophysics* 21.6, pp. 685–698.

Ashley, G. (1975). "Rhythmic sedimentation in glacial lake Hitchcock, Massachusetts, Connecticut." In: *Glaciofluvial and Glaciolacustrine Sedimentation*. Ed. by A.V. Jopling and McDonald B.C. Tulsa, Oklahoma, U.S.A.: Society of Economic Paleontologists and Mineralogists. Chap. 15, pp. 304–320. DOI: 10.2110/pec.75.23.

Atkinson, N., L.D. Andriashek, and S.R. Slattery (2013). "Morphological analysis and evolution of buried tunnel valleys in northeast Alberta, Canada." In: *Quaternary Science Reviews* 65, pp. 53–72. DOI: 10.1016/j.quascirev.2012.11.031.

Attig, J.W., D.M. Mickelson, and L. Clayton (1989). "Late Wisconsin landform distribution and glacier-bed conditions in Wisconsin." In: *Sedimentary Geology* 62.2, pp. 399–405. DOI: 10.1016/0037-0738(89)90128-0.

Augustinus, P.C. (1991). "Rock resistance to erosion: Some further considerations." In: *Earth Surface Processes and Landforms* 16.6, pp. 563–569. DOI: 10.1002/esp.3290160608.

Augustinus, P.C. (1992). "The influence of rock mass strength on glacial valley cross-profile morphometry: A case study from the Southern Alps, New Zealand." In: *Earth Surface Processes and Landforms* 17.1, pp. 39–51. DOI: 10.1002/esp.3290170104.

Augustinus, P.C. (1995). "Glacial valley cross-profile development: the influence of in situ rock stress and rock mass strength, with examples from the Southern Alps, New Zealand." In: *Geomorphology* 14.2, pp. 87–97. DOI: 10.1016/0169-555X(95)00050-X.

Bamber, J. L., J. A. Griggs, R. T. W. L. Hurkmans, J. A. Dowdeswell, S. P. Gogineni, I. Howat, J. Mouginot, J. Paden, S. Palmer, E. Rignot, and D. Steinhage (2013). "A new bed elevation dataset for Greenland." In: *The Cryosphere* 7.2, pp. 499–510. DOI: 10.5194/tc-7-499-2013.

Barrell, D.J.A. (2011). "Chapter 75 - Quaternary Glaciers of New Zealand." In: *Quaternary Glaciations - Extent and Chronology*. Ed. by Jürgen Ehlers, Philip L. Gibbard, and Philip D. Hughes. Vol. 15. Developments in Quaternary Sciences. Elsevier, pp. 1047–1064. DOI: 10.1016/B978-0-444-53447-7.00075-1.

Beaney, C.L. (2002). "Tunnel channels in southeast Alberta, Canada:: evidence for catastrophic channelized drainage." In: *Quaternary International* 90.1, pp. 67–74. ISSN: 1040-6182. DOI: 10.1016/S1040-6182(01)00093-3.

Beaud, F., G. E. Flowers, and J. G. Venditti (2016). "Efficacy of bedrock erosion by subglacial water flow." In: *Earth Surface Dynamics* 4.1, pp. 125–145. DOI: 10.5194/esurf-4-125-2016.

Beaud, F., G.E. Flowers, and S. Pimentel (2014). "Seasonal-scale abrasion and quarrying patterns from a two-dimensional ice-flow model coupled to distributed and channelized subglacial drainage." In: *Geomorphology* 219, pp. 176–191. DOI: 10.1016/j.geomorph.2014.04.036.

Beaud, F., G.E. Flowers, and J.G. Venditti (2018a). "Modeling Sediment Transport in Ice-Walled Subglacial Channels and Its Implications for Esker Formation and Proglacial Sediment Yields." In: *Journal of Geophysical Research: Earth Surface* 123.12, pp. 3206–3227. DOI: 10.1029/2018JF004779.

Beaud, F., J.G. Venditti, G.E. Flowers, and M. Koppes (2018b). "Excavation of subglacial bedrock channels by seasonal meltwater flow." In: *Earth Surface Processes and Landforms* 43.9, pp. 1960–1972. DOI: 10.1002/esp.4367.

Bentley, M.J., C. Ó Cofaigh, J.B. Anderson, H. Conway, B. Davies, A.G.C. Graham, C.D. Hillenbrand, D.A. Hodgson, S.S.R. Jamieson, R.D. Larter, A. Mackintosh, J.A. Smith, E. Verleyen, R.P. Ackert, P.J. Bart, S. Berg, D. Brunstein, M. Canals, E.A. Colhoun, X. Crosta, W.A. Dickens, E. Domack, J.A. Dowdeswell, R. Dunbar, W. Ehrmann, J. Evans, V. Favier, D. Fink, C.J. Fogwill, N.F. Glasser, K. Gohl, N.R. Golledge, I. Goodwin, D.B. Gore, S.L. Greenwood, B.L. Hall, K. Hall, D.W. Hedding, A.S. Hein, E.P. Hocking, M. Jakobsson, J.S. Johnson, V. Jomelli, R.S. Jones, J.P. Klages, Y. Kristoffersen, G. Kuhn, A. Leventer, K. Licht, K. Lilly, J. Lindow, S.J. Livingstone, G. Massé, M.S. McGlone, R.M. McKay, M. Melles, H. Miura, R. Mulvaney, W. Nel, F.O. Nitsche, P.E. O'Brien, A.L. Post, S.J. Roberts, K.M. Saunders, P.M. Selkirk, A.R. Simms, C. Spiegel, T.D. Stolldorf, D.E. Sugden, N. van der Putten, T. van Ommen, D. Verfaillie, W. Vyverman, B. Wagner, D.A. White, A.E. Witus, and D. Zwartz (2014). "A community-based geological reconstruction of Antarctic Ice Sheet deglaciation since the Last Glacial Maximum." In: *Quaternary Science Reviews* 100, pp. 1–9. DOI: 10.1016/j.quascirev.2014.06.025.

Berger, G.W. (1985). "Thermoluminescence dating studies of rapidly deposited silts from south-central British Columbia." In: *Canadian Journal of Earth Sciences* 22.5, pp. 704–710. DOI: 10.1139/e85-076.

Booth, D.B. (1987). "Timing and processes of deglaciation along the southern margin of the Cordillera ice sheet." In: *North America and Adjacent Oceans During the Last Deglaciation*. Ed. by W.F. Ruddiman and H.E. Wright. Geological Society of America, pp. 71–90.

Boulton, G. S. and N. Eyles (1979). "Sedimentation by valley glaciers: A model and genetic classification." In: *Moraines and Varves*. Ed. by C. H. Schliichter. Balkema, pp. 11–23.

Boulton, G.S., M. Hagdorn, P.B. Maillot, and S. Zatsepin (2009). "Drainage beneath ice sheets: groundwater–channel coupling, and the origin of esker systems from former ice sheets." In: *Quaternary Science Reviews* 28.7, pp. 621–638. DOI: 10.1016/j.quascirev.2008.05.009.

Boulton, G.S. and R.C.A. Hindmarsh (1987). "Sediment deformation beneath glaciers: rheology and geological consequences." In: *Journal of Geophysical Research: Solid Earth* 92.B9, pp. 9059–9082. DOI: 10.1029/JB092iB09p09059.

Boulton, G.S., R. Lunn, P. Vidstrand, and S. Zatsepin (2007). "Subglacial drainage by groundwater-channel coupling, and the origin of esker systems: Part 1—glaciological observations." In: *Quaternary Science Reviews* 26.7, pp. 1067–1090. DOI: 10.1016/j.quascirev.2007.01.007.

Boyd, R., D. Scott, and M. Douma (1988). "Glacial tunnel valleys and Quaternary history of the outer Scotian shelf." In: *Nature* 333, pp. 61–64. DOI: 10.1038/333061a0.

Braedstrup, C.F., D.L. Egholm, S.V. Ugelvig, and V.K. Pedersen (2016). "Basal shear stress under alpine glaciers insights from experiments using the iSOSIA and ElmerIce models." In: *Earth Surface Dynamics* 4.1, pp. 159–174. DOI: 10.5194/esurf-4-159-2016.

Brennand, T.A. and J. Shaw (1994). "Tunnel channels and associated landforms, south-central Ontario: their implications for ice-sheet hydrology." In: *Canadian Journal of Earth Sciences* 31.3, pp. 505–522. DOI: 10.1139/e94-045.

Briner, J.P. and D.S. Kaufman (2008). "Late Pleistocene mountain glaciation in Alaska: key chronologies." In: *ournal of Quaternary Science* 23.6-7, pp. 659–670. DOI: 10.1002/jqs.1196.

Brocklehurst, S.H. and K.X. Whipple (2006). "Assessing the relative efficiency of fluvial and glacial erosion through simulation of fluvial landscapes." In: *Geomorphology* 75.3, pp. 283–299. DOI: 10.1016/j.geomorph.2005.07.028.

Brodie, J.W. and J. Irwin (1970). "Morphology and sedimentation in lake Wakatipu, New Zealand." In: *New Zealand Journal of Marine and Freshwater Research* 4.4, pp. 479–496. DOI: 10.1080/00288330.1970.9515362.

Broecker, W. S., G. Bond, M. Klas, E. Clark, and J. McManus (1992). "Origin of the northern Atlantic's Heinrich events." In: *Climate Dynamics* 6, pp. 265–273. DOI: 10.1007/BF00193540.

Brook, M.S., Kirkbride M.P., and Brock B.W. (2004). "Rock Strength and Development of Glacial Valley Morphology in the Scottish Highlands and Northwest Iceland." In: *Geografiska Annaler. Series A, Physical Geography* 86.3, pp. 225–234. DOI: 10.1111/j.0435-3676.2004.00227.x.

Brown, R.L. and J. Murray (1987). "Tectonic denudation of the Shuswap metamorphic terrane of southeastern British Columbia." In: *Geology* 15.2, pp. 142–146. DOI: 10.1130/0091-7613(1987)15%3C142:TDOTSM%3E2.0.CO;2.

Buechi, M.W., S.M. Frank, H.R. Graf, J. Menzies, and F.S. Anselmetti (2017). "Subglacial emplacement of tills and meltwater deposits at the base of overdeepened bedrock troughs." In: *Sedimentology* 64.3, pp. 658–685. DOI: 10.1111/sed.12319.

Cadwell, D.H. and E.H. Muller (1986). "Surficial Geologic Map of New York, New York State Museum – Geological Survey." In: *Map and Chart Series* 40.

Camerlenghi, A., E. Domack, M. Rebesco, R. Gilbert, S. Ishman, A. Leventer, S. Brachfeld, and A. Drake (2001). "Glacial morphology and post-glacial contourites in northern Prince Gustav Channel (NW Weddell Sea, Antarctica)." In: *Marine Geophysical Researches* 22, pp. 417–443. DOI: 10.1023/A:1016399616365.

Carrara, P.E. (1990). "Surficial Geologic Map of Glacier National Park, Montana." In: DOI: 10.3133/i1508D.

Carrara, P.E., S.K. Short, and R.E. Wilcox (1986). "Deglaciation of the Mountainous Region of Northwestern Montana, U.S.A., as Indicated by Late Pleistocene Ashes." In: *Arctic and Alpine Research* 18.3, pp. 317–325. DOI: 10.1080/00040851.1986.12004093.

Carrivick, J.L., B.J. Davies, W.H.M. James, D.J. Quincey, and N.F. Glasser (2016). "Distributed ice thickness and glacier volume in southern South America." In: *Global and Planetary Change* 146, pp. 122–132. ISSN: 0921-8181. DOI: 10.1016/j.gloplacha.2016.09.010.

Carter, G.S. and M.R. Lane (1996). "Modelling surface oscillations in New Zealand lakes." In: *New Zealand Journal of Marine and Freshwater Research* 30.3, pp. 341–353. DOI: 10.1080/00288330.1996.9516721.

Chandler, D.M., J.L. Wadham, G.P. Lis, T. Cowton, A. Sole, I. Bartholomew, J. Telling, P. Nienow, E.B. Bagshaw, D. Mair, and S Vinen (2013). "Evolution of the subglacial drainage system beneath the Greenland Ice Sheet revealed by tracers." In: *Nature Geosci* 6.3, pp. 195–198. DOI: 10.1038/ngeo1737.

Church, M., J.M. Ryder, R.G. Pike, T.E. Redding, R.D. Moore, R.D. Winker, and K.D. Bladon (2010). "Compendium of forest hydrology and geomorphology in British

Columbia." In: *Land Management Handbook*. Ed. by R.G. Pike, T.E. Redding, R.D. Moore, R.D. Winker, and K.D. Bladon. Vol. 66. Physiography of british columbia, pp. 17–46.

Clague, J.J. (1981). "Late Quaternary geology and geochronology of British Columbia, 2. Summary and discussion of radiocarbon-dated Quaternary history." In: *Geolo. Surv. Can. pap.* 41, pp. 80–35.

Clapperton, C.M. (1968). "Channels Formed by the Superimposition of Glacial Meltwater Streams, with Special Reference to the East Cheviot Hills, North-East England." In: *Geografiska Annaler: Series A, Physical Geography* 50.4, pp. 207–220. doi: 10.1080/04353676.1968.11879784.

Clark, C.D., D.J. Evans, A. Khatwa, T. Bradwell, C.J. Jordan, S.H. Marsh, W.A. Mitchell, and M.D. Bateman (2004). "Map and GIS database of glacial landforms and features related to the last British Ice Sheet." In: *Boreas* 33.4, pp. 359–375. doi: 10.1111/j.1502-3885.2004.tb01246.x.

Clark, P.U. and J.S. Walder (1994). "Subglacial drainage, eskers, and deforming beds beneath the Laurentide and Eurasian ice sheets." In: *Geological Society of America Bulletin* 106.2, pp. 304–314. doi: 10.1130/0016-7606(1994)106<0304:SDEADB>2.3.CO;2.

Clarke, G.K.C., D.W. Leverington, J.T. Teller, A.S. Dyke, and S.J. Marshall (2005). "Fresh arguments against the Shaw megaflood Hypothesis A reply to comments by David Sharpe on Paleohydraulics of the last outburst flood from glacial Lake Agassiz and the 8200 BP cold event." In: *Quaternary Science Reviews* 24.12-13, pp. 1533–1541.

Clayton, L., J.W. Attig, and D.M. Mickelson (1999). "Tunnel channels formed in Wisconsin during the last glaciation." In: *Special Papers-Geological Society of America*, pp. 69–82.

Colonia, D., J. Torres, W. Haeberli, S. Schauwecker, E. Braendle, C. Giraldez, and A. Cochachin (2017). "Compiling an Inventory of Glacier-Bed Overdeepenings and Potential New Lakes in De-Glaciating Areas of the Peruvian Andes: Approach, First Results, and Perspectives for Adaptation to Climate Change." In: *Water* 9.5. doi: 10.3390/w9050336.

Cook, S.J. and D.A. Swift (2012). "Subglacial basins: Their origin and importance in glacial systems and landscapes." In: *Earth-Science Reviews* 115.4, pp. 332–372. doi: 10.1016/j.earscirev.2012.09.009.

Cooper, M.A., K. Michaelides, M.J. Siegert, and J.L. Bamber (2016). "Paleofluvial landscape inheritance for Jakobshavn Isbræ catchment, Greenland." In: *Geophysical Research Letters* 43.12, pp. 6350–6357. doi: 10.1002/2016GL069458.

Craddock, C. (1970). "Geologic Maps of Antarctica." In: *American Geographical Society of New York*.

Creyts, T.T. and G.K. Clarke (2010). "Hydraulics of subglacial supercooling: theory and simulations for clear water flows." In: *Journal of Geophysical Research: Earth Surface* 115.F3. doi: 10.1029/2009JF001417.

Creyts, T.T., Clarke G.K.C., and Church. M. (2013). "Evolution of subglacial overdeepenings in response to sediment redistribution and glaciohydraulic supercooling." In: *Journal of Geophysical Research: Earth Surface* 118.2, pp. 423–446. doi: 10.1002/jgrf.20033.

Cui, Y., D. Miller, P. Schiarizza, and L.J. Diakow (2017). "British Columbia digital geology." In: *British Columbia Ministry of Energy, Mines and Petroleum Resources* British Columbia Geological Survey Open File 2017-8, p. 9.

Cutler, P.M., P.M. Colgan, and D.M. Mickelson (2002). "Sedimentologic evidence for outburst floods from the Laurentide Ice Sheet margin in Wisconsin, USA: implications for tunnel-channel formation." In: *Quaternary International* 90.1, pp. 23–40. DOI: 10.1016/S1040-6182(01)00090-8.

Dawes, P.R. (2009). "The bedrock geology under the Inland Ice: the next major challenge for Greenland mapping." In: *GEUS Bulletin* 17, pp. 57–60. DOI: 10.34194/geusb.v17.5014.

Dehnert, A., S.E. Lowick, F. Preusser, F.S. Anselmetti, R. Drescher-Schneider, H.R. Graf, F. Heller, H. Horstmeyer, H.A. Kemna, N.R. Nowaczyk, A. Züger, and H. Furrer (2012). "Evolution of an overdeepened trough in the northern Alpine Foreland at Niederweningen, Switzerland." In: *Quaternary Science Reviews* 34, pp. 127–145. DOI: 10.1016/j.quascirev.2011.12.015.

Denton, G.H. and D.E. Sugden (2005). "Meltwater features that suggest miocene ice-sheet overriding of the transantarctic mountains in victoria land, antarctica." In: *Geografiska Annaler: Series A, Physical Geography* 87.1, pp. 67–85. DOI: 10.1111/j.0435-3676.2005.00245.x.

Douillet, G., J.F. Ghienne, Y. Geraud, A. Abueladas, M. Diraison, and A. Al-Zoubi (2012). "Late Ordovician tunnel valleys in southern Jordan." In: *Geological Society, London, Special Publications* 368.1, pp. 275–292. DOI: 10.1144/SP368.4.

Dove, D., D.J.A. Evans, J.R. Lee, D.H. Roberts, D.R. Tappin, C.L. Mellett, David Long, and S.L. Callard (2017). "Phased occupation and retreat of the last British–Irish Ice Sheet in the southern North Sea; geomorphic and seismostratigraphic evidence of a dynamic ice lobe." In: *Quaternary Science Reviews* 163, pp. 114–134. DOI: 10.1016/j.quascirev.2017.03.006.

Duford, J.M. and G.D. Osborn (1978). "Holocene and latest Pleistocene cirque glaciations in the Shuswap Highland, British Columbia." In: *Canadian Journal of Earth Sciences* 15.6, pp. 865–873. DOI: 10.1139/e78-098.

Duhnforth, M., R.S. Anderson, D. Ward, and G.M. Stock (2010). "Bedrock fracture control of glacial erosion processes and rates." In: *Geology* 38.5, pp. 423–426. DOI: 10.1130/G30576.1..

Dürst Stucki, M., R. Reber, and F. Schlunegger (2010). "Subglacial tunnel valleys in the Alpine foreland: an example from Bern, Switzerland." In: *Swiss Journal of Geoscience* 103, pp. 363–374. DOI: 10.1007/s00015-010-0042-0.

Dürst Stucki, M. and F. Schlunegger (2013). "Identification of erosional mechanisms during past glaciations based on a bedrock surface model of the central European Alps." In: *Earth and Planetary Science Letters* 384, pp. 57–70. DOI: 10.1016/j.epsl.2013.10.009.

Dürst Stucki, M., F. Schlunegger, F. Christener, J. Otto, and J. Götz (2012). "Deepening of inner gorges through subglacial meltwater — An example from the UNESCO Entlebuch area, Switzerland." In: *Geomorphology* 139-140, pp. 506–517. DOI: 10.1016/j.geomorph.2011.11.016.

Egholm, D.L., V.K. Pedersen, M.F. Knudsen, and N.K. Larsen (2012). "Coupling the flow of ice, water, and sediment in a glacial landscape evolution model." In: *Geomorphology* 141-142, pp. 47–66. DOI: 10.1016/j.geomorph.2011.12.019.

Ehlers, J. and G. Linke (1989). "The origin of deep buried channels of Elsterian age in Northwest Germany." In: *Journal of Quaternary Science* 4.3, pp. 255–265. DOI: 10.1002/jqs.3390040306.

Ehlers, J., K.D. Meyer, and H.J. Stephan (1984). "The pre-weichselian glaciations of North-West Europe." In: *Quaternary Science Reviews* 3.1, pp. 1–40. DOI: 10.1016/0277-3791(84)90003-9.

Ehlers, J. and R. Wingfield (1991). "The extension of the late Weichselian/late Devensian ice sheets in the North Sea basin." In: *Journal of Quaternary Science* 6.4, pp. 313–326. DOI: 10.1002/jqs.3390060406.

Erdmer, P. and Y. Cui (2009). "Geological Map of British Columbia." In: *British Columbia Ministry of Energy, Mines and Petroleum Resources* 2009-1.scale 1:1,500,000.

Eyles, N. (1987). "Late Pleistocene depositional systems of Metropolitan Toronto and their engineering and glacial geological significance." In: *Canadian Journal of Earth Sciences* 24.5, pp. 1009–1021. DOI: 10.1139/e87-098.

Eyles, N., E. Arnaud, A.E. Scheidegger, and C.H. Eyles (1997). "Bedrock jointing and geomorphology in southwestern Ontario, Canada: an example of tectonic predesign." In: *Geomorphology* 19.1, pp. 17–34. DOI: 10.1016/S0169-555X(96)00050-5.

Eyles, N., J.I. Boyce, J.D. Halfman, and B. Koseoglu (2000). "Seismic stratigraphy of Waterton Lake, a sediment-starved glaciated basin in the Rocky Mountains of Alberta, Canada and Montana, USA." In: *Sedimentary Geology* 130.3, pp. 283–311. DOI: 10.1016/S0037-0738(99)00120-7.

Eyles, N. and P. de Broekert (2001). "Glacial tunnel valleys in the Eastern Goldfields of Western Australia cut below the Late Paleozoic Pilbara ice sheet." In: *Palaeogeography, Palaeoclimatology, Palaeoecology* 171.1, pp. 29–40. DOI: 10.1016/S0031-0182(01)00265-6.

Eyles, N., M. Doughty, J.I. Boyce, Mullins H.T., J.D. Halfman, and B. Koseoglu (2003). "Acoustic architecture of glaciolacustrine sediments deformed during zonal stagnation of the Laurentide Ice Sheet; Mazinaw Lake, Ontario, Canada." In: *Sedimentary Geology* 157.1, pp. 133–151. DOI: 10.1016/S0037-0738(02)00229-4.

Eyles, N. and H.T. Mullins (1997). "Seismic-stratigraphy of Shuswap Lake, British Columbia, Canada." In: *Sedimentary Geology* 109.3, pp. 283–303. DOI: 10.1016/S0037-0738(96)00060-7.

Eyles, N., H.T. Mullins, and A.C. Hine (1991). "The seismic stratigraphy of Okanagan Lake, British Columbia; a record of rapid deglaciation in a deep 'fiord-lake' basin." In: *Sedimentary Geology* 73.1, pp. 13–41. DOI: 10.1016/0037-0738(91)90021-5.

Farrand, W.R. and D. Bell (1982). "Quaternary Geology of Southern Michigan." In: *Department of Natural Resources* 1:500,000.

Fischer, U.H., D. Cohen, T.T. Creyts, M. Detert, G.E. Flowers, W. Haeberli, R.L. Hooke, J. Menzies, P. Molnar, D.A. Swift, J. Turowski, and M.A. Werder (2017). "Subglacial-fluvial Erosion, Transport and Deposition: Results of a workshop held at Kartause Ittingen, Swizerland." In: *Quaternary International* AktennotiZ AN 17-518, pp. 87–115.

Fisher, D.W., Y.W. Isachsen, and L.V. Rickard (1970a). "Geologic map of New York, Hudson–Mohawk sheet." In: *N.Y. State Mus. Sci. Serv.* Map and Chart Ser. No. 15.

Fisher, D.W., Y.W. Isachsen, and L.V. Rickard (1970b). "Geologic map of New York, Lower Hudson sheet." In: *N.Y. State Mus. Sci. Serv.* Map and Chart Ser. No. 15.

Fisher, T.G. and L.D. Taylor (2002). "Sedimentary and stratigraphic evidence for subglacial flooding, south-central Michigan, USA." In: *Quaternary International* 90.1, pp. 87–115. DOI: 10.1016/S1040-6182(01)00095-7.

Fitzsimons, S.J. and H. Veit (2001). "Geology and Geomorphology of the European Alps and the Southern Alps of New Zealand." In: *Mountain Research and Development* 21.4, pp. 340–349. DOI: 10.1659/0276-4741(2001)021[0340:GAGOTE]2.0.CO;2.

Flain, M. (1970). "Lake Coleridge, Provision Bathymetry." In: *New Zealand oceanographic institute* chart lake series.1: 50 000.

Fountain, A.G. and J.S. Walder (1998). "Water flow through temperate glaciers." In: *Reviews of Geophysics* 36.3, pp. 299–328. DOI: 10.1029/97RG03579.

Fretwell, P., H. D. Pritchard, D. G. Vaughan, J. L. Bamber, N. E. Barrand, R. Bell, C. Bianchi, R. G. Bingham, D. D. Blankenship, G. Casassa, G. Catania, D. Callens, H. Conway, A. J. Cook, H. F. J. Corr, D. Damaske, V. Damm, F. Ferraccioli, R. Forsberg, S. Fujita, Y. Gim, P. Gogineni, J. A. Griggs, R. C. A. Hindmarsh, P. Holmlund, J. W. Holt, R. W. Jacobel, A. Jenkins, W. Jokat, T. Jordan, E. C. King, J. Kohler, W. Krabill, M. Riger-Kusk, K. A. Langley, G. Leitchenkov, C. Leuschen, B. P. Luyendyk, K. Matsuoka, J. Mouginot, F. O. Nitsche, Y. Nogi, O. A. Nost, S. V. Popov, E. Rignot, D. M. Rippin, A. Rivera, J. Roberts, N. Ross, M. J. Siegert, A. M. Smith, D. Steinhage, M. Studinger, B. Sun, B. K. Tinto, B. C. Welch, D. Wilson, D. A. Young, C. Xiangbin, and A. Zirizzotti (2013). "Bedmap2: improved ice bed, surface and thickness datasets for Antarctica." In: *The Cryosphere* 7.1, pp. 375–393. DOI: 10.5194/tc-7-375-2013.

Frey, H., W. Haeberli, A. Linsbauer, C. Huggel, and F. Paul (2010). "A multi-level strategy for anticipating future glacier lake formation and associated hazard potentials." In: *Natural Hazards and Earth System Sciences* 10.2, pp. 339–352. DOI: 10.5194/nhess-10-339-2010.

Fulton, R.J. (1965). "Surficial geology Vernon, British Columbia." In: *Geological Survey of Canada* Map 1245A.scale 1:126.

Fulton, R.J. (1969). "Glacial lake history, southern interior British Columbia." In: *Geological Survey of Canada paper* 69-37, p. 14.

Fulton, R.J. (1972). "Stratigraphy of unconsolidated till and Quaternary development of North Okanagan Valley." In: *Geological Survey of Canada paper* 72-8.Part B, pp. 9–17.

Fulton, R.J. (1984). "Quaternary glaciation, Canadian Cordillera." In: *Geological Survey of Canada paper* 84-10, pp. 39–48.

Fulton, R.J. (1995). "Surficial materials of Canada / Matériaux superficiels du Canada." In: *Geological Survey of Canada* "A" Series Map 1880A.1 sheet.

Fulton, R.J. and G.W. Smith (1978). "Late Pleistocene stratigraphy of south-central British Columbia." In: *Canadian Journal of Earth Sciences* 15.6, pp. 971–980. DOI: 10.1139/e78-105.

Gabriel, G., R. Kirsch, Siemon B., and H. Wiederhold (2003). "Geophysical investigation of buried Pleistocene subglacial valleys in Northern Germany." In: *Journal of Applied Geophysics* 53.4, pp. 159–180. DOI: 10.1016/j.jappgeo.2003.08.005.

Galon, R. (1983). "On the origin of subglacial channels." In: *Studies in Quaternary geomorphology: Proceedings of the VIth*. Ed. by D.J. Briggs and R.S. Waters. Norwich: Institute of British Geographers. Geo. Books, pp. 85–95.

Gannett, H. (1898). "Lake Chelan." In: *National Geographic* 9, pp. 417–428.

Gerald, M.R. (1986). “Stratigraphy and correlation of glacial deposits of the Rocky Mountains, the Colorado Plateau and the ranges of the Great Basin.” In: *Quaternary Science Reviews* 5, pp. 99–127. DOI: https://doi.org/10.1016/0277-3791(86)90178-2.

Gilbert, G.K. (1877). “Report on the geology of the Henry Mountains.” In: *US Government Printing Office*.

Gilgannon, S.M., D.A Swift, and S.J. Livingstone (2019). “Report of literature review "Bedrock landforms produced by focused glacial and glaciofluvial incision - formation mechanisms, morphology and potential analogue sites".” In: *AN 19-353* part I.

Gilgannon, S.M., D.A Swift, and S.J. Livingstone (2020). “Report of literature review "Bedrock landforms produced by focused glacial and glaciofluvial incision - formation mechanisms, morphology and potential analogue sites".” In: *AN 19-353* part II.

Glasser, N.F. and M.C. Ghiglione (2009). “Structural, tectonic and glaciological controls on the evolution of fjord landscapes.” In: *Geomorphology* 105.3, pp. 291–302. DOI: 10.1016/j.geomorph.2008.10.007.

Glasser, N.F. and G.H. Sambrook Smith (1999). “Glacial meltwater erosion of the Mid-Cheshire Ridge: implications for ice dynamics during the Late Devensian glaciation of northwest England.” In: *Journal of Quaternary Science* 14, pp. 703–710. DOI: 10.1002/(SICI)1099-1417(199912)14:7<703::AID-JQS465>3.0.CO;2-9.

Golledge, N.R. and M.S. Stoker (2006). “A palaeo-ice stream of the British Ice Sheet in eastern Scotland.” In: *Boreas* 35.2, pp. 231–243. DOI: 10.1111/j.1502-3885.2006.tb01153.x.

Graf, W.L. (1970). “The Geomorphology of the Glacial Valley Cross Section.” In: *Arctic and Alpine Research* 2.4, pp. 303–312. DOI: 10.1080/00040851.1970.12003589.

Grau Galofre, A., A. M. Jellinek, G. R. Osinski, M. Zanetti, and A. Kukko (2018). “Subglacial drainage patterns of Devon Island, Canada: detailed comparison of rivers and subglacial meltwater channels.” In: *The Cryosphere* 12.4, pp. 1461–1478. DOI: 10.5194/tc-12-1461-2018.

Greenwood, S.L., C.D. Clark, and A.L. Hughes (2007). “Formalising an inversion methodology for reconstructing ice-sheet retreat patterns from meltwater channels: application to the British Ice Sheet.” In: *Journal of Quaternary Science* 22.6, pp. 637–645. DOI: 10.1002/jqs.1083.

Greenwood, S.L., C.C. Clason, C. Helanow, and M. Margold (2016). “Theoretical, contemporary observational and palaeo-perspectives on ice sheet hydrology: Processes and products.” In: *Earth-Science Reviews* 155, pp. 1–27. DOI: 10.1016/j.earscirev.2016.01.010.

Gudmundsson, H.J. (1997). “A review of the holocene environmental history of Iceland.” In: *Quaternary Science Reviews* 16.1, pp. 81–92. DOI: 10.1016/S0277-3791(96)00043-1.

Gustavson, T.C. and J.C. Boothroyd (1987). “A depositional model for outwash, sediment sources, and hydrologic characteristics, Malaspina Glacier, Alaska: A modern analog of the southeastern margin of the Laurentide ice sheet.” In: *Geological Society of America Bulletin* 99, pp. 187–200. DOI: 10.1130/0016-7606(1987)99<187:ADMFOS>2.0.CO;2.

Haeberli, W., A. Linsbauer, A. Cochachin, C. Salazar, and U.H. Fischer (2016). "On the morphological characteristics of overdeepenings in high-mountain glacier beds." In: *Earth Surface Processes and Landforms* 41.13, pp. 1980–1990. DOI: 10.1002/esp.3966.

Haeberli, W. and C. Whiteman (2015). "Chapter 1 - Snow and Ice-Related Hazards, Risks, and Disasters: A General Framework." In: *Snow and Ice-Related Hazards, Risks, and Disasters*. Ed. by J.F. Shroder, W. Haeberli, and C. Whiteman. Hazards and Disasters Series. Boston: Academic Press, pp. 1–34. DOI: 10.1016/B978-0-12-394849-6.00001-9.

Hanson, B., L.R. Hooke, and E.M. Grace (1998). "Short-term velocity and water-pressure variations down-glacier from a riegel, Storglaciären, Sweden." In: *Journal of Glaciology* 44.147, pp. 359–367. DOI: 10.3189/S0022143000002689.

Haran, T., J. Bohlander, T. Scambos, T. Painter, and M. Fahnestock (2015). "MEaSUREs MODIS Mosaic of Greenland 2005." In: *Boulder, Colorado, National Snow and Ice Data Center* Image Map.version 1. DOI: 10.5067/IAGYM8Q26QRE.

Harbor, J.M. (1989). "Early Discoverers XXXVI: W.J. McGee On Glacial Erosion Laws and the Development of Glacial Valleys." In: *Journal of Glaciology* 35.121, pp. 419–425. DOI: 10.3189/S0022143000009357.

Harbor, J.M. (1992). "Numerical modelling of the development of U-shaped valleys by glacial erosion." In: *Geological Society of America Bulletin* 104.10, pp. 1364–1375. DOI: 10.1130/0016-7606(1992)104<1364:NMOTDO>2.3.CO;2.

Harbor, J.M. (1995). "Development of glacial-valley cross sections under conditions of spatially variable resistance to erosion." In: *Geomorphology* 14.2, pp. 99–107. DOI: 10.1016/0169-555X(95)00051-1.

Harbor, J.M. and D.A. Wheeler (1992). "On the mathematical description of glaciated valley cross sections." In: *Earth Surface Processes and Landforms* 17.5, pp. 477–485. DOI: 10.1002/esp.3290170507.

Harrison, S., N. Glasser, V. Winchester, E. Haresign, C. Warren, G.A.T. Duller, Bailey R., S. Ivy-Ochs, K. Jansson, and P. Kubik (2008). "Glaciar León, Chilean Patagonia: late-Holocene chronology and geomorphology." In: *The Holocene* 18.4, pp. 643–652. DOI: 10.1177/0959683607086771.

Henriksen, N., A.K. Higgins, F. Kalsbeek, and T.C.R. Pulvertaft (2009). "Greenland from Archaean to Quaternary." In: *Geological Survey of Denmark and Greenland Bulletin* 18, p. 126.

Herman, F., F. Beaud, J.D. Champagnac, J.M. Lemieux, and P. Sternai (2011). "Glacial hydrology and erosion patterns: A mechanism for carving glacial valleys." In: *Earth and Planetary Science Letters* 310.3, pp. 498–508. DOI: 10.1016/j.epsl.2011.08.022.

Herman, F., O. Beyssac, M. Brughelli, S.N. Lane, S. Leprince, T. Adatte, Lin J.Y.Y., Avouac J.P., and Cox S.C. (2015). "Erosion by an Alpine glacier." In: *Science* 350.6257, pp. 193–195. DOI: 10.1126/science.aab2386.

Hindmarsh, R.C., J.M. Gwendolyn, M.J. Raymond, and G.H. Gudmundsson (2006). "Draping or overriding: the effect of horizontal stress gradients on internal layer architecture in ice sheets." In: *Journal of geophysical research: earth surface* 111.F2. DOI: 10.1029/2005JF000309.

Hirano, M. and M. Aniya (1988). "A rational explanation of cross-profile morphology for glacial valleys and of glacial valley development." In: *Earth Surf. Process. Landforms* 13, pp. 707–716. DOI: 10.1002/esp.3290130805.

Holtedahl, H. (1967). "Notes on the Formation of Fjords and Fjord-Valleys." In: *Geografiska Annaler: Series A, Physical Geography* 49.2-4, pp. 188–203. doi: 10.1080/04353676.1967.11879749.

Hooke, R.L. (1991). "Positive feedbacks associated with erosion of glacial cirques and overdeepenings." In: *Geological Society of America Bulletin* 103.8, pp. 1104–1108. doi: 10.1130/0016-7606(1991)103<1104:PFAWEO>2.3.CO;2.

Hooke, R.L. and C.E. Jennings (2006). "On the formation of the tunnel valleys of the southern Laurentide ice sheet." In: *Quaternary Science Reviews* 25.11, pp. 1364–1372. doi: 10.1016/j.quascirev.2006.01.018.

Hooke, R.L., B. Wold, and J.O. Hagen (1985). "Subglacial hydrology and sediment transport at Bondhusbreen, southwest Norway." In: *Geological Society ofAmerica Bulletin* 96, pp. 388–397. doi: 10.1130/0016-7606(1985)96<388:SHASTA>2.0.CO;2.

Horton, R.E. (1945). "Erosional development of streams and their drainage basins; hydrophysical approach to quantitative morphology." In: *Geological Society ofAmerica Bulletin* 56.3, pp. 275–370. doi: 10.1130/0016-7606(1945)56[275:EDOSAT]2.0.CO;2.

Howat, I. M., C. Porter, B. E. Smith, M.-J. Noh, and P. Morin (2019). "The Reference Elevation Model of Antarctica." In: *The Cryosphere* 13.2, pp. 665–674. doi: 10.5194/tc-13-665-2019.

Hsu, K.J. and K.R. Kelts (1984). "Quaternary Geology ofLake Zurich: An Interdisciplinary Investigation by Deep-Lake Drilling." In: *Stuttgart: Schweizerbartsche.*, p. 210.

Hubbard, B. P., M. J. Sharp, I. C. Willis, M. K. Nielsen, and C. C. Smart (1995). "Borehole water-level variations and the structure of the subglacial hydrological system of Haut Glacier d'Arolla, Valais, Switzerland." In: *Journal of Glaciology* 41.139, pp. 572–583. doi: 10.3189/S0022143000034894.

Huuse, M. and H. Lykke-Andersen (2000). "Overdeepened Quaternary valleys in the eastern Danish North Sea: morphology and origin." In: *Quaternary Science Reviews* 19.12, pp. 1233–1253. doi: 10.1016/S0277-3791(99)00103-1.

Irwin, J. (1970). "Lake Ohau, Provision Bathymetry." In: *New Zealand oceanographic institute chart lake series* 1:31,680.scale 1:50,000.

Irwin, J. (1971). "Lake Te Anau, Provision Bathymetry." In: *New Zealand oceanographic institute chart lake series* 1:63,36.scale 1:50,000.

Irwin, J. (1973). "Lake Tekapo Bathymetry." In: *New Zealand oceanographic institute chart lake series* l:3l, 680.Lake Series.

Irwin, J. (1978). "Bottom sediments of Lake Tekapo compared with adjacent Lakes Pukaki and Ohau, South Island, New Zealand." In: *New Zealand Journal of Marine and Freshwater Research* 12.3, pp. 245–250. doi: 10.1080/00288330.1978.9515749.

Isachsen, Y.W. and D.W. Fisher (1970). "Geologic map of New York." In: *University of the State of New York, State Education Department*.

Iverson, N.R. (2012). "A theory of glacial quarrying for landscape evolution models." In: *Geology* 40.8, pp. 679–682. doi: 10.1130/G33079.1.

Jakobsson, M., L. Mayer, B. Coakley, J.A. Dowdeswell, S. Forbes, B. Fridman, H. Hodnesdal, R. Noormets, R. Pedersen, M. Rebesco, and H.W. Schenke (2012). "The international bathymetric chart of the Arctic Ocean (IBCAO) version 3.0." In: *Geophysical Research Letters*. doi: 10.1029/2012GL052219.

Jansen, J.D., A.T. Codilean, A.P. Stroeven, D. Fabel, C. Hättestrand, J. Kleman, J.M. Harbor, J. Heyman, P.W. Kubik, and S. Xu (2014). "Inner gorges cut by subglacial meltwater during Fennoscandian ice sheet decay." In: *Nature Communications* 5.3815. DOI: 10.1038/ncomms4815.

Jordan, P. (2010). "Analysis of overdeepened valleys using the digital elevation model of the bedrock surface of Northern Switzerland." In: *Swiss Journal of Geoscience* 103, pp. 375–384. DOI: 10.1007/s00015-010-0043-z.

Jørgensen, F., H. Lykke-Andersen, P.B.E. Sandersen, E. Auken, and E. Nørmark (2003). "Geophysical investigations of buried Quaternary valleys in Denmark: an integrated application of transient electromagnetic soundings, reflection seismic surveys and exploratory drillings." In: *Journal of Applied Geophysics* 53.4, pp. 215–228. DOI: 10.1016/j.jappgeo.2003.08.017.

Jørgensen, F. and P.B.E. Sandersen (2006). "Buried and open tunnel valleys in Denmark—erosion beneath multiple ice sheets." In: *Quaternary Science Reviews* 25.11, pp. 1339–1363. DOI: 10.1016/j.quascirev.2005.11.006.

Jørgensen, F. and P.B.E. Sandersen (2009). "Buried valley mapping in Denmark: evaluating mapping method constraints and the importance of data density." In: *Zeitschrift der Deutschen Gesellschaft für Geowissenschaften* 160.3, pp. 211–223. DOI: 10.1127/1860-1804/2009/0160-0211.

Joughin, I., B.E. Smith, I.M. Howat, T. Scambos, and T. Moon (2010). "Greenland flow variability from ice-sheet-wide velocity mapping." In: *Journal of Glaciology* 56.197, pp. 415–430. DOI: 10.3189/002214310792447734.

Joughin, I., S. Tulaczyk, J.L. Bamber, D. Blankenship, J.W. Holt, T. Scambos, and D.G. Vaughan (2009). "Basal conditions for Pine Island and Thwaites Glaciers, West Antarctica, determined using satellite and airborne data." In: *Journal of Glaciology* 55.190, pp. 245–257. DOI: 10.3189/002214309788608705.

Kehew, A.E., S.K. Ewald, J.M. Esch, and A.L. Kozlowski (2013). "On the origin of tunnel valleys of the Saginaw Lobe of the Laurentide Ice Sheet; Michigan, USA." In: *Boreas* 42.2, pp. 442–462. DOI: 10.1111/j.1502-3885.2012.00295.x.

Kehew, A.E., Piotrowski J.A., and F. Jørgensen (2012). "Tunnel valleys: Concepts and controversies — A review." In: *Earth-Science Reviews* 113.1, pp. 33–58. DOI: 10.1016/j.earscirev.2012.02.002.

Kehew, A.E. and A.L. Kozlowski (2007). "Tunnel channels of the Saginaw lobe, Michigan, USA." In: *Applied Quaternary research in the central part of glaciated terrain* Special Paper.46, pp. 69–78.

Kessler, M.A., R.S. Anderson, and J.P. Briner (2008). "Fjord insertion into continental margins driven by topographic steering of ice." In: *Nature Geoscience* 1.6, pp. 365–369. DOI: 10.1038/ngeo201.

King, J.W., S.K. Banerjee, J. Marvin, and S. Lund (1983). "Use of small-amplitude paleomagnetic fluctuations for correlation and dating of continental climatic changes." In: *Palaeogeography, Palaeoclimatology, Palaeoecology* 42.1, pp. 167–183. DOI: https://doi.org/10.1016/0031-0182(83)90043-3.

Kirkbride, M.P. (1993). "The temporal significance of transitions from melting to calving termini at glaciers in the central Southern Alps of New Zealand." In: *The Holocene* 3.3, pp. 232–240. DOI: 10.1177/095968369300300305.

Kirkham, J.D., K.A. Hogan, R.D. Larter, N.S. Arnold, F.O. Nitsche, G. Kuhn, K. Gohl, J.B. Anderson, and J.A. Dowdeswell (2020). "Morphometry of bedrock meltwater channels on Antarctic inner continental shelves: Implications for channel development and subglacial hydrology." In: *Geomorphology* 370, p. 107369. doi: 10.1016/j.geomorph.2020.107369.

Kluiving, S.J., J.H Aleid Bosch, Ebbing J.H.J., Mesdag C.S., and R.S. Westerhoff (2003). "Onshore and offshore seismic and lithostratigraphic analysis of a deeply incised Quaternary buried valley system in the Northern Netherlands." In: *Journal of Applied Geophysics* 53.4, pp. 249–271. doi: 10.1016/j.jappgeo.2003.08.002.

Knighton, D. (2014). "Fluvial forms and processes: a new perspective." In: *Hodder Headline Group*.

Kor, P.S.G., J. Shaw, and D.R. Sharpe (1991). "Erosion of bedrock by subglacial meltwater, Georgian Bay, Ontario: a regional view." In: *Canadian Journal of Earth Sciences* 28.4, pp. 623–642. doi: 10.1139/e91-054.

Korup, O. and F. Schlunegger (2007). "Bedrock landsliding, river incision, and transience of geomorphic hillslope-channel coupling: Evidence from inner gorges in the Swiss Alps." In: *Journal of Geophysical Research: Earth Surface* 112.F3. doi: 10.1029/2006JF000710.

Kozlowski, A.L. (1999). "Three dimensional mapping of the East Leroy and Union City 7.5 minute quadrangles in southwest Michigan." In.

Krall, D.B. (1977). "Late Wisconsinan ice recession in east-central New York." In: *GSA Bulletin* 88.12, pp. 1697–1710. doi: 10.1130/0016-7606(1977)88<1697:LWIRIE>2.0.CO;2.

Kristensen, T.B., M. Huuse, J.A. Piotrowski, and O.R. Clausen (2007). "A morphometric analysis of tunnel valleys in the eastern North Sea based on 3D seismic data." In: *Journal of Quaternary Science: Published for the Quaternary Research Association* 22.8, pp. 801–815. doi: 10.1002/jqs.1123.

Kristensen, T.B., J.A. Piotrowski, M. Huuse, O.R. Clausen, and L. Hamberg (2008). "Time-transgressive tunnel valley formation indicated by infill sediment structure, North Sea–the role of glaciohydraulic supercooling." In: *Earth Surface Processes and Landforms: The Journal of the British Geomorphological Research Group* 33.4, pp. 546–559. doi: 10.1002/esp.1668.

Kühni, A. and O.A. Pfiffner (2001). "The relief of the Swiss Alps and adjacent areas and its relation to lithology and structure: topographic analysis from a 250-m DEM." In: *Geomorphology* 41.4, pp. 285–307. doi: 10.1016/S0169-555X(01)00060-5.

Kuster, H. and K.D. Meyer (1979). "Glaziare Rinnen im mittleren und nordlichen Niedersachsen." In: *EG Quaternary Science Journal* 29.1, pp. 135–156. doi: 10.3285/eg.29.1.12.

Lai, J. and A.M. Anders (2021). "Climatic controls on mountain glacier basal thermal regimes dictate spatial patterns of glacial erosion." In: *Earth Surface Dynamics* 9.4, pp. 845–859. doi: 10.5194/esurf-9-845-2021.

Lajeunesse, P. (2014). "Buried preglacial fluvial gorges and valleys preserved through Quaternary glaciations beneath the eastern Laurentide Ice Sheet." In: *GSA Bulletin* 126.3-4, pp. 447–458. doi: 10.1130/B30911.1.

Lesemann, J., G.I. Alsop, and J.A. Piotrowski (2010). "Incremental subglacial meltwater sediment deposition and deformation associated with repeated ice-bed decoupling: a case study from the Island of Funen, Denmark." In: *Quaternary Science Reviews* 29.23, pp. 3212–3229. doi: 10.1016/j.quascirev.2010.06.010.

Lewis, A.R., D.R. Marchant, D.E. Kowalewski, S.L. Baldwin, and L.E. Webb (2006). "The age and origin of the Labyrinth, western Dry Valleys, Antarctica: Evidence for extensive middle Miocene subglacial floods and freshwater discharge to the Southern Ocean." In: *Geology* 34.7, pp. 513–516. DOI: 10.1130/G22145.1.

Lewis, W.V. (1945). "Nick points and the curve of water erosion." In: *Geological Magazine* 82.6, pp. 256–266. DOI: 10.1130/B30911.1.

Li, Y., G. Liu, and Z. Cui (2001). "Glacial valley cross-profile morphology, Tian Shan Mountains, China." In: *Geomorphology* 38.1, pp. 153–166. DOI: 10.1016/S0169-555X(00)00078-7.

Lindbäck, K., R. Pettersson, S.H. Doyle, C. Helanow, P. Jansson, S.S. Kristensen, L. Stenseng, R. Forsberg, and A.L. Hubbard (2014). "High-resolution ice thickness and bed topography of a land-terminating section of the Greenland Ice Sheet." In: *Earth System Science Data* 6.2, pp. 331–338. DOI: 10.5194/essd-6-331-2014.

Linsbauer, A., H. Frey, W. Haeberli, H. Machguth, M.F. Azam, and S. Allen (2016). "Modelling glacier-bed overdeepenings and possible future lakes for the glaciers in the Himalaya—Karakoram region." In: *Annals of Glaciology* 57.71, pp. 119–130. DOI: 10.3189/2016AoG71A627.

Linton, D.L. (1963). "The Forms of Glacial Erosion." In: *Transactions and Papers (Institute of British Geographers)* 33, pp. 1–28. DOI: 10.2307/620998.

Little, H.W. (1962). "Geological Map of British Columbia." In: *Department of Mines and Technical Surveys*.

Livingstone, S.J., W. Chu, J.C. Ely, and J. Kingslake (June 2017). "Paleofluvial and subglacial channel networks beneath Humboldt Glacier, Greenland." In: *Geology* 45.6, pp. 551–554. DOI: 10.1130/G38860.1.

Livingstone, S.J. and C.D. Clark (2016). "Morphological properties of tunnel valleys of the southern sector of the Laurentide Ice Sheet and implications for their formation." In: *Earth Surface Dynamics* 4.3, pp. 567–589. DOI: 10.5194/esurf-4-567-2016.

Lloyd, C.T. (2015). "Controls upon the location and size of glacial overdeepenings." In: *University of Sheffield*.

Locke, W.W. (1995). "Modelling of icecap glaciation of the northern Rocky Mountains of Montana." In: *Geomorphology* 14.2, pp. 123–130. DOI: 10.1016/0169-555X(95)00053-5.

Lonergan, L., S.C. Maidment, and J.S. Collier (2006). "Pleistocene subglacial tunnel valleys in the central North Sea basin: 3-D morphology and evolution." In: *Journal of Quaternary Science: Published for the Quaternary Research Association* 21.8, pp. 891–903. DOI: 10.1002/jqs.1015.

Lowe, A.L. and J.B. Anderson (2003). "Evidence for abundant subglacial meltwater beneath the paleo-ice sheet in Pine Island Bay, Antarctica." In: *Journal of Glaciology* 49.164, pp. 125–138. DOI: 10.3189/172756503781830971.

Lowe, D.J. and J.D. Green (1992). "Lakes." In: *GLandforms of New Zealand: Second Edition*. Ed. by Soons J.M. and Selby M.J. Auckland, New Zealand: Longman Paul, pp. 107–143.

Ludlam, S.D. (1967). "Sedimentation in Cayuga Lake, New YORK1." In: *Limnology and Oceanography* 12.4, pp. 618–632. DOI: 10.4319/lo.1967.12.4.0618.

MacAulay, H.A. and G. Hobson (1972). "A seismic refraction survey of the North Okanagan and South Shuswap Valleys. Bedrock topography of the North Okanagan Valley and the stratigraphy of the Unconsolidated Valley Fill. Part A." In: *Geological Survey of Canada, Paper* 72.8, pp. 1–8.

MacGregor, K.R., R.S. Anderson, S.P. Anderson, and E.D. Waddington (Nov. 2000). "Numerical simulations of glacial-valley longitudinal profile evolution." In: *Geology* 28.11, pp. 1031–1034. DOI: 10.1130/0091-7613(2000)28<1031:NSOGLP>2.0.CO;2.

MacGregor, K.R., R.S. Anderson, and E.D. Waddington (2009). "Numerical modeling of glacial erosion and headwall processes in alpine valleys." In: *Geomorphology* 103.2, pp. 189–204. DOI: 10.1016/j.geomorph.2008.04.022.

Mackin, J.H. (1948). "Concept of the graded river." In: *GSA Bulletin* 59.5, pp. 463–512. DOI: 10.1130/0016-7606(1948)59[463:COTGR]2.0.CO;2.

Magnin, F., W. Haeberli, A. Linsbauer, P. Deline, and L. Ravanel (2020). "Estimating glacier-bed overdeepenings as possible sites of future lakes in the de-glaciating Mont Blanc massif (Western European Alps)." In: *Geomorphology* 350, p. 106913. DOI: 10.1016/j.geomorph.2019.106913.

Magnusson, E., F. Palsson, H. Bjornsson, and S. Guomundsson (2012). "Removing the ice cap of Oraefajokull central volcano, SE Iceland: mapping and interpretation of bedrock topography, ice volumes, subglacial troughs and implications for hazards assessments." In: *Jokull* 62, pp. 131–150.

Magrani, F., P.G. Valla, N. Gribenski, and E. Serra (2020). "Glacial overdeepenings in the Swiss Alps and foreland: Spatial distribution and morphometrics." In: *Quaternary Science Reviews* 243, p. 106483. DOI: 10.1016/j.quascirev.2020.106483.

Margerison, H.R., W.M. Phillips, F.M. Stuart, and D.E. Sugden (2005). "Cosmogenic 3He concentrations in ancient flood deposits from the Coombs Hills, northern Dry Valleys, East Antarctica: interpreting exposure ages and erosion rates." In: *Earth and Planetary Science Letters* 230.1-2, pp. 163–175.

Margold, M., C.R. Stokes, and C.D. Clark (2015). "Ice streams in the Laurentide Ice Sheet: Identification, characteristics and comparison to modern ice sheets." In: *Earth-Science Reviews* 143, pp. 117–146. DOI: 10.1016/j.earscirev.2015.01.011.

McDougall, I. (1979). "Age of shield-building volcanism of Kauai and linear migration of volcanism in the Hawaiian island chain." In: *Earth and Planetary Science Letters* 46.1, pp. 31–42.

McGee, W.J. (1894). "Glacial Canons." In: *The Journal of Geology* 2.4, pp. 350–364. DOI: 10.2307/30054312.

Menzies, J. (2009). "Glacial Geomorphology." In: *Encyclopedia of Paleoclimatology and Ancient Environments*. Ed. by V. Gornitz. Dordrecht: Springer. DOI: 10.1007/978-1-4020-4411-3_92.

Mickelson, D.M. and P.M. Colgan (2003). "The southern Laurentide Ice Sheet." In: *The Quaternary Period in the United States*. Vol. 1. Developments in Quaternary Sciences. Elsevier, pp. 1–16. DOI: 10.1016/S1571-0866(03)01001-7.

Monaghan, G.W., G.J. Larson, and G.D. Gephart (1986). "Late Wisconsinan drift stratigraphy of the Lake Michigan Lobe in southwestern Michigan." In: *GSA Bulletin* 97.3, pp. 329–334. DOI: 10.1130/0016-7606(1986)97<329:LWDSOT>2.0.CO;2.

Montgomery, D. and O. Korup (2011). "Preservation of inner gorges through repeated Alpine glaciations." In: *Nature Geosc* 4, pp. 62–67. DOI: 10.1038/ngeo1030.

Montgomery, D.R. (2002). "Valley formation by fluvial and glacial erosion." In: *Geology* 30.11, pp. 1047–1050. DOI: 10.1130/0091-7613(2002)030<1047:VFBFAG>2.0.CO;2.

Moores, H.D. (1989). "On the Formation of the Tunnel Valleys of the Superior Lobe, Central Minnesota." In: *Quaternary Research* 32.1, pp. 24–35. DOI: 10.1016/0033-5894(89)90029-X.

Morlighem, M., E. Rignot, T. Binder, D. Blankenship, R. Drews, G. Eagles, O. Eisen, F. Ferraccioli, R. Forsberg, P. Fretwell, and V. Goel (2020). "Deep glacial troughs and stabilizing ridges unveiled beneath the margins of the Antarctic ice sheet." In: *Nature Geoscience* 13.2. DOI: 10.1038/s41561-019-0510-8.

Morlighem, M., C.N. Williams, E.A.L. Rignot, J.E. Arndt, J.L. Bamber, G. Catania, N. Chauché, J.A. Dowdeswell, B. Dorschel, and I. Fenty (2017). "BedMachine v3: Complete bed topography and ocean bathymetry mapping of Greenland from multi-beam echo sounding combined with mass conservation." In: *Geophysical Research Letters* 44.21. DOI: 10.1002/2017GL074954.

Motyka, R.J., M. Truffer, E.M. Kuriger, and A.K. Bucki (2006). "Rapid erosion of soft sediments by tidewater glacier advance: Taku Glacier, Alaska, USA." In: *Geophysical Research Letters* 33.24. DOI: 10.1029/2006GL028467.

Mudge, M.R. (1977). "General geology of Glacier National Park and adjacent areas, Montana." In: *Bulletin of Canadian Petroleum Geology* 25.4, pp. 736–751. DOI: 10.35767/gscpgbull.25.4.736.

Muller, E.H. and P.E. Calkin (1993). "Timing of Pleistocene glacial events in New York state." In: *Canadian Journal of Earth Sciences* 30.9, pp. 1829–1845.

Mullins, H.T., N. Eyles, and E.J. Hinchey (1990). "Seismic reflection investigation of Kalamalka Lake: a "fiord lake" on the Interior Plateau of southern British Columbia." In: *Canadian Journal of Earth Sciences* 27.9, pp. 1225–1235. DOI: 10.1139/e90-130.

Mullins, H.T., N. Eyles, and E.J. Hinchey (1991). "High-Resolution Seismic Stratigraphy of Lake Mcdonald, Glacier National Park, Montana, U.S.A." In: *Arctic and Alpine Research* 23.3, pp. 311–319. DOI: 10.1080/00040851.1991.12002850.

Mullins, H.T. and E.J. Hinchey (1989). "Erosion and infill of New York Finger Lakes: Implications for Laurentide ice sheet deglaciation." In: *Geology* 17.7, pp. 622–625. DOI: 10.1130/0091-7613(1989)017<0622:EAIONY>2.3.CO;2.

Mullins, H.T., E.J. Hinchey, R.W. Wellner, D.B. Stephens, W.T. Anderson, T.R. Dwyer, and A.C. Hine (1996). "Seismic stratigraphy of the Finger Lakes: a continental record of Heinrich event H-1 and Laurentide ice sheet instability." In: *SPECIAL PAPERS-GEOLOGICAL SOCIETY OF AMERICA*, pp. 1–36.

Nasmith, H. (1962). "Late glacial history and surficial deposits of the Okanagan Valley, British Columbia." In: *British Columbia Department of Mines and Petroleum Resources, Bulletin* 46.

Nesje, A. and I.M. Whillans (1994). "Erosion of Sognefjord, Norway." In: *Geomorphology* 9.1, pp. 33–45. DOI: 10.1016/0169-555X(94)90029-9.

Nienow, P., M. Sharp, and I. Willis (1998). "Seasonal changes in the morphology of the subglacial drainage system, Haut Glacier d'Arolla, Switzerland." In: *Earth Surface Processes and Landforms* 23.9, pp. 825–843. DOI: 10.1002/(SICI)1096-9837(199809)23:9<825::AID-ESP893>3.0.CO;2-2.

Nye, J.F. (1973). "Water at the bed of a glacier." In: *Symposium at Cambridge 1969 – Hydrology of Glaciers* 95, pp. 189–194.

Nye, J.F. and F.C. Frank (1973). "Hydrology of the intergranular veins in a temperate glacier." In: *In Symposium on the Hydrology of Glaciers* 95, pp. 157–161.

Ó Cofaigh, C. (1996). "Tunnel valley genesis." In: *Progress in Physical Geography: Earth and Environment* 20.1, pp. 1–19. DOI: 10.1177/030913339602000101.

Oerlemans, J. (1984). "Numerical experiments on glacial erosion." In: *Zeitschrift für Gletscherkunde und Glazialgeologie* 20, pp. 107–126.

Okulitch, A.V. (1979). "Lithology, stratigraphy, structure and mineral occurrences of the Thompson-Shuswap-Okanagan area, British Columbia." In: *Geological Survey of Canada*, p. 3.

Okulitch, A.V. (1984). "The role of the Shuswap Metamorphic Complex in Cordilleran tectonism: a review." In: *Canadian Journal of Earth Sciences* 21.10, pp. 1171–1193. DOI: 10.1139/e84-123.

Okulitch, A.V. (1989). "Revised stratigraphy and structure in the Thompson-Shuswap-Okanagan map area, southern British Columbia." In: *Geological Survey of Canada*, pp. 51–60.

St-Onge, M.R., J.A.M. Van Gool, A.A. Garde, and D.J. Scott (2009). "Correlation of Archaean and Palaeoproterozoic units between northeastern Canada and western Greenland: constraining the pre-collisional upper plate accretionary history of the Trans-Hudson orogen." In: *Geological Society, London, Special Publications* 318.1, pp. 193–235. DOI: 10.1144/SP318.7.

Pair, D.L. (1997). "Thin film, channelized drainage, or sheetfloods beneath a portion of the Laurentide Ice Sheet: an examination of glacial erosion forms, northern New York State, USA." In: *Sedimentary Geology* 111.1, pp. 199–215. DOI: 10.1016/S0037-0738(97)00015-8.

Patterson, C.J. (1997). "Southern Laurentide ice lobes were created by ice streams: Des Moines Lobe in Minnesota, USA." In: *Sedimentary Geology* 111.1, pp. 249–261. DOI: 10.1016/S0037-0738(97)00018-3.

Patton, H., A. Hubbard, K. Andreassen, M. Winsborrow, and A.P. Stroeven (2016a). "The build-up, configuration, and dynamical sensitivity of the Eurasian ice-sheet complex to Late Weichselian climatic and oceanic forcing." In: *Quaternary Science Reviews* 153, pp. 97–121. DOI: 10.1016/j.quascirev.2016.10.009.

Patton, H., D.A. Swift, C.D. Clark, S.J. Livingstone, and S.J. Cook (2016b). "Distribution and characteristics of overdeepenings beneath the Greenland and Antarctic ice sheets: Implications for overdeepening origin and evolution." In: *Quaternary Science Reviews* 148, pp. 128–145. DOI: 10.1016/j.quascirev.2016.07.012.

Patton, H., D.A. Swift, C.D. Clark, S.J. Livingstone, S.J. Cook, and A. Hubbard (2015). "Automated mapping of glacial overdeepenings beneath contemporary ice sheets: Approaches and potential applications." In: *Geomorphology* 232, pp. 209–223. DOI: 10.1016/j.geomorph.2015.01.003.

Pattyn, F. and W. Van Huele (1998). "Power law or power flaw?" In: *Earth Surface Processes and Landforms: The Journal of the British Geomorphological Group* 23.8, pp. 761–767. DOI: 10.1002/(SICI)1096-9837(199808)23:8<761::AID-ESP892>3.0.CO;2-K.

Paxman, G.J., S.S. Jamieson, F. Ferraccioli, M.J. Bentley, N. Ross, E. Armadillo, E.G. Gasson, G. Leitchenkov, and R.M. DeConto (2018). "Bedrock erosion surfaces record former East Antarctic Ice Sheet extent." In: *Geophysical Research Letters* 45.9, pp. 4114–4123. DOI: 10.1029/2018GL077268.

Penck, A. (1900). "Die Uebertiefung der Alpentäler." In: *12th International Geographical Congress* 2, pp. 232–240.

Peterson, G. and M.D. Johnson (2018). "Hummock corridors in the south-central sector of the Fennoscandian ice sheet, morphometry and pattern." In: *Earth Surface Processes and Landforms* 43.4, pp. 919–929. DOI: 10.1002/esp.4294.

Petruccione, J.L. and R.W. Wellner (1996). "Seismic reflection investigation of Montezuma wetlands, central New York State: Evolution of a Late Quaternary subglacial meltwater channel system." In: *Subsurface Geologic Investigations of New York Finger Lakes: Implications for Late Quaternary Deglaciation and Environmental Change* 311, p. 77.

Pietsch, J. and P. Jordan (2014). "Digitales Höhenmodell Basis Quartär der Nordschweiz – Version 2014 (SGT E2) und ausgewählte Auswertungen, Tech." In: *Nagra Arbeitsbericht* NAB 14-02.

Piotrowski, J.A. (1994). "Tunnel-valley formation in northwest Germany—geology, mechanisms of formation and subglacial bed conditions for the Bornhöved tunnel valley." In: *Sedimentary Geology* 89.1, pp. 107–141. DOI: 10.1016/0037-0738(94)90086-8.

Piotrowski, J.A. (1997). "Subglacial hydrology in north-western germany during the last glaciation: groundwater flow, tunnel valleys and hydrological cycles." In: *Quaternary Science Reviews* 16.2, pp. 169–185. DOI: 10.1016/S0277-3791(96)00046-7.

Piotrowski, J.A., J. Geletneky, and R. Vater (1999). "Soft-bedded subglacial meltwater channel from the Welzow-Sud opencast lignite mine, Lower Lusatia, eastern Germany." In: *Boreas* 28.3, pp. 363–374. DOI: 10.1111/j.1502-3885.1999.tb00226.x.

Porter, C., P. Morin, I. Howat, M. Noh, B. Bates, K. Peterman, S. Keesey, M. Schlenk, J. Gardiner, K. Tomko, M. Willis, C. Kelleher, M. Cloutier, E. Husby, S. Foga, H. Nakamura, M. Platson, M. Wethington, C. Williamson, G. Bauer, J. Enos, G. Arnold, W. Kramer, P. Becker, A. Doshi, C. D'Souza, P. Cummens, F. Laurier, and M. Bojesen (2018). "ArcticDEM." In: https://doi.org/10.7910/DVN/OHHUKH.V1. DOI: 10.7910/DVN/OHHUKH. URL: https://doi.org/10.7910/DVN/OHHUKH.

Praeg, D. (2003). "Seismic imaging of mid-Pleistocene tunnel-valleys in the North Sea Basin—high resolution from low frequencies." In: *Journal of Applied Geophysics* 53.4, pp. 273–298. DOI: 10.1016/j.jappgeo.2003.08.001.

Prasicek, G., I.J. Larsen, and D.R. Montgomery (2015). "Tectonic control on the persistence of glacially sculpted topography." In: *Nature communications* 6, p. 8028. DOI: 10.1038/ncomms9028.

Prentice, I.C., P.J. Bartlein, and T. Webb (1991). "Vegetation and Climate Change in Eastern North America Since the Last Glacial Maximum." In: *Ecology* 72.6, pp. 2038–2056.

Prest, V.K., D.R. Grant, and V.N. Rampton (1968). "Glacial map of Canada." In: *Geological Survey of Canada* Map 1253A. DOI: 10.4095/108979.

Preusser, F., J.M. Reitner, and C. Schluchter (2010). "Distribution, geometry, age and origin of overdeepened valleys and basins in the Alps and their foreland." In: *Swiss Journal of Geosciences* 103.3, pp. 407–426. DOI: 10.1007/s00015-010-0044-y.

Ravier, E., J. Buoncristiani, M. Guiraud, J. Menzies, S. Clerc, B. Goupy, and Portier E. (2014). "Porewater pressure control on subglacial soft sediment remobilization and tunnel valley formation: A case study from the Alnif tunnel valley (Morocco)." In: *Sedimentary Geology* 304, pp. 71–95. DOI: 10.1016/j.sedgeo.2014.02.005.

Regis, R.S., C.J. Patterson, N. Wattrus, and D. Rausch (2003). "Relationship of deep troughs in the eastern Lake Superior basin and large-scale glaciofluvial landforms in the central Upper Peninsula of Michigan." In: *North Central Geological Society of America Abstracts with Program, Paper*, pp. 19–10.

Rickard, L.V. and D.W. Fisher (1970a). "Geologic map of New York: Finger Lakes sheet." In: *New York State Museum and Science Service* The University of the State of New York, Albany, New York, Map and Chart Series, 15.

Rickard, L.V. and D.W. Fisher (1970b). "Geologic Map of New York: Niagara Sheet." In: *New York State Museum and Science Service* The University of the State of New York, Albany, New York, Map and Chart Series, 15.

Rose, K.C., N. Ross, R.G. Bingham, H.F.J. Corr, F. Ferraccioli, T.A. Jordan, A.M. Le Brocq, D.M. Rippin, and M.J. Siegert (2014). "A temperate former West Antarctic ice sheet suggested by an extensive zone of subglacial meltwater channels." In: *Geology* 42.11, pp. 971–974. DOI: 10.1130/G35980.1.

Ross, C.P. (1959). "Geology of Glacier National Park and the Flathead region, northwestern Montana." In: *U.S. Geological Survey Professional Paper* 296, p. 125. DOI: 10.3133/pp296.

Ross, J.V. (1981). "A geodynamic model for some structures within and adjacent to the Okanagan Valley, southern British Columbia." In: *Canadian Journal of Earth Sciences* 18.10, pp. 1581–1598. DOI: 10.1139/e81-146.

Russell, A.J., A.R. Gregory, A.R.G. Large, P.J. Fleisher, and T.D. Harris (2007). "Tunnel channel formation during the November 1996 jökulhlaup, Skeioarárjokull, Iceland." In: *Annals of Glaciology* 45, pp. 95–103. DOI: 10.3189/172756407782282552.

Salcher B.C.and Hinsch, R. and M. Wagreich (2010). "High-resolution mapping of glacial landforms in the North Alpine Foreland, Austria." In: *Geomorphology* 122.3, pp. 283–293. DOI: 10.1016/j.geomorph.2009.09.037.

Sandersen, P.B., F. Jørgensen, N.K. Larsen, J.H. Westergaard, and E. Auken (2009). "Rapid tunnel-valley formation beneath the receding Late Weichselian ice sheet in Vendsyssel, Denmark." In: *Boreas* 38.4, pp. 834–851. DOI: 10.1111/j.1502-3885.2009.00105.x.

Sandersen, P.B.E. and F. Jørgensen (2003). "Buried Quaternary valleys in western Denmark—occurrence and inferred implications for groundwater resources and vulnerability." In: *Journal of Applied Geophysics* 53.4, pp. 229–248. DOI: 10.1016/j.jappgeo.2003.08.006.

Sauli, C., M. Busetti, L. De Santis, and N. Wardell (2014). "Late Neogene geomorphological and glacial reconstruction of the northern Victoria Land coast, western Ross Sea (Antarctica)." In: *Marine Geology* 355, pp. 297–309. DOI: 10.1016/j.margeo.2014.06.008.

Schoof, C. (2007). "Ice sheet grounding line dynamics: Steady states, stability, and hysteresis." In: *Journal of Geophysical Research: Earth Surface* 112.F3. DOI: 10.1029/2006JF000664.

Schumm, S.A. and F.G. Ethridge (1994). "Origin, Evolution and Morphology of Fluvial Valleys." In: *Society for Sedimentary Geology* 51.

Scipy (2020). "scipy.signal.find_peaks." In: https://docs.scipy.org/doc/scipy/reference/generated/scipy.signal.findpeaks.html. URL: https://docs.scipy.org/doc/scipy/reference/generated/scipy.signal.find$%5C_$peaks.html.

Seidl, M.A., W.E. Dietrich, and J.W. Kirchner (1994). "Longitudinal Profile Development into Bedrock: An Analysis of Hawaiian Channels." In: *The Journal of Geology* 102.4, pp. 457–474. DOI: 10.1086/629686.

Shaw, J. (1977). "Sedimentation in an Alpine Lake During Deglaciation, Okanagan Valley, British Columbia, Canada." In: *Geografiska Annaler: Series A, Physical Geography* 59.3-4, pp. 221–240. DOI: 10.1080/04353676.1977.11879954.

Shaw, J. and T.R. Healy (1977). "The formation of the Labyrinth, Wright Valley, Antarctica." In: *New Zealand Journal of Geology and Geophysics* 20.5, pp. 933–947.

Shaw, J., D. Kvill, and B. Rains (1989). "Drumlins and catastrophic subglacial floods." In: *Sedimentary Geology* 62.2, pp. 177–202. DOI: 10.1016/0037-0738(89)90114-0.

Shreve, R.L. (1972). "Movement of Water in Glaciers." In: *Journal of Glaciology* 11.62, pp. 205–214. DOI: 10.3189/S002214300002219X.

Sjogren, D.B., T.G. Fisher, L.D. Taylor, H.M. Jol, and M.J. Munro-Stasiuk (2002). "Incipient tunnel channels." In: *Quaternary International* 90.1, pp. 41–56. DOI: 10.1016/S1040-6182(01)00091-X.

Sly, P.G. and J.W. Prior (1984). "Late glacial and postglacial geology in the Lake Ontario basin." In: *Canadian Journal of Earth Sciences* 21.7, pp. 802–821. DOI: 10.1139/e84-087.

Smed, P. (1998). "Die Entstehung der danischen und norddeutschen Rinnentaler (Tunneltaler) Glaziologische Gesichtspunkte." In: *E&G Quaternary Science Journal* 48.1, pp. 1–18. DOI: 10.3285/eg.48.1.01.

Smith, L.C., L.C. Andrews, L.H. Pitcher, B.T. Overstreet, A.K. Rennermalm, M.G. Cooper, S.W. Cooley, J.C. Ryan, C. Miege, C. Kershner, and C.E. Simpson (2021). "Supraglacial river forcing of subglacial water storage and diurnal ice sheet motion." In: *Geophysical Research Letters* 48.7, e2020GL091418. DOI: 10.1029/2020GL091418.

Smith, L.N. (2004). "Late Pleistocene stratigraphy and implications for deglaciation and subglacial processes of the Flathead Lobe of the Cordilleran Ice Sheet, Flathead Valley, Montana, USA." In: *Sedimentary Geology* 165.3, pp. 295–332. DOI: 10.1016/j.sedgeo.2003.11.013.

Soller, D.R. and C.P. Garrity (2018). "Map of bedrock topography, sheet 2 in Quaternary sediment thickness and bedrock topography of the glaciated United States east of the Rocky Mountains." In: *U.S. Geological Survey Scientific Investigations* Map 3392 2 sheets.scale 1:5,000,000. DOI: 10.3133/sim3392.

Spedding, N. and D.J.A. Evans (2002). "Sediments and landforms at Kviarjokull, southeast Iceland: a reappraisal of the glaciated valley landsystem." In: *Sedimentary Geology* 149.1, pp. 21–42. DOI: 10.1016/S0037-0738(01)00242-1.

Spotila, J.A. and J.T. Buscher (2004). "Long-term glacial erosion of active mountain belts: Example of the Chugach–St. Elias Range, Alaska." In: *Geology* 32.6, pp. 501–504.

Stackebrandt, W. (2009). "Subglacial channels of Northern Germany a brief review." In: *Zeitschrift der Deutschen Gesellschaft fur Geowissenschaften* 160.3, pp. 203–210. DOI: 10.1127/1860-1804/2009/0160-0203.

Staiger, J.K., J.C. Gosse, J.V. Johnson, J. Fastook, J.T. Gray, D.F. Stockli, L. Stockli, and R. Finkel (2005). "Quaternary relief generation by polythermal glacier ice." In: *Earth Surface Processes and Landforms: The Journal of the British Geomorphological Research Group* 30.9, pp. 1145–1159. DOI: 10.1002/esp.1267.

Stewart, M.A. (2009). "3D seismic analysis of Pleistocene tunnel valleys in the Central North Sea." PhD thesis.

Stewart, M.A., Lonergan L., and Hampson G. (2013). "3D seismic analysis of buried tunnel valleys in the central North Sea: morphology, cross-cutting generations and glacial history." In: *Quaternary Science Reviews* 72, pp. 1–17. DOI: 10.1016/j.quascirev.2013.03.016.

Stewart, M.A. and L. Lonergan (2011). "Seven glacial cycles in the middle-late Pleistocene of northwest Europe: Geomorphic evidence from buried tunnel valleys." In: *Geology* 39.3, pp. 283–286. DOI: 10.1130/G31631.1.

Studinger, M., R.E. Bell, G.D. Karner, A.A. Tikku, J.W. Holt, D.L. Morse, T.G. Richter, S.D. Kempf, M.E. Peters, D.D. Blankenship, R.E. Sweeney, and V.L. Rystrom (2003). "Ice cover, landscape setting, and geological framework of Lake Vostok, East Antarctica." In: *Earth and Planetary Science Letters* 205.3, pp. 195–210. DOI: 10.1016/S0012-821X(02)01041-5.

Stumm, D. (2010). "Deep glacial erosion: Review with focus on tunnel valleys in northern Europe." In: *Nagra Arbeitsbericht* NAB 10-33.

Sugden, D.E., G.H. Denton, and D.R. Marchant (1991). "Subglacial Meltwater Channel Systems and Ice Sheet Overriding, Asgard Range, Antarctica." In: *Geografiska Annaler: Series A, Physical Geography* 73.2, pp. 109–121. DOI: 10.1080/04353676.1991.11880335.

Sugden, D.E. and B.S. John (1976). In: *Glaciers and landscape*. E. Arnold.

Svensson, H. (1959). "Is the Cross-Section of a Glacial Valley a Parabola?" In: *Journal of Glaciology* 3.25, pp. 362–363. DOI: 10.3189/S0022143000017032.

Swift, D.A., S.J. Cook, D.J. Graham, N.G. Midgley, A.E. Fallick, R. Storrar, M. Toubes Rodrigo, and D.J.A. Evans (2018). "Terminal zone glacial sediment transfer at a temperate overdeepened glacier system." In: *Quaternary Science Reviews* 180, pp. 111–131. DOI: 10.1016/j.quascirev.2017.11.027.

Swift, D.A., P.W. Nienow, and T.B. Hoey (2005). "Basal sediment evacuation by subglacial meltwater: suspended sediment transport from Haut Glacier d'Arolla, Switzerland." In: *Earth Surface Processes and Landforms* 30.7, pp. 867–883. DOI: 10.1002/esp.1197.

Swift, D.A., C. Persano, F.M. Stuart, K. Gallagher, and A. Whitham (2008). "A reassessment of the role of ice sheet glaciation in the long-term evolution of the East Greenland fjord region." In: *Geomorphology* 97.1, pp. 109–125. DOI: 10.1016/j.geomorph.2007.02.048.

Tabacco, I.E., C. Bianchi, A. Zirizzotti, E. Zuccheretti, A. Forieri, and A. Della Vedova (2002). "Airborne radar survey above Vostok region, east-central Antarctica: ice thickness and Lake Vostok geometry." In: *Journal of Glaciology* 48.160, pp. 62–69. DOI: 10.3189/172756502781831656.

Tarr, R.S. (1904). "Artesian Well Sections at Ithaca, N, Y." In: *The Journal of Geology* 12.2, pp. 69–82.

Tweed, F.S., M.J. Roberts, and A. J. Russell (2005). "Hydrologic monitoring of supercooled meltwater from Icelandic glaciers." In: *Quaternary Science Reviews* 24.22, pp. 2308–2318. DOI: 10.1016/j.quascirev.2004.11.020.

Ugelvig, S.V., D.L. Egholm, R.S. Anderson, and N.R. Iverson (2018). "Glacial erosion driven by variations in meltwater drainage." In: *Journal of Geophysical Research: Earth Surface*. DOI: 10.1029/2018JF004680.

Ugelvig, S.V., D.L. Egholm, and N.R. Iverson (2016). "Glacial landscape evolution by subglacial quarrying: a multiscale computational approach." In: *Journal of Geophysical Research: Earth Surface* 121.11, pp. 2042–2068. DOI: 10.1002/2016JF003960.

Upton, P. and E.C. Osterberg (2007). "Paleoseismicity and mass movements interpreted from seismic-reflection data, Lake Tekapo, South Canterbury, New Zealand." In: *New Zealand Journal of Geology and Geophysics* 50.4, pp. 343–356. DOI: 10.1080/00288300709509841.

USGS (2018). "The National Elevation Dataset (NED)." In: https://www.usgs.gov/core-science-systems/national-geospatial-program/national-map. URL: https://www.usgs.gov/core-science-systems/national-geospatial-program/national-map.

Ussing, N.V. (1903). "Om Jyllands hedesletter og teorierne for deres dannelse." In.

van der Vegt, P., A. Janszen, and A. Moscariello (2012). "Tunnel valleys: current knowledge and future perspectives." In: *Geological Society, London, Special Publications* 368.1, pp. 75–97. DOI: 10.1144/SP368.13.

Vanderburgh, S. and M.C. Roberts (1996). "Depositional systems and seismic stratigraphy of a Quaternary basin: north Okanagan Valley, British Columbia." In: *Canadian Journal of Earth Sciences* 33.6, pp. 917–927. DOI: 10.1139/e96-069.

Vivian, R. (1970). "Hydrologie et erosion sous-glaciaires." In: DOI: 10.3406/rga.1970.3471.

Walder, J. and B. Hallet (1979). "Geometry of Former Subglacial Water Channels and Cavities." In: *Journal of Glaciology* 23.89, pp. 335–346. DOI: 10.3189/S0022143000029944.

Warren, C.R. and M.P. Kirkbride (1998). "Temperature and bathymetry of ice-contact lakes in Mount Cook National Park, New Zealand." In: *New Zealand Journal of Geology and Geophysics* 41.2, pp. 133–143. DOI: 10.1080/00288306.1998.9514797.

Warren, C.R. and M.P. Kirkbride (2003). "Calving speed and climatic sensitivity of New Zealand lake-calving glaciers." In: *Annals of Glaciology* 36, pp. 173–178. DOI: 10.3189/172756403781816446.

Wellner, J.S., D.C. Heroy, and J.B. Anderson (2006). "The death mask of the antarctic ice sheet: Comparison of glacial geomorphic features across the continental shelf." In: *Geomorphology* 75.1, pp. 157–171. DOI: 10.1016/j.geomorph.2005.05.015.

Wellner, R.W. and J.L. Petruccione (1996). "Correlation of drillcore and geophysical results from Canandaigua." In: *Subsurface Geologic Investigations of New York Finger Lakes: Implications for Late Quaternary Deglaciation and Environmental Change* 311, p. 37.

Wenau, S. and T.M. Alves (2020). "Salt-induced crestal faults control the formation of Quaternary tunnel valleys in the southern North Sea." In: *Boreas* 49.4, pp. 799–812. DOI: 10.1111/bor.12461.

Werder, M.A. (2016). "The hydrology of subglacial overdeepenings: A new supercooling threshold formula." In: *Geophysical Research Letters* 43.5, pp. 2045–2052. DOI: 10.1002/2015GL067542.

Wheeler, D.A. (1984). "Using parabolas to describe the cross-sections of glaciated valleys." In: *Earth Surface Processes and Landforms* 9.4, pp. 391–394. DOI: 10.1002/esp.3290090412.

Whipple, J.W. (1992). "Geologic map of Glacier National Park, Montana." In: *(No. 1508-F)*.

White, L.F., I. Bailey, G.L. Foster, G. Allen, S.P. Kelley, J.T. Andrews, K. Hogan, J.A. Dowdeswell, and C.D. Storey (2016). "Tracking the provenance of Greenland-sourced, Holocene aged, individual sand-sized ice-rafted debris using the Pb-isotope compositions of feldspars and 40Ar/39Ar ages of hornblendes." In: *Earth and Planetary Science Letters* 433, pp. 192–203. DOI: 10.1016/j.epsl.2015.10.054.

Wingfield, R.T.R. (1990). "The origin of major incisions within the Pleistocene deposits of the North Sea." In: *Marine Geology* 91.1, pp. 31–52. DOI: 10.1016/0025-3227(90)90131-3.

Woodland, A. W. (1970). "The Buried Tunnel-Valleys of East Anglia." In: *Proceedings of the Yorkshire Geological Society* 37.4, pp. 521–578. DOI: 10.1144/pygs.37.4.521.

Wright, H.E. (1973). "Tunnel Valleys, Glacial Surges, and Subglacial Hydrology of the Superior Lobe, Minnesota." In: *The Wisconsinan Stage*. Geological Society of America. DOI: 10.1130/MEM136-p251.

Yager, R.M., T.S. Miller, and W.M. Kappel (2001). "Simulated effects of salt-mine collapse on ground- water flow and land subsidence in a glacial aquifer system, Livingston County, New York." In: *US Geological Survey* 1611.97. DOI: 10.3133/pp1611.

Young, D.A., A.P. Wright, J.L. Roberts, R.C. Warner, N.W. Young, J.S. Greenbaum, D.M. Schroeder, J.W. Holt, D.E. Sugden, D.D. Blankenship, and T.D. van Ommen (2011). "A dynamic early East Antarctic Ice Sheet suggested by ice-covered fjord landscapes." In: *Nature* 474.7349, pp. 72–75. DOI: 10.1038/nature10114.

Zimmer, P.D. and E.J. Gabet (2018). "Assessing glacial modification of bedrock valleys using a novel approach." In: *Geomorphology* 318, pp. 336–347. DOI: 10.1016/j.geomorph.2018.06.021.

Zorn, T.G. (2017). "Ecology and Management of Stream Resident Brown Trout in Michigan (USA)." In: *Brown Trout: Biology, Ecology and Management*, pp. 667–696. DOI: 10.1002/9781119268352.ch27.

Zumberge, J.H. (1960). "CORRELATION OF WISCONSIN DRIFTS IN ILLINOIS, INDIANA, MICHIGAN, AND OHIO." In: *GSA Bulletin* 71.8, pp. 1177–1188. DOI: 10.1130/0016-7606(1960)71[1177:COWDII]2.0.CO;2.

Part V

APPENDIX

APPENDIX A

Table A.1: Table of all potential analogue sites found and the potential available published data.

Analogue Locations	Region	Location	Feature Types	Data Type	Data Source
USA	Northern New York State	Finger Lakes	Tunnel valleys	Seismic Stratigraphy	Mullins and Hinchey (1989)
USA	Northern New York State	Finger Lakes	Tunnel valleys	Seismic Stratigraphy	Mullins et al. (1996)
USA	Northern New York State	Finger Lakes	Tunnel valleys	Seismic Stratigraphy	Petruccione and Wellner (1996)
USA	New York State	Adirondack	N/A	Geological maps	Isachsen and Fisher (1970)
USA	New York State	Finger Lakes	N/A	Geological maps	Rickard and Fisher (1970a)
USA	New York State	Hudson/Mohawk	N/A	Geological maps	Fisher et al. (1970a)
USA	New York State	Lower Hudson	N/A	Geological maps	Fisher et al. (1970b)
USA	New York State	Niagara	N/A	Geological maps	Rickard and Fisher (1970b)
USA	New York State	-	Tunnel valleys	Map of spatial extent	Pair (1997)
USA	Michigan	-	Tunnel valleys	Map of spatial extent	Sjogren et al. (2002)
USA	Michigan	-	Tunnel valleys	Map of spatial extent	Fisher and Taylor (2002)
USA	Michigan	-	Tunnel valleys	Map of spatial extent	Kehew and Kozlowski (2007)
USA	Wisconsin	-	Tunnel valleys	Map of spatial extent	Clayton et al. (1999)
USA	Wisconsin	-	Tunnel valleys	Map of spatial extent	Cutler et al. (2002)
USA	Minnesota	-	Tunnel valleys	Map of spatial extent	Clayton et al. (1999)
USA	Wisconsin	Late Wisconsin ice lobes	Tunnel valleys	Map of glacier bed conditions	Attig et al. (1989)
USA	Minnesota	Superior Lobe, Central Minnesota	Tunnel valleys	Map of spatial extent	Moores (1989)
USA	Glacier National Park	Lake McDonald	Overdeepening	Seismic Stratigraphy	Mullins et al. (1991)
Canada	British Columbia	Okanagan Lake	Overdeepening	Seismic Stratigraphy	Eyles et al. (1991)
Canada	British Columbia	North Okanagan Valley	Overdeepening	Seismic Stratigraphy	Vanderburgh and Roberts (1996)

Table A.1: continued

Analogue Locations	Region	Location	Feature Types	Data Type	Data Source
Canada	British Columbia	Kalamalka Lake	Overdeepening	Seismic Stratigraphy	Mullins et al. (1990)
Canada	British Columbia	Shuswap Lake	Overdeepening	Seismic Stratigraphy	Eyles and Mullins (1997)
Canada	Ontario	Southwestern Ontario	Overdeepening	Bedrock maps	Eyles et al. (1997)
Canada	British Columbia	Mazinaw Lake	Overdeepening	Seismic Stratigraphy	Eyles et al. (2003)
Canada	Ontario	Lake Ontario Basin	Overdeepening	Seismic Stratigraphy	Sly and Prior (1984)
Canada	Toronto	Laurentian Channel	Tunnel valleys	Borehole data reconstruction	Eyles (1987)
Canada	Alberta	Waterton Lake	Overdeepening	Sonar	Eyles et al. (2000)
New Zealand	Southern Alps	Lake Tekapo	Overdeepening	Bathymetry	Irwin (1978)
New Zealand	Southern Alps	Godley Lake	Overdeepening	Bathymetry	Warren and Kirkbride (2003) Warren and Kirkbride (1998)
New Zealand	Southern Alps	Classen Lake	Overdeepening	Bathymetry	Warren and Kirkbride (2003)
New Zealand	Southern Alps	Maud Lake	Overdeepening	Bathymetry	Warren and Kirkbride (2003) Warren and Kirkbride (1998)
New Zealand	Southern Alps	Hooker Lake	Overdeepening	Bathymetry	Warren and Kirkbride (2003) Warren and Kirkbride (1998)
New Zealand	Southern Alps	Lake Ohau	Overdeepening	Bathymetry	Carter and Lane (1996)
New Zealand	Southern Alps	Lake Coleridge	Overdeepening	Bathymetry	Carter and Lane (1996)
New Zealand	Southern Alps	Lake Te Anau	Overdeepening	Bathymetry	Carter and Lane (1996)
New Zealand	Southern Alps	Lake Wakatipu	Overdeepening	Bathymetry	Brodie and Irwin (1970)
New Zealand	North and South Island	Multiple Lakes	Overdeepening	Bathymetry	Lowe and Green (1992)
Australia	Eastern Goldfields	-	Tunnel valleys	Sedimentary cross section	Eyles and de Broekert (2001)
Greenland	Greenland	Greenland	Overdeepening	Bed-topography DEM	Patton et al. (2016a)
Greenland	Greenland	Humboldt Glacier	Tunnel valleys	Ice-penetrating radar	Livingstone et al. (2017)

Table A.1: continued

Analogue Locations	Region	Location	Feature Types	Data Type	Data Source
Greenland	Greenland	Western Greenland	Overdeepening	Bed-topography DEM	Greenland Analogue Project
Greenland	Greenland	Greenland	Overdeepening	Bed-topography DEM	BedMachine v3, Morlighem et al. (2017)
Antarctica	Antarctica	Antarctica	Overdeepening	Bed-topography DEM	Patton et al. (2016a)
Antarctica	Former East Antarctic Ice Sheet	Victoria Land	Overdeepening	Radar	Paxman et al. (2018)
Antarctica	Northern Victoria Land Coast	Northwestern Ross Sea	Tunnel valleys	Seismic Stratigraphy	Sauli et al. (2014)
Peru	Peruvian Andes	Overdeepening	Bathymetry	Haeberli et al. (2016)	
South America	Patagonia	South America	Overdeepening	ASTER GDEM V2	Carrivick et al. (2016)
South America	Chile	Glaciar Leon	Overdeepening	Bathymetry	Harrison et al. (2008)
Jordan	Southern Jordan	Southern Jordan	Tunnel valleys	Sedimentary cross section	Douillet et al. (2012)
UK	East Anglia	East Anglia	Tunnel valleys	Sedimentary cross section	Woodland (1970)
UK	East Anglia	-	Tunnel valleys	Smed (1998)	
UK	-	Tunnel valleys	Seismic Stratigraphy	Golledge and Stoker (2006)	
Germany	Germany	Northern Germany /Denmark	Tunnel valleys	map of subglacial channels	Stackebrandt (2009)
Germany	Germany	-	Tunnel valleys	Sedimentary cross section	Kuster and Meyer (1979)
Germany	Germany	-	Tunnel valleys	Sedimentary cross section	Ehlers et al. (1984)
Germany	Germany	-	Tunnel valleys	Sedimentary cross section	Piotrowski (1994)
Germany	Germany	-	Tunnel valleys	Sedimentary cross section	Piotrowski (1997)
Germany	Germany	-	Tunnel valleys	Seismic Stratigraphy	Gabriel et al. (2003)
Denmark	Denmark	Jutland	Tunnel valleys	Seismic Stratigraphy	Jørgensen and Sandersen (2006)
Denmark	Denmark	Northern Germany /Denmark	Tunnel valleys	map of subglacial channels	Stackebrandt (2009)

Table A.1: continued

Analogue Locations	Region	Location	Feature Types	Data Type	Data Source
Denmark	Denmark	-	Tunnel valleys	Sedimentary cross section	Ehlers et al. (1984)
Denmark	Denmark	Off the coast of Jutland	Tunnel valleys	Seismic Stratigraphy	Huuse and Lykke-Andersen (2000)
Denmark	Denmark	-	Tunnel valleys	Seismic Stratigraphy	Jørgensen et al. (2003)
Denmark	Denmark	-	Tunnel valleys	Seismic Stratigraphy	Sandersen and Jørgensen (2003)
Poland	Poland	-	Tunnel valleys	Galon (1983)	
Netherlands	-	-	Tunnel valleys	Seismic Stratigraphy	Kluiving et al. (2003)
North Sea	North Sea	-	Tunnel valleys	Seismic Stratigraphy	Kluiving et al. (2003)
North Sea	North Sea	-	Tunnel valleys	Seismic Stratigraphy	Praeg (2003)
North Sea	North Sea	-	Tunnel valleys	Sedimentary cross section	Woodland (1970)
North Sea	North Sea	-	Tunnel valleys	map of subglacial channels	Smed (1998)
North Sea	North Sea	-	Tunnel valleys	Seismic Stratigraphy	Jørgensen and Sandersen (2006)
North Sea	North Sea	-	Tunnel valleys	Seismic Stratigraphy	Huuse and Lykke-Andersen (2000)
North Sea	North Sea	-	Tunnel valleys	Seismic Stratigraphy	Wingfield (1990)
North Sea	North Sea	-	Tunnel valleys	map of subglacial channels	Clark et al. (2004)
North Sea	North Sea	-	Tunnel valleys	Seismic Stratigraphy	Lonergan et al. (2006)
North Sea	North Sea	-	Tunnel valleys	Seismic Stratigraphy	Kristensen et al. (2007)
North Sea	North Sea	-	Tunnel valleys	Seismic Stratigraphy	Kristensen et al. (2008)
North Sea	North Sea	-	Tunnel valleys	Multi	Stewart (2009)
North Sea	North Sea	-	Tunnel valleys	Seismic Stratigraphy	Stewart and Lonergan (2011)
Switzerland	Whole of Switzerland	-	TV/OD?	DEM	Dürst Stucki and Schlunegger (2013)
Switzerland	Zurich Canton	Near Bulach	TV/OD?	Borehole data reconstruction	Buechi et al. (2017)
Switzerland	Zurich Canton	Near Niederweningen	TV/OD?	Seismic Stratigraphy	Dehnert et al. (2012)
Switzerland	Zurich Canton	-	TV/OD?	DEM	Jordan (2010)

Table A.1: continued

Analogue Locations	Region	Location	Feature Types	Data Type	Data Source
Switzerland	Alps	-	TV/OD?	Seismic Stratigraphy	Preusser et al. (2010)
Switzerland	Bern Canton	-	TV/OD?	Seismic Stratigraphy	Dürst Stucki et al. (2010)
Switzerland	Entlebuch area	-	Inner Gorge	DEM	Dürst Stucki et al. (2012)

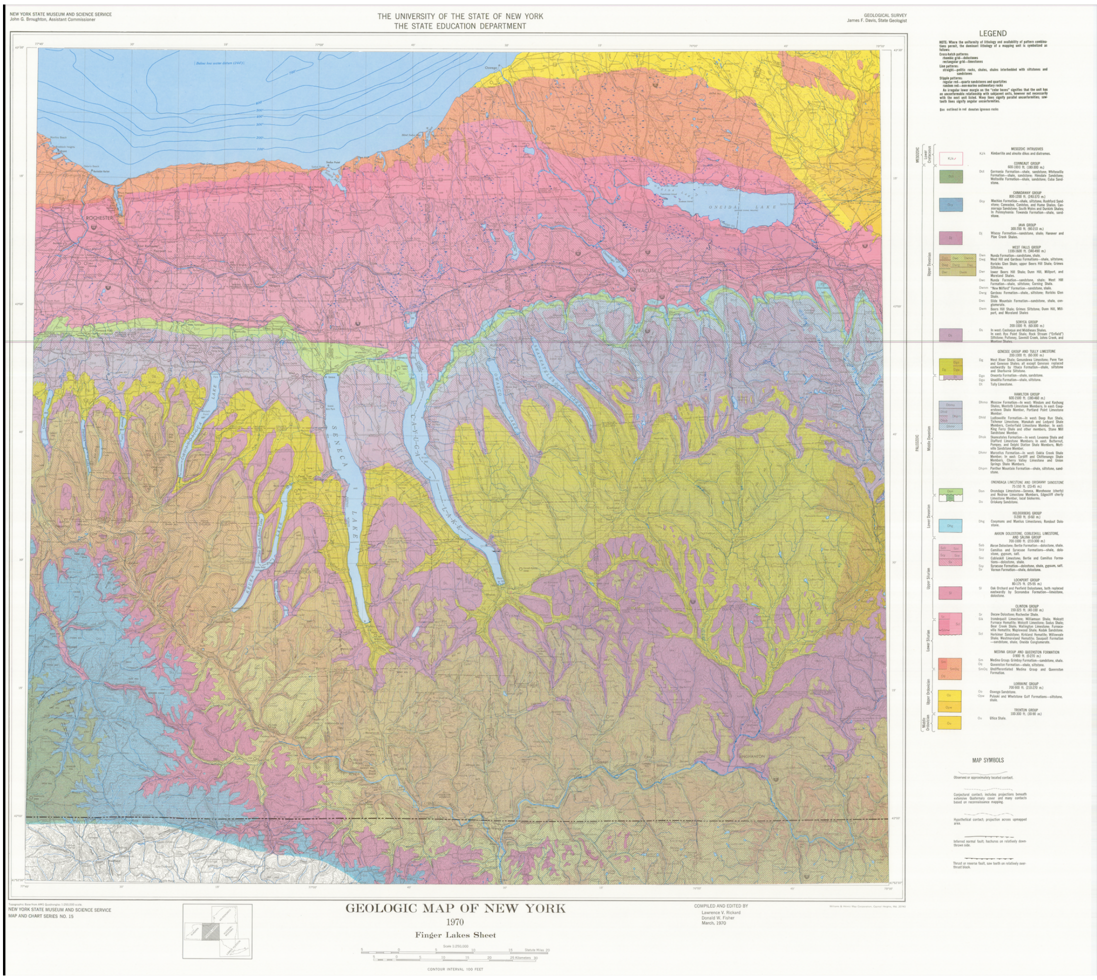

Figure A.1: Bedrock geologic map of Finger Lakes, New York, (1:250,000). Figure downloaded from the New York State Museum. (*nysm.nysed.gov/research − collections/geology/gis*)

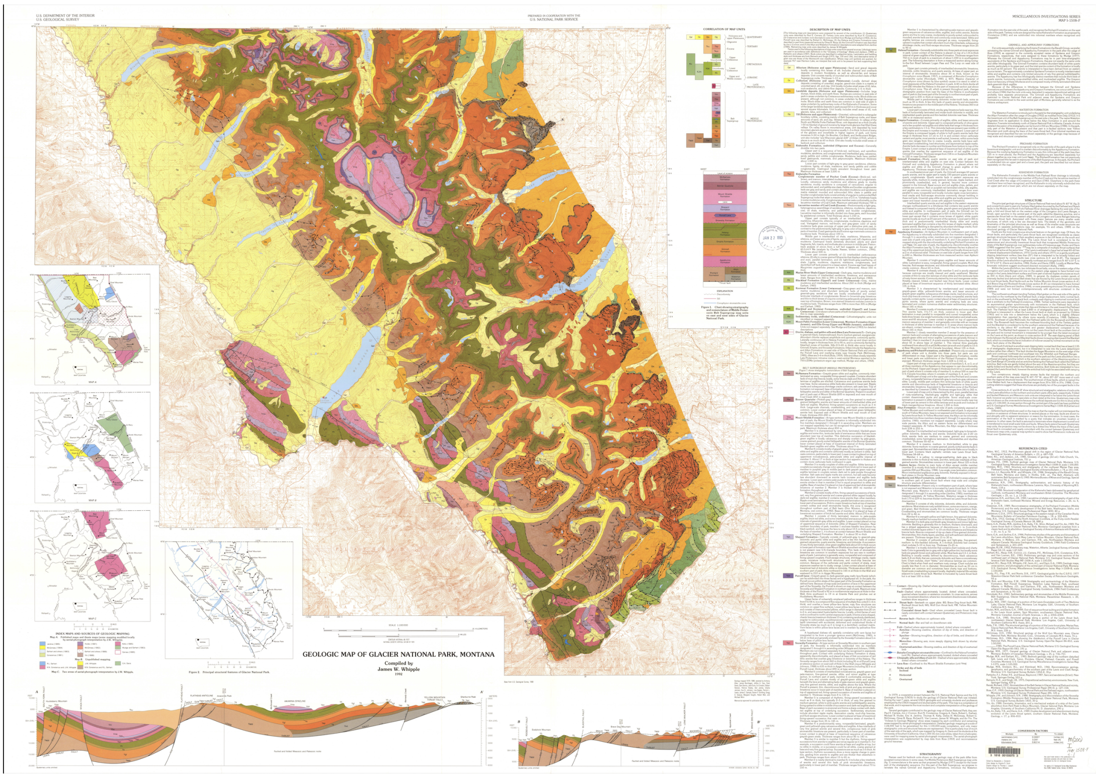

Figure A.2: Geologic map of Glacier National Park, Montana (1:100,000). Figure downloaded from National Park maps (*ngmdb.usgs.gov/Prodesc/proddesc*9273)

B

APPENDIX B

Table B.1: Table showing the location of faults and its effect on location of nested features

Number of features near a nested basin	<500 (m)	>500 (m)	>1 km	>5 km	Number of faults	Number of nested features
F1	-	1	3	7	11	9
F2	1	-	-	-	1	3
F3	1	-	-	-	1	2
F4	-	-	4	1	5	7
F5	-	-	-	2	2	2
F6	-	1	2	-	3	4
F7	-	-	-	1	1	1
F8	-	-	-	1	1	1
F9	-	-	5	-	5	7
F10	-	-	2	-	2	8
F11	-	-	2	1	3	4

Table B.2: Table showing northern Switzerland

	Peak KDE Depth	Peak KDE width	Peak KDE Fr	Peak KDE b exponent	Peak KDE V-index
Peak KDE Depth	N/A	0.002288	N/A	0.059766	0.051509
Peak KDE width	0.002288	N/A	N/A	0.001707	0.080599
Peak KDE Fr	N/A	N/A	N/A	0.025218	0.001613
Peak KDE b exponent	0.059766	0.001707	0.025218	N/A	0.107743
Peak KDE V-index	0.110559	0.157354	0.012805	0.347634	N/A

Table B.3: Table showing Finger Lakes

	Peak KDE Depth	Peak KDE width	Peak KDE Fr	Peak KDE b exponent	Peak KDE V-index
Peak KDE Depth	N/A	0.002288	N/A	0.059766	0.051509
Peak KDE width	0.002288	N/A	N/A	0.001707	0.080599
Peak KDE Fr	N/A	N/A	N/A	0.025218	0.001613
Peak KDE b exponent	0.059766	0.001707	0.025218	N/A	0.107743
Peak KDE V-index	0.051509	0.080599	0.001613	0.107743	N/A

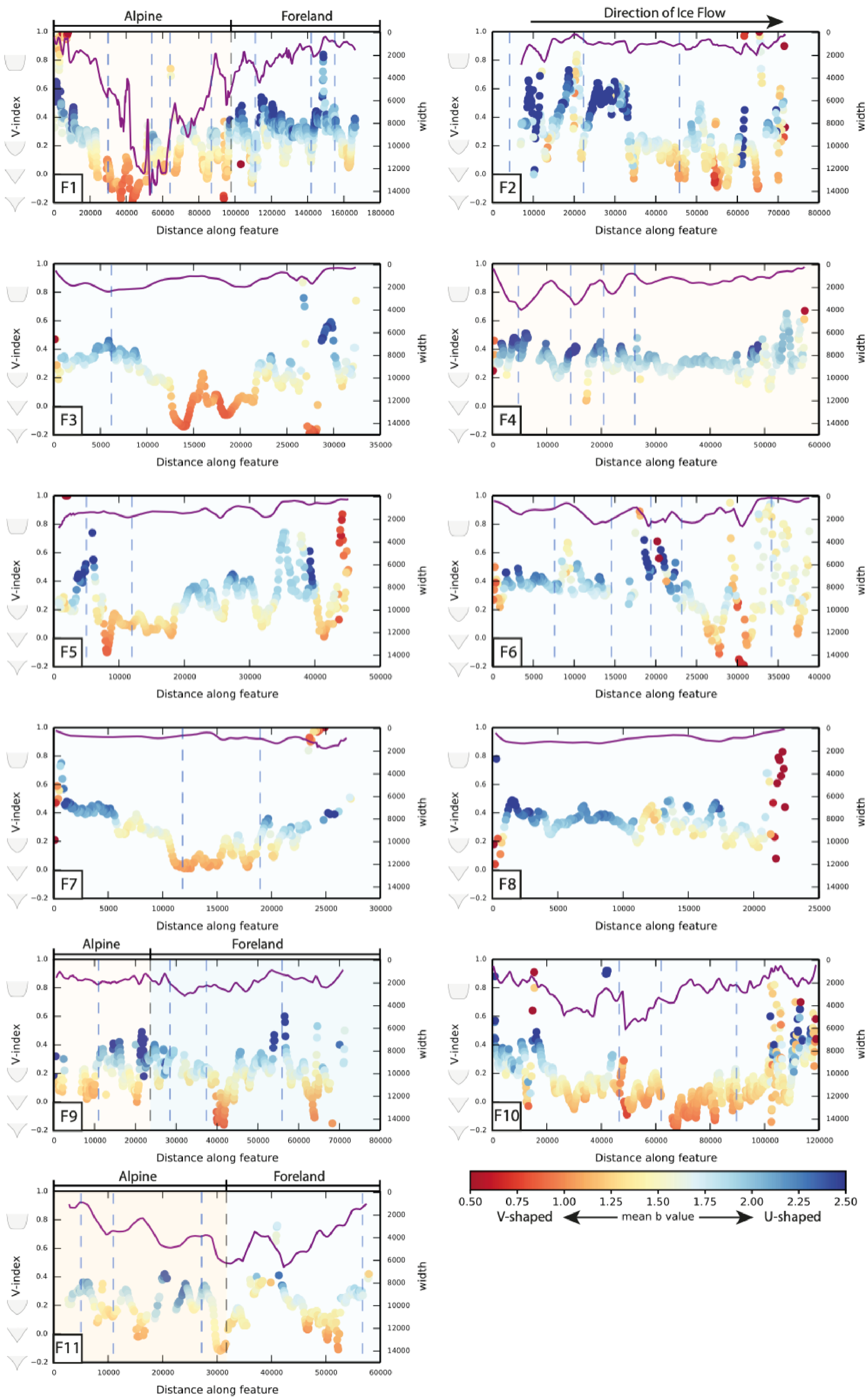

Figure B.1: Long-profiles of the features of northern Switzerland showing changes in feature width (purple), the location of tributary valleys (dashed blue lines, location of the boundary between the alpine and foreland regions, and the V-index and b-exponents of each CGBL. The scatter plots of the V-index data are colour coded to its corresponding b-exponent value.

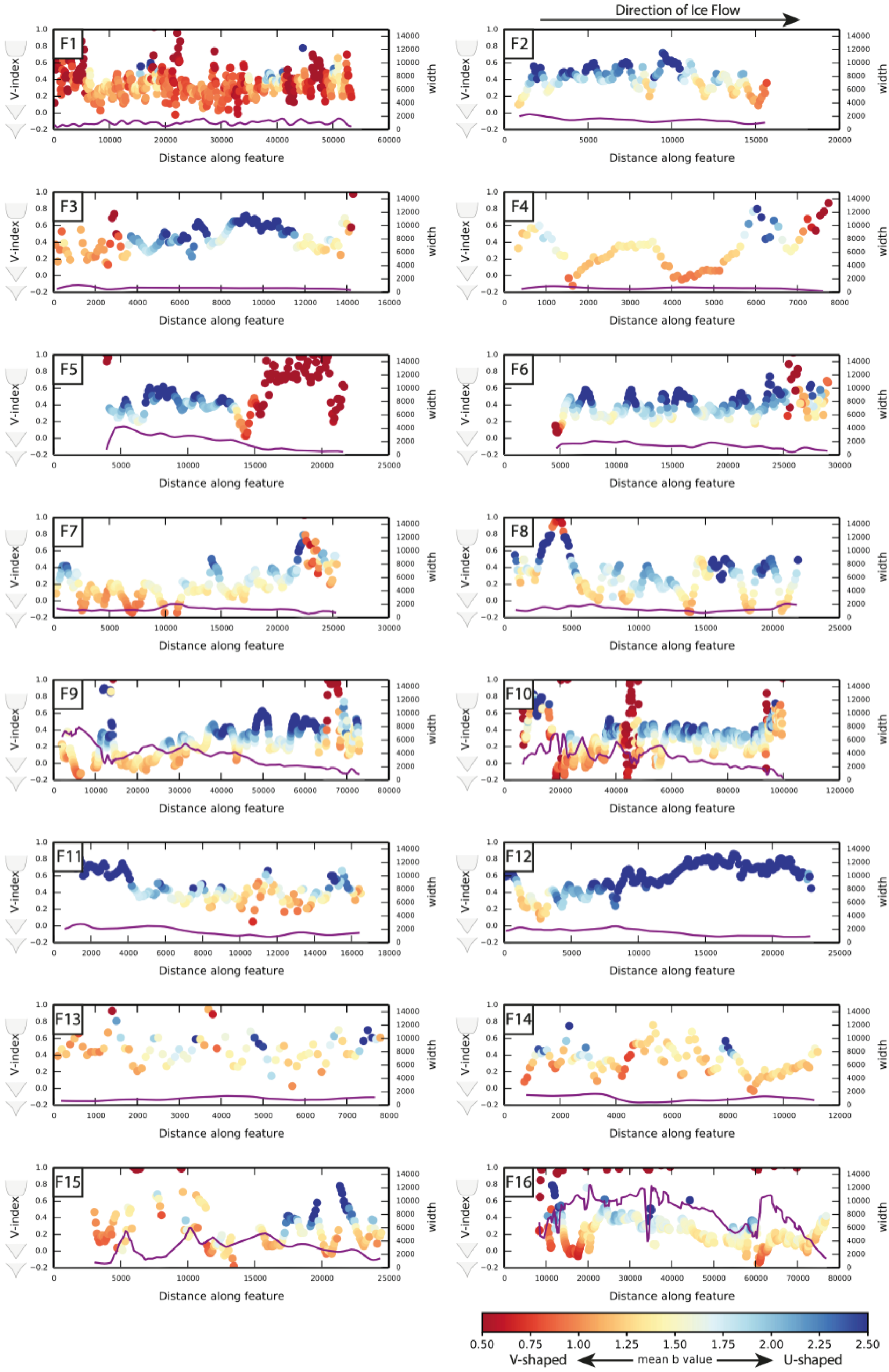

Figure B.2: Long-profiles of the features of the Finger Lakes showing changes in feature width (purple), and the V-index and b-exponents of each feature. The scatter plots of the V-index data are colourcoded to its corresponding b-exponent value.

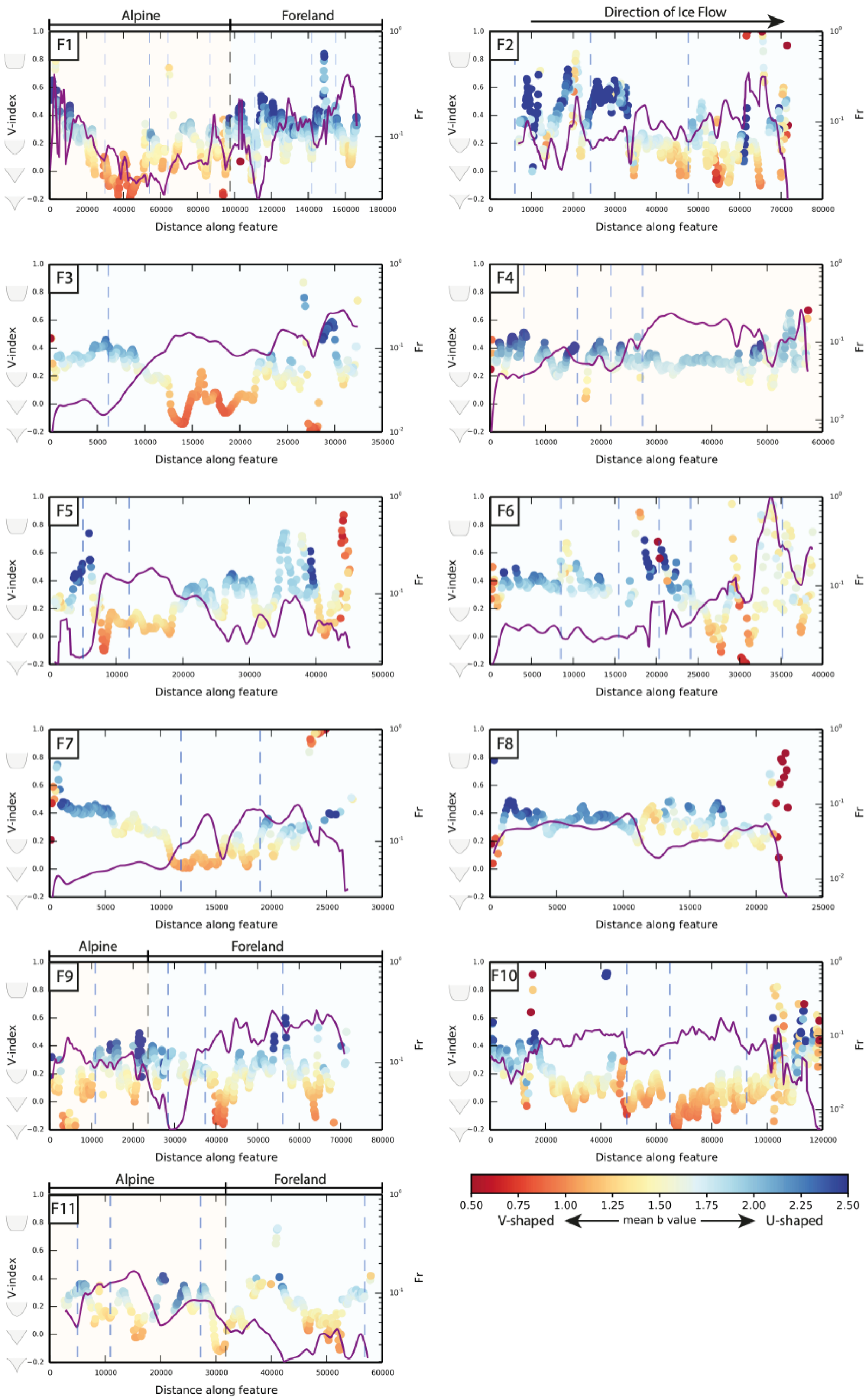

Figure B.3: Long-profiles of the features of northern Switzerland showing changes in form ratio (Fr) along feature (purple), the location of tributary valleys (dashed blue lines), location of the boundary between the alpine and foreland regions, and the V-index and b-exponents of each CGBL. The scatter plots of the V-index data are colour coded to its corresponding b-exponent value.

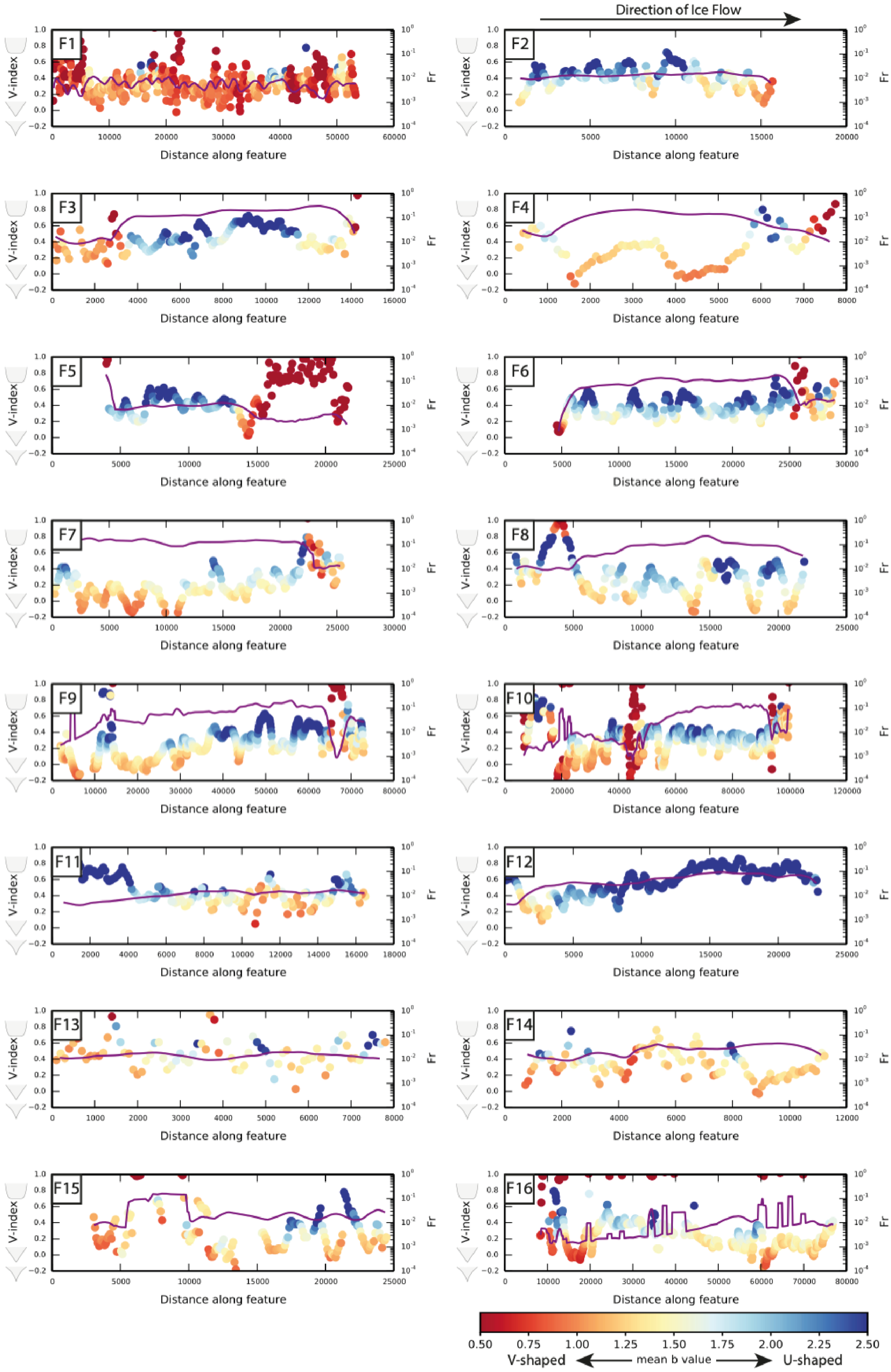

Figure B.4: Long-profiles of the features of the Finger Lakes showing changes in form ratio (Fr) along feature (purple), and the V-index and b-exponents of each features. The scatter plots of the V-index data are colour coded to its corresponding b-exponent value.

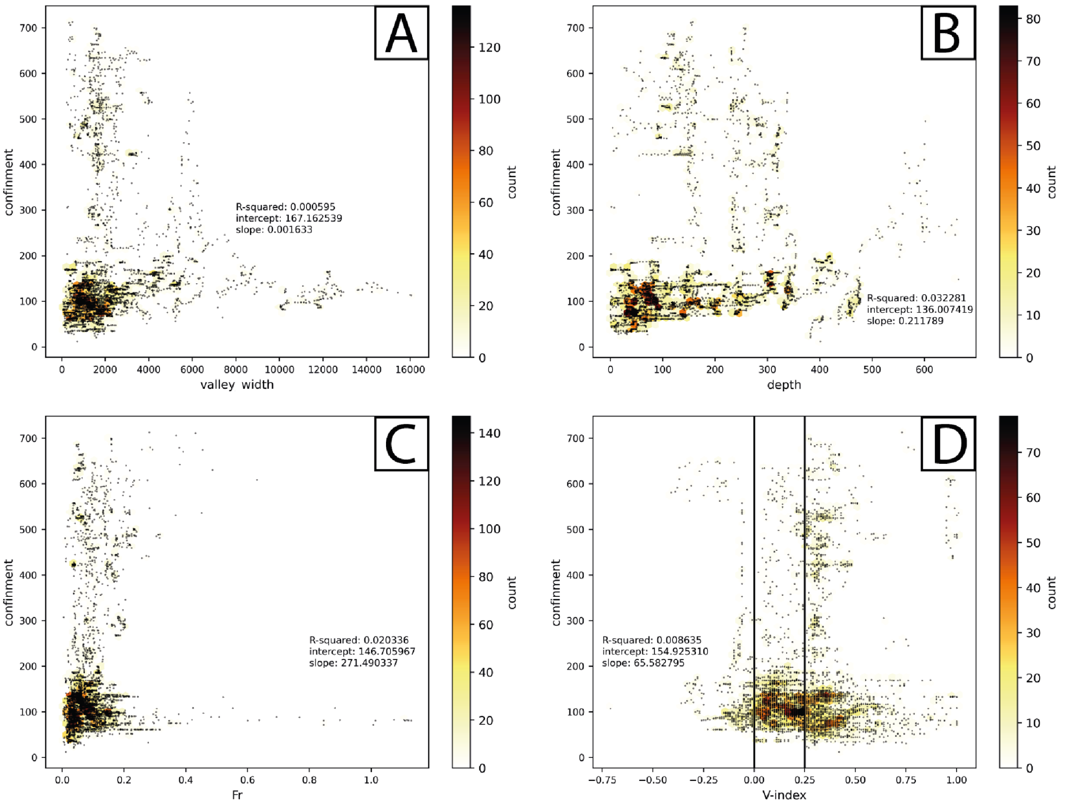

Figure B.5: Scatter plot hexbin of topographic confinement for foreland features of northern Switzerland. A) hexbin scatter plot of width vs confinement, B) hexbin scatter plot of depth vs confinement, C) hexbin scatter plot of Form ratio vs confinement, D) hexbin scatter plot of V-index vs confinement. Hexbins are colour coded according to the frequency of points in each 50 hexbin.